Integrated Reflection Seismic Monitoring and Reservoir Modeling for Geologic CO_2 Sequestration

Final Technical Report

Reporting Period: October 1, 2009 through December 31, 2011

PRINCIPAL AUTHOR
John D Rogers, PhD, PMP, PE

Report Date: March 2012

DOE Award : DE-FE 0001111

Fusion Petroleum Technologies, Inc.
8665 New Trails Drive, Suite 125
The Woodlands, TX 77381

DISCLAIMER

1 ABSTRACT

The US DOE/NETL CCS MVA program funded a project with Fusion Petroleum Technologies Inc. (now SIGMA^3) to model the proof of concept of using sparse seismic data in the monitoring of CO_2 injected into saline aquifers. The goal of the project was to develop and demonstrate an active source reflection seismic imaging strategy based on deployment of spatially sparse surface seismic arrays. The primary objective was to test the feasibility of sparse seismic array systems to monitor the CO_2 plume migration injected into deep saline aquifers.

The USDOE/RMOTC Teapot Dome (Wyoming) 3D seismic and reservoir data targeting the Crow Mountain formation was used as a realistic proxy to evaluate the feasibility of the proposed methodology. Though the RMOTC field has been well studied, the Crow Mountain as a saline aquifer has not been studied previously as a CO_2 sequestration (storage) candidate reservoir.

A full reprocessing of the seismic data from field tapes that included prestack time migration (PSTM) followed by prestack depth migration (PSDM) was performed. A baseline reservoir model was generated from the new imaging results that characterized the faults and horizon surfaces of the Crow Mountain reservoir. The 3D interpretation was integrated with the petrophysical data from available wells and incorporated into a geocellular model. The reservoir structure used in the geocellular model was developed using advanced inversion technologies including Fusion's ThinMAN^{TM} broadband spectral inversion. Seal failure risk was assessed using Fusion's proprietary GEOPRESS^{TM} pore pressure and fracture pressure prediction technology. CO_2 injection was simulated into the Crow Mountain with a commercial reservoir simulator.

Approximately 1.2MM tons of CO_2 was simulated to be injected into the Crow Mountain reservoir over 30 years and subsequently let "soak" in the reservoir for 970 years. The relatively small plume developed from this injection was observed migrating due to gravity to the apexes of the double anticline in the Crow Mountain reservoir of the Teapot dome.

Four models were generated from the reservoir simulation task of the project which included three saturation models representing snapshots at different times during and after simulated CO_2 injection and a fully saturated CO_2 fluid substitution model. The saturation models were used along with a Gassmann fluid substitution model for CO_2 to perform fluid volumetric substitution in the Crow Mountain formation. The fluid substitution resulted in a velocity and density model for the 3D volume at each saturation condition that was used to generate a synthetic seismic survey. FPTI's (Fusion Petroleum Technologies Inc.) proprietary SeisModelPRO^{TM} full acoustic wave equation software was used to simulate acquisition of a 3D seismic survey on the four models over a subset of the field area. The simulated acquisition area included the injection wells and the majority of the simulated plume area.

The four sets of shot gathers, one for each of the four CO_2 simulation models were further decimated to obtain sparse seismic data sets. Each gather set was processed using the same processing flow for consistency. The analysis of the sparse data sets demonstrated that sparse seismic arrays can be utilized to monitor effectively the CO_2 injection process and migration of the CO_2 plumes for gas storage and sequestration applications.

Contents

2 EXECUTIVE SUMMARY

The goal of the project was to develop and demonstrate an active source reflection seismic imaging strategy based on deployment of spatially sparse surface seismic arrays. Funded under US DOE/NETL project DEFE0001111, Fusion Petroleum Technology Inc. developed and demonstrated a fully integrated multidisciplinary software system and proved the feasibility of sparse seismic methodology for CO_2 MVA (Monitoring, Verification, and Accounting) in a realistic field system.

The project was divided into three phases and two budget periods with tasks associated with project management and administration outside of the three phases. These included the following: Phase I – Baseline CO_2 Reservoir Model; Phase II – Proof-of-Concept; and Phase III-Integration into GeoPRO™ software. The data set from the DOE RMOTC Teapot Dome site was used in the project as a proxy to demonstrate an active source reflection seismic imaging strategy based on the deployment of spatially sparse surface seismic arrays, integrated with a dense baseline array.

Phase I results consisted of processing seismic data from the DOE RMOTC site and interpreting the reservoir structure from the processed seismic and well log analysis. The initial time and depth processing of the Teapot Dome 3D seismic have yielded results which are superior to previously published results from other sources. Based on Fusion's high end imaging and reservoir analysis tools a physical model of the reservoir was developed. The reservoir model incorporates rock physics, well information, and derived formation geopressure distribution, and the overall reservoir characterization defined from the efforts in Phase II.

Phase II was a Proof of Concept effort which consisted of developing a reservoir geocellular model to characterize the reservoir based on the reservoir structural interpretation from Phase I, reservoir simulation of CO_2 injection, and rock physics seismic simulation and analysis to develop the sparsity analysis objective of the project. The simulation of injecting CO_2 into the Crow Mountain aquifer incorporating the geochemistry of the water/gas/rock systems has proven to be computationally difficult. The reservoir simulation of injection and developing a simulated plume into the Crow Mountain aquifer was eventually accomplished[1] with a very simplified rock mineral composition (three minerals. Task 6.1, the reservoir simulation task, started approximately one month later and finished almost six months later than the baseline projected due to difficulty with the commercial reservoir simulator and the coupling of geochemistry and transport module. Four CO_2 saturation realizations were exported from the simulator and used with seismic modeling software to prove the feasibility concept of sparse seismic data acquisition in CO_2 MVA.

The dense amplitude differences showed the possibility of evaluating a migrating CO_2 plume with dense seismic information. Procedures to decimate or reduce the amount of data from the synthetically produced dense data were accomplished by reducing the number of gathers in the dense data set without rerunning the seismic simulator. Comparison of the synthetic seismic and actual field seismic showed high confidence that the synthetic seismic was modeling the reservoir correctly. The synthetic data set with a limited offset of six fold was reimaged. The dense data set had relatively good resolution while the decimated or less dense data appears grainy but the boundaries of the plume can be resolved in both cases and remain relatively unchanged. This is also seen in further reduction using a limited offset of three fold data sets. Again the boundaries of the plume are discernible and consistent though the resolution becomes a little grainier.

Modifying fold is one way of modifying the amount of data and ultimately modifying the quality of the stack (Signal/Noise ratio if assuming the presence of noise). Another way to reduce the amount of data gathered is to increase the bin size. We looked at increasing the bin size of the data from 110 ft to 220 feet. We concluded that increasing the bin size can affect the spatial resolution but not necessarily change the amount of data that goes in the stack.

The decimation exercise in this project shows that limiting seismic data by fold does not influence the time lapse detectability as much as changing the bin size. When the bin size is doubled we are still able to detect with reasonable confidence the effect of CO_2 movement inferred only from saturation changes over time. Changes in fluid densities effect on the seismic data due to aqueous reactions in the reservoir were not studied. From the current work and the binning concept further optimization is needed in regards to the minimum fold of data needed and the maximum bin size needed in a sequestration project.

Phase III was executed in parallel with Phases I and II and contained the software development efforts for this project. Phase III started October 1, 2009 (start of project) and was completed September 30, 2011 (original completion date of project). At the beginning of the project we revisited the planning stage for software development and concluded that integration and development of the software environment and infrastructure to accomplish both computational and visualization components of CO_2 MVA in parallel from the start of the project would be advantageous to Fusion and quicker introduction of the software and possible use in other parts of the project.

Software development has concentrated on the data base, interchangeable data formats, and visualization. In addition to applications such as depth imaging and reservoir simulation, the system includes tools for automatic model updating and optimal control of full-field reservoir models, and for the inference of CO_2 plume location and detection of leaks from seismic data. Fusion will continue improving and adding to this suite of software as it is an important market

driver for Fusion in the oil and gas arena as well as in the potential CO_2 sequestration and environmental geosciences and engineering area. Vizpro™ and Geopro™ developed in phase III were used to a limited degree in Phase II tasks to integrate and develop the sparse seismic workflow.

3 INTRODUCTION

3.1 Project Objectives

The goal of this project was to develop and demonstrate an active source reflection seismic imaging strategy based on deployment of spatially sparse surface seismic arrays, integrated with a dense baseline array. The primary objective was to test the feasibility of sparse seismic CO_2 MVA for deep saline aquifers. The project used a phased approach: Phase I – Baseline CO_2 Reservoir Model; Phase II – Proof-of-Concept; and Phase III-Integration into GeoPRO™ software.

Phase III developed software useful in MVA independent and simultaneously with the other two phases (Phase I and II). The software was useful in converting reservoir simulation grid data for input into the Seismic simulation modeling software and developing the sparse CO_2 MVA workflow methodology.

3.2 Management of Project

3.2.1 Approach

The project was a seismic and reservoir simulation modeling effort and was developed in three phases originally scheduled for two years . The effort in the first two phases was to define a realistic seismic reservoir model provided by the US DOE RMOTC unit and processed and interpreted by Fusion personnel.

- Phase I developed a Baseline Reservoir Analysis consisting of processing a realistic baseline test 3D seismic data set (RMOTC Crow Mountain Saline Aquifer) through depth migration, petrophysical analysis of well logs, interpreting the reservoir structure from the seismic and well log analysis.
- Phase II of the project developed the Proof of Concept consisting of, developing a geocellular model to characterize the reservoir based on the structural interpretation in Phase I, reservoir simulation of CO_2 injection, and rock physics seismic simulation and analysis. The Synthetic seismic simulation modeled the CO_2 injected at various times during the injection and subsequent storage to monitor the CO_2 plume with seismic.

The data set from the DOE RMOTC Teapot Dome site is used in this project as a proxy to demonstrate the objective on a realistic data set.

Phase III was accomplished parallel to the other two phases and developed software useful in MVA CCS program. The third phase developed an integrated a software system for CO_2 MVA.

- Phase III Develop visualization and database foundation software to integrate complex seismic and engineering applications in a unified data base for seamless systems workflow between application software. Systematically aids with the analysis of subsurface data for MVA of CO_2 injection in brine formations

The software was useful in converting reservoir simulation grid data for input into the Seismic simulation modeling software and developing the sparse CO_2 MVA workflow methodology for some of the tasks in other phases.

3.2.2 Challenges and Difficulties

The simulation of CO_2 with the equilibrium solubility and mineral chemistry into the Crow Mountain aquifer (reservoir) proved to be computationally difficult; however, the reservoir simulation of injection and developing a simulated plume into the Crow Mountain aquifer (Task 6.1) was completed but increased the schedule by approximately ninety days. The vendor is still working on fixing the geochemistry coupling in the reactive transport reservoir simulator.

The loss of a key team member created a temporary discontinuity in the direction and execution of the spasity analysis workflow. Skilled technical resources had to be redirected to accomplish the tasks and additional understanding as to how to accomplish the scheduled tasks had to be ascertained.

3.3 Background

The Crow Mountain reservoir is used to prove the concept of using Sparse Seismic methodology for monitoring, verification and accounting (MVA) technology for anthropogenic CO_2 injection into Brine or saline aquifers (an aquifer defined as a water saturated rock through which water can flow or move). The targeted Crow Mountain reservoir for this study is contained within the lease boundaries of the US DOE Naval Petroleum Reserve No. 3 (NPR-3). Though the formations and reservoirs in the NPR-3 lease have been well studied, the Crow Mountain as a saline water repository for anthropogenic CO_2 has not been extensively studied for CO_2 sequestration or storage. The complex structure, lack of hydrocarbon producing potential and the available seismic and reservoir data make Crow Mountain formation a good proxy for a realistic and general analysis for CO_2 storage in a confined brine aquifer. Other formations within the NPR-3 site, primarily oil producing strata in the Tensleep and Dakota (Frontier) Formations have been studied for CO_2 EOR/Sequestration but the Crow Mountain reservoir

(aquifer) has not been studied to any detail. RMOTC personnel have been very helpful and attentive in supplying data to Fusion for this project.

The Naval Petroleum Reserve No. 3 (NPR-3) commonly referred to as Teapot Dome field Figure 1 is operated by the U.S. Department of Energy (DOE) through its Rocky Mountain Oilfield Testing Center (RMOTC). NPR-3 is located in the southwest portion of the Powder River Basin, 35 miles north of Casper, Natrona County, Wyoming. Production from the Teapot Dome commenced in the 1920's with full development activities beginning in 1976 after the effects of the first Arab oil embargo. Production has been from nine (9) productive horizons with the Shannon, Steele and Niobrara Shales, Second Wall Creek, and Tensleep Formations being the most productive. The stratigraphy present at Teapot Dome is illustrated in the geologic column shown in Figure 2.

The geographic expanse of the Crow Mountain aquifer is not exactly known but there are outcrop petrographic studies defining the lithology in Northwest Wyoming. There appears to be pinchouts and structural unconformities. Lying between oil and gas reservoirs in the RMOTC lease boundaries the data for analysis of the Crow Mountain aquifer in the Teapot Dome area was primarily a vestige of activity to define the oil and gas horizons and producing capabilities in the boundaries of the RMOTC NPR-3 Teapot Dome. In the boundaries of the DOE NPR-3 the Crow Mountain formation or reservoir is considered a brine aquifer for oilfield waste water disposal, but has been reported to produce significant amounts of oil in several anticlines in the Big Horn and Wind River basins of Northwestern and Northcentral Wyoming and outcrops near Ten Sleep and Dubois, Wyoming and near the southeastern end of the Washakie Range.

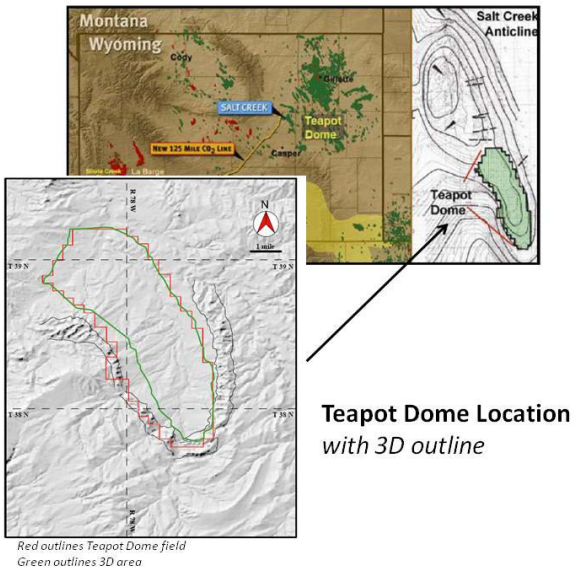

Figure 1: Geographical location of Teapot Dome with lease boundaries and seismic survey delineated

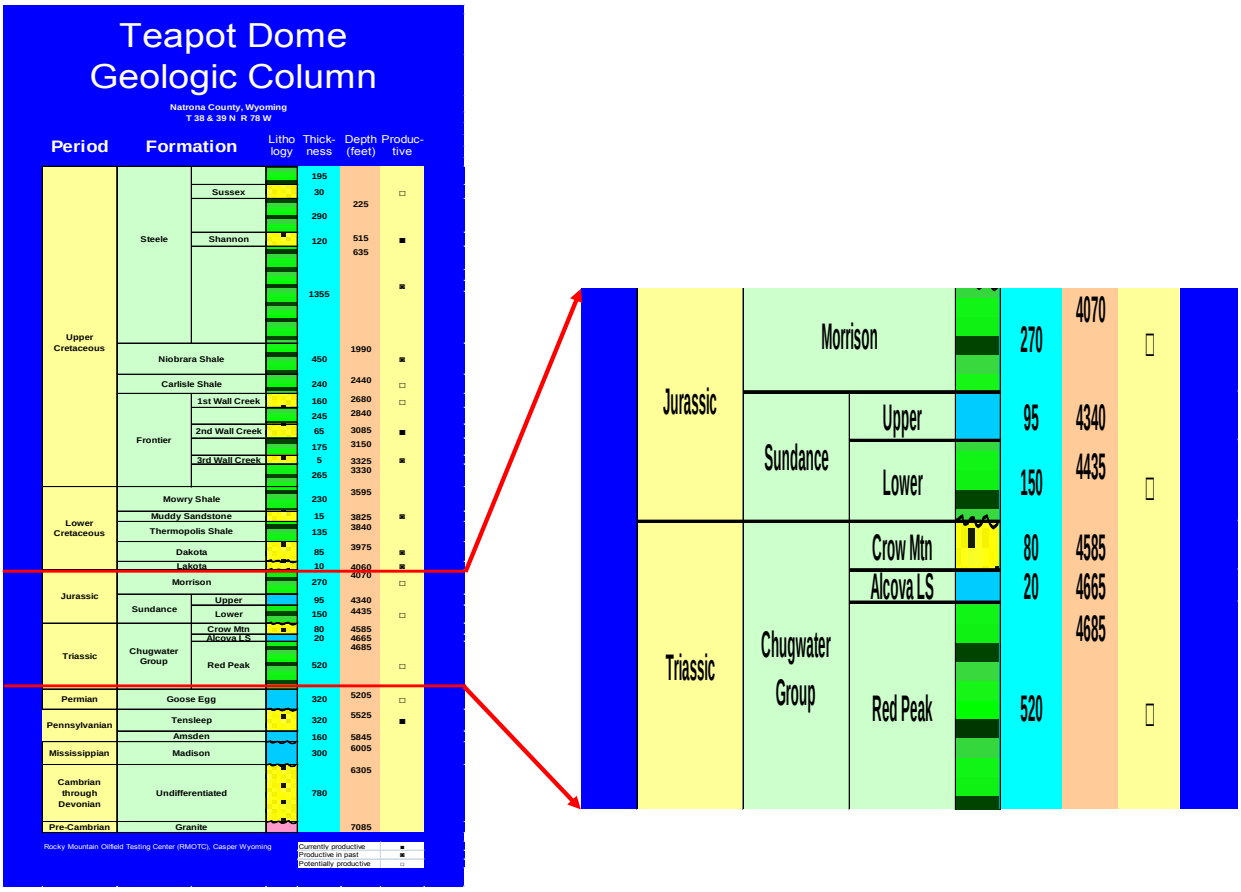

Figure 2:Geologic Column of the Teapot Dome field showing the Triassic Crow Mountain saline aquifer and surrounding formation

NPR-3 Teapot Dome surface boundaries encompass approximately 10,000 acre +/-. However, the extent of the Crow Mountain reservoir does not end at the boundaries of the RMOTC NPR-3 lease. Though the formations surrounding the Crow Mountain e.g. Red Peak (below) and Sundance members (above) have considerable clay compositions they are not considered impermeable shale aquitards or aquicludes. These silty claystones would conventionally be considered a shale but here they cleave in more sub-conchoidal to conchoidal fractures and exhibit poor fissility[2] and are not defined as a true shale that generally cleave along planes into thin sheets.

Picard et al[2,3,4] has presented several works in the 1960's and 1970's with a few more current works[5] on the petrography and stratigraphy of the Red Beds of the Triassic Chugwater Group in Northwestern and South-central Wyoming. His and others work provide a basis for the petrography and stratigraphy used in this study. The Crow Mountain, Alcova and Red Peak are members of the Chugwater group.

3.3.1 Structure

The Teapot Dome is a large northwest-southeast trending highly faulted, doubly plunging, basement-cored, Laramide-age asymmetrical anticline[6]. The anticline is an extension of the larger Salt Creek anticline to the north. The structure drops much more rapidly on the west flank than on the east side of the structure. For most of this study the entire aerial extent of the Teapot Dome property is utilized. The second phase of the project evaluated the available petrophysical and seismic data and provided basic mineralogy and lithological facies, and structural definition of the Crow Mountain and immediate surrounding rock.

Petrophysical data across the Crow Mountain Aquifer is limited. Three wells are completed in the Crow Mountain (primarily used as disposal wells) and over 33 wells penetrating to below the lower horizons primarily targeting the Tensleep oil producing formation. Fourteen of the wells penetrating the Crow Mountain have sonic logs and were evaluated with the density neutron logs to estimate rock and fluid properties.

3.3.2 Project Geology Overview

The Chugwater Group (Triassic) consists, in ascending order, of the Red Peak Formation, the Alcova Limestone, the Crow Mountain Sandstone, and the Jelm or Popo Agie Formations. With the exception of the Alcova, which is a marine limestone, the remainder of the Chugwater Group is mainly red mudrock interbedded with very fine to medium-grained sandstone[7]. The Crow Mountain is thought to be of tidal flat to shallow marine origin[7]. In the RMOTC Teapot dome area Central Wyoming the Jelm or Popo Agie Formations are disconformable and the Crow Mountain Formation of the Chugwater group is overlain by the Sundance Formation (Jurassic).

The Red Peak consists of silty claystone to sandstone and has casts of salt, mud cracks, and raindrop impressions, indicating tidal flat to nearshore marine depositional environments and underlays the Alcova and Crow Mountain formations[8]. The origin of other units, consisting of continuous sandstone or claystone units, is much less certain. However, continuous sandstones observed near Alcova Reservoir have irregular bedding that may be sabkha (coastal salt flat) related. Other units exposed near Dubois, Wyoming, have distinct channel forms[8]. In the current project model the Red Peak is defined to be the lower aquitard or seal. The top fifty feet is modeled.

The Alcova Limestone consists of marine limestone and dolomite and contains minor mollusks and abundant algal structures. The unit is a minor reservoir that produces hydrocarbons from fractured limestone with no primary porosity at Big Sand Draw field[8].

Above the Alcova is a well lithified Upper Triassic sandstone formation called the Crow Mountain. The Crow Mountain is characterized by fine- to medium-grained crossbedded sandstone and has produced about 2 million barrels of oil with associated gas in the Beaver Creek, Pilot Butte, Poison Spider, Rolff Lake, Sheldon northwest, and Steamboat Butte fields Wyoming. These fields are west and southwest of RMOTC NPR-3 site. The Crow Mountain is considered a minor reservoir[8]. The Crow Mountain is the targeted reservoir to simulate CO_2 sequestration for this project.

For the project the Lower Sundance Formation is defined as the upper aquitard and possible seal to the CO_2 injected into the Crow Mountain. In general the Sundance Formation is about 200 to 550 ft thick in the RMOTC area. We are modeling the lower 50 foot section immediately above the Crow Mountain. The overall formation consists of interbedded sandstone and siltstone, with some limestone and shale that were deposited in marine to eolian environments[8]. Some strata are glauconitic (iron potassium phyllosilicate) and highly fossiliferous[8]. The unit may be effectively sealed off from Phosphoria-generated oil in the western half of the Wind River Basin by anhydrite beds in the underlying Gypsum Spring Formation. About 3.5 million barrels of oil has been produced from the Sundance at Bolton Creek, Poison Spider, Schrader Flats, and Spindletop fields[8] all located at the extreme eastern margin of the Wind River province where the Gypsum Spring anhydrite beds are not present (west and southwest of the NPR-3 Teapot Dome area).

4 RESULTS AND DISCUSSIONS

4.1 Baseline Field Seismic Reservoir Analysis

Reprocessing the Teapot Dome 3D seismic program was undertaken in Phase I during November 2009 to February 2010 at Fusion Petroleum Technologies, Inc.'s offices in Houston, Texas. The reprocessing activities included time reprocessing, 3D pre-stack time migration (PSTM), and 3D pre-stack depth migration of the 3D data recorded in 2001 over the Naval Petroleum Reserve No. 3 (NPR-3) or more commonly referred to as Teapot Dome. The reprocessing was undertaken to provide a baseline, high quality 3D data volume utilized in other aspects of this project.

Key factors encountered during the reprocessing of these data included:

- Removing distorting effects due to variable near-surface conditions using 3D refraction statics.
- Addressing strong interfering coherent noise and improving the signal-noise ratio within the data.

- Tuning of Pre-Stack Migration parameters for a optimal curved ray PSTM and PSDM final volumes.
- Maximizing signal resolution and reflector continuity during the post-processing phase to prepare the data for the subsequent seismic attribute and geopressure stages of the project.

A summary of the processing flows and deliverables are discussed in this section and the detailed report is provided in Appendix A : Seismic Processing and 3D Pre-Stack Migration of this report.

4.1.1 Seismic Processing

The RMOTC Teapot Dome 3D seismic data set used in this study covers about 28 square miles of the Naval Petroleum Reserve No. 3 (NPR-3). Figure 3 is a representation of the 3D seismic survey plan view, showing source and receiver lines, fold, and a common receiver gather in the middle of the survey.

The following data processing flow was applied to the Teapot Dome data before imaging:

- Format Conversion: SEG-Y -> Internal Format
- Geometry Application & Correction
- 3D Refraction Statics - Renegade Tomo-Hybrid Solution (Datum 6700ft, Vr = 9600'/s)
- Edit
- Spherical Divergence (v2t)
- Noise Attenuation (WIND – Shot Domain)
- Velocity Analysis – Pass 1 (½mi)
- 3D Surface-Consistent Residual Statics – Pass 1 (MASTT)
- 3D Surface-Consistent Amplitude Scaling
- Minimum Phase Conversion
- 3D Surface-Consistent Spiking Deconvolution - 240ms Operator
- Spectral Equalization
- 2nd Pass Velocity (½mi) + 3D Residual Statics (MASTT)
- Trim Statics
- 3D Interpolation/Regularization
- Noise Attenuation (WIND – Common Offset Domain)

The above workflow includes proprietary Fusion processing algorithms.

A suite of prestack time migration (PSTM) results were developed. These will be input to the initial attribute and reservoir analysis. The 3D volumes are raw and post-processed:

- Preprocessed including spectral equalization (SPEQ) to PSTM
- Preprocessed, regularized/interpolated, including SPEQ to PSTM
- Preprocessed, regularized/interpolated to PSTM.

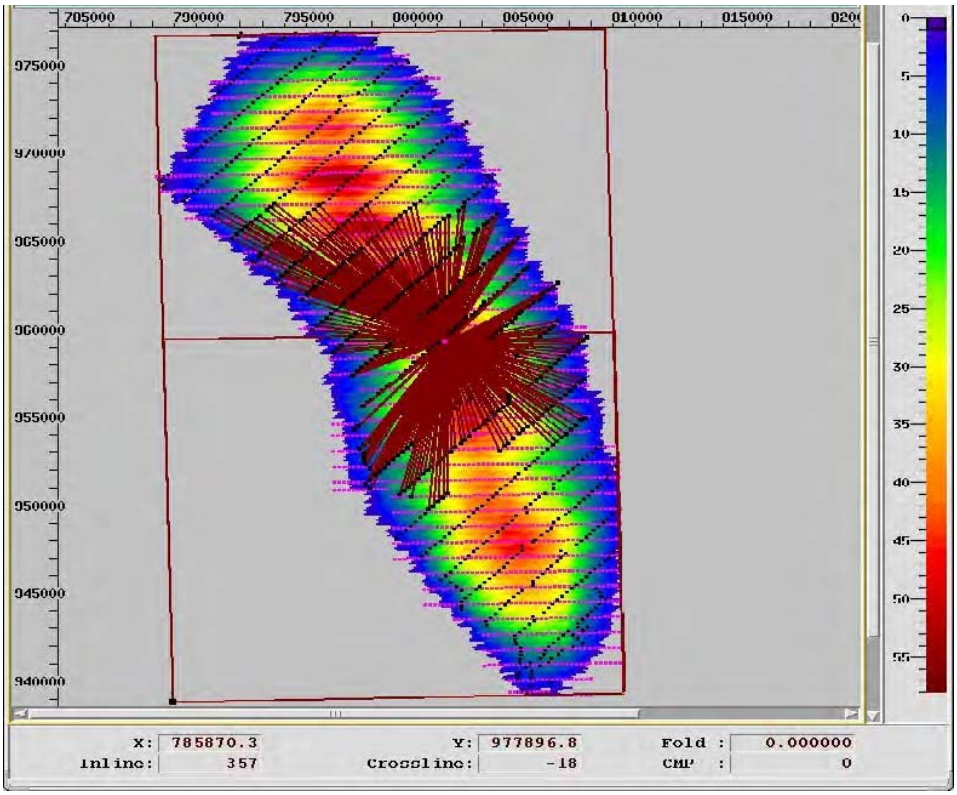

Figure 3: Teapot Dome 3D seismic survey plan view, showing source and receiver lines, fold in color, and a common receiver gather in the approximate center of the survey.

4.1.1.1 Time Processing

The objective of the seismic processing program was to provide a 3D volume that fully reflected the subsurface structural and stratigraphic characteristics of the Teapot Dome field to facilitate the later tasks in this CO_2 MVA program. An intensive effort was exerted to remove unnecessary distorting effects while preserving valid subsurface information. As the production processing flow evolved, several key factors emerged as critical to success of the project:

- Removal of near-surface travel-time distorting effects.
- Noise Attenuation of the diverse coherent noises encountered on the shot as well as high “random” noise degrading signal-noise ratio.
- Optimizing signal bandwidth

- Accurate definition of the RMS velocity variations across the Teapot Dome field
- 3D Pre-stack Imaging
  - Algorithm selection
  - Aperture design
  - Velocity Modeling
- Post-Stack signal enhancement

4.1.1.2 Depth Processing

3D Pre-Stack Depth Migration (PSDM) was undertaken to provide a data volume that could most effectively be tied to wells for the later reservoir-related stages of this project. A typical workflow utilizes the following approach

- Velocity Model Building: Vint-Z from PSTM-derived RMS-Time field
- Iterative Pre-stack Depth Migration with 3D Tomographic Updating.
- Model Building and Velocity Update: at each iteration stage.
- Final Pre-stack Depth Migration
  - 20 degree opening, 50 degree final angle
  - 20000ft aperture
  - 40 output offset bins, 330ft spacing
  - 10ft depth step
- Residual NMO: applied to all depth gathers.
- Gather Mute and Stack
- Convert from Depth to Time, using final velocity field (if required)
- Post migration processes
- Output SEG Y PSDM Gathers and Volume

4.1.1.3 Summary of Fusion Processed Teapot Dome 3D Seismic Data

The processing of the Teapot Dome 3D data delivered a high quality pre-stack imaged data base in both two-way-time and depth for the continuing stages of the CO_2 MVA project. No major problems were encountered during this portion of the project and the primary emphasis was assuring the amplitude integrity and frequency resolution of the data was sufficient for the subsequent attribute and modeling stages of the project.

3D refraction modeling using Fusion's Seismic Studio™ system provided a three-dimensional near surface model that removed any possible long-wavelength or high frequency near-surface travel time distortions. The stack response of the data versus a basic elevation-based correction showed noticeable improvement. Coherent noise energy was effectively removed using Fusion's WIND noise attenuation workflow allowing later processes such as deconvolution to be more properly designed on valid signal energy without noise contaminating the design. The use of 3D surface-consistent processes provided robust design of deconvolution filters and also allowed amplitude variations associated with differing near-surface conditions, source and or receiver coupling problems etc. to be corrected without damaging the integrity of the seismic amplitudes containing valid subsurface stratigraphic and/or fluid content information. Two passes of 3D surface consistent reflection residual statics removed minor high-frequency near surface related travel-time variations before the detailed 3D velocity estimation stage.

The geologic column of interest only extended to around 7000-ft and with offsets extending to greater than 13000-ft, RMS velocity estimates could be accurately determined using one-half mile spacing. While velocity variation across the Teapot Dome 3D area proved to be stable, an additional one-half mile grid generated after PSTM did improve the stability of the velocity model and the PSTM result and final PSTM stack. Within the limits of the 8-96 Hz Vibroseis sweep frequency range, a broadband spectrum was achieved. Consistent with the expectations of later processes, a volume with and without spectral equalization before stack was produced. Post-processed imaging volumes with spectral equalization applied were generated. Amplitude fidelity was preserved wherever possible and no processes likely to distort the temporal or offset amplitude relationships were applied.

Pre-stack imaging in both time and depth indicated a slowly varying velocity model laterally and consistent with vertical velocity relationships. The 3D area was elongated along the crest of the anticline with the narrower East-West (E-W) dimension in the dominant dip direction. After 3D migration the anticlinal features were compressed (Figure 4) and, as energy migrated in the generally E-W updip direction, there is a loss of useful information at the edges of the survey. The original 3D design with limited East-West aperture limited the useful fully migrated 3D area available for analysis. From observation of the time and depth slices through the final 3D

volumes a clearly focused 3D image emerged over the center of the area of interest (see Figure 5).

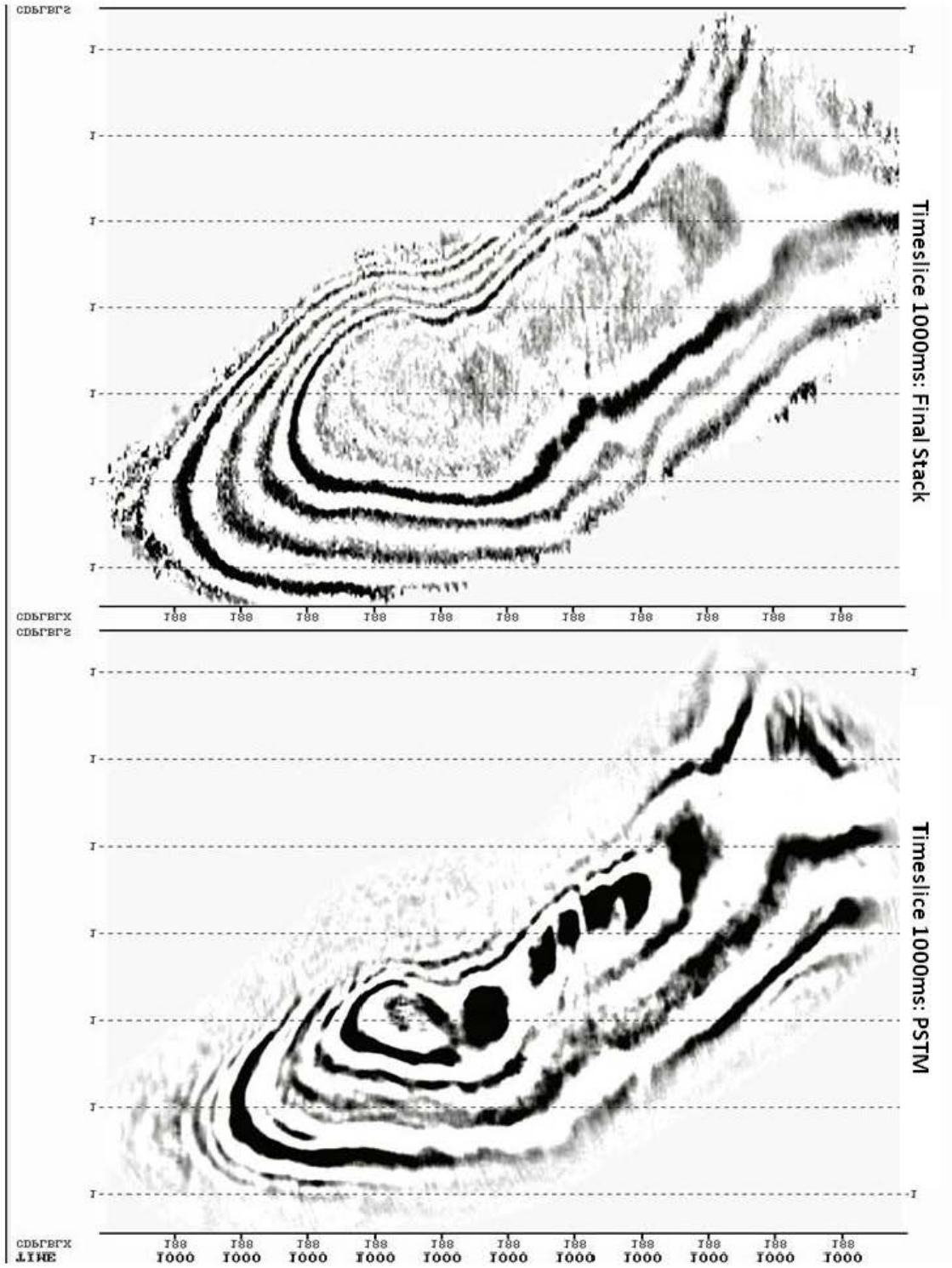

Figure 4 Time sliice 1000 ms: Final Stack versus Final PSTM

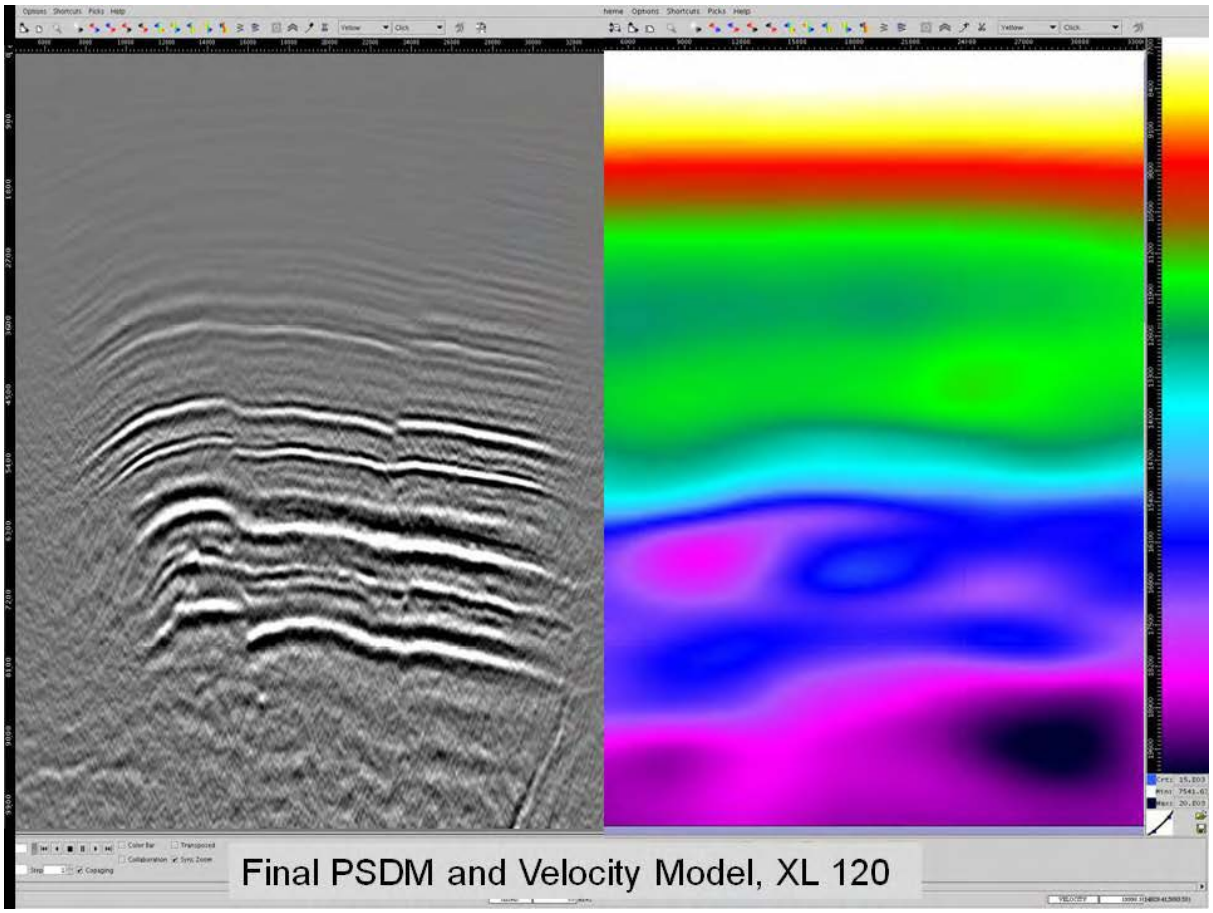

Figure 5: Final PSDM (no post-processing) with Velocity Model -- Crossline 120.

4.1.2 Geophysical Interpretation/Analysis

Using advanced seismic analysis techniques the statigraphy and lithology of the targeted Crow Mountain brine aquifer reservoir was modeled[9]. Spectral decomposition and acoustic impedance inversion provide useful analysis of the CO_2 injection and storage, even in relatively well lithified stratigraphy. Initially fluid substitution modeling indicated that CO_2 injection could be detectable with surface seismic data in this reservoir.

With the reprocessed 3D seismic data described in the previous sections, we performed structural mapping of the Crow Mountain sandstone, fluid replacement modeling of well log data replacing in-situ brine with injected CO_2, and calculation of synthetic offset models from the well data. The preliminary fluid replacement and synthetic offsets model indicated that a CO_2 plume should be evident from amplitude differences in a full field analysis. A full reservoir simulation of CO_2 injection is discussed in section 4.3 followed by the sparsity analysis.

Figure 2 is a geologic column diagram emphasizing the stratigraphy associated with the Jurrasic and Triassic portions of the Teapot Dome structure. The Crow Mountain Sandstone is in the

Upper Triassic with an unconformity at the top where it is overlain by the Lower Sundance Formation. Below the Crow Mountain are the Alcova Limestone and the well lithified Red Peak Shale. The Crow Mountain appears to be hydraulically isolated from the surrounding geologic section which adds to the viability of this aquifer as a CO_2 storage reservoir albeit small.

Figure 6 is a time map of the top of the Crow Mountain Formation contoured at 10ms intervals. The structure is an asymmetric ridge trending North-Northwest (NNW) to South-Southwest) SSE and appears to be the result of compressional tectonic forces. Some internal faulting suggests that these force axes may have rotated over time. The highest point on the structure occurs in the south one-third of the survey and this high is bounded on the north by a normal fault. There is another opposing normal fault with throw down to the south, with both of these faults creating a low-relief depression in the central portion of the survey. This feature is somewhat enigmatic since opposing normal faults usually indicate crustal extension. These might possibly document wrenching stresses and accommodation. The Crow Mountain Sandstone is eroded to approximately 40 feet in thickness in the north one-quarter of the survey while it appears to remain relatively constant at approximately 80 feet in thickness throughout the rest of the 3D survey.

The central portion of the structure has approximately 80 feet in thickness as shown in Figure 7. The low impedance of the Crow Mountain Formation in relation to the bounding stratigraphy is observed in Figure 8a and the top and base of the crow mountain is clearly resolvable in the synthetic seismogram displayed in Figure 8b.

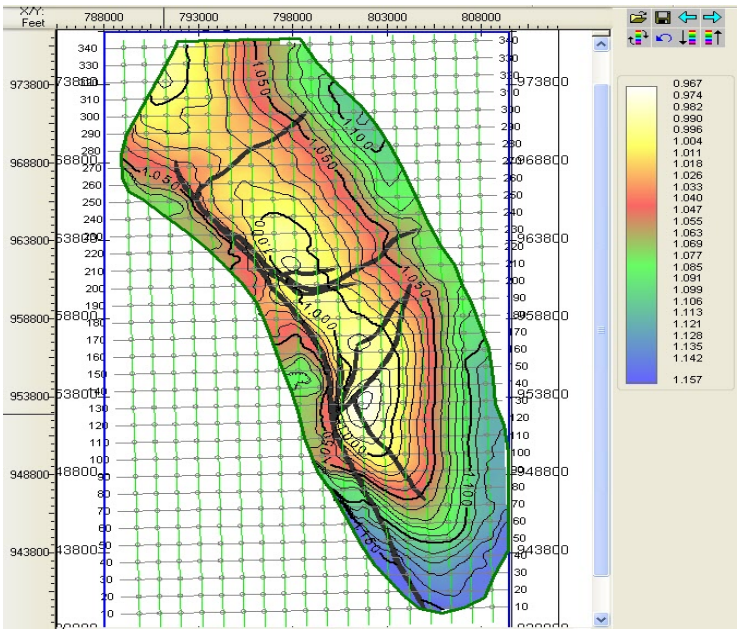

Figure 6: Time map of the Crow Mountain formation with 10ms contour interval. Solid black lines are Fusion interpreted faults from Fusion processed 3D seismic information

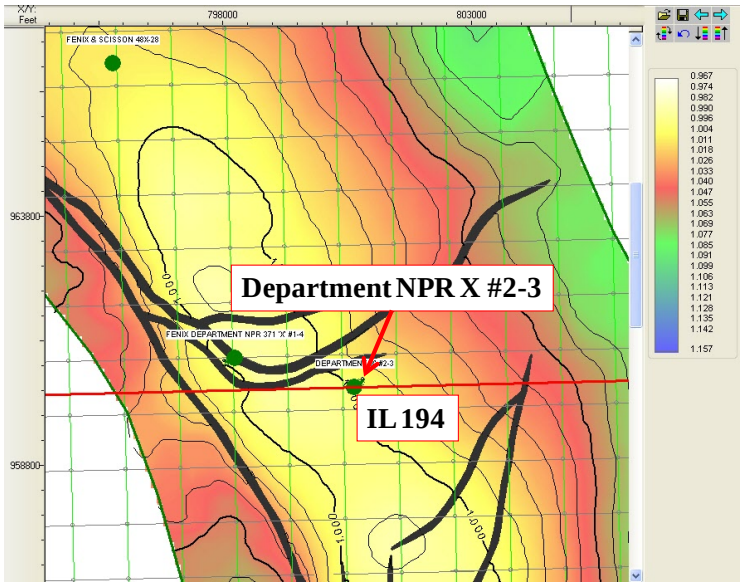

Figure 7: Central portion of the Crow Mountain structure with inline 194 intersecting the Department NPR X #2-3 well near the crest of the central portion of the structure

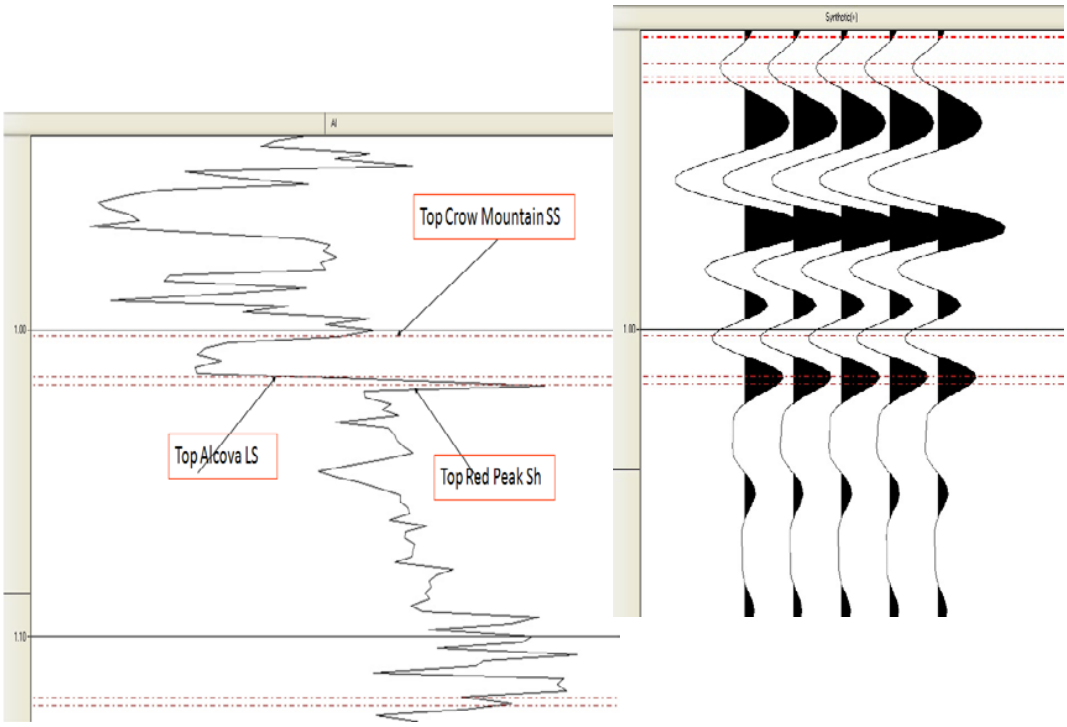

a b

Figure 8: a) low impedance log b) Synthetic seismogram

4.1.3 Geopressure -- Pore Pressure Analysis from Seismic Data

Fusion Petroleum Technologies Inc. (FPTI) performed integrated geopressure prediction on the 3D seismic in the Teapot Dome Area RMOTC site. A summary of the study is discussed below and details of geopressure analysis are presented in the complete report duplicated in *Appendix B: Crow Mountain Geopressure Analysis.*

Fluid and fracture pressure interpretation based on well control and seismic interval velocities were performed. Well control included seven (7) wells located within the seismic survey area. These wells contained mud weight data and wireline logs. The dense velocities were input to REVEL™, proprietary software developed by FPTI for residual velocity analysis, which refined the velocity field for pressure prediction. The velocity data were used to calibrate for pressure using the control well locations, and then predict pressures in 3D across the prospective area using the GEOPRESS™ tool. Attributes were generated for pore pressure (PP), overburden pressure (OB), fracture pressure (FP), effective stress (ES) in pounds per square inch (PSI) and gradients of these attributes in pounds per gallon (PPG).

Fluid and fracture pressure predictions were performed on a sub-sampled grid of the 3D velocity volume Figure 9 (Figure 3.1 of original report). Time values were converted to depth within GEOPRESS™, utilizing the seismic interval velocity data. The calibrations defined in section 4 of the report were applied to the data and depth and time values of effective stress, pore pressure, fracture pressure and overburden pressure were generated along with their gradients. The calculations were performed using the application of Bowers unloading above the horizon “top reversal surface”(magenta), and in the second calculation and inverted Bowers trend, followed by a deep Bowers calculation below the horizon “top second compaction surface” (blue).

The fluid pressure calculation set a minimum gradient of 8.5 pounds/gallon (hydrostatic). The time-depth relationship at each calculation function allowed generation of time-based calculations of vertical stress, effective stress, and fluid and fracture pressure. The output data volume for this project contains time-based data for fluid pressure and its gradient, fracture pressure and its gradient, vertical stress and its gradient and effective stress.

The fluid pressure gradient and fracture pressure gradient results along Arbitrary Line A-A’ are shown in Figure 10 (Figure 5.1 in original geopressure report see Appendix B: Crow Mountain Geopressure Analysis) and Figure 11 (Figure 5.2 in original geopressure report). The pore pressure above the “top reversal surface” (magenta) is in a regime of normal compaction. Below the TUL surface, the regime changes from normal compaction to the inverted Bowers trend. The fluid pressure gradients below the top second compaction surface increase however the pressure remain generally benign throughout.

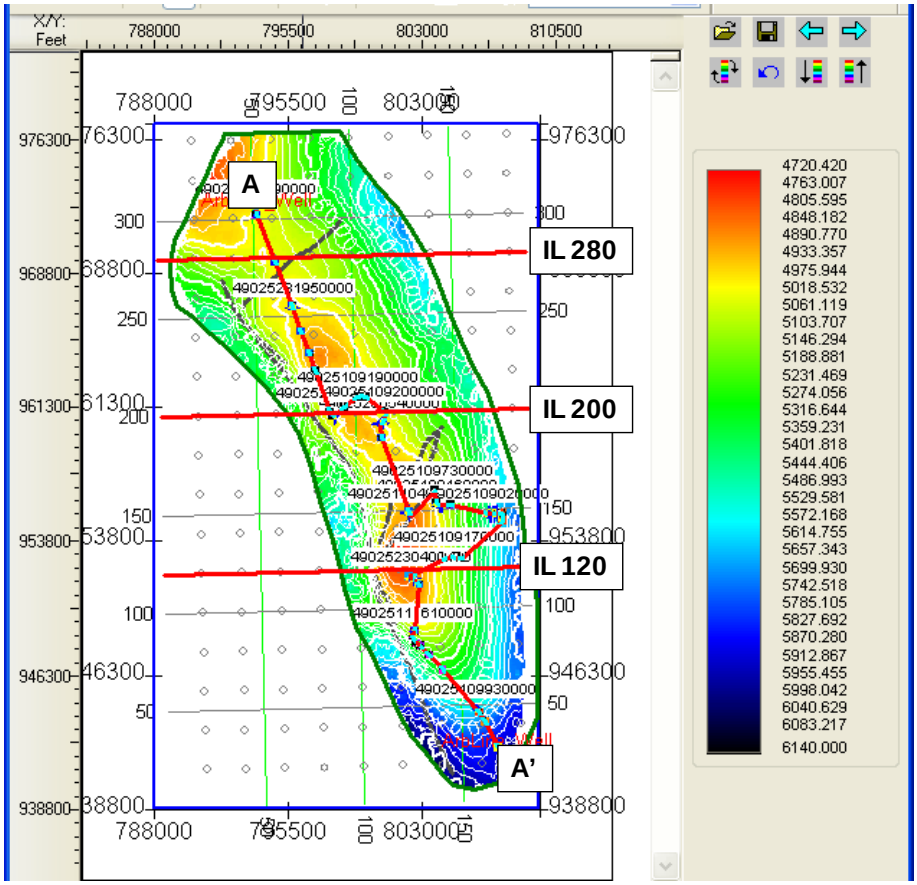

Figure 9: Base map for study area showing the 4 display lines used in this report (arbitrary line A-A', IL 120, IL 200 and IL 280).

The fracture pressure gradient consistently demonstrates that the predicted fracture gradient gently increase to approximately 20 ppg in the formation above the vicinity of the Crow Mountain formation at approximately 1 second two way time.

Figure 12 and Figure 13 (figures 5.3 and 5.4 of geopressure report) show the pore pressure gradient and fracture pressure gradient results for both cases for Inline 280. Figure 14 and Figure 15 (figures 5.5 and 5.6 of geopressure report) show the same displays for Inline 200. Figure 16 and Figure 17 (figures 5.7 and 5.8 of geopressure report) show the same displays for Inline 120. The maps for the "top velocity reversal" and "top second compaction" surfaces are also shown in Figure 18 and Figure 19 (figures 5.9 and 5.10 of geopressure report).

A prediction was extracted from the 3D volume at each calibration well location. These raw predictions are generated within GEOPRESS™ and are used to double-check the results. Figure 20 through Figure 33 (Original Internal Fusion report Figures 5.11 to 5.24 see Appendix B: Crow Mountain Geopressure Analysis) show the predictive results for the fourteen available wells in

the study area. The Top Reversal and Top Second Compaction surfaces are shown on each prediction panel as magenta and blue lines that cut across the figure. The small changes in pressure can be observed at each boundary.

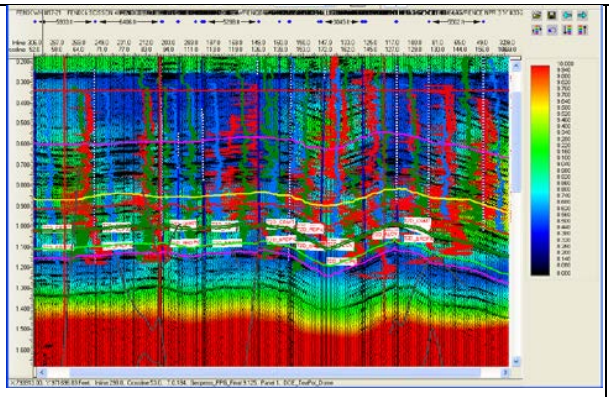

Figure 10:Pore pressure gradient section for arbitrary line A-A' showing the top of velocity reversal (magenta) and top of the deep compaction (yellow) horizons. Units are in PPG.

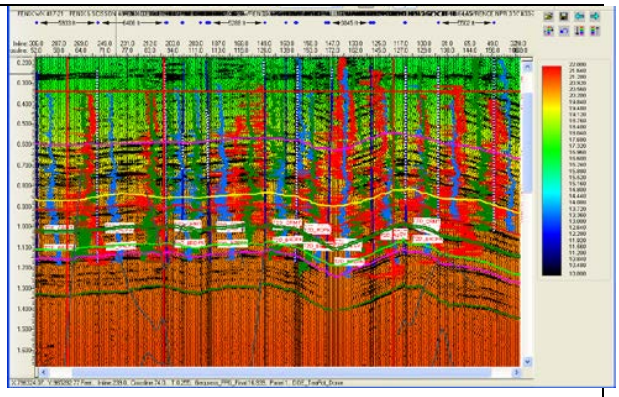

Figure 11:Fracture pressure gradient section for arbitrary line A-A' showing the top unloading (magenta) and top chemical compaction (yellow) horizons. Units are in PPG.

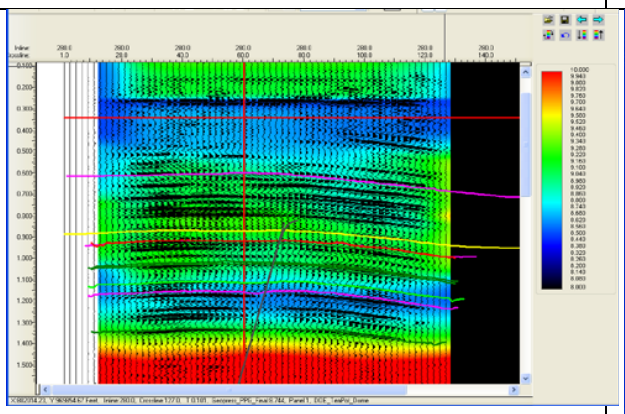

Figure 12: Pore pressure gradient section for inline 280 showing the top of velocity reveral (magenta) and top of the deep compaction (yellow) horizons. Units are in PPG.

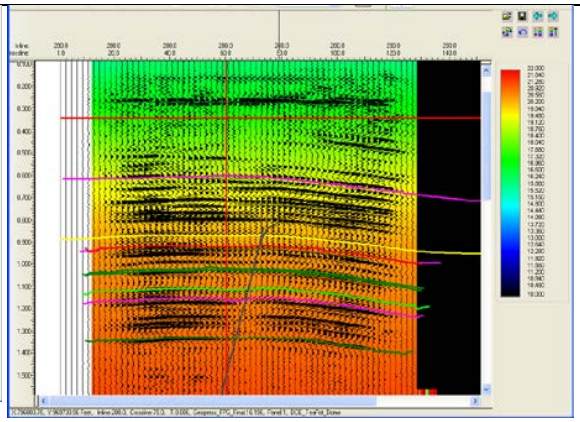

Figure 13: Fracture pressure gradient section for inline 280 showing the top of velocity reversal (magenta) and top of the deep compaction (yellow) horizons. Units are in PPG.

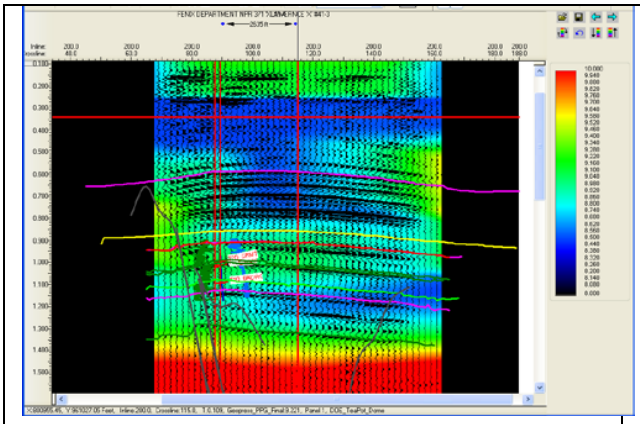

Figure 14: Pore pressure gradient section for Inline 200 showing the top of velocity reversal (magenta) and top of the deep compaction (yellow) horizons. Units are in PPG.

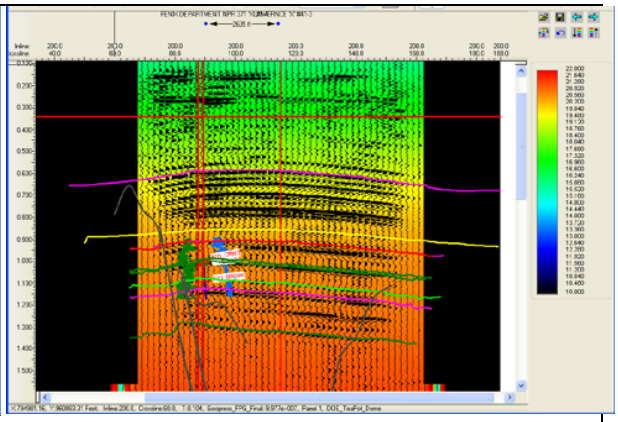

Figure 15: Fracture pressure gradient section for inline 200 showing the top of velocity reversal (magenta) and top of the deep compaction (yellow) horizons. Units are in PPG.

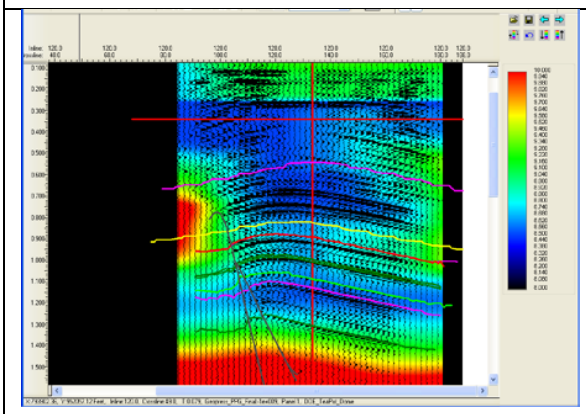

Figure 16: Pore pressure gradient section for Inline 120 showing the top of velocity reversal (magenta) and top of the deep compaction (yellow) horizons. Units are in PPG.

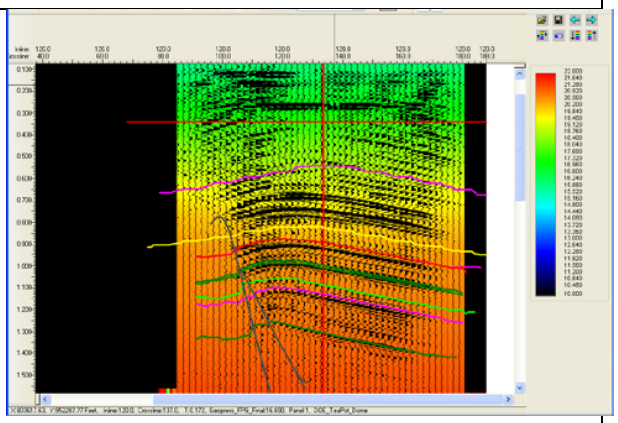

Figure 17: Fracture pressure gradient section for inline 120 showing the top of velocity reversal (magenta) and top of the deep compaction (yellow) horizons. Units are in PPG

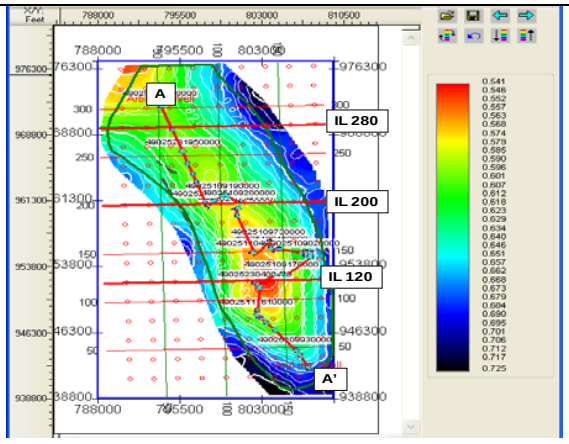

Figure 18: Map showing the top of the velocity reversal surface with 10 msec time contours.

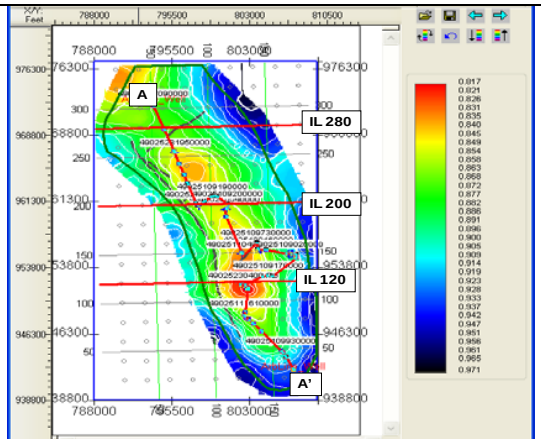

Figure 19: Map showing the top of the velocity reversal surface with 10 msec time contours

Pore pressure gradient (red), fracture pressure gradient (brown) and overburden gradient (orange) are labeled in the right panel.

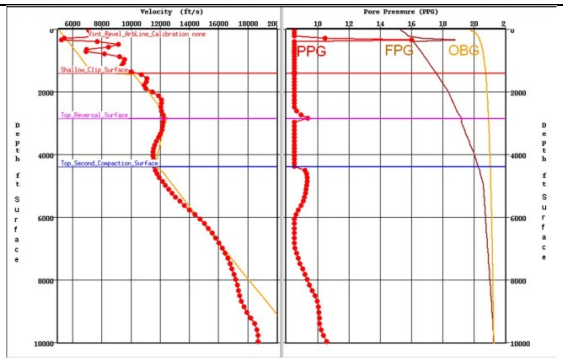

Figure 20: Prediction panel for the NPR 3LX #28-34 well.

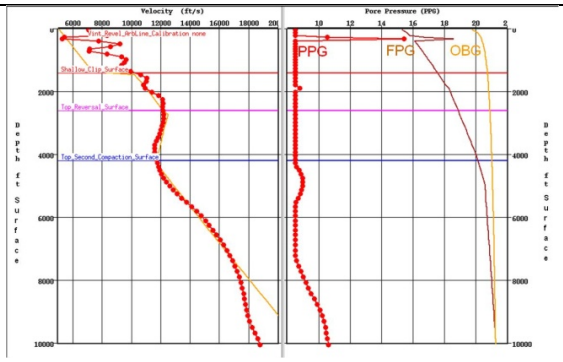

Figure 21: Prediction panel for the NPR3 X #67-1 well.

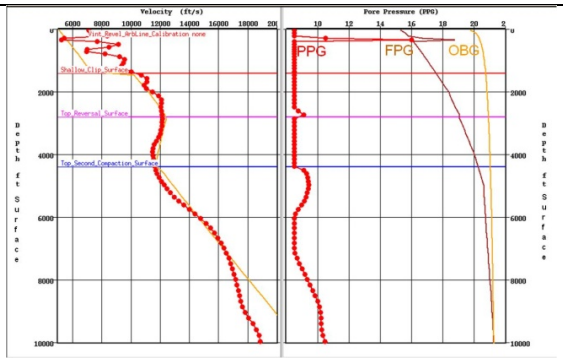

Figure 22: Prediction panel for the Dept #2-3 well.

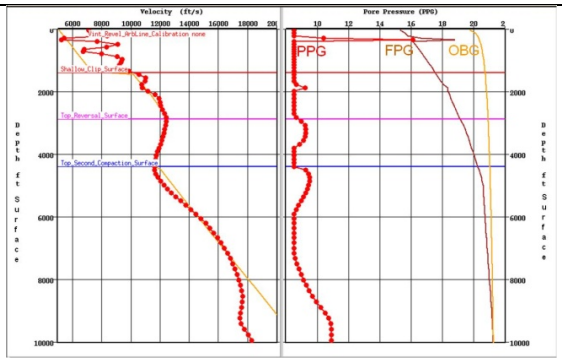

Figure 23: Prediction panel for the FNX X #48-28 well.

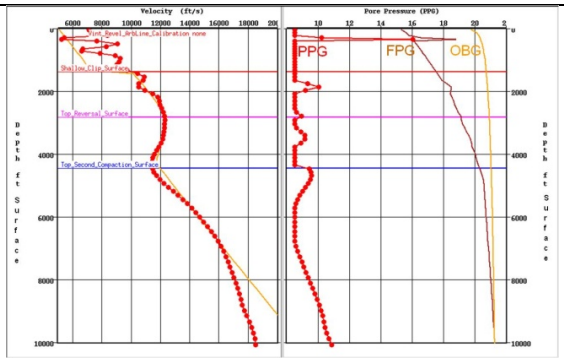

Figure 24: Prediction panel for the FNX WX #17-21 well.

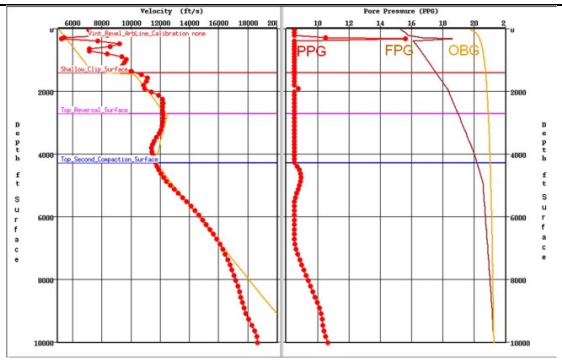

Figure 25: Prediction panel for the Law 62TPX #10-10 well.

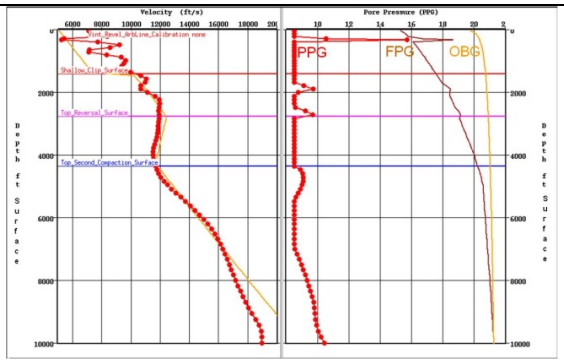

Figure 26: Prediction panel for the Law X #11-11 well.

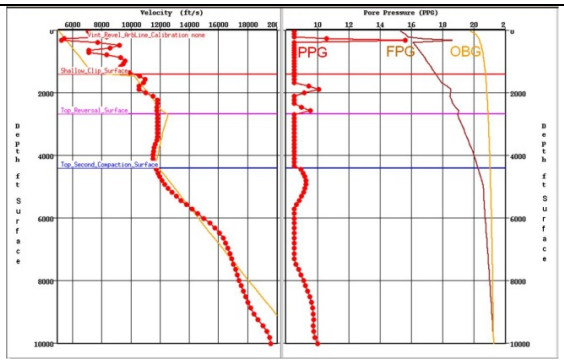

Figure 27: Prediction panel for the Law X #25-11 well.

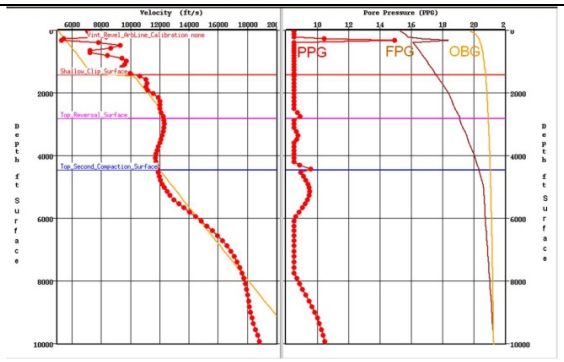

Figure 28: Prediction panel for the Law X #64-15 well.

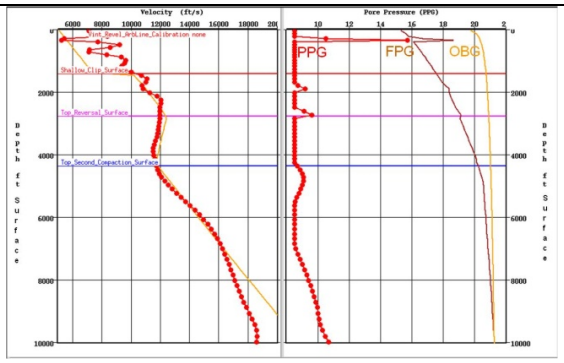

Figure 29: Prediction panel for the Law X #88-3 well.

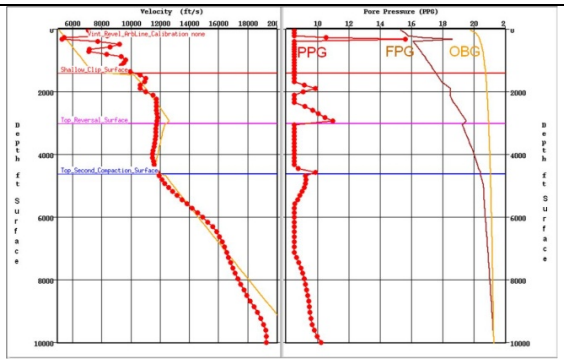

Figure 30: Prediction panel for the Law X #62-11 well.

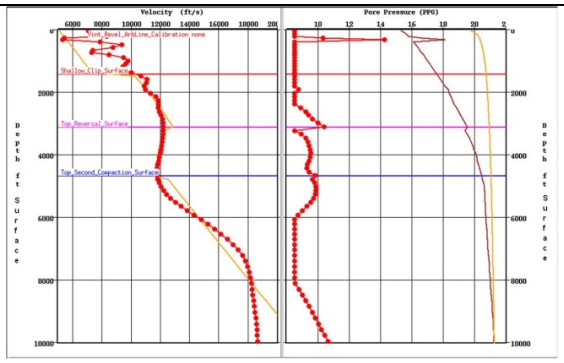

Figure 31: Prediction panel for the NPR3X #33-23 well.

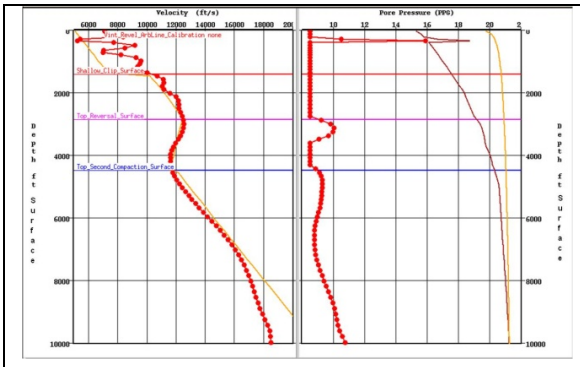

Figure 32: Prediction panel for the NPR #371X well.

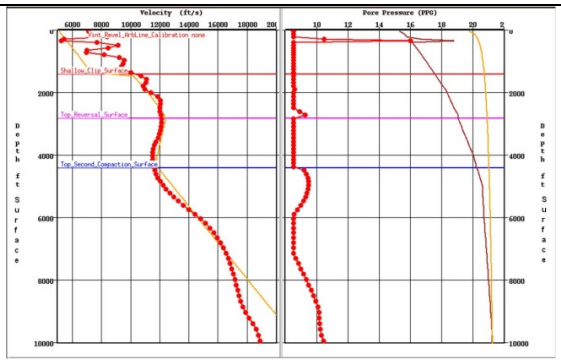

Figure 33: Prediction panel for the Law X #41-3 well.

4.1.4 Petrophysical, Log and Mineral Analysis

There is little petrophysical data available to establish good rock and fluid flow characteristics in the Crow Mountain and immediately neighboring rock. There is one known core taken over the Crow Mountain in well 34-CMX-10 (API number 490251092900) and one Drill Stem Test (DST) in that same well. The DST was not analyzed for any reservoir characteristics for this project.

A critical parameter used to determine reservoir rock and fluid low characteristics for engineering analysis (and simulation) is permeability. This is usually obtained by core analysis and then scaled appropriately to develop a porosity/permeability relationship to relate porosity and reservoir resistivity from well logs and estimate water saturations and permeability of the reservoir at the appropriate scale. The data from the one core in the Crow Mountain reservoir was used to make a cross plot of core permeability vs. core porosity. This cross plot data was compared with published correlations to estimate the permeability strictly from log data to determine that the Timur correlation fit the data fairly well. Based on the limited amount of information for analysis and comparison and because there is such sparse core data available, the use of a correlation to estimate the permeability based on porosity and irreducible water saturation is justified.

4.1.4.1 Well Log Analysis

The Timur Correlation[10,11] is given in equation 1.1 and is presented in modified form as equations 1.2 and 1.3, which are used to calculate permeability from ten logs penetrating the Crow Mountain based on effective porosity from the neutron density logs:

$$k = 0.136 \frac{\emptyset_{eff}^{4.4}}{S^2{}_{wirr}} \qquad (1.1)$$

$$k = \left(100 \frac{{\emptyset_{eff}}^{2.25}}{S_{wirr}}\right)^2 \quad (1.2)$$

Where irreducible water saturation was calculated using a simple approximation:

$$S_{wirr} = \frac{0.065}{\emptyset_{NDe}} \quad (1.3)$$

And the following definitions apply:

k	Permeability (md)
$\emptyset_{eff}$	Effective porosity
S_{wirr}	Irreducible water saturation
$\emptyset_{NDe}$	Effective Porosity determined from neutron density log cross plot with shale correction applied[1]

An empirical correlation to a measured core/permeability relationship was performed (Figure 34 through Figure 36) where core had been gathered from the upper 30 feet of the Crow Mountain formation on one well. Timur correlation approximated the permeability well enough for the purposes of this project in light of the scant data available. Time and project scope did not allow for separate zonal calibration of core-porosity and core-permeability relationships. None of the core measurements appeared to be conducted at reservoir pressures, so the core relationship if analyzed based on core data available in other zones could be misleading.

We note that the Timur Correlation was developed for clean sands, which should be valid for the relatively clean Crow Mountain sandstone. However, for this project scope we extended the use of the Timur equation without modification or justification to calculate permeability in shale areas and in limestone/dolomite formations. Normally the Timur correlation as well as other correlations to determine permeability is calibrated with more core, production data, and pressure transient data to ensure the values are representative of the permeability of the particular formation. At the time this report was written there is currently little known work developing correlations for shale permeability. Some R&D in shale gas mechanism is proceeding and some efforts to evaluate the conductivity of shale have been accomplished and

[1] In this case $\emptyset_{NDe}$ is the shale corrected porosity calculated from the total porosity from a typical neutron density cross-plot. The shale volume used to adjust the total porosity is equal to the bentonite volume plus the shale volume ($Neutron_{Shale}$ = 12-14% $Density_{Shale}$ = 2.44 to 2.46 g/cc and S_{wirr} is the water saturation irreducible estimate.

published recently. The magnitude of the shale permeability calculated using the Timur Correlation seems to be consistent with published laboratory conductivity and permeability of shale.

Seal permeabilities can range over many orders of magnitude. Shale permeabilities have been reported to range from 0.1 to 10^{-8} md.[12] Hart et al. [13] recently measured the permeability of shale aquitards of the Maquoketa Formation in Wisconsin, and found the permeability to range from 1.8×10^{-6} to 4.1×10^{-4} md while other researchers [14] have measured a wider range, between 0.01 to 10^{-8} md. Blasingame [15] documents the progression of technology for the evaluation and characterization of low permeability reservoir systems and remarks that the estimation of shale permeability remains difficult and that Neuzil's[14] work focuses less on specific values of shale permeability and more on the "regions" shown on a plot of porosity versus logarithm of permeability. Blasingame suggests that this perspective is useful in understanding that shales/clays have high porosity and low permeability, and some predictability in terms of trends.

The use of a power-law model for estimating permeability in shaley-sands using porosity and shale volume has been suggested. This exercise is somewhat similar to that of Timur, in that ultimately a power law (or in some cases, a modified power law) relation is obtained. We used this technique to estimate the effective porosity by reducing the total porosity based on the shale volume and used the effective porosity to calculate the permeability for modeling the Crow Mountain aquifer in this project.

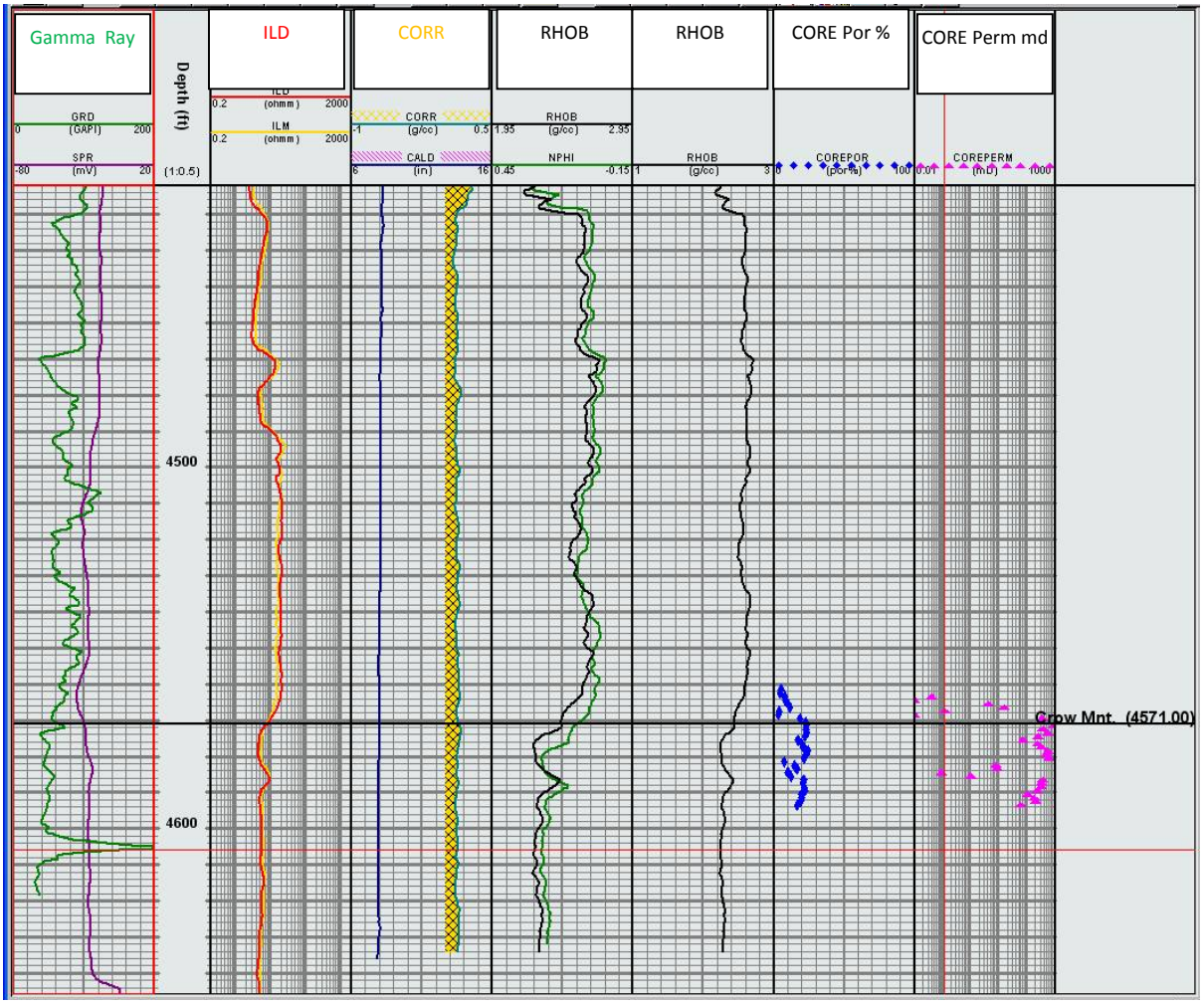

Figure 34. The 34-CMX-10 (API number 490251092900) well has core data in the upper 30 feet of the Crow Mountain formation. The core porosity (blue points) & core permeability (pink points) are illustrated in the last two tracks.

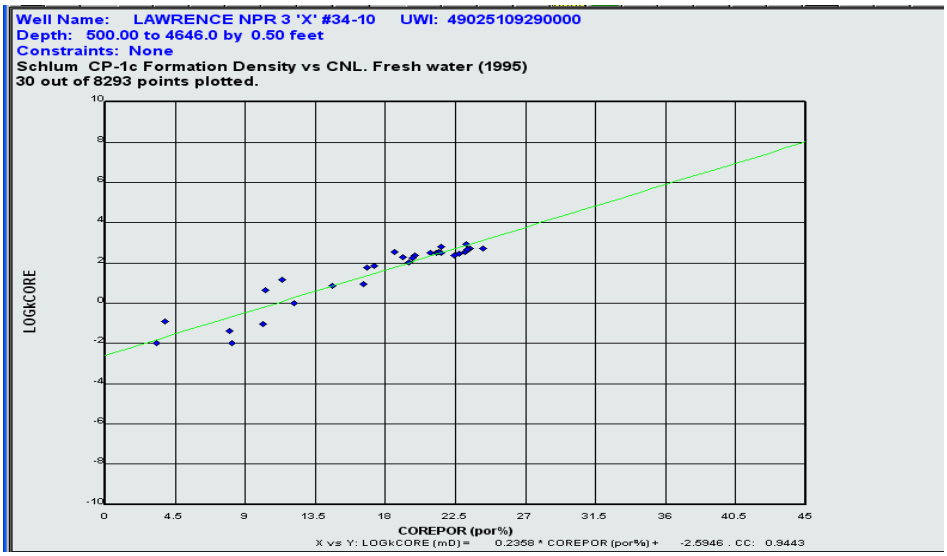

Figure 35. Core Relationship for Crow Mountain: $k = 10^{(0.23568\emptyset_{core} - 2.5946)}$

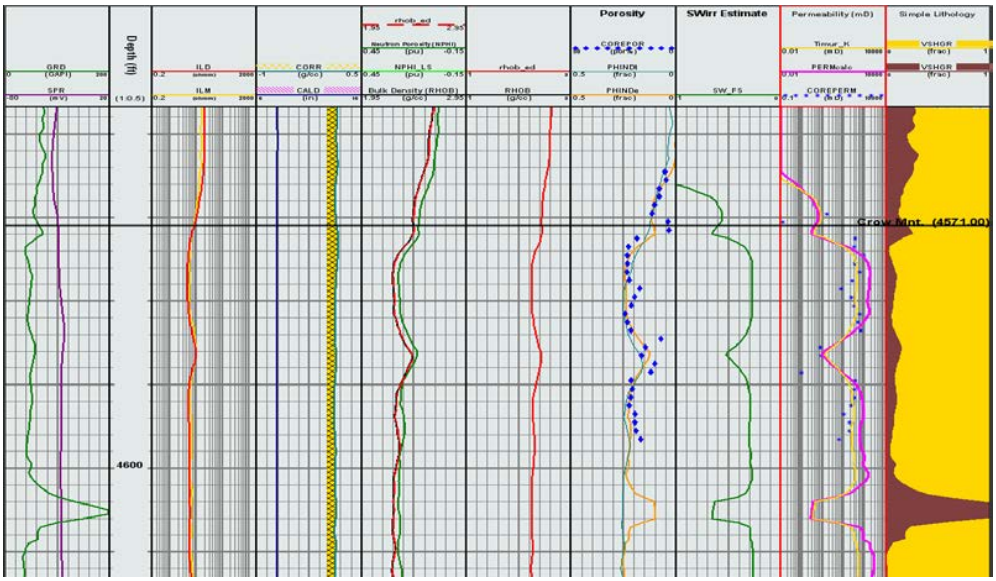

Figure 36. Timur curve (yellow) in last track appears to be good if not better fit than the pink statistical fit to measured porosity/permeability core data (blue points).

4.1.4.2 Mineralogy Estimates

Working with a small ten (10) well log subset a limited mineralogy study was performed. The purpose was to determine if the general lithology encountered in the Teapot Dome area could be modeled with the available data. Based on mud log cutting descriptions we were able to establish a model that does a good job of representing the major lithology types. Because log

quality was generally good this model demonstrated robustness in that we were able to accomplish the lithology representation with minimal iterations and significantly less time than typical multi-mineral analysis. This multi-mineral representation of the rocks from well logs helps to develop a facies distribution model for effect on flow and geochemical reactions during the injection and storage of CO_2. Figure 37 illustrates an example of the mineralogy form one of the wells.

Eight (8) of the ten wells used for the mineralogy study show the lithology of the Chugwater in Figure 38. The arrangement of the wells shown in Figure 38 is not in any particular pattern or order (e.g. no specific cross-section is depicted) the wells were hung on the top of crow mountain drillers depth. The purpose of this illustration is to show the Crow Mountain lithology and surrounding formations. The Crow Mountain is fairly clean sandstone but has stringers of calcium carbonate with bentonite clays present. The Sundance formation above the Crow Mountain shows considerable "liminess" with some areas having sandy permeable stringers.

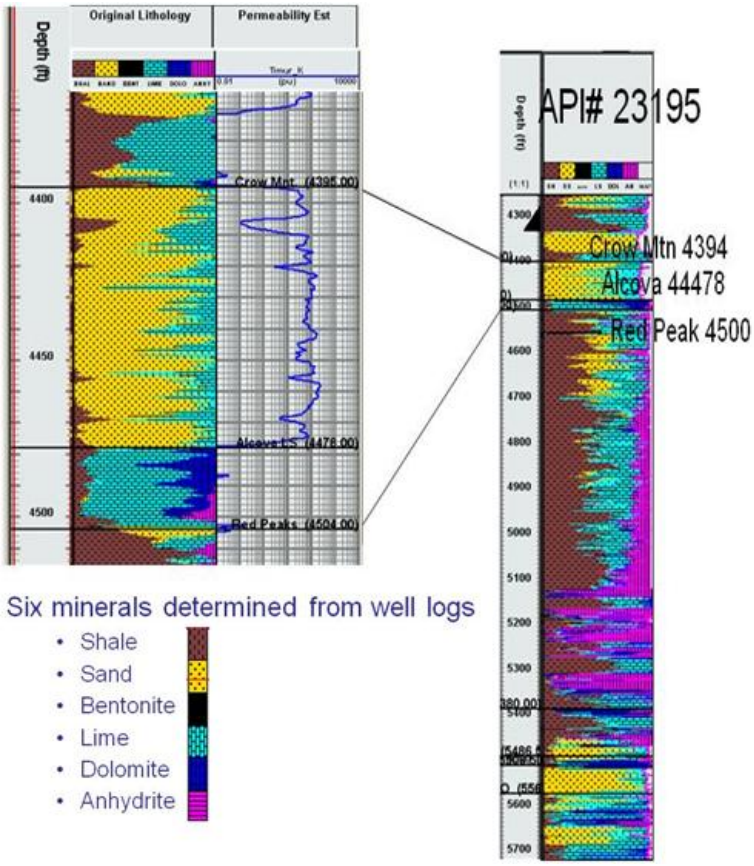

Figure 37: Limited mineralogy study example from well logs

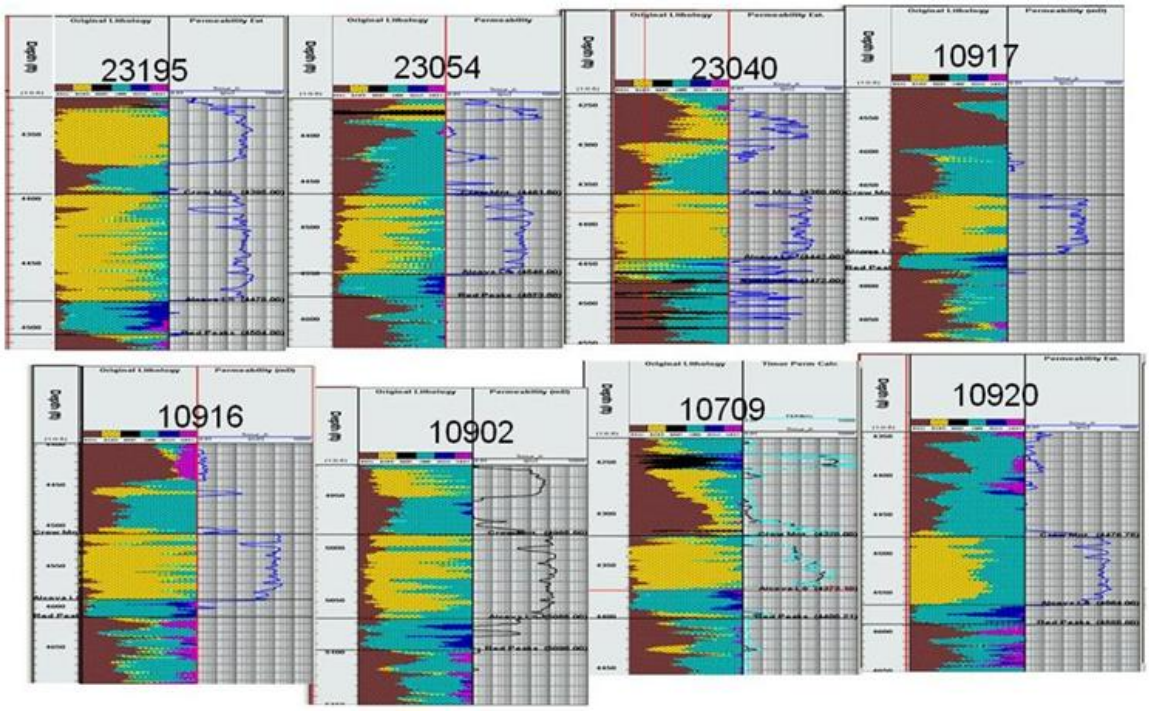

Figure 38: Eight of the ten wells used for the mineralogy study show the lithology of the Chugwater across the RMOTC lease Note the order of these wells do not depict any particular or specifi cross-section in the reservoir.

4.2 Reservoir Modeling

4.2.1 Creation of the Reservoir Static model

The Teapot Dome geological structure (horizons and faults) was defined based on the interpretation of 3D seismic time data converted to depth using Fusion's in house time-to-depth conversion process and well ties. The depth seismic cube, well tops, faults and horizons were then imported to the JewelSuite™ (JS) geocellular reservoir modeling software.

Fourteen faults and four horizon surfaces (Crow Mountain, Alcova, Dakota and Tensleep) were interpreted from seismic data and correlated to top depth using ten wells that penetrated the Crow Mountain see Figure 39 and Figure 40. Six of the interpreted faults extended above and below the Crow Mountain formation. The Dakota formation is about 650 feet above the Crow Mountain and the Tensleep is 840 feet below the Crow Mountain. The Sundance forms a Caprock of about 245 feet of silty and Limestone/Dolomite claystone and the Red Peak forms the lower seal of about 520 feet of claystone. In the NPR-3 the Dakota and Tensleep both produce hydrocarbons while the Crow Mountain is an aquifer currently used as a brine disposal formation.

4.2.1.1 Geocellular Reservoir Model

After faults and surface are imported into JewelSuite™ either in polyline (faultline) format or as 2D surfaces, they are triangulated, smoothed, and wellmatched to log tops from the log analysis. These trimesh surfaces are then evaluated and the structure building process workflow used to build a properly connected structural geological network. This part of the reservoir model building can take considerable time and can be tedious. The reservoir model definition is based on the imported surfaces or other workflow process (well tops or well correlations) to generate the network as discussed in previous sections. The layering in the model was chosen to be proportional to the top and base of the surface defining the horizon.

Two horizons and six faults from the fourteen interpreted faults and four horizons from seismic data and validated by log analysis for the area of interest (Crow Mountain and Alcova) are used in the model. Parallel copies of the Alcova surface were made in JewelSuite™ and matched to well tops of the Red Peak and base of the Red Peak to form the surfaces at the bottom of the Alcova (Top of the Red Peak) and the Red Peak Base. This procedure works well to formulate boundaries where surfaces were not interpreted or could not be interpreted and when the surfaces consistently parallel each other, as they seem to in the Teapot Dome. The Top of the Red peak is a fairly consistent twenty feet below the Alcova and could not be mapped with seismic. The Top of the Alcova and Top of the Red Peak fell in the approximate same peak/trough on the seismic cube since the seismic has a minimum resolution of approximately 30 feet.

One of the most critical tasks in building a reservoir model for use in reservoir simulation is to ensure that any surface to surface intersections and gaps are eliminated and a smooth fit between all structural surfaces is achieved. Seismic interpretation data is often imprecise and faults that should truncate against one another may either overlap or not even touch each other. There may be large gaps between horizons and faults, and horizon data might be on the wrong side of a fault, resulting in incorrect fault throws. The structural framework modeling task addresses these issues and was completed in the JS geocellular modeling software.

Figure 41 and Figure 42 display the horizons and faults after the structure building process. Figure 43 displays the actual surfaces used in the model. Once surfaces are interpreted and matched to the tops of the well logs, a grid can be generated and that grid can then be used to generate other surfaces to aid in defining a reservoir model emphasizing the proposed modeling and simulation effort. In this case the surfaces defined sufficient seal characteristics on either side of the targeted reservoir to evaluate the geochemistry and geotechnical effects of injecting CO_2 in the Crow Mountain on the claystones and the mineralogy associated with the claystones and aquifer rock.

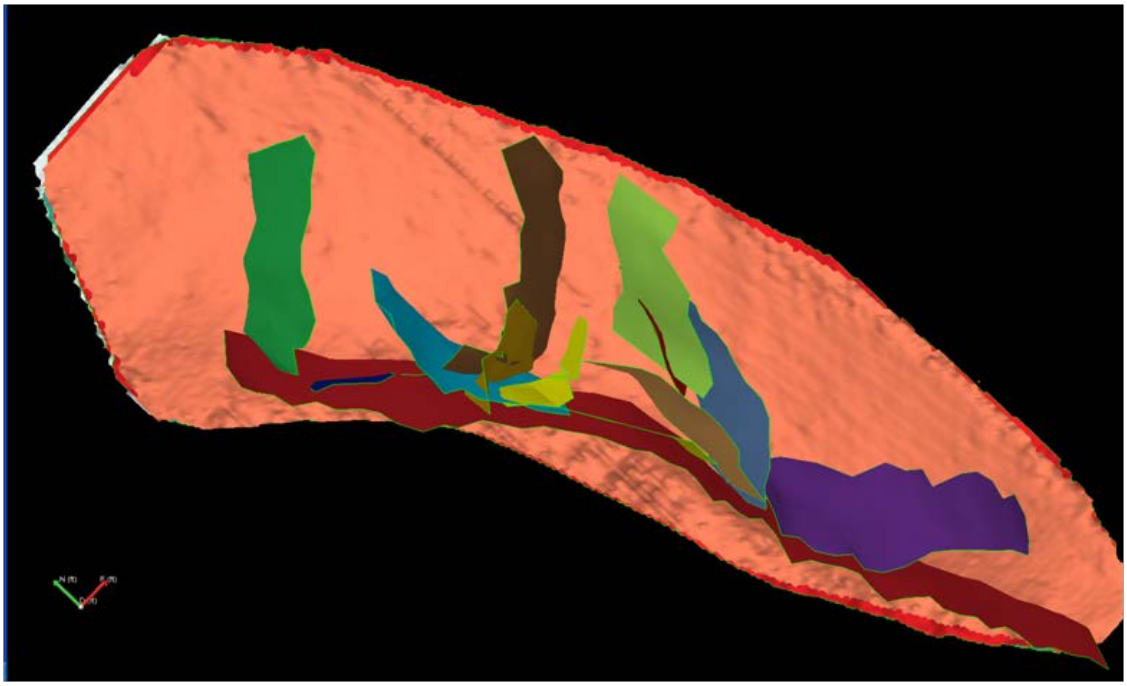

Figure 39. 14 faults and four horizons are imported into Jewel Suite. The top of the Dakota is interpreted from seismic

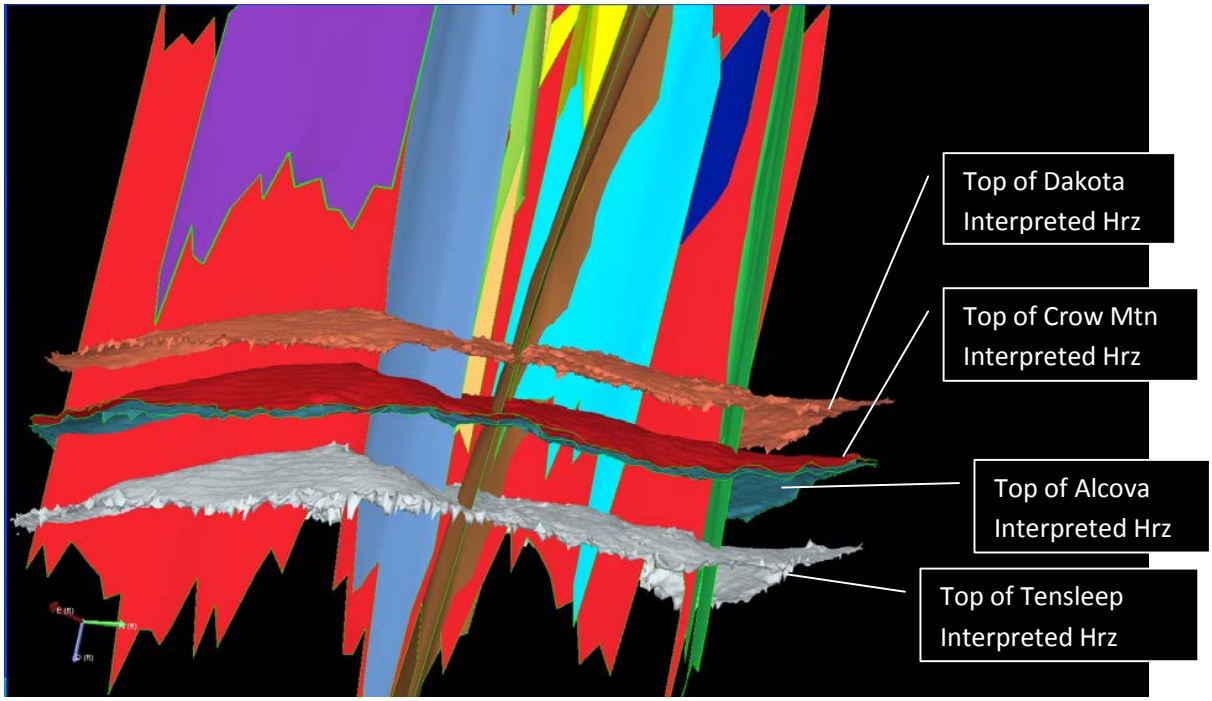

Figure 40. Close-up of the 14 faults and four horizons with horizons labeled. Though not real clear in this picture there are only 6 interpreted faults that penetrate the Crow Mountain

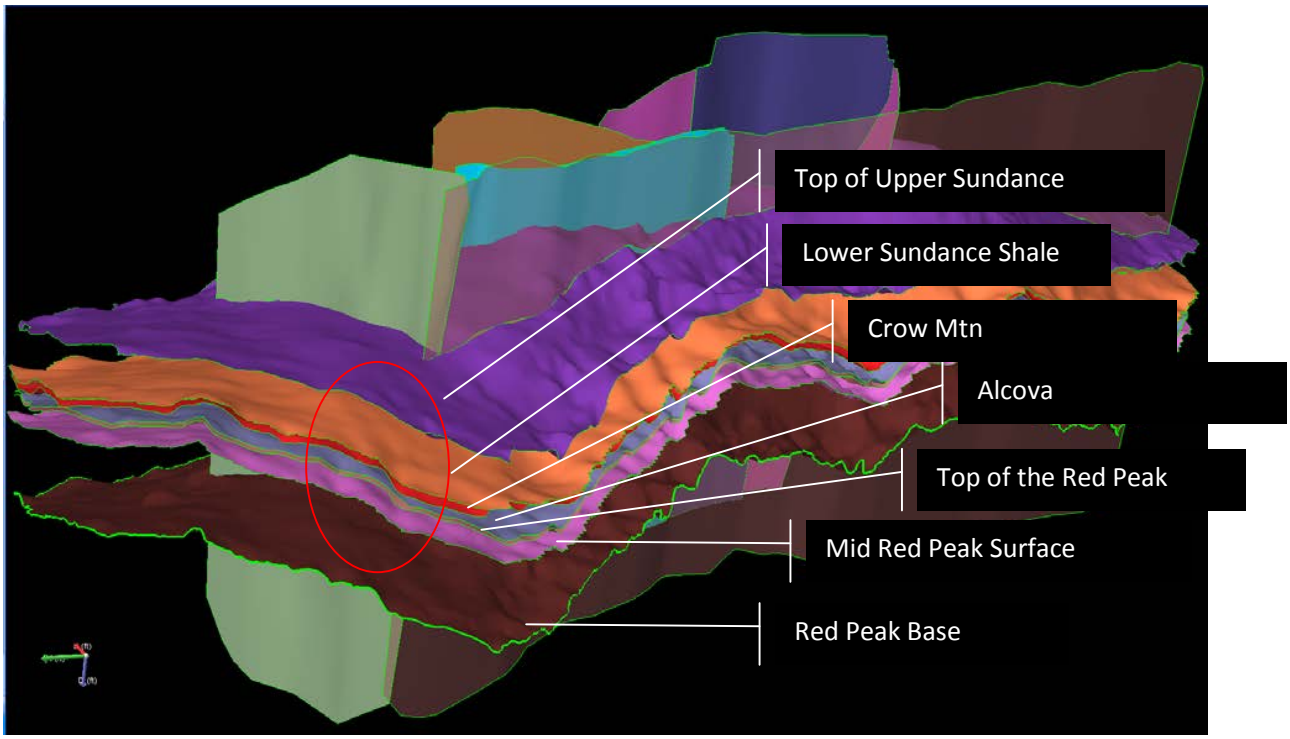

Figure 41. Model with representative surfaces and faults after structure building process.

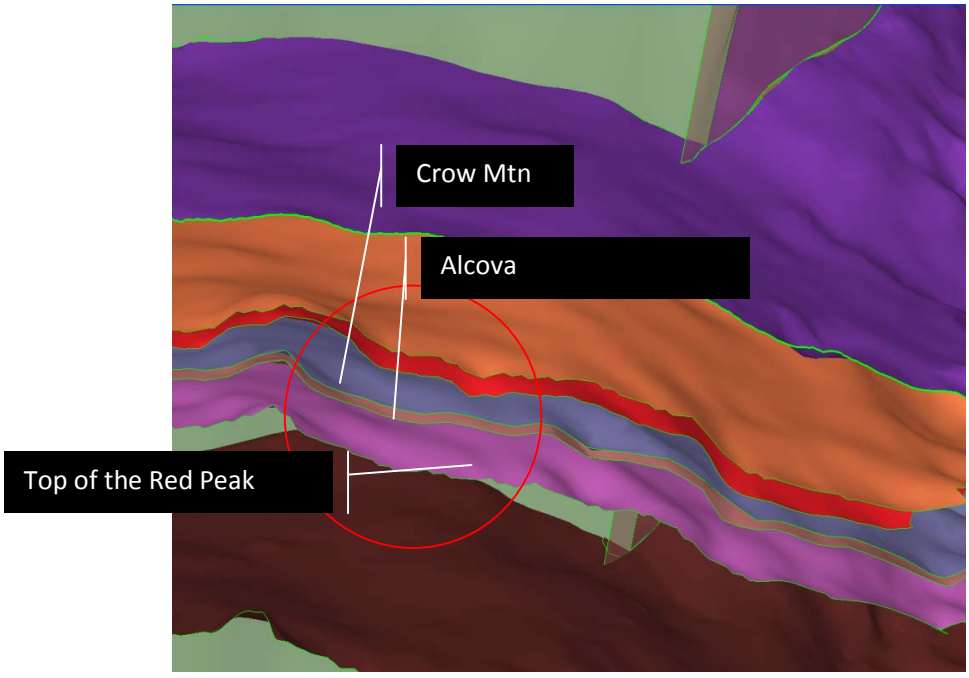

Figure 42. Close-up of horizons to delineate top of Alcova and top of Red Peak.

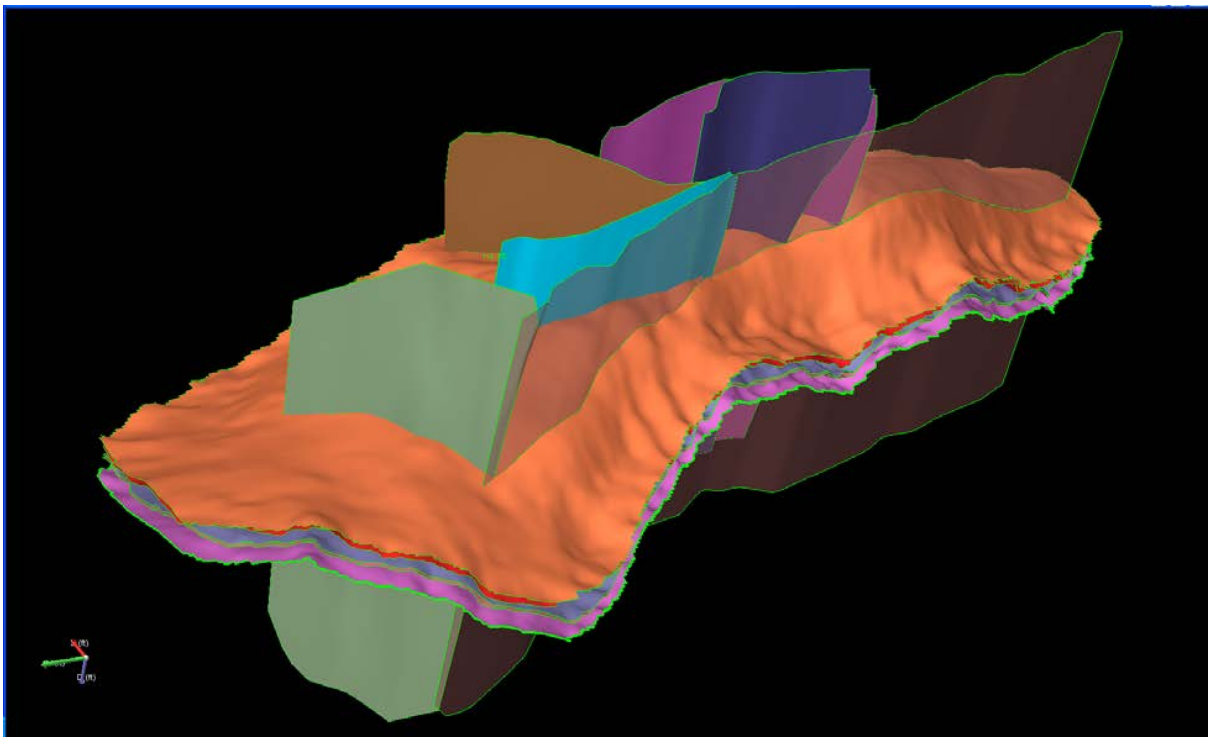

Figure 43. Surfaces used in the model definition: Top surface is the lower Sundance shale (approximately 50 foot of shale caprock above the Crow Mountain). Note the thickness is not the same between the top of the Lower Sundance and the top of the Crow Mountain. Top of the Crow Mountain (red), Alcova gray/blue, Top of the Red Peak brown sliver under Alcova. Magenta is Mid Red Peak shale approximately 50 ft of Red Peak shale however this is based on grid layer of previous gridding.

4.2.1.2 Reservoir Model definition

The reservoir model was originally planned to include the Top of the Sundance to the base of the Red Peak. This would model approximately 150 foot of the limey dolomitic claystone caprock in the Sundance formation, 80 foot of sandstone aquifer in the Crow Mountain (target for CO_2 sequestration), 20 feet in the Limestone aquitard in the Alcova directly below the Crow Mountain aquifer and another 520 feet of Red Peak Shale (see Figure 44). Initially two foot internal layers over the entire sections were evaluated but the number of cells would be over $24x10^6$; which, even for fine grid static models can start to encumber the computer and time resources allocated to the project. The model in Figure 44 shows 2 foot internal layers for Crow Mountain and Alcova and 10 foot internal layering for the shale capstones. Though this could be modeled, the volume of "shale" were felt to under emphasize the projects main goal of evaluating sparse reflective seismic of a CO_2 plume for MVA in the Crow Mountain Aquifer.

A more manageable reservoir model definition is defined as shown in Figure 45. In this model two additional surfaces were developed based on the gridding of previous model definitions (see gridding section) -- the lower Sundance and the mid-red Peak. Upper and lower model boundaries were defined at 50 ft above the Crow Mountain and 50 feet below the Alcova

respectively. Vertical resolution was two feet (lateral resolution was the same as the other model) to evaluate CO_2 injection effects on water movement into the shale, and CO_2 plume movement with the synthetic seismic in later tasks (the key focus of this project). The Teapot Dome model is shown in 3-D is shown in Figure 46.

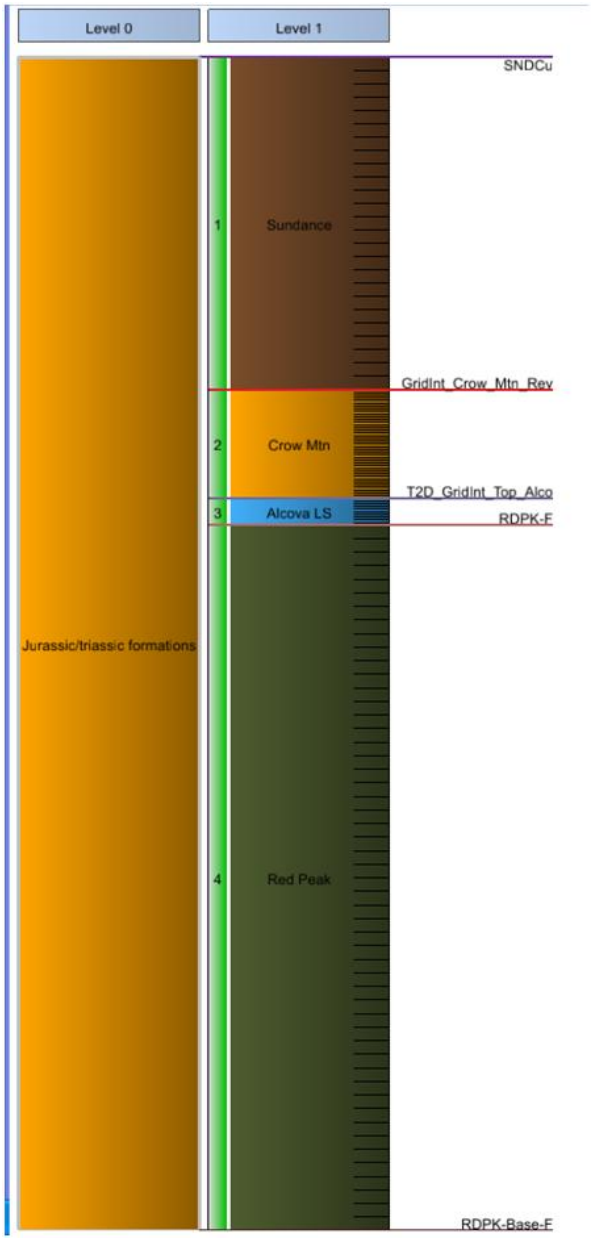

Figure 44. Initial Reservoir Model Definition.

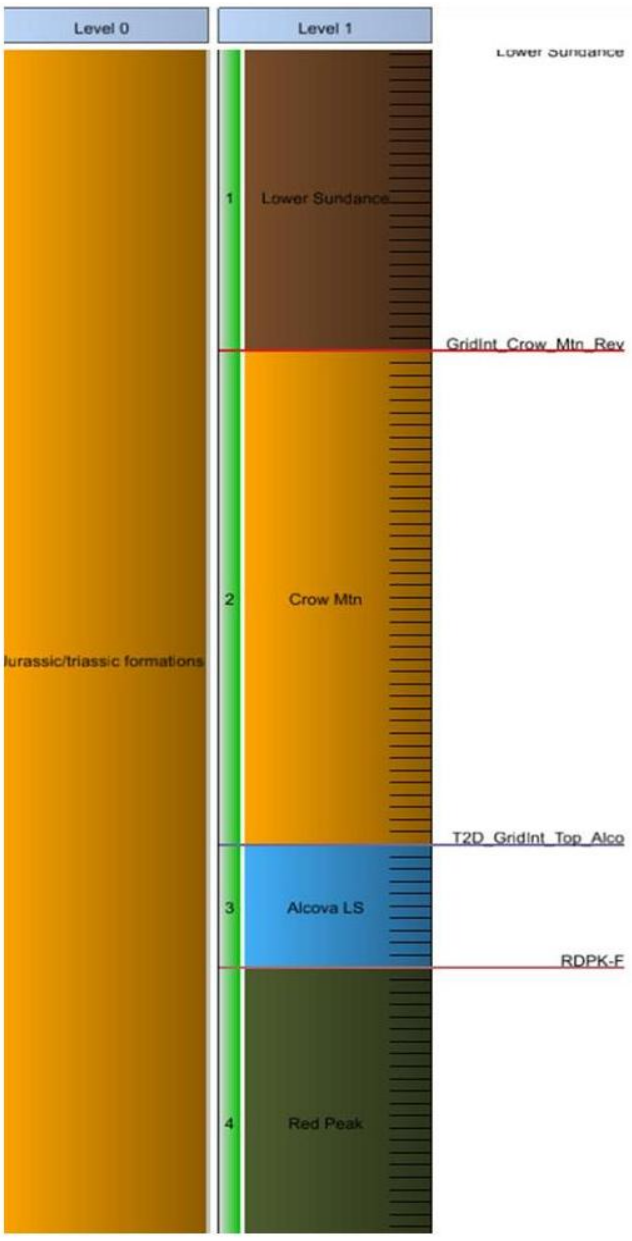

Figure 45. Current Reservoir Model Definition.

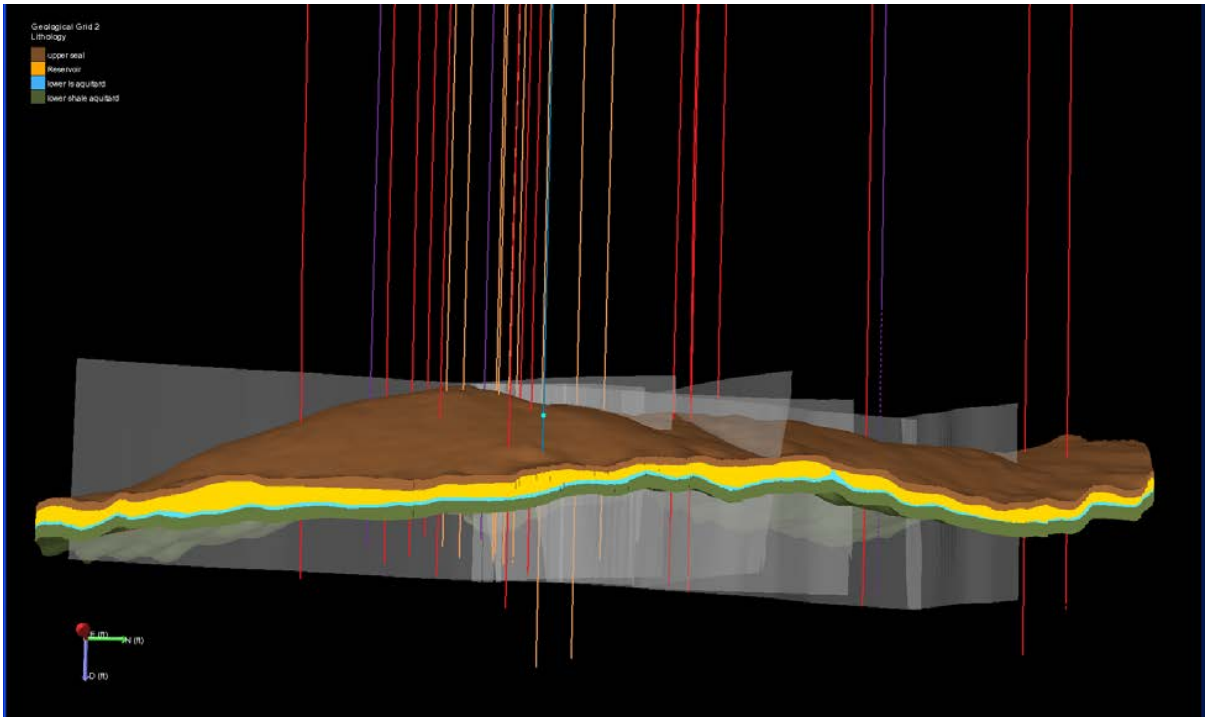

Figure 46: RMOTC Teapot Dome reservoir model Lower Sundance (brown), Crow Mtn (yellow), Alcova (blue), Red Peak (green) with wells penetrating below Crow Mountain.

4.2.2 Reservoir Grid Development

Geologic modeling is the process used to create grids used for property modeling, volumetric, upscaling, and reservoir simulation. Three grids were generated based on different reservoir definitions. The current geologic grid is approximately 3.5 million cells with lateral dimensions of 107 ft x 110 ft x 2 ft. Figure 47 shows the fine geocellular grid looking toward the southeast with the k_z (vertical permeability) parameter shown. Note the permeability parameter varies by orders of magnitude (e.g. 10^{-5}md in aquitard seals to over 500 md in the Crow Mountain clean sand). Figure 48 is an approximate same view of the upscaled grid prepared for input to simulator. The upscaled grid has 144,018 variable cells roughly 500 ft x500 ft x2 ft.

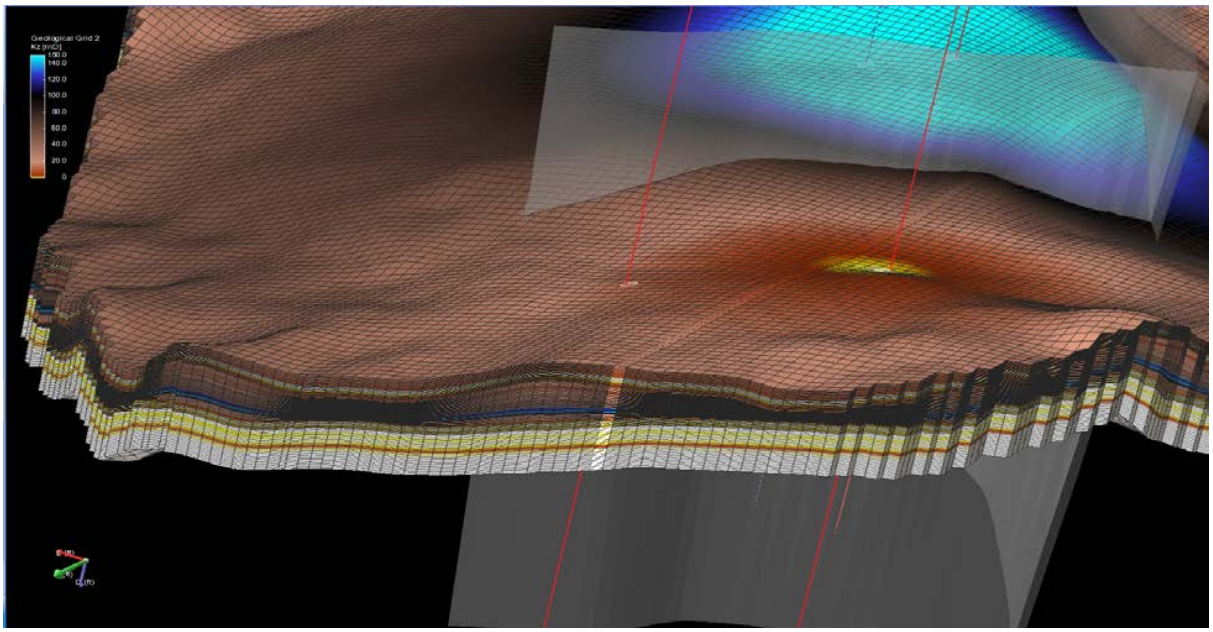

Figure 47: Fine Grid Geologic model Grid looking South Easterly k_z permeability parameter.

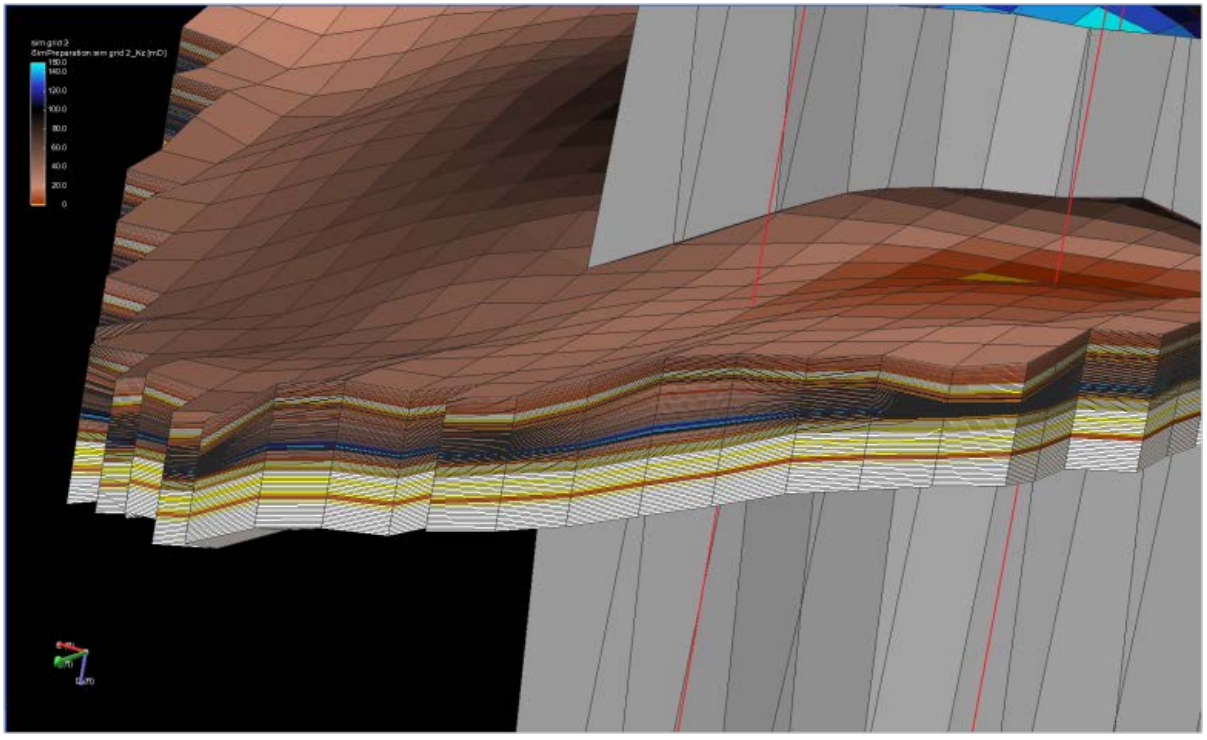

Figure 48:Upscale Grid prepared for simulation roughly 500ft x500ft x 2 ft. Cells are variable dimensions

4.2.2.1 Parameter Modeling

Interpolation of the parameters to populate the grids used inverse distance weighted average with a power of two. No attempt has been made to optimize the property modeling methods (using Kriging, Gaussian Sequential Simulation or facies property modeling, etc.) as there is little core information within the Crow Mountain and there is no core analysis of shales (claystones) in the RMOTC field and little production or injection data in the Crow Mountain to validate any efforts in this direction. Mineral analysis of the shales or reservoir seals would be important for CO_2 sequestration sites as this could define how open/closed the system is and impact the CO_2 capacity. If the RMOTC site is to be used as a CO_2 sequestration either in the Crow Mountain aquifer or as EOR/Sequestration in mature oil/gas formations, then the hydraulic conductivity (and permeability) of the shale would be of value to determine the closed or open nature of the storage site. An open site can store much more CO_2 than a closed site.

Based on the petrophysical analysis of ten well logs a rock mineralogy was developed (ratios of shale, bentonite, sand, limestone, dolomite, anhydrite volumes, effective and total porosity, S_{wirr}, and Timur permeability). The Timur permeability was used with the directional permeability set to be isotropic (e.g., $k_x=k_y=k_z$). During the parameter modeling, the permeability changes due to the location of the well with weighted difference changes away from each well. The scatter plots (not shown) do not indicate large variations of directional permeability in each individual cell but from cell to cell there could be significant differences. A lateral view of the permeability parameter model is shown in Figure 49 and shows some high permeability streaks in the Red Peak formation and also some tighter layers in the Crow Mountain. The model is one realization based on the data available and the assumptions considered.

4.3 Dynamic Reservoir Simulation

Most reservoir simulators are designed based on no flow boundary conditions that basically predefine a system to be closed. This works well for estimation of the oil and gas reserves and reservoir analysis especially where there is more than one immiscible phase. For CO_2 sequestration, however, orders of magnitude smaller permeability are required to create a seal and aquifers may not be considered a locally closed system.

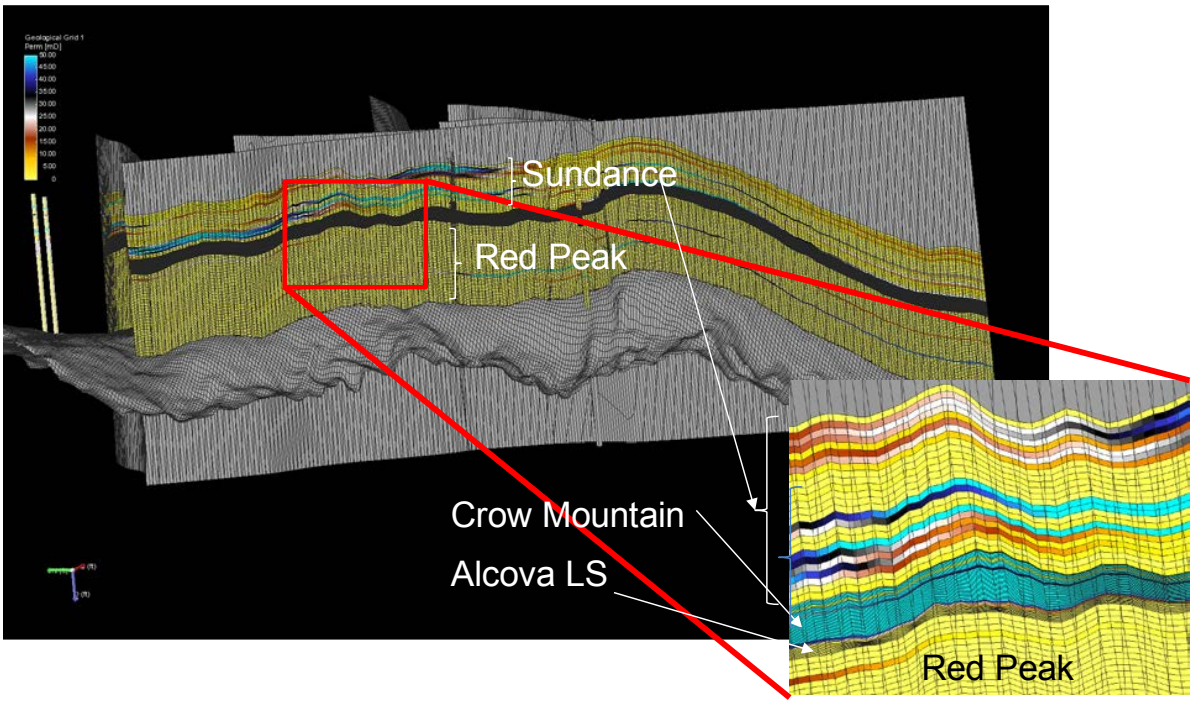

Figure 49: Permeability Property along the main fault. This figure shows all of the red peak structure. Note that there appears to be high permeability stringers in the upper and lower seal structures and low permeability stringers in the Upper Crow Mountain unit.

Closed systems may not offer sufficiently large capacity to sequester any reasonable amount of CO_2 and the aquifers are not closed systems. The ability for single phase system of water and gas to flow is not necessarily impeded at the definitions for uneconomic oil and gas development. Single phase fluids do not encounter significant restriction to movement in porous media until very low permeability or capillary restrictive conditions exist generally due to more than one immiscible phase present in the system. Water can hydraulically flow through very "tight" (micro and even nano darcy range) reservoir rocks albeit very slowly. Seal permeabilities above 10^{-18} m^2 (10^{-3} md) behave as open systems while systems below 10^{-19} m^2 (10^{-4} md) exhibit closed-system behavior[16]. Most aquifers would be too large aerially to be modeled as a closed system if the aquitards (seals) surrounding the aquifers are included in the modeling effort and the vast lateral extension of an aquifer is also included.

As an example the fresh water Ogallalla Aquifer covers 174,000 mi^2 in portions of eight states. Though this aquifer (being a fresh water aquifer) is not suggested as a target for CO_2 sequestration its expanse gives an indication of how large aquifers can be. Multiple phases in a reservoir rock retard the non-wetting phases from flowing as readily, but aquifer rock can be considered water wet and water can flow less impeded than other non-wetting phases e.g. defining CO_2 to be a non-wetting phase.

- Most reservoirs are initially bounded by competent cap rock that is sealing.
- There exists a pressure differential across the cap rock.
- During injection phase, when this pressure drop becomes sufficiently large, the seal provided by the cap rock may be breached, and flow across the breach/caprock may occur.

However, since the pressure drop across the cap rock may be driven higher by external influences (even though fluid can now move across it), further seal degeneration could occur, resulting in larger and larger outflow.

4.3.1 Reservoir Simulation Model

Based on the reservoir model as defined above a reservoir simulation model was populated with the porosity and permeability determined from the logs and the Timur correlation. The 3-D images (Figure 50 and Figure 51) show the heterogeneity and layering of different permeabilities and infer possible transmissivity variations and barriers to flow both horizontally and vertically.

Permeability

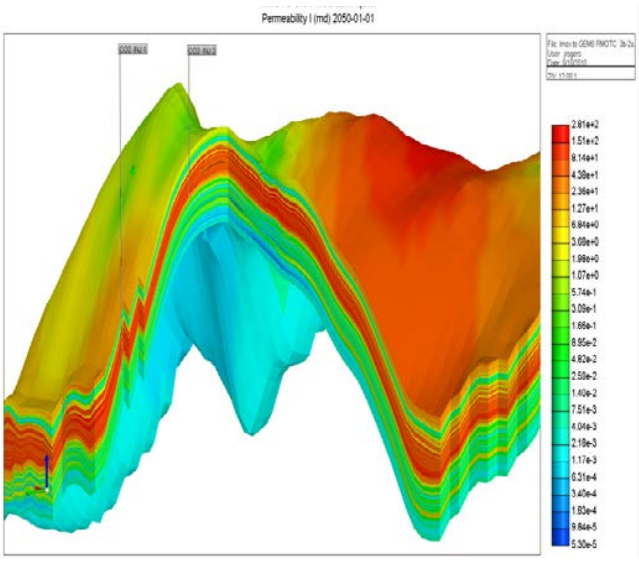

Figure 50: Cutaway view off permeability parameter model in the Teapot Dome by Timur correlation. The vertical scale is overemphasized.

Porosity

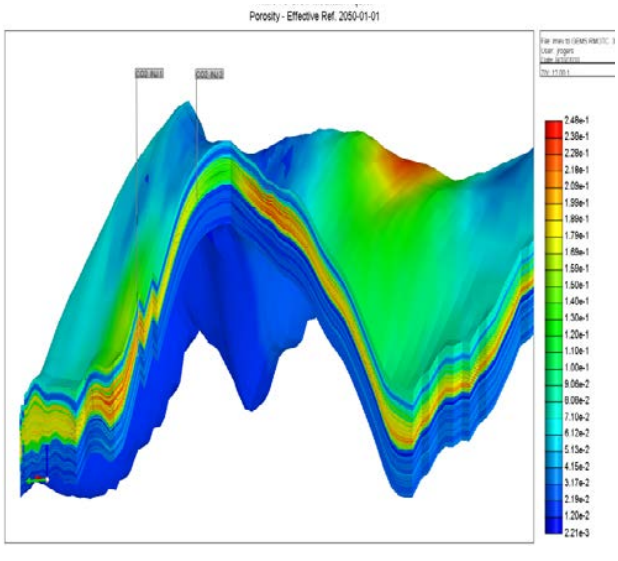

Figure 51: Cutaway of Teapot Dome showing prosity map of Crow Mountain and surrounding reservoir

4.3.2 Initialization of the Reservoir Model

4.3.2.1 Reservoir Temperature

The reservoir temperature in the Crow Mountain based on temperature gradient, varies from a minimum of 170°F to 194°F and average of 178°F. The gradient was determined from temperature recordings on logs in the Dakota (163°F at 3800 ft) and the Tensleep (190°F at 5500 ft). The gradient is calculated internally in the simulator and each cell temperature is populated according to its depth from the gradient.

4.3.2.2 Reservoir Pressure

The initial pressure for each block of the reservoir was developed using a specific gravity of sea water of 1.03 and an average surface elevation of 5218 feet above sea level and is a close approximation to the vertical equilibrium models assuming a water saturation of 100%.

4.3.2.3 Fluid and Rock Composition

The simulation model uses six reactions, three mineral components, and seven aqueous components H^+, Ca^{++}, Al^{+++}, $SiO_2(aq)$, HCO_3^-,CO_3^{--}, OH^-. The mineral components used are Anorthite ($CaAl_2Si_2O_8$) a calcium rich feldspar, Calcite or calcium carbonate ($CaCO_3$), and Kaolinite a common clay mineral ($Al_2Si_2O_5(OH)_4$) prevalent in sandstone rocks. The volume fraction of rock input into the model is Anorthite 0.0088, calcite 0.0088, and Kaolinite 0.0176 with the remainder considered or assumed to be inert. There are a number of other minerals that can be used from the commercial reactive transport reservoir simulator data base. We chose three of the most common and prevalent for initial runs for this project. The six equilibrium reactions are:

$CO_2\ (aq) + H_2O \rightleftharpoons (H^+) + (HCO_3^-)$

$(CO_3^{--}) + (H^+) \rightleftharpoons (HCO_3^-)$

$(OH^-) + (H^+) \rightleftharpoons H_2O$

$Anorthite + 8\ (H^+) \rightleftharpoons 4\ H_2O + (Ca^{++}) + 2\ (Al^{+++}) + 2\ SiO_2\ (aq)$

$Calcite + (H^+) \rightleftharpoons (Ca^{++}) + (HCO_3^-)$

$Kaolinite + 6\ (H^+) \rightleftharpoons 5\ H_2O + 2\ (Al^{+++}) + 2\ SiO_2\ (aq)$

The above equilibrium equations define the chemistry during the injection of the CO_2 and the subsequent dissolution/deposition during the shutin periods. However, since the primary purpose of this project was to inject CO_2 and determine the ability to monitor the plume using synthetic seismic additional chemistry was not advisable since the more complex the chemistry

the more computer resource time is needed. The parameters used for the aqueous phase chemical equilibrium reactions and the mineral dissolution and precipitation reactions are used to define the mineral reaction system and are determined from the commercial equation of state software. Mineralization of CO_2 is possible with providers of Ca^{++}, Mg^{++} and Fe^{++} however the actual physical process takes a long time. Henry's solubility model was used to calculate the solubility of CO_2 in water.

4.3.2.4 Rock Fluid Data Relative Permeability data

The relative permeability data was a published source provided by the vendor of the commercial reservoir software. The reader should note that though this relative permeability curve is not valid for all of the rocks within this study e.g. caprock above the Crow Mountain, the Alcova, and the seal below the Alcova, it provides a useable proxy for the lack of a core derived model for each different lithology. We recognize each facies have different fluid rock interactions especially in the tight shale (see for example discussions by Bennion and Bachu[17,18,19]) and Stanford Universities Relative Permeability Explorer website[20]. The current curves used in this study provided a tool to simulate the injection of the CO_2 and develop a reasonable plume in light of the fact no relative permeability or capillary data for the specific reservoir rocks of Chugwater Group and fluids (CO_2 and water) exist.

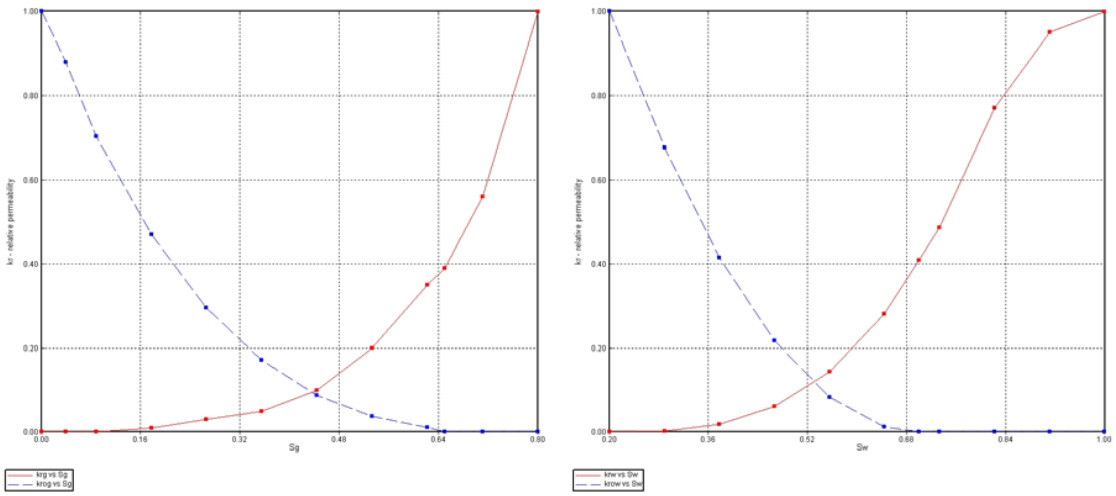

Figure 52: CO_2 water relative permeability curves used in the model

4.3.2.5 Simulation Grid

In order to emulate an open or infinite reservoir system the cells in the outer pillars of the grid system had a pore volume multiplier of 10^6 applied to each cell (see Figure 53). Applying this multiplier resulted in a large total pore volume of approximately 1.092 x10^{15} cubic feet. And, if we assume a 200 ft. height for the reservoir of interest (50 ft sandy/shale/siltstone above the

crow mountain, 80 ft. Crow Mountain aquifer, 20 ft. Alcova Limestone/dolomite, and 50 ft. of Shale/Claystone in the red peak) an area of 5.45 x 10^{12} sq. feet or approximately 195,400 sq. miles is calculated. For comparison the area of Wyoming is 97,814 sq. miles. The magnitude of this area may seem somewhat unrealistic as the Crow Mountain and its parent geologic member's outcrop in northwestern Wyoming and may in fact be substantially smaller if truly hydraulically bounded as some have suggested. The model, however, provides an axiom to define the Crow Mountain as an open system and as a proxy to mimic a fairly constant pressure realization for sequestering CO_2 in the Crow Mountain aquifer. The simulation grid consists of 256,632 blocks of which 124,331 are active and 132,301 blocks are blocks with pinchout characteristics e.g. pore volumes that are small enough that could cause high transmissibility with their neighboring cells and cause convergence problems or cells outside of the reservoir model.

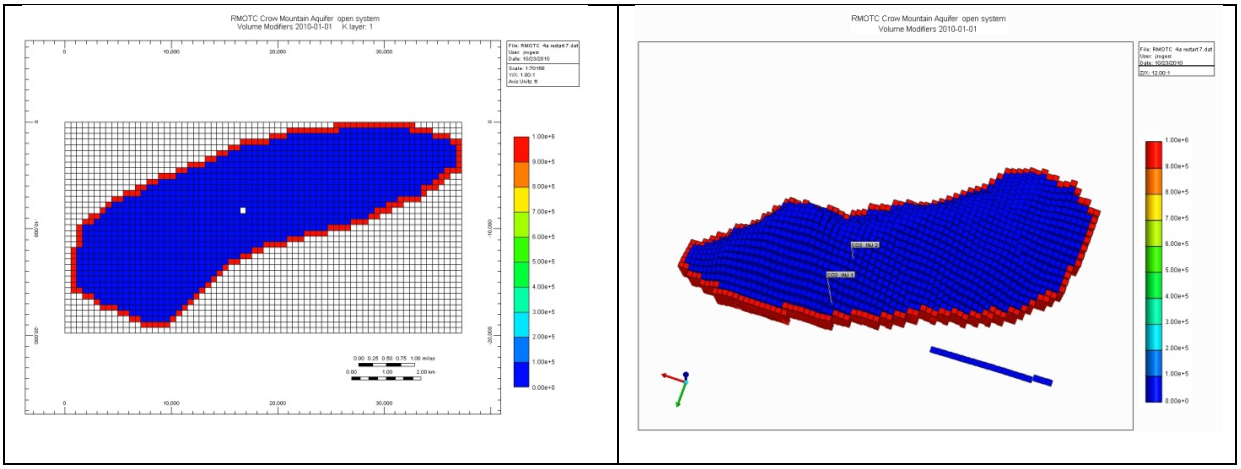

Figure 53: Left is a 2-D aerial view of the input grid. Right is a 3D view of the input grid. Note red cells indicate the cells that have large multipliers to emulate an open (infinite) reservoir.

4.3.3 Simulation of CO_2 Injection

Simulated supercritical CO_2 injection into the Crow Mountain was through two wells. Injection well one was placed close to the Teapot Dome boundaries on the south end of the east edge of the field away from the main fault line and at one of the lowest areas in the reservoir. Injection well 2 was placed up dip of Injection well 1 but not quite at the apex of the anticlines or higher structures prevalent in the Teapot Dome. Both wells had rates of 1MM cuft/day (total of 2 MM cuft/day for approximately 106 tons per day and a total of approximately 1.2 MM tons of CO_2). Both wells were completed in the bottom ten feet in layers 50-55. Each layer in the model is approximately two feet thick.

Preliminary simulation evaluations indicated gravity segregation seems to be a prevailing mechanism in CO_2 injection in the Crow Mountain due to the structural nature of the Teapot Dome formations. Figure 54 shows four snapshots of layer 22 (slightly above the top of the

Crow Mountain) at various times during the injection of carbon dioxide. Layer 22 shows the largest plume accumulation of CO_2 during the injection. The accumulation is under a layer of dolomitic claystones above the Crow Mountain aquifer. Figure 55 is a cross-section or cutaway view that shows the gravity segregation as the CO_2 accumulated at the higher portions apexes of the aquifer. The CO_2 does not diffuse laterally but appears to flow very rapidly vertically in the immediate injection blocks and then flows below the low permeability layers at the top of the Crow Mountain to the apex of the anticlines where the gas concentrates due to gravity. Though there is some lateral convective flow along the longitudinal axis during injection of the reservoir the primary flow is in the southwest as a result of gravity segregation and density differences of the dense supercritical CO_2 and the water. The dense gaseous phase flows along a less permeable layer but the CO_2 still appears to penetrate the upper "seal" as is illustrated in the "fence diagrams" of the different time realizations in Figure 56.

The simulation data was exported from the simulator and readied for the sparsity analysis task via GeoPRO™. Several time fluid saturation realizations (time "snapshots") were exported so a synthetic seismic image of the CO_2 plume for each "snapshot" could be visualized using SeisModelPRO™ in the seismic modeling effort of the project.

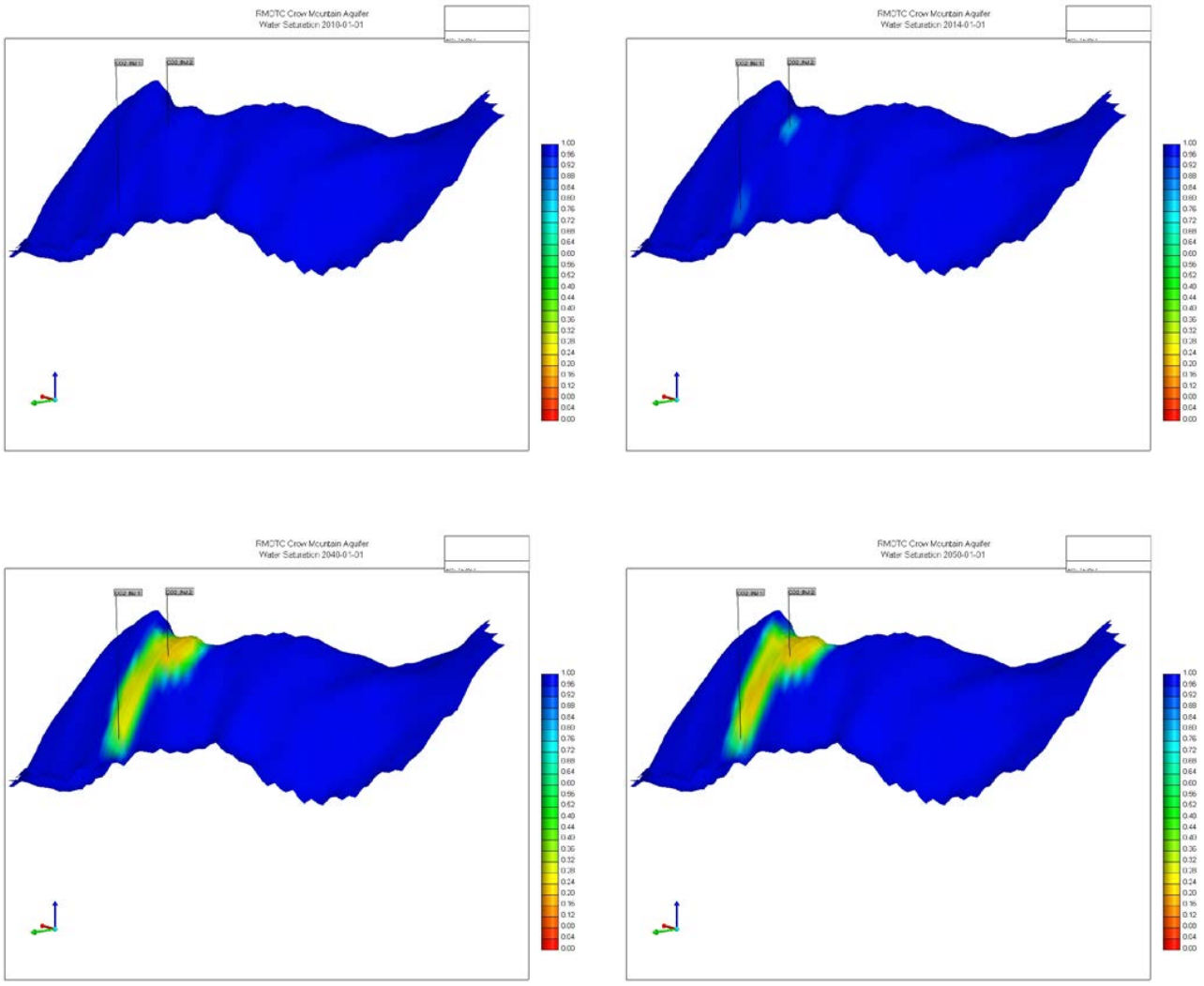

Figure 54: a) Start of Injection b) 4 years after injection c) at end of injection 2040 d) after 10 year soak. The images are of a layer approximately at the top of the Crow Mountain

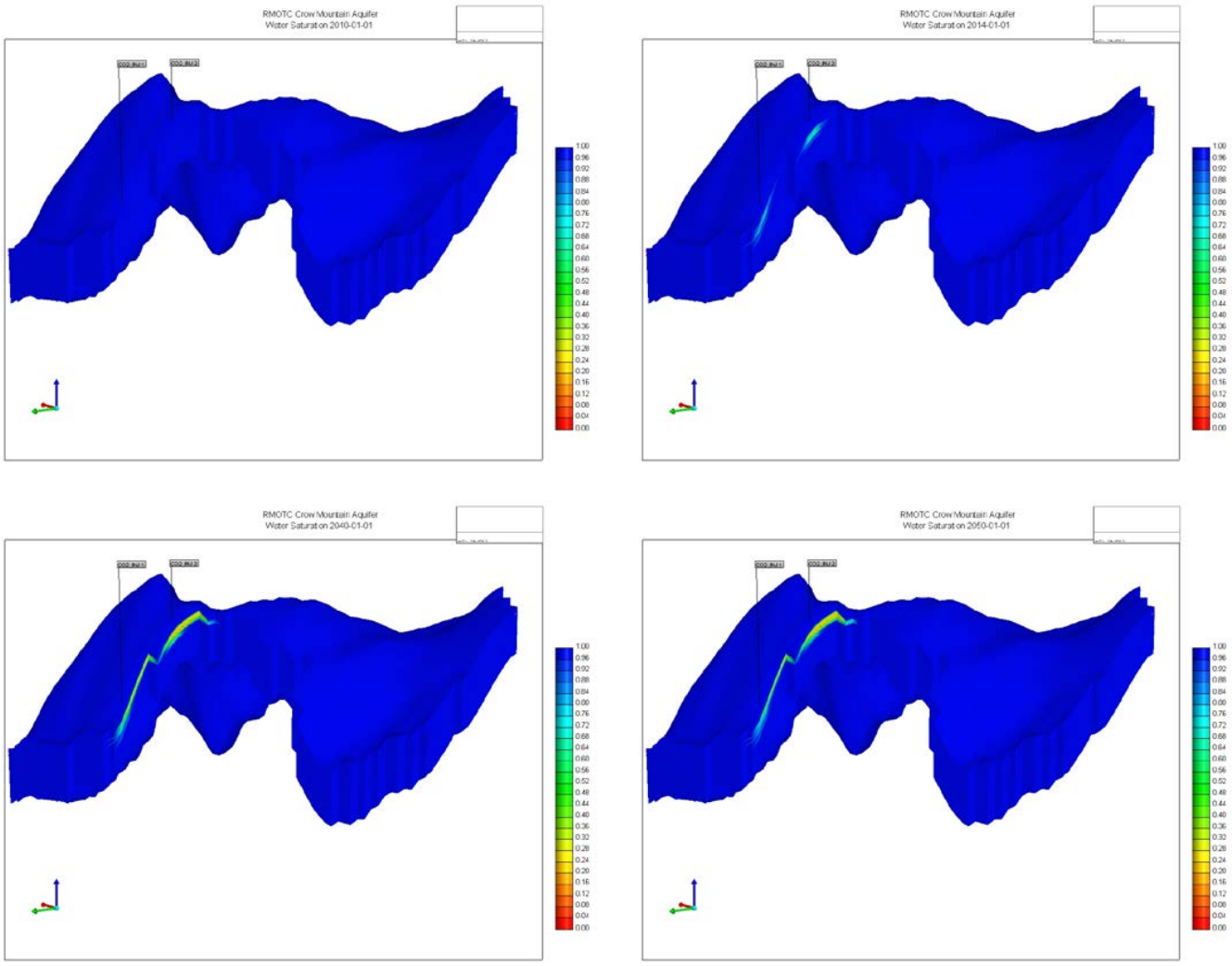

Figure 55: a) Start of Injection b) 4 years after injection c) at end of injection 2040 d) after 10 year soak and equilibration time.

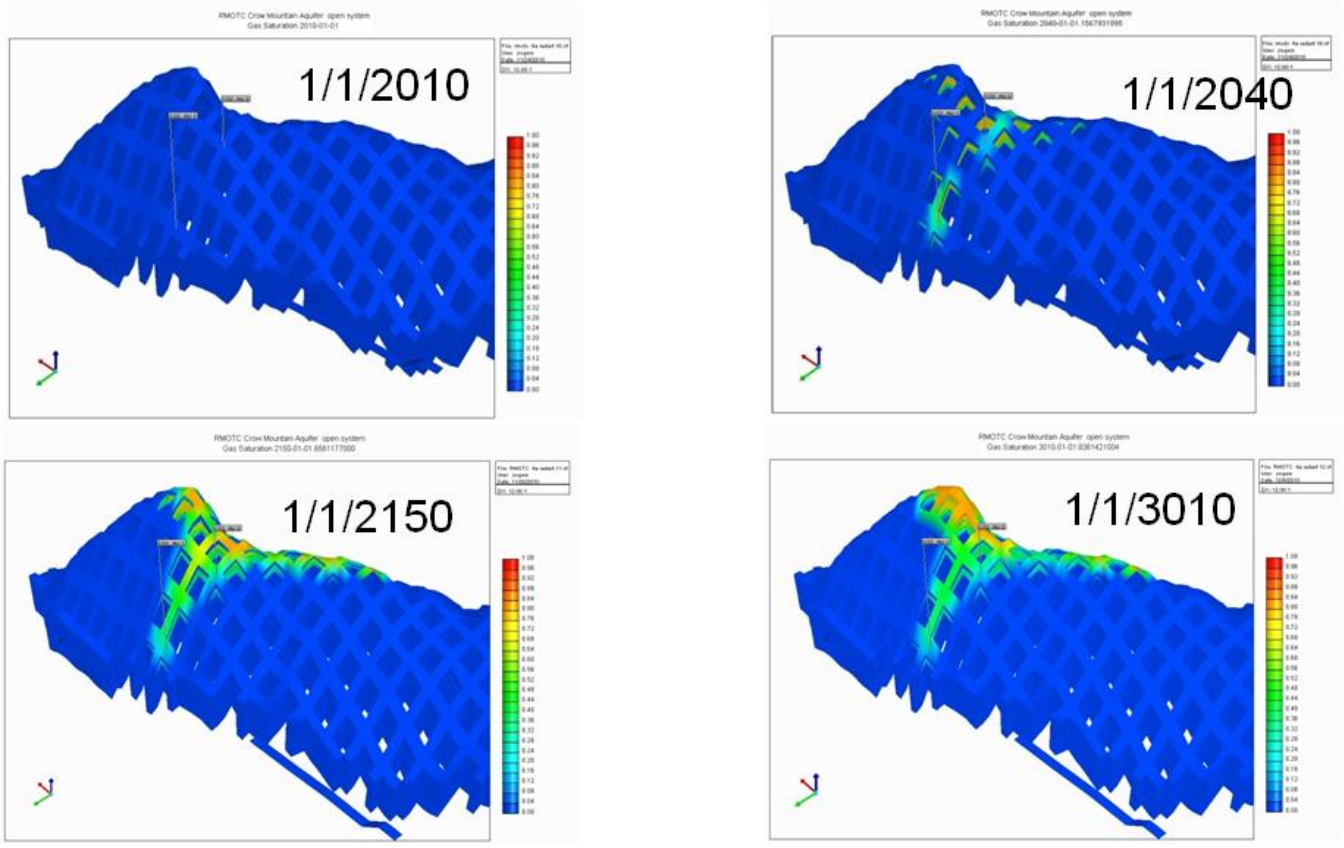

Figure 56: 3D "fence diagrams" of the gas saturation from the reservoir simulation of CO_2 injected into the Crow Mountain. The injection simulation started at 1/1/2010 and injection ceased at 1/1/2040 -- 30 years later. Note that the gas continues to displace vertically as well as in the two lateral directions after injection ceases.

4.4 Feasibility of sparse Seismic CO_2 MVA

One of the primary objectives of this project was to demonstrate that flow performance of the CO_2 injection into deep saline reservoirs can be monitored with much sparser, and therefore more economic, spatial seismic coverage. The necessary temporal coverage was also to be addressed.

4.4.1 Seismic Modeling

The procedure to create synthetic seismograms is discussed in this section. Developing synthetic seismograms is computationally intensive and time consuming; thus, only a portion of the original volumes were used to create the synthetic surveys. Synthetic surveys for the four models (snapshots of simulated saturation changes in the reservoir) were run on areas close to the two injection wells. The software (GeoPRO™ and VizPRO™) developed in the third phase of this project was used to aid in developing the input for the SeisModelPRO™ from four

snapshots models exported from the reservoir simulation. The four time saturation realizations used to generate 3D synthetic seismograms were

- Baseline model (100% water saturation)
- CO_2 model (complete fluid replacement by CO_2)
- 2040 model (30 years of CO_2 injection)
- 3010 model (960 years soak)

4.4.1.1 Preparation of data using GeoPRO™ and VizPRO™

The time-lapse reservoir results from the reservoir modeling and simulation efforts previously described were input to SeisModelPRO™ through GeoPRO™. SeisModelPRO™ is a Fusion proprietary computer system designed to "shoot" a synthetic seismic survey at user-defined surface locations.

The workflow for the seismic model data preparation is

1. Using GeoPRO™, each model was windowed as follows:
    a. ep: 1-345 (inline)
    b. cdpt: 12-187 (xline)
    c. Depth: 0-7000 ft.
2. All models were exported to VizPRO™ format. This task was performed using the "Project Catalog" in GeoPRO™.
3. In VizPRO™, the velocity/Density models were smoothed:
    a. Results from the simulator make the cells appear blocky on the Velocity/Density models. The models need to be smoothed to prevent the blocky structure of the models from causing instabilities in the Finite-Difference modeling in SeisModelPRO™.
    b. Smoothing of the models was performed, for each Volume, (using a three step procedure in VizPRO™):
    Step 1. **Volume_Differences** = **Volume** - **Baseline_Model** .
    Step 2. Smooth **Volume_Differences** (using a XYZ=443 stencil) -> **Volume_Differences_Smooth443.**
    Step 3. **Smooth_Volume** = **Baseline_Model + Volume_Differences_Smooth44**

    The three step procedure in VizPRO™ was used instead of a trivial one step procedure since the one-step procedure smoothes the whole Volume, thus changing the values of Velocity/Density in the shallow part of the model (above the injection area), and a direct comparison of the synthetic models would be difficult.
    Step 1. Smooth Volume (using a XYZ=443 stencil) -> Smooth_Volume.

The three step procedure will keep the Volume models identical to the baseline model (except for the plume region), so the seismograms will be identical above the plume, and a direct comparison of the seismograms will be possible.

4. Final conditioning of the models.
   All the models were prepared for use by the SeisModelPRO™ software by eliminating all the zero values (SeisModelPRO™ will check for zero values in velocities and densities and will not run if any have values of zero) and eliminates outliers, which will create discontinuities in the computation of the synthetic seismograms.

An example of this workflow for the smoothing of the 2040 density model:

1. In GeoPRO™: Load density data in DOE project.
2. In GeoPRO™: Window the data:
   a. Depth: 0-7000 ft
   b. ep: 1-345 (IL)
   c. cdpt: 12-187 (XL).
3. In VizPRO™:
   Using the volume calculator, compute the residuals:
   volume_2040 –baseline = **volume_baseline – volume_2040**.
   Using the Smooth Volume function, smooth the residuals using an xyz=443 stencil, and save to file **volume_2040–baseline_smooth443**.
4. In VizPRO™:
   Using the volume calculator, compute the perturbed density model:
   volume_perturbed = volume_baseline + volume_2040–baseline_smooth443
5. Using GeoPRO™, condition the perturbed model for SeisModelPRO™:
   a. Eliminate outliers.
   b. Eliminate zero-valued amplitudes.
6. Use the conditioned, perturbed model as input to SeisModelPRO™.
7. Figure 57 shows the residuals density volume (**volume_2040 –baseline**).

Figure 58 through Figure 60 show three different views of the residual density volume, with the baseline model in the background in VizPRO™ visualization software. No details are discernible from these images but they illustrate the usefulness of GeoPRO in developing a workflow.

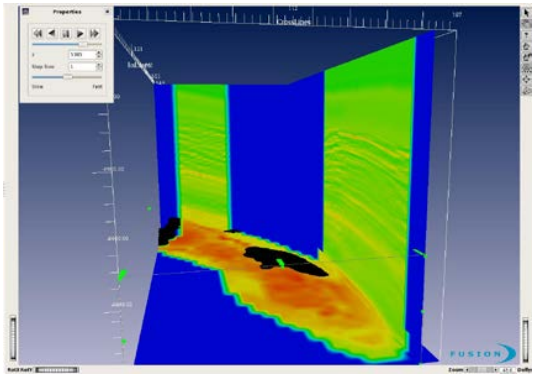

Figure 58:Differences between Baseline and 2040 density models.

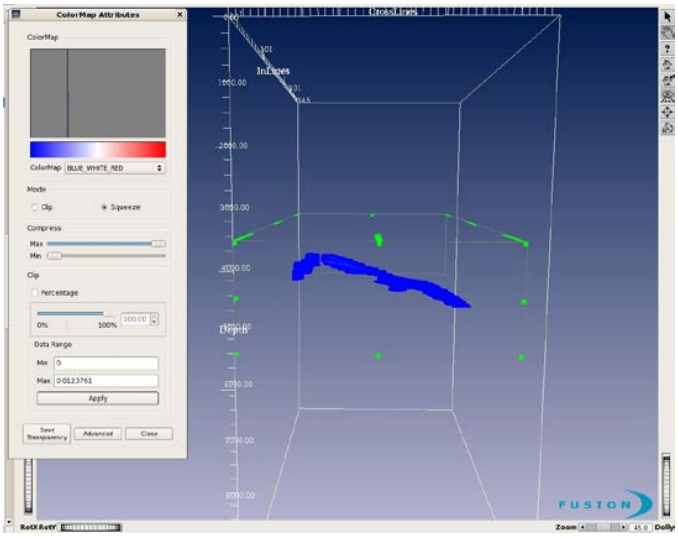

Figure 57: Differences between Baseline and 2040 density models in VizPRO™.

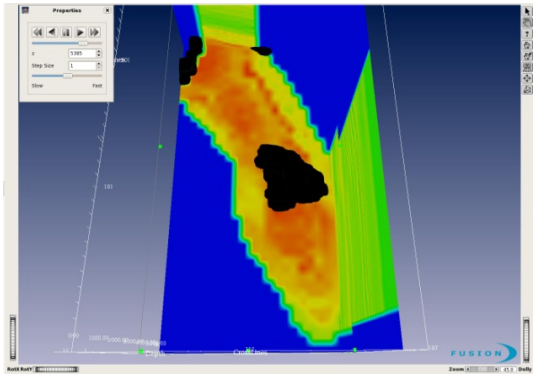

Figure 59: Differences between Baseline and 2040 density models.

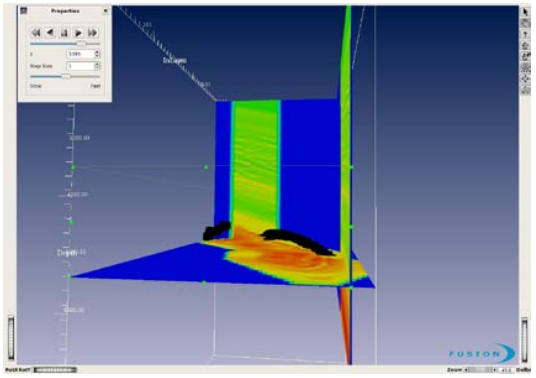

Figure 60: Differences between Baseline and 2040 density models.

4.4.1.2 Generating Synthetic Seismic Survey for Each Snapshot

Synthetic seismograms were created on a section of the volumes close to the injection wells. The seismograms were computed using Fusion's SeisModelPRO™ software. SeisModelPRO™ is a

computer system designed to simulate a synthetic seismic survey at user-defined surface locations. A real seismic survey is simulated using a full Acoustic Wave Equation algorithm, which simulates most of the interesting seismic events that are used in conventional seismic processing/interpretation.

The procedure to create synthetic seismograms is discussed in this section. Due to the computational intensity of seismic modeling and project time constraints, only a portion of the volumes were used to create initial synthetic surveys. To define a basis for comparison between the four models or snapshots, synthetic surveys for the four models were run on areas close to the two injection wells.

The coordinates of the two injection wells are:

Well Co2_1: Inline 157, crossline-Line 167
Well Co2_2: Inline 167, crossline-Line 137

The area for the initial limited synthetic survey was defined by the inlines 160-173 and crosslines 117-167. The limited survey area is shown in

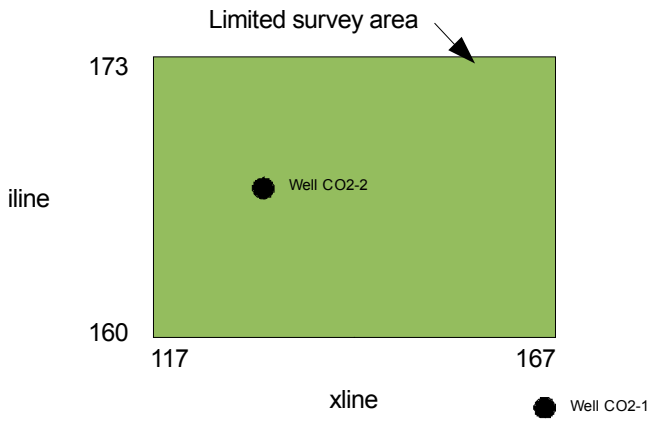

Figure 61: Area where limited survey was performed. Black dots indicate injection wells locations.

The results of the seismic modeling performed on the area of the 4 models are discussed in this section. For each one of the 4 velocity/density models, a synthetic survey was generated using the parameters discussed above. These surveys include seismograms in areas close to the injection wells, and will be used to perform a preliminary comparison of the seismic response of the 4 models.

These four synthetic surveys include just the areal extent of the CO_2 plume for the velocity/density models corresponding to the following time snapshots from the reservoir simulator:

1. A Baseline brine-saturated state e.g. beginning of injection at 2010
2. A CO_2 flooded state e.g. at the end of injection of the CO_2 at 2040
3. A soak state for 970 years after the 30 year injection state ending at 3010 and
4. A CO_2 fluid replacement synthetic model with 100% CO_2 in the pores of the Crow Mountain reservoir

The synthetic survey contain data with a maximum frequency of 80 Hz

Figure 62 shows a comparison between the seismograms computed for the 4 models. All the seismograms were computed along line IL167. The source is at location XL117. Every fourth receiver is shown. In the figure, the first section is the seismogram computed using the Baseline model. The second, third and fourth sections are the differences (residuals) between the first section (Baseline) and the seismograms computed using the CO_2, 2040 and 3010 models, respectively.

Relative differences in amplitudes between the 3 residuals (Baseline - CO_2, Baseline - 2040 and Baseline - 3010) can be observed in this Figure 62. As expected, models CO_2 and 2040 have the biggest differences compared to the Baseline model.

Figure 63 shows the zero-offset traces of each seismogram (Baseline, CO_2, 2040 and 3010, respectively). The difference between the seismograms is difficult to see by just looking at the amplitude of the seismograms. A more detailed view of the differences between the 4 seismograms is shown in Figure 64 and Figure 65. Figure 64 is similar to Figure 62, but only the zero-offset traces are shown. Differences between the amplitudes of the residuals can be observed in Figure 64.

Figure 65 is also based on Figure 62 but in this case only the traces with offset=2200 ft. are shown. Figure 64 and Figure 65 present a picture of the difference in seismic response at different offsets from the 3 injected models, compared to the Baseline model.

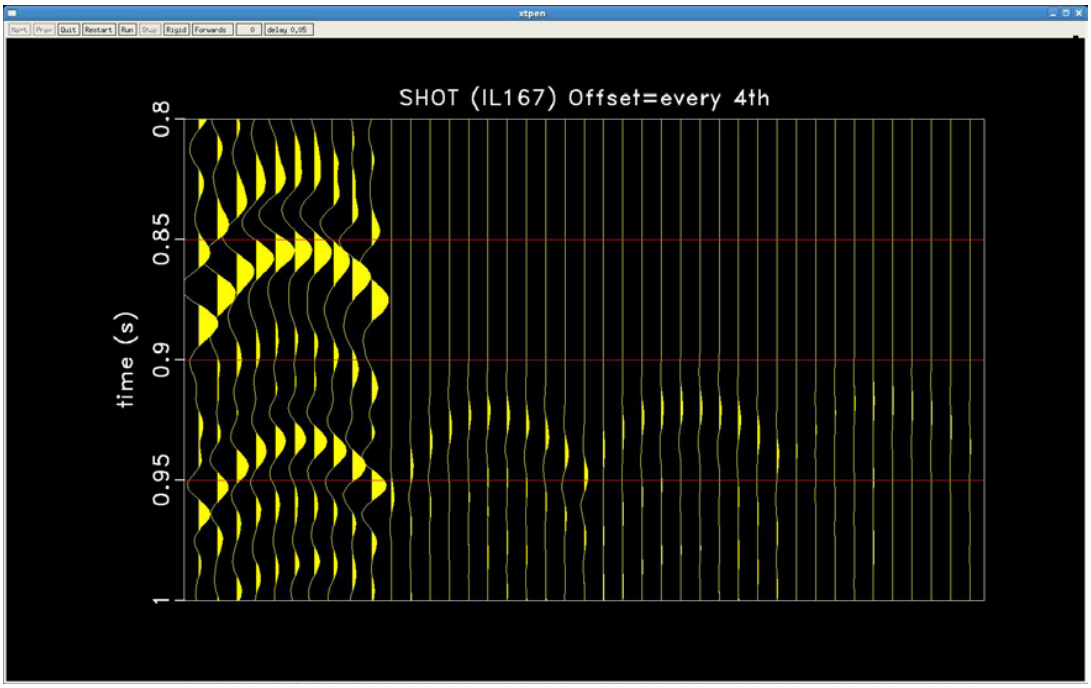

Figure 62 Comparison between the differences of the three injected models (CO2, 2040 and 3010) and the Baseline model. The first section shows the seismogram computed using the Baseline model. The second, third and fourth sections show the result of subtracting the seismograms computed using models CO2, 2040 and 3010 (respectively) from the Baseline seismogram in first section.

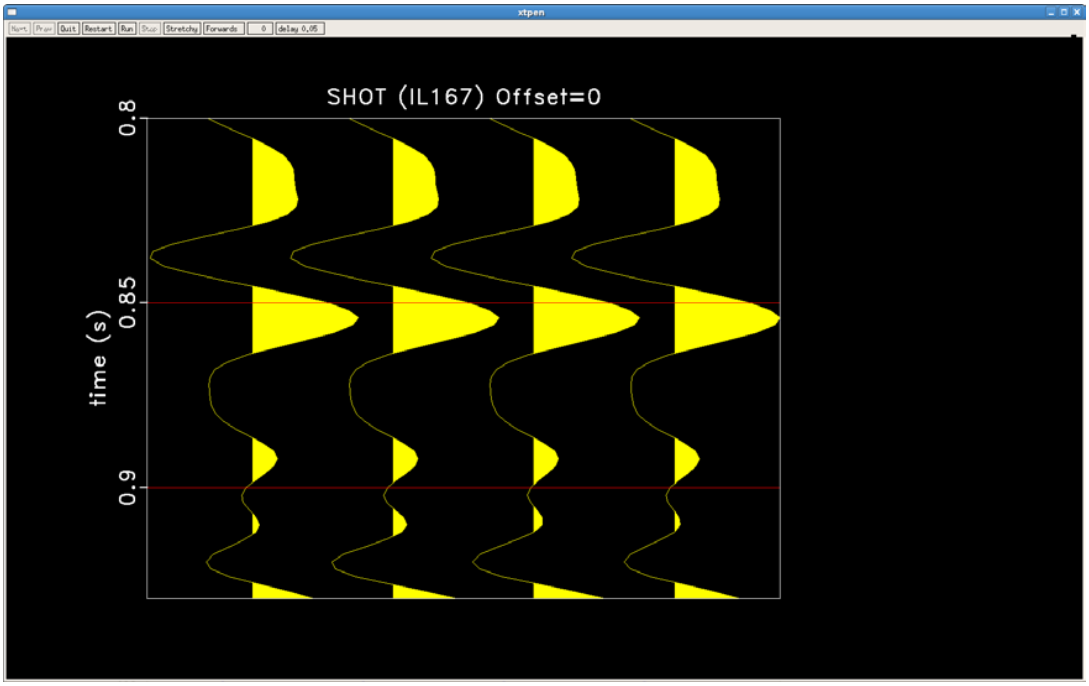

Figure 63: Comparison between the amplitudes of the three injected models (CO2, 2040 and 3010) and the Baseline model. The first section shows the seismogram computed using the Baseline model. The second, third and fourth sections show the seismogram computed using the three injected models (CO2, 2040 and 3010, respectively).

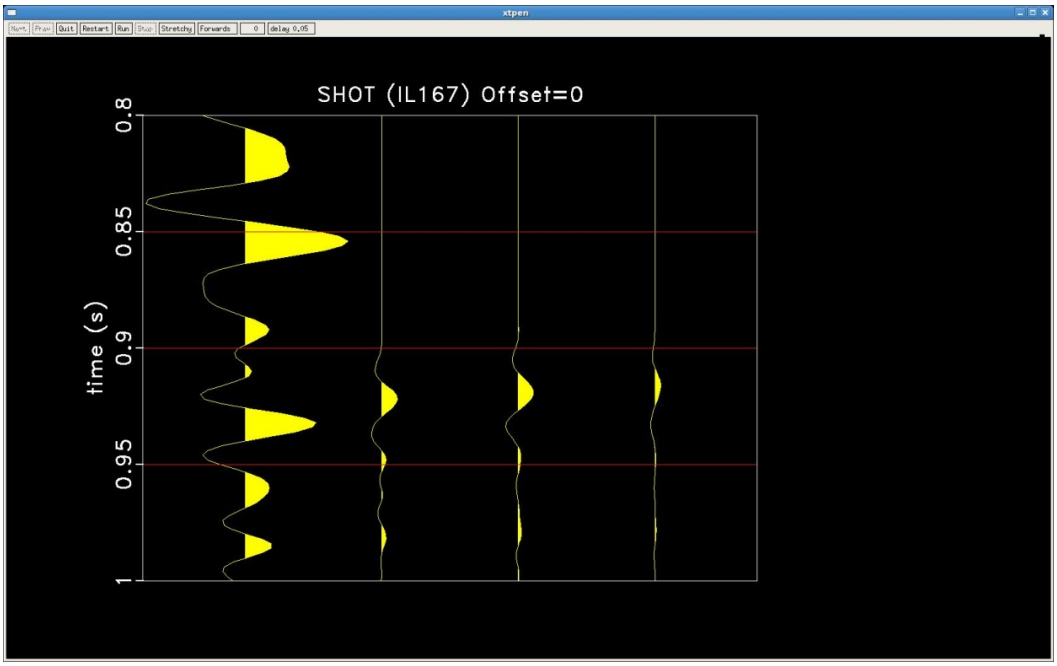

Figure 64: Comparison between the differences of the three injected models (CO2, 2040 and 3010) and the Baseline model. The first section shows the seismogram computed using the Baseline model. The second, third and fourth sections show the result of subtracting the seismograms computed using models CO2, 2040 and 3010 (respectively) from the Baseline seismogram in first section. Only the zero-offset seismogram is shown for all 4 sections.

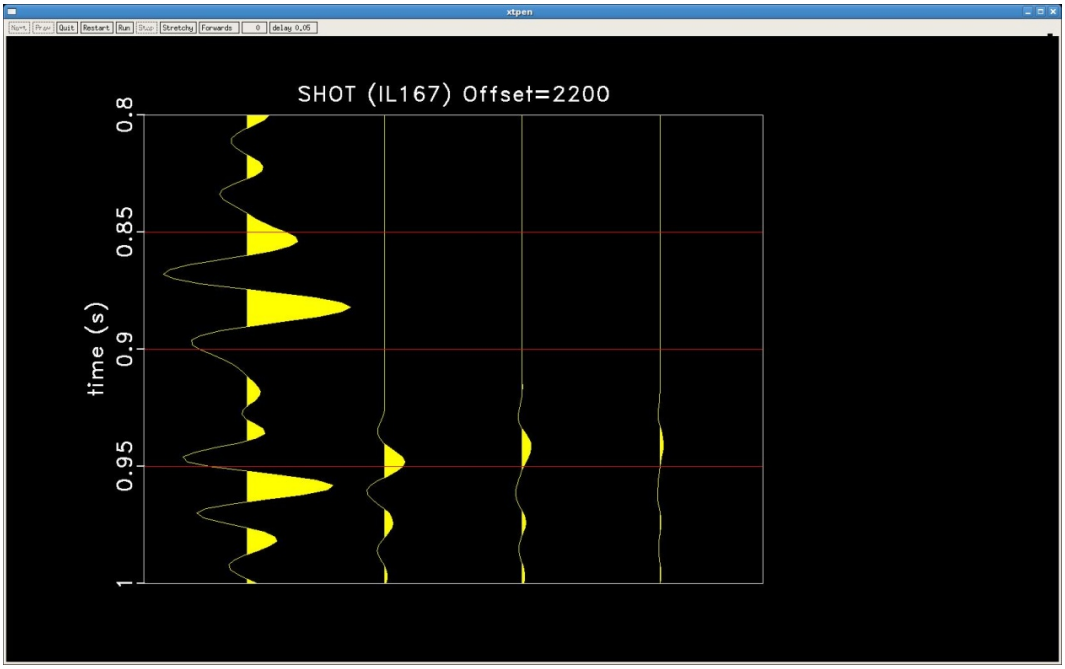

Figure 65: Comparison between the differences of the three injected models (CO2, 2040 and 3010) and the Baseline model. The first section shows the seismogram computed using the Baseline model. The second, third and fourth sections show the result of subtracting the seismograms computed using models CO2, 2040 and 3010 (respectively) from the Baseline seismogram in first section. Only a far-offset seismogram is shown for all 4 sections (Offset = 2200 ft).

4.4.1.3 Imaging Synthetic Seismic

The synthetic seismic data obtained was imaged using Fusion's high-fidelity seismic imaging algorithms, and analyzed using Fusion's proprietary reservoir analysis tools.

After synthetic data generation, the four synthetic seismic snapshots were formatted and sorted into standard industry formats for reflection seismic processing and imaging. The formatting and data sorting were confirmed by generation of pre-migration "stack" volumes, which test the spatial alignment of the model and the synthetic seismic. A bulk static correction of -16 ms was applied to the seismic to correct for the delay incurred in generating the seismic source signal during modeling.

After reformatting, pre-stack image volumes were generated using Fusion's K3D Kirchhoff pre-stack depth migration software to position seismic reflections into their correct spatial positions for all four synthetic snapshots. Input to K3D included the preprocessed synthetic seismic and the time-lapse models used to generate the seismic. The pre-stack synthetic image volumes were then converted to vertical two-way seismic travel time for comparison with the field seismic image volume, and stack image volumes were generated for all four synthetic seismic snapshots.

Using these four synthetic seismic data volumes the following efforts were accomplished

1. Completion of pre-stack imaging
2. Calibration of synthetic and field seismic data
3. Image analysis of processed data and differentiating between time shots
4. Decimation of data for Sparsity analysis. Comparison of sparse 4D data with dense 4D data

Noise was not added to the synthetic data as it is not a simple issue to model and was not felt to be germane to the purpose and scope of this project. A more realistic evaluation or comparison to a realistic field data set could be accomplished if noise was added. Due to time constraints noise was not modeled but should be considered in the synthetic data possibly as a future effort.

4.4.1.4 Calibrate Synthetic and Field Data

In order to validate the reservoir model synthetic seismic baseline the simulated seismic models were calibrated with the actual field data from RMOTC processed and interpreted by Fusion.

Comparing Figure 66 and Figure 67 below illustrates that the synthetic data (Figure 67) agrees well with real data (Figure 66). Figure 68 is the same as Figure 67 but the green horizon (top of Crow Mountain) interpreted from real data has been replaced in the display with the yellow horizon interpreted from synthetic data (also top of Crow Mountain). The point is that there is very good agreement at the calibration well between real and synthetic data. Thus we are confident in having identified the top of the Crow Mountain in the synthetic data and knowing that it represents the upper boundary of the injection interval. We should expect to be able to detect differences between seismic data from different saturation stages if present, and bounded by this top (yellow horizon).

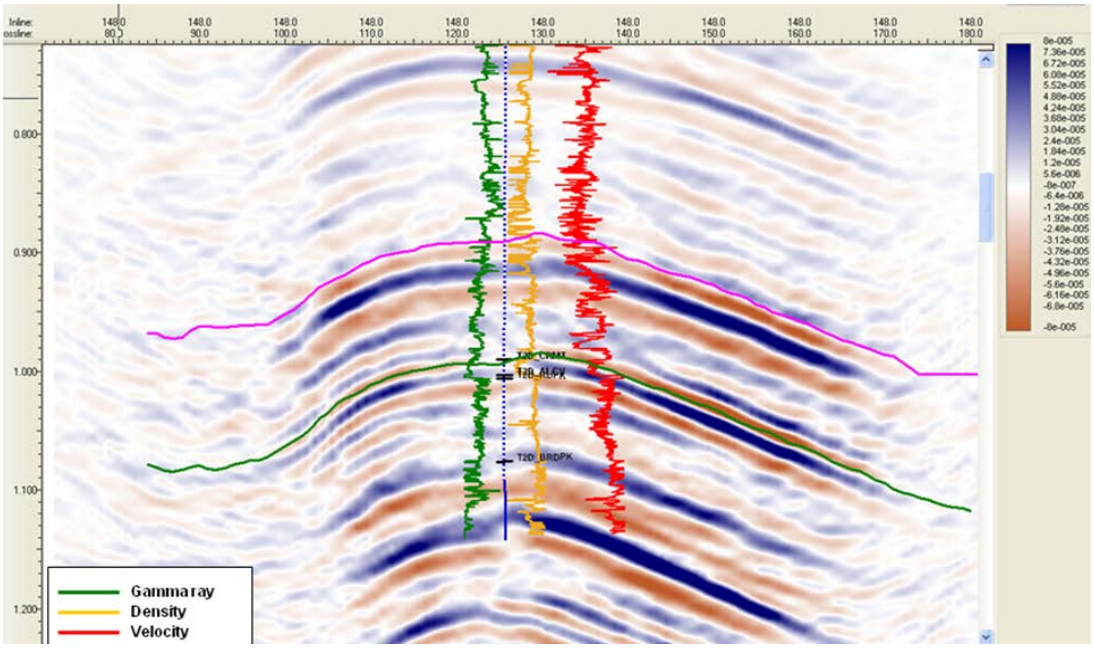

Figure 66:True seismic at calibration well. Green horizon is Top of Crow Mountain. In-line 148 crossline 181 at well Lawrence 62 TPX #10-10

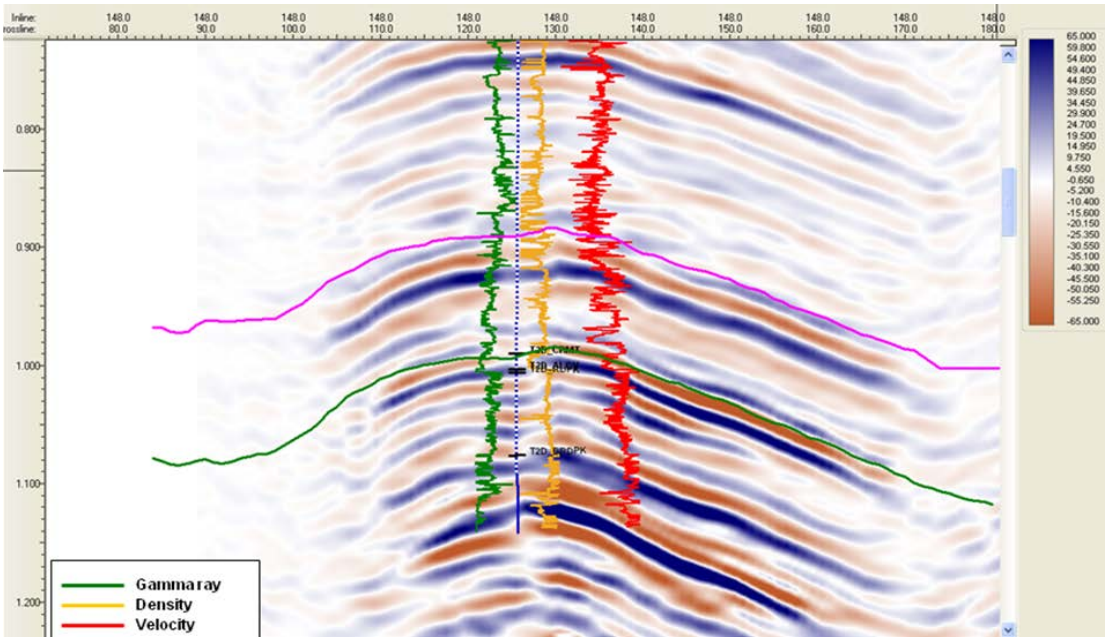

Figure 67: Synthetic seismic at calibration well. Green horizon is Top of Crow Mountain interpreted from true seismic at In-line 148 crossline 181 at well Lawrence 62 TPX #10-10

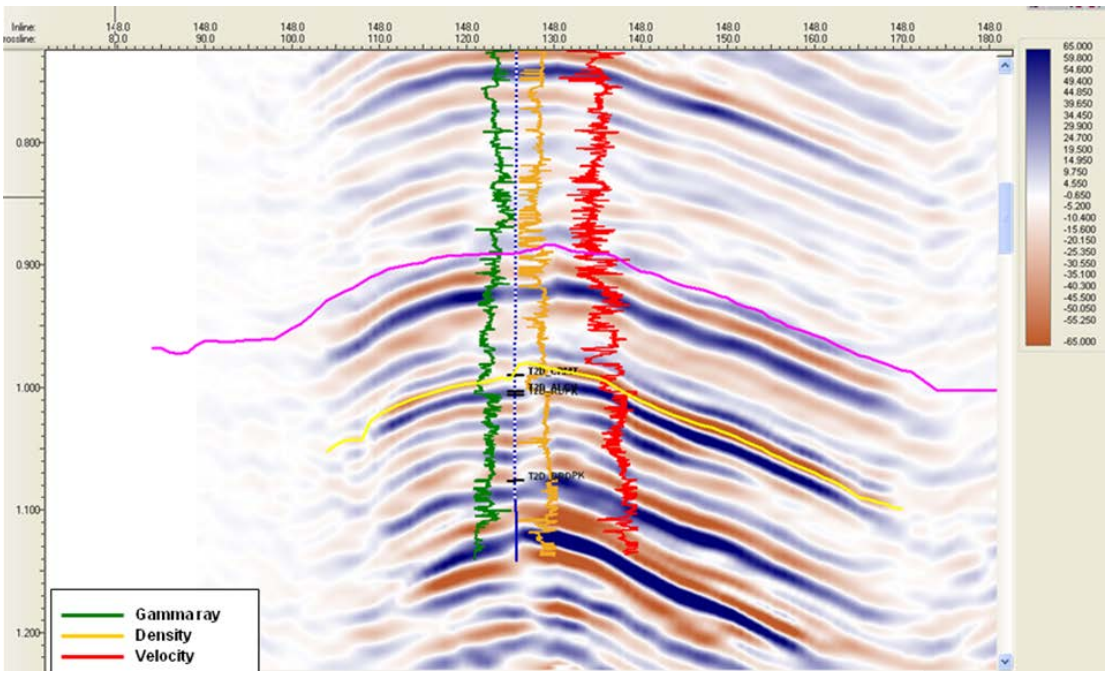

Figure 68:Synthetic seismic at calibration well. Yellow horizon is Top of Crow Mountain interpreted in synthetic seismic

4.4.2 Sparsity Determination

Figure 69 illustrates that small time delays can be detected in the seismic data due to changes in the fluid saturations. Figure 69 shows that the velocity is slower through the CO_2 saturated reservoir than through the brine saturated reservoir. Thus the reflection time is greater through the gas saturated reservoir and that the time differences between the gas filled reservoir and brine filled baseline reservoir will allow us to monitor and detect the migration of the gas within the injected reservoir.

Figure 70 through Figure 73 illustrate the synthetic seismic amplitude changes due to saturation changes at the top of the Crow Mountain reservoir. The two top images (Figure 70 and Figure 71) show the two different types of fluid at 100% saturation for each fluid in the simulated seismic area. Figure 70 image is the amplitude of 100% brine saturated base case. Figure 71 is an image of the amplitude of 100% CO_2 saturation. Figure 72 and Figure 73 show two time snapshots of the seismic data amplitudes of the Crow Mountain reservoir at the end of the thirty year injection period (2040) and after 970 years of soak (3010). Note that both time and amplitude anomalies are detectable.

Dense acquisition images developed using the three models (baseline, 2040 injection state, 3010 soak state) were used to develop amplitude difference maps between the two flooded states (e.g. 2040 and 3010) and the baseline state or 100% brine filled state (see Figure 74 and Figure 75) developed in task 7. From these difference images the CO_2 migration at different times can be seen as the carbon dioxide migrates updip of well 1 to the apexes of the anticline south (lower part of the image). The saturation changes can also be seen along the east side from the anticline updip of injection well 1.

For comparison Figure 76 and Figure 77 are 3D "fence diagrams" from the reservoir simulation of the CO_2 injected into the Crow Mountain. The upperleft corner of both figures is south-southwest and northeast is to the lower left corner where CO_2 injection well 1 is located. Figure 76 and Figure 77 are rotated clockwise about 180° from Figure 74 and Figure 75. Figure 76 and Figure 77 illustrate the CO_2 plume saturation at the top of the Sundance from the reservoir simulator while Figure 74 and Figure 75 show 2D maps of the amplitude differences from the synthetic seismic at the top of the Crow Mountain at the two time states of the reservoir e.g. at 2040 (end of injection and 3010 end of simulated soak).

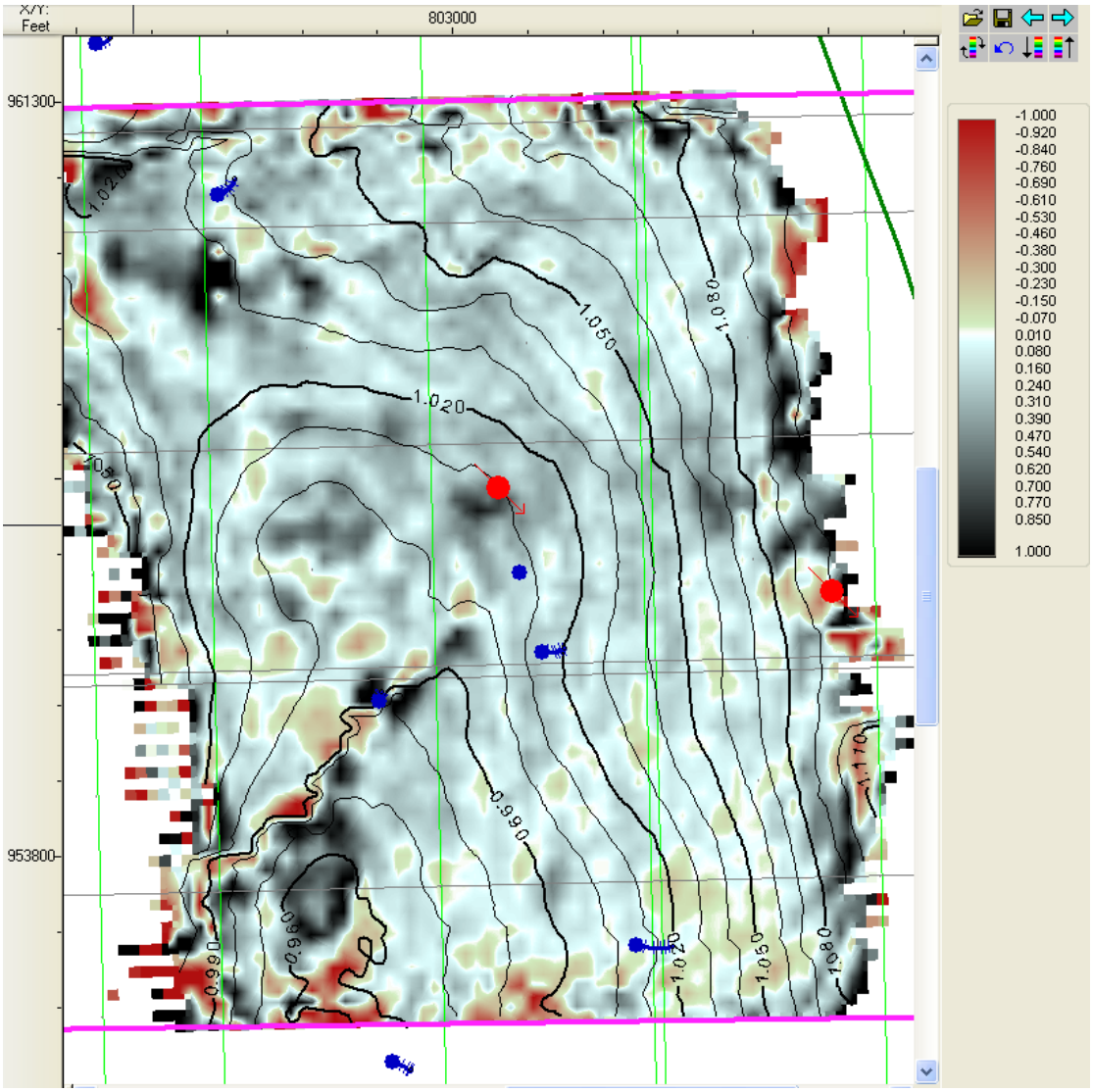

Figure 69: Seismic data time differences (msec) at the Top of Crow Mountain (CO_2 – Brine) dues to saturation changes from brine to 100% CO_2 saturated.

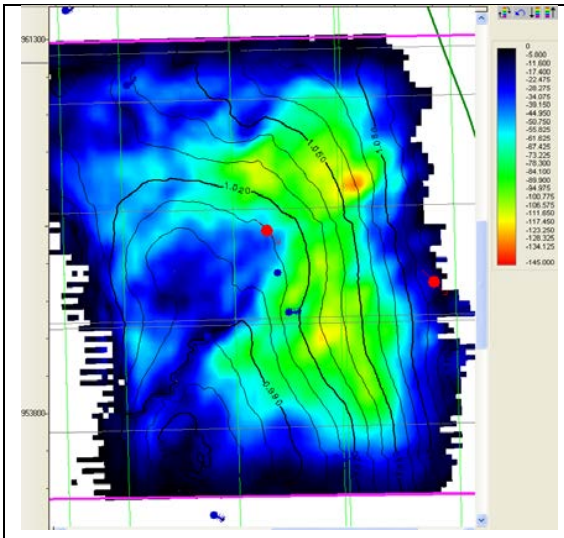

Figure 70:Amplitude at Top of Crow Mtn (Brine case (Baseline))

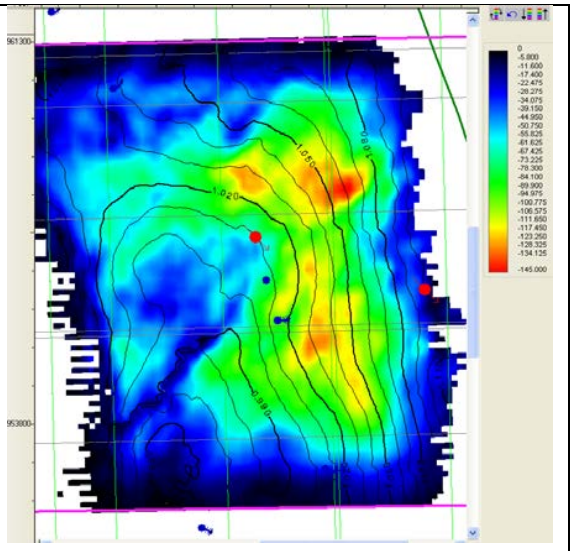

Figure 71:Amplitude at Top of Crow Mtn (CO_2 case)

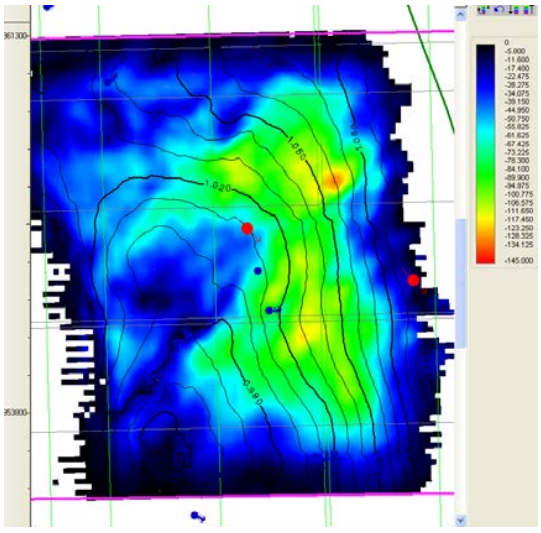

Figure 72: Amplitude at Top of Crow Mtn (2040 case)

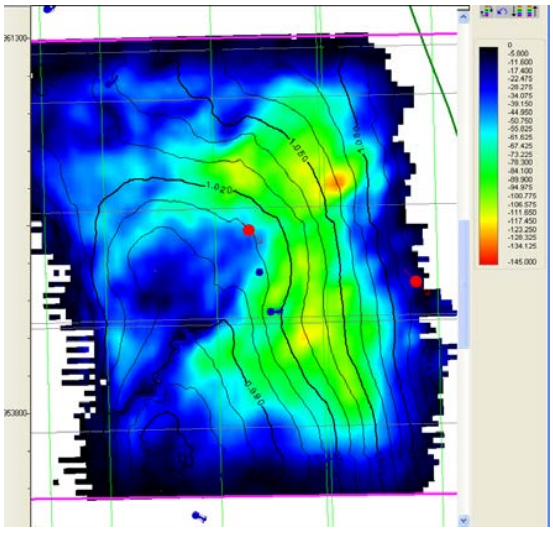

Figure 73: Amplitude at Top of Crow Mtn (3010 case)

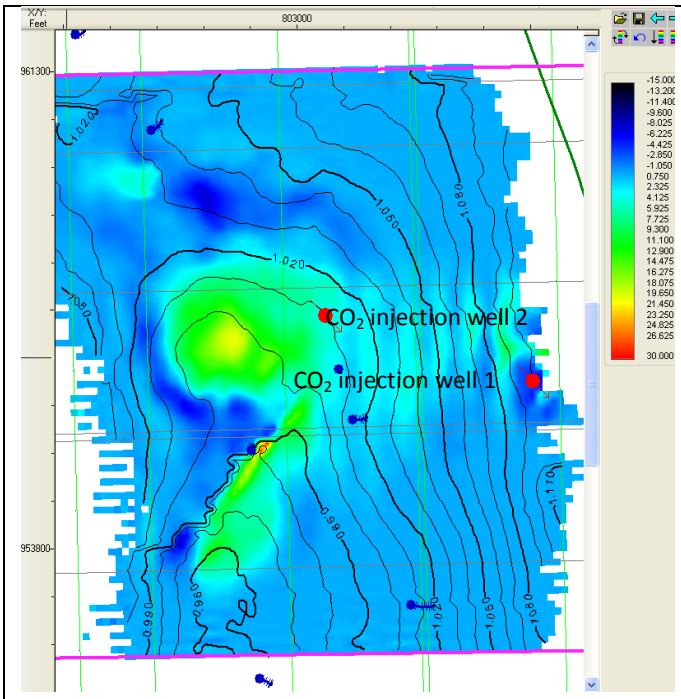

Figure 74:Time lapse Amplitude Anomalies Dense acquisition (110 by 110 bin size) 2040 state minus baseline. Red Dots are two simulated CO_2 injection wells.

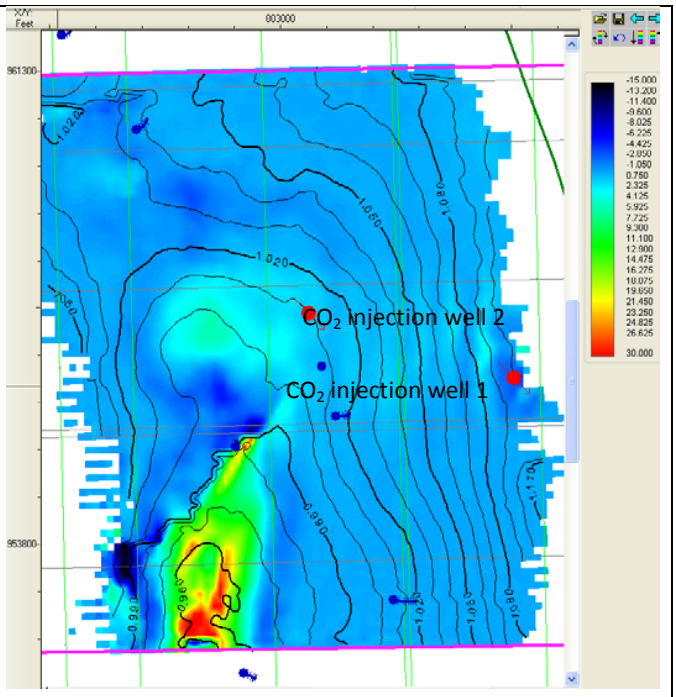

Figure 75: Time lapse Amplitude Anomalies Dense acquisition (110 by 110 bin size) 3010 state minus baseline. Red Dots are two simulated CO_2 injection wells.

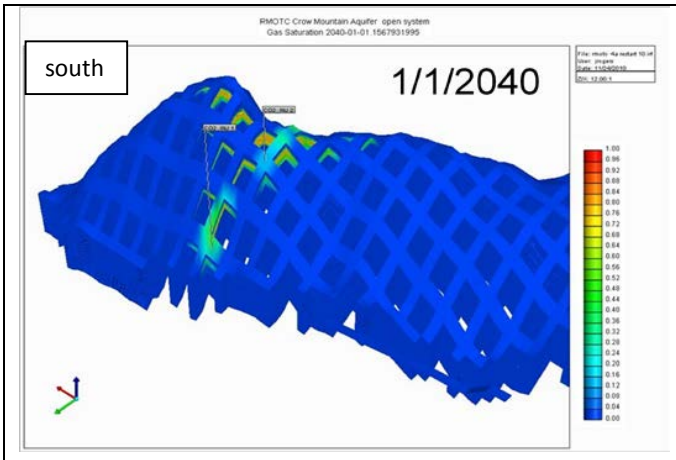

Figure 76: Simulated injection of CO_2 into Crow Mountain at end of 30 year injection period

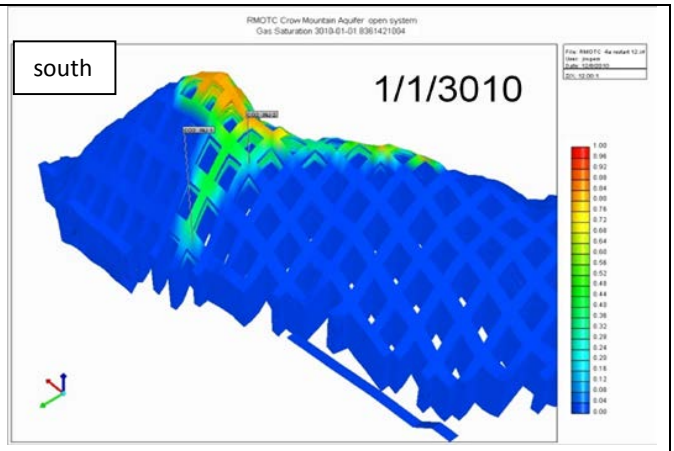

Figure 77: Simulated injection of CO_2 into Crow Mountain at end 970 year soak period

4.5 Development of Software to Aid in MVA

The GeoPRO™ Database developed in this project consists of many different and unique types of data needed for a full cycle of reservoir analysis processing especially for MVA. The data types include seismic, gridded velocities, velocity picks, surfaces, faults, grids, wells, and events to name a few. The infrastructure included all base C++ classes needed for processing CO_2 MVA data. This includes components and tools to process data using many geophysical modules within a workflow process. A new processing engine was created to efficiently process data on large distributed systems. Intelligent parameterization was added to help the users define parameters in complex flows. These improvements required design of a common native format for each data type (seismic, horizons, wells, etc.) in order for each to be shared and used among internal Tools. Originally we targeted Open Spirit for a common format, but changed to R5000 to talk directly with R5000 support applications and removing the middle-ware

- Launcher starts the tools used for CO_2 MVA analysis that uses seismic or other reservoir data or tools integrated into GeoPRO™.
- A data Catalog manages all data through GeoPRO™ and VizPRO™
- VizPRO™ is an advanced visualization tool that runs within the GeoPRO™operating environment. VizPRO™ allows the user to interrogate their data after any processing or analysis step, and also allows the interpretation of surfaces for analysis or model building in real time as the model is built. VizPRO™ allows the display of well paths, logs and other critical information, and has full opacity, sub-cube and volume rendering

capability to meet your most challenging project needs. Multiple value surfaces can be viewed in all directions and many other very elegant features.

- VelPRO™ is a next-generation velocity modeling tool that allows the user to have interactive control over multiple velocity functions at one time. VelPRO™ will improve a user's ability to construct complex models needed for seismic analysis especially if used in CO_2 MVA. VelPRO™ links back to VizPRO™ and will enable efficient quality control of the velocity field within the GeoPRO™ environment without porting the data to another platform.
- GeoPRO's Flow Builder has a full parallel processing capability to allow the user to process seismic data on LINUX clusters with custom node assignment on each specific job. The platform also provides a developer environment that allows for efficient implementation of the user´s own software with full linkage to the visualization environment
- Additional tools incorporated into the software development of this software effort--SegyPRO™ Viewer, TomoPRO™ and Module Builder

Details of developing this type of MVA software and the purpose of each is discussed below.

4.5.1 Enhancement and Re-architecture of the Prototype GeoPRO Software

GeoPRO's design to include Intelligent Parameterization, Multi-Component data, and Improved Data Management Capabilities was successfully completed. Creating long and complex work flows as in MVA analysis is made easier for users by intelligent parameterization which allows the passing of descriptions about the data between modules. For example, when sample rates change between modules, the downstream module would alert the user to the data's maximum frequency. The capability to hide parameters that do not need to be parameterized because of other parameter's options was added. An example of this capability is when the user specifies time in a migration module, all depth related parameters would be hidden. The addition of intelligent parameters removes possibility of errors in the flows, alerts users to errors before submitting jobs into a distributed queuing system, and helps guide users to good parameter choices. The items designed in this task were implemented in subsequent tasks in developing the software.

4.5.2 Enhancement of the Prototype Data

Enhancements to the GeoPRO™ Database and implementation and testing has been completed as a deliverable of this project. Improved Data management capabilities include a Database architecture necessary to process MVA modules. Improvements included:

1. Analysis of the differences in the internal proprietary software data structures (Geometry, Seismic Processing and Seismic Analysis)

2. Sharing of each data type among all of the available internal tools.

These improvements required design of a common native format for each data type (seismic, horizons, wells, etc.) in order for each to be shared and used among internal Tools. Originally we targeted Open Spirit for a common format, but changed to R5000 to talk directly with R5000 support applications and removing the middle-ware. Middle-ware, such as Open Spirit, adds complexity to the software that was not needed for CO_2 MVA processing. A simpler direct connection to database required for CO_2 MVA processing was a better choice. The reservoir modeling tool was changed from the third party JOA JewelSuite™ to Crystal.

We successfully created our own GeoPRO™ Database and connected both GeoPRO™ applications and Crystal. The GeoPRO™ Database consists of many different and unique types of data needed for a full cycle of MVA processing. The data types include seismic, gridded velocities, velocity picks, surfaces, faults, grids, wells, and events to name a few.

VizPRO™ is successfully integrated to use the new database and a new tool to interact with the database was created. VizPRO™ is an advanced visualization tool that runs within the GeoPRO™operating environment. VizPRO™ allows the user to interrogate their data after any processing or analysis step, and also allows the interpretation of surfaces for analysis or model building in real time as the model is built. VizPRO™ allows the display of well paths, logs and other critical information, and has full opacity, sub-cube and volume rendering capability to meet your most challenging project needs. It allows multiple value surfaces in all directions and many other very elegant features. Other tools are actively being integrated to use the database, such as Flow Builder and VelPRO™. In the near future, all tools and applications, companywide, will use this database.

VelPRO™ is a next-generation velocity modeling tool that allows the user to have interactive control over multiple velocity functions at one time improving the user's ability to construct complex models needed for CO_2 MVA. VelPRO™ links back to VizPRO™ to enable efficient quality control of the velocity field within the GeoPRO™ environment without porting the data to another platform.

GeoPRO's Flow Builder has a full parallel processing capability to allow the user to process seismic data on LINUX clusters with custom node assignment on each specific job. The platform also provides a developer environment that allows for efficient implementation of the user´s own software with full linkage to the visualization environment.

4.5.3 Primary Infrastructure for the CO_2 MVA System Software

The infrastructure includes all base C++ classes needed for processing CO_2 MVA data. This includes components and tools to process data using many geophysical modules within a

workflow process. A new processing engine was created to efficiently process data on large distributed systems. Intelligent parameterization was added to help the users define parameters in complex flows.

An example of a complex flow used to cleanup noisy land data is shown in Figure 78. This flow has thirty-nine modules and hundreds of parameters for a user to enter. Without intelligent parameters this workflow would be error prone because parameters for certain modules are affected by parameters in upstream modules.

The ability to analyze, view, and interpret seismic velocity models was incorporated. These tools are needed to build accurate velocity models for CO_2 MVA. In order to see CO_2 from acquired seismic data, the data must be processed with the most accurate velocities using the best migration algorithms. This requires tools to visualize and work/process many different data types, such as seismic, velocities, well logs, reservoir models, etc. An example of a velocity analysis and model building workflow is shown in Figure 79.

Due to the very wide scope of the nature of operations needed for building the primary infrastructure, we have developed several applications inside the GeoPRO™ system, each catering to a specific field of study. This makes each application have a specific purpose and make the user interactivity very simple.

Migration of seismic data is handled by Flow Builder and the outputs of these migrations are provided to Crystal. Crystal is a reservoir characterization software to develop static reservoir models and populate reservoir parameters into the grid cells of the static model. Characterization of the reservoir is handled in Crystal to develop static reservoir models. These static reservoir models can be passed to a reservoir simulator where dynamic reservoir flow models are developed. The output of these models is provided to VizPRO™, where the reservoir realizations are done using the seismic and reservoir data. The process can be repeated for multiple scenarios and different times. The resultant 4D data is interactively viewed in VizPRO™ as time series navigation.

Teapot_NoisePRO_Flow
- Segy Disk Read
  - Header Math
  - Header Math
  - Header Math
  - Filter
  - Ensemble AGC
  - Decon
- SC Decon
  - Spherical Divergence
- SC Amplitude Balance
  - Static Shift
  - NoisePRO - Frequency Split
  - Header Math
  - Header Math
- Trace Stack
- Trace Sort
  - NoisePRO - ampAtt
- Trace Sort
- Trace Stack
  - Static Shift
  - Header Manager
  - Header Manager
  - Filter
  - Header Manager
  - Header Math
  - FX Decon
- Trace Sort
  - Header Manager
  - Header Math
  - Header Manager
  - NoisePRO - ampAtt
  - NoisePRO - ampAtt
  - Filter
  - Spherical Divergence
- Segy Disk Write
  - Spherical Divergence
  - Filter
  - Spherical Divergence
- Segy Disk Write

Figure 78: Example of complex flow used to cleanup noisy land data

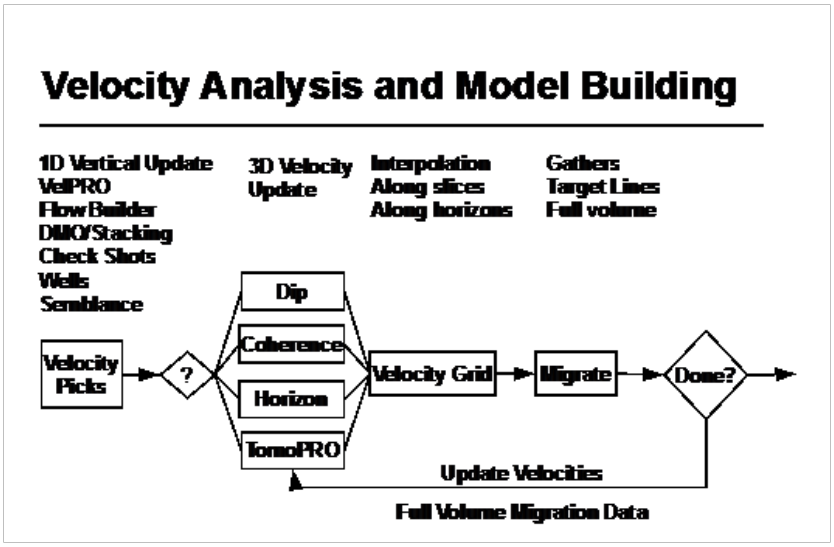

Figure 79: Example velocity analysis and model building workflow

4.5.4 Optimized Grid Operation

A parallel grid based system called Overlord is integrated into GeoPRO™ and includes many enhancements to the parallel engine. Overlord (OVE) is a parallel processing system designed to minimize time spent on large processing jobs or other computationally intensive computer routines by spreading data and work to a set of slave machines. A secondary goal is to minimize the impact of slave machine failure. A set of configurable algorithms within OVE controls data staging and distribution of executable commands. Dependence on long term node stability is minimized, and failures in data communication between the master process

and worker processes do not halt the entire processing job. Parallel engines that rely on constant communications between master and worker process will kill a job when any worker within the job fails. Failed jobs are rescheduled without interruption and data collection occurs in parallel thus making the process much more efficient and less manpower intensive or interactive and reducing cost of processing massive sets of data.

4.5.5 Unified Data Format

The ultimate goal of a unified data format is to allow an application to read from any data base regardless of format. This can only be achieved by a combination or unifying data formats for each item in the GeoPRO™ database and creating a unified data framework layer on top of multiple databases; thus, when the applications have to interact with a new database, the modification of the source code is not significantly limited. The unified database creates a highly efficient method to integrate data and applications to share one database. A data framework that all the GeoPRO™ applications can communicate with was successfully developed, without requiring the application to directly interface with the underlying data base. This framework layer acts as a bridge between the applications and the databases (see Figure 81).

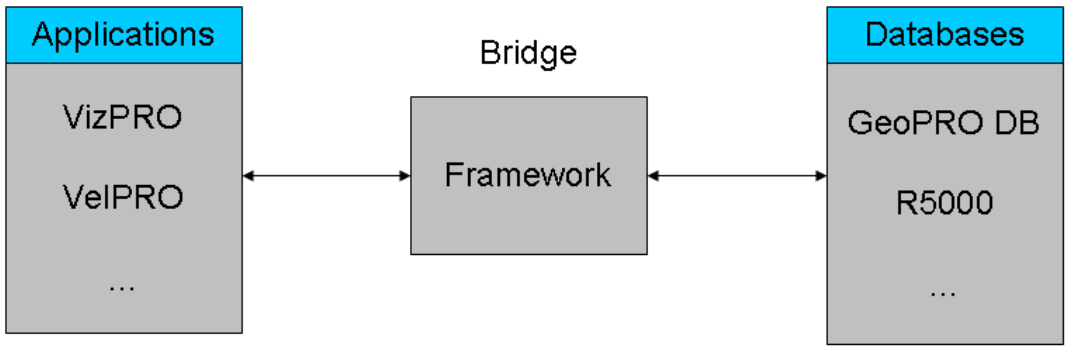

Figure 80: Architecture of framework of GeoPRO™ database

Fusion has successfully ported the R5000 data base into this framework model. R5000 is Landmark Graphics OpenWorks Project Management system and is a database for landmark suite of software, such as interpretation software. Integration with this data base is necessary since many of the volumes used in CO_2 MVA are used between GeoPRO™ and Landmark's tools. The R5000 database layer allows for additional layers of data to be incorporated on top of the existing database and is especially useful a database does not support a specific data item. For example, R5000 does not support the multi-z surfaces (as seen in complex reservoirs of reverse

faulting or salt intrusions etc), so we could easily add a layer for multi-z surfaces on top of the R5000 database.

Implemented in the unified framework is a capability that enables all tools within Fusion Geo to seamlessly access data from any database system. Both the GeoPRO™ Database and R5000 database are integrated with this framework and will be available for commercial use in the GeoPRO 3.0 release scheduled for April 1, 2012

4.5.6 Collaboration and Visualization

A wide range of visualization tools have been provided in the software developed in DEFE0001111 to handle different kinds of data (e.g., 1D, 2D, 3D, 4D). Collaboration in simple 1D and 2D domains can be easily achieved by using VNC. VNC is remote control software which allows you to view and fully interact with one computer desktop (the "VNC server") using a simple program (the "VNC viewer") on another computer desktop anywhere on the Internet. The two computers don't even have to be the same type. A user of VNC can view a Windows Vista desktop at the office on a Linux or Mac computer at home. Visualization of 3D and 4D is much more complicated as 3D/4D data has to be transferred across the network to display on the remote machine.

Remote Visualization allows users to view and interact with very large data sets from almost any client machine located almost anywhere. Distant users who need to access and visualize large data can take advantage of remote rendering to avoid bringing back data locally and overcome graphics limitations of their workstation or laptop. The data server generates images with high performance, and those images are transported efficiently across the network by remote rendering.

Remote visualization is an ideal choice for people to collaborate who are in different locations. If the remote machine cannot be used, the data has to be copied on to the local network and all the computers would need high-end graphics cards to view the images. Without remote visualization, all persons working with the data would need to be at the same physical location to view the data simultaneously. This is not an ideal solution as it would introduce latency and also there might be GPU differences between the host and the remote machines. Latency is a result of transferring all the graphics commands and data over network before visualizing on the local machine and results not only in very slow behavior but also improper visualization and poor resolution in some cases.

From our research we have concluded that the best solution for collaboration of 3D and 4D visualization is to use the power of the remote GPU servers and transfer the rendered image (compressed if necessary) across multiple collaborating nodes. Using a combination of VirtualGL and VNC we accomplish remote visualization. VirtualGL redirects 3D commands from a

Unix/Linux OpenGL application onto a server-side 3D graphics card and converts the rendered 3D images into a video stream with which remote clients can interact to view and control the 3D application in real time.

Several different kinds of stereo capabilities were included based on the available hardware. Visualization of 3D data on a desktop is not completely 3D, as the interface between the user and the 3D display is a 2D monitor. Stereo allows complete 3D with the use of special 3D glasses. There are several different ways stereo could be achieved, based on the hardware example: active stereo, passive stereo, etc. The advantage of stereo viewing is that the user is more immersed into the scene.

4.5.7 Installation and Testing at a Selected CO_2 Sequestration Site

As part of the software effort scripts that can be used to install the MVA software at a CO_2 Sequestration Site were written and tested.

Installation scripts:

a. Install GeoPRO™ Platform

b. Create GeoPRO™ Database using SQL scripts

c. GeoPRO™ environment

d. Run-time execution scripts

5 CONCLUSIONS

5.1 Direct Conclusions from the many tasks and efforts of this project:

1. RMOTC data were successfully processed and analyzed to provide a reservoir model of a realistic brine formation using Fusion proprietary software and utilization of some software developed in this project.
2. Simulated injection of approximately 1.2 MM tons of CO_2 into the Crow Mountain Formation was modeled as an open system with limited geochemical effects.
3. Sparse seismic array modeling was performed and compared successfully with actual seismic data.
4. Sparsely acquired seismic data have the potential to reduce the cost of data acquisition to monitor effectively CO_2 sequestration.
5. Software incorporating advanced database management and visualization concepts should help to analyze MVA data more efficiently and allow better QC of critical information.
6. Workflow for seismic sparsity analysis has been demonstrated and is incorporated in the GeoPRO^{TM} software platform.

5.2 DEFE0001111 Relevancy to the Aims of the CCS Program

- This project in its entirety addresses the overall goal of the DOE's Carbon Storage Program "to develop and advance technologies that will significantly improve the efficacy of the geologic carbon storage technology, reduce the cost of implementation, and be ready for widespread commercial deployment between 2020 and 2030... and without hindering economic growth." The project does this by
    1. primarily addressing the technical focus area of MVA but also integrates the Carbon Storage program technical focus area of simulation and risk assessment
    2. Developing a workflow from processing and interpretation, reservoir modeling, reservoir simulation of injection of CO_2 in a real reservoir proxy, and modeling of 4D seismic based on realistic surrogate sequestration site, and development of advanced database management for visualization and modeling efforts.
- The migration of CO_2 injected into saline aquifers by source reflection seismic imaging strategy based on deployment of spatially sparse surface seismic arrays was

shown by simulation to be feasible and the concept methodology scientifically proven for field testing and application. Substantial cost savings can be inferred from this successful proof of concept as the acquisition of the 4D seismic data is substantial and reducing the acquisition effort and maintaining the resolution of the data is relevant to three CCS programs MVA programmatic goals

1. "to develop technology, methodology and protocols to effectively evaluate and provide assurance of CO_2 storage permanence in geologic formations reliably and cost effectively" and
2. will help in "demonstrating that 99 percent of injected CO_2 remains in the injection zone(s)" economically as well as
3. "improving efficiency of storage operations."

- The application and use of 3D seismic to evaluate the reservoir strength or integrity using the advanced geopressure analysis as was done as part of this project is relevant to the MVA CCS program in that the methodology and technology applied can help determine safe injection pressures so that the wellbore and the mechanical integrity of the formation seals at the wellbore and boundaries are intact and not vulnerable to mechanical failure at the operating or injection pressures. This is relevant to the CCS program goals of
    1. " Developing improved tools and interpretation of data from well logging and seismic surveys that may increase the resolution of existing technologies and assess integrity of wellbores"
    2. "improving efficiency of storage operations"
    3. "estimating CO_2 storage capacity in geologic formations "
- The sparsity analysis proof of concept demonstrated in this project modeled small changes from background levels and identified changes in CO_2 levels could be monitored outside the intended target storage formation. This is relevant to the CCS program in
    1. "demonstrating that 99 percent of injected CO_2 remains in the injection zone(s)"
    2. "improving efficiency of storage operations "

  The software development efforts in this project addressed the need for advanced geophysical methods and protocols to image CO_2 or sense changes in geochemistry in the target or surrounding formations in the MVA focus area.

6 LITERATURE CITED

1. Rogers, J. D. *Integrated Reflection Seismic Monitoring and Reservoir Modeling for Geologic CO2 Sequestration Seventh Quarterly Report;* Quarterly Report; Fusion Petroleum Technology Inc, 2011, April 1, 2011 to June 20, 2011.

2. Picard, D. M. Petrography of Red Peak Member, Chugwater (Triassic), West-Central Wyoming. *Journal of Sedimentary Petrology* **1966,** *36* (4), 904-925.

3. Picard, D. M. Iron Oxides and Fine Grained Rocks of Red Peak and Crow Mountain Sandstone Members, Chugwater (Triassic) Formation, Wyoming. *Journal of Sedimentary Petrology* **1965,** *35* (2), 484-479.

4. High Jr., L.; Picard, D. M. Stratigraphic Relations within the Upper Chugwater Group (Triassic) Wyoming. *The American Association of Petroleum Geologists Bulletin* **1969,** *53* (5), 1091-1104.

5. Cavaroc, V. V.; Flores, R. M. Red Beds of the Triassic Chugwater Group, Southwestern Powder River Basin Wyoming. *USGS Bulletin: 1917-E* **1991**.

6. Cooper, S. P.; Goodwin, L. B.; Lorentz, J. C. Fracture and fault Patterns associated with basement cored anticlines: The example of Teapot Dome Wyoming. *AAPG Bulletin* **2006,** *90* (12), 1903-1920.

7. Tohill, B.; Picard, D. M. Stratigraphy and Petrology of Crow Mountain Sandstone Member (Triassic) Chugwater Formation, Northwestern Wyoming. *Bulletin of the American Association of Petroleum Geologists* **1960,** *50* (12), 2347-2565.

8. Kirschbaum, M. A.; Lillis, P. G.; Roberts, L. N. R. Chapter 3 Geologic Assessment of Undiscovered Oil and Gas Resources in the Phosphoria Total Petroleum System of the Wind River Basin Province, Wyoming. In *Petroleum Systems and Geologic Assessment of Oil and gas in the Wind River Basin Province Wyoming*.

9. Sparlin, M.; Meyer, J.; Bevc, D.; Cabrera, R.; Hibbits, T.; Rogers, J. Seismic Analysis and Characterization of a Brine Reservoir for CO2 Sequestration. *Society of Exploration Geophysicists*, Denver, 2010, presentation.

10. Timur, A. An Investigation of Permeability, Porosity, and Residual Water Saturation Relationships. *The Log Analyst,* July/August 1968.

11. Holditch, S. A. Chapter 7: Tight Gas Reservoirs. In *SPE Handbook vol VI;* Warner Jr., H. R., Lake, L., Eds.; SPE: Richardson, Texas, 2007; Vol. VI, pp 297-353.

12. Birkholzer, J.; Quanlin, A.; Rutqvist, J.; Jordan, P.; Zhang, K.; Tsang, C.-F. *Research Project on CO2 Geological Storage and Groundwater Resources: Large-Scale Hydrological Evaluation and Modeling of the Impact on Groundwater Systems;*, 2007, Annual Report october 1, 2006 to September 30, 2001.

13. Hart, D. J.; Bradbury, K. R.; Feistein, D. T. The Vertical Hydraulic Conductivity of an Aquitard at Two Spatial Scales. *Ground Water* **2006,** 201-211.

14. Neuzil, C. E. How Permaeable are Clays and Shales? *Water Resources Research* **1994,** *30,* 145-150.

15. Blasingame, T. A. The characteristic Flow Behavior of Low-Permeability Reservoir Systems. *2008 SPE Unconventional Conference*, Keystone, 2008.

16. Quanlin, Z.; Birkholzer, J.; Rutqvist, J.; Tsang, C.-F. Sensitivity Study of CO2 Sorage Capacity in Brine Aquifers with Closed Boundaries: Dependence on Hydrogeologic Properties. *Sixth Annual Conference on Carbon Capture and Sequestration DOE/NETL*, 2007, May 7-10.

17. Bennion, B. D.; Bachu, S. Permeability and Relative Permeability Measurements at Reservoir Conditions for CO2-Water Systems in Ultra Low Permeability Confining Caprocks. *SPE/EAGE Conference London June 11-14, 2007.*, 2007.

18. Bennion, B. D.; Bachu, S. Relative Permeability Characteristics for Supercritical CO2 Displacing Water in a Variety of Ptential Sequestration Zones in the Western Canada Sdementary Basin. *SPE Annual Technical Conference Dallas October 9-12*, 2005.

19. Bennion, Brant D; Bachu, Stefen. Drainage and Imbibition Relative Permeability Relationships for Supercritical CO2/Brine and H2S/Brine Systems in Intergranular Sandstone, Carbonate, Shale, and Anhydrite Rocks. *SPE Reservoir & Engineering* **2008,** 487-496.

20. Benson, Sally. Relative Permeability Explorer. http://pangea.stanford.edu/research/bensonlab/relperm/index.html (accessed 2011).

7 LIST OF ACRONYMS AND ABBREVIATIONS

Acronym or abbreviation	Meaning	Acronym or abbreviation	Meaning
3D	three dimensional	nano	10^{-9}
AAPG	American Association of Petroleum Geologists	NETL	National Energy Technology Laboratory
API	American Petroleum Institute	NMO	normal move out
aq	aqueous	NNW	north-northwest
BP	Budget Period	no.	Number
BP1	First Budget Period	NPR	Naval Petroleum Reserve
BP2	Second Budget Period	OB	overburden
cc	cubic centimeter	PE	State Registered Professional Engineer
CCS	Carbon Capture and Storage	PG	State Registered Professional Geoscientist
Co.	Colorado	PI	principal investigator
DOE	US Department of Energy	PMP	Project Management Professional; Project Management Plan
DST	drill stem test	PP	pore pressure
EAGE	European Association of Geoscientists and Engineers	PPG	pound-force per gallon
ed	editor	PSDM	pre-stack depth migration
EOR	enhanced oil recovery	PSI	pound -force per square inch
ES	effective stress	PSTM	pre-stack time migration
F	Fahrenheit	R&D	research and development
FP	fracture pressure	REVEL	residual velocity analysis. Proprietary software by FUSION
FPTI	Fusion Petroleum Technology Inc.	RMO	residual normal moveout
ft	feet	RMOTC	Rocky Mountain Oilfield Testing Center
g	gram	RMS	root mean square
GHG	green house gas	SEG	society of Exploration Geophysicists
GPU	graphics processing unit	SEG Y	currently accepted standardized data exchange file format for seismic data developed by the SEG. The "Y" component of the acronym reflects the azimuthal component of the main storage base indexing.
Hrz	Horizon	sh	shale
Hz	hertz frequency	SPE	Society of Petroleum Engineers
IL	in-line	SPEQ	spectral equalization
Inc	Incorporated	sr	Senior
JS	JewelSuite™	SS	sandstone
k_x	permeability in x direction	SSE	south southeast
ky	permeability in the y direction	TOMO	tomographic
kz	permeability in the z direction	Tx	Texas
LFAF	low frequency array forming	™	Trade mark
LS	limestone	US	United States
M	thousand	USGS	United States Geological Society
m^2	square meter	VNC	virtual network computing
MASTT	Third party commercial software for calculating residual reflection statics	vol	volume
md	millidarcy	VP	vice president
mi	mile	WIND	FUSION proprietary noise attenuation software
micro	10^{-6}	XL	cross-line
MM	million		
ms	millisecond		
msec	millisecond		
Mtn	mountain		
MVA	Monitoring, Verification and Accounting		

APPENDICES

Appendix A : Seismic Processing and 3D Pre-Stack Migration

Final Report
Seismic Processing
and
3D Pre-Stack Migration

for

U.S. Department of Energy

INTEGRATED REFLECTION SEISMIC MONITORING AND RESERVOIR MODELING FOR GEOLOGIC CO2 SEQUESTRATION
Phase 1 Task 3.0

February 2010

Table of Contents

1. Project Overview

The Teapot Dome 3D seismic reprocessing program was undertaken during November 2009 to February 2010 at Fusion Petroleum Technologies, Inc.'s offices in Houston, Texas. It comprised the time reprocessing, 3D pre-stack time migration (PSTM), and 3D pre-stack depth migration of 3D data recorded in 2001 over the Naval Petroleum Reserve No. 3 (NPR-3) located in the southwest portion of the Powder River Basin, approximately twenty-seven (27) miles north of Casper, Wyoming. This is commonly referred to as the Teapot Dome field. The reprocessing was undertaken to provide a baseline, high quality 3D data volume to support Fusion's Integrated Reflection Seismic Monitoring and Reservoir Modeling for Geologic CO2 Sequestration project for the U.S Department of Energy.

The objective of the integrated program was to develop and demonstrate a fully integrated multidisciplinary CO_2 MVA (Monitoring, Verification, and Accounting) software system, based on using a novel approach to the deployment and utilization of seismic imaging, and the innovative integration of the seismic with reservoir modeling. The system was planned to include an accurate reservoir modeling package which will account for geomechanical and geochemical processes of CO_2 injection into a brine aquifer. This reservoir simulation will be linked via rock physical relationships to seismic rock properties.

This report provides an overview of the Fusion 3D reprocessing program and discusses the key factors encountered during the reprocessing of these data. These included:

- Removing distorting effects due to variable near-surface conditions using 3D refraction statics.
- Addressing strong interfering coherent noise and improving the signal-noise ratio within the data.
- Tuning of Pre-Stack Migration parameters for a optimal curved ray PSTM and PSDM final volumes.
- Maximizing signal resolution and reflector continuity during the post-processing phase to prepare the data for the subsequent seismic attribute and geopressure stages of the project.

2. Geologic Setting

Teapot Dome is a large northwest-southeast trending anticline from which production began in the 1920's with full development activities ramping up in the 1970's. The Teapot Dome anticline is basement-cored and an extension of the larger Salt Creek anticline to the north. It is a doubly plunging, asymmetrical anticline. Structural dips are steeper on the west flank than on the east side of the structure. The producing formations of interest include nine productive horizons with the Shannon, Steele and Niobrara shales, Second Wall Creek, and Tensleep formations being the most productive. As a result, depths of interest extend to approximately 7000ft beneath a surface exceeding 5000ft above sea level. The structural setting and stratigraphic column are characterized below.

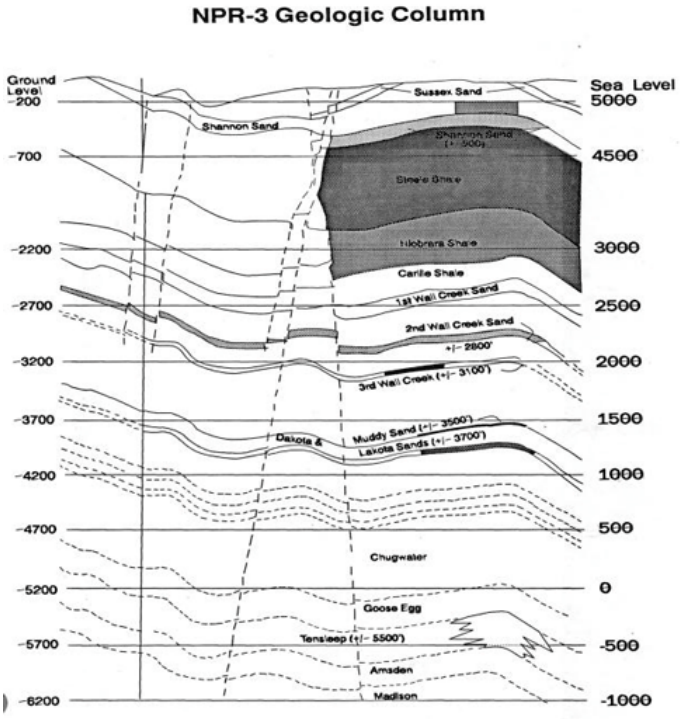

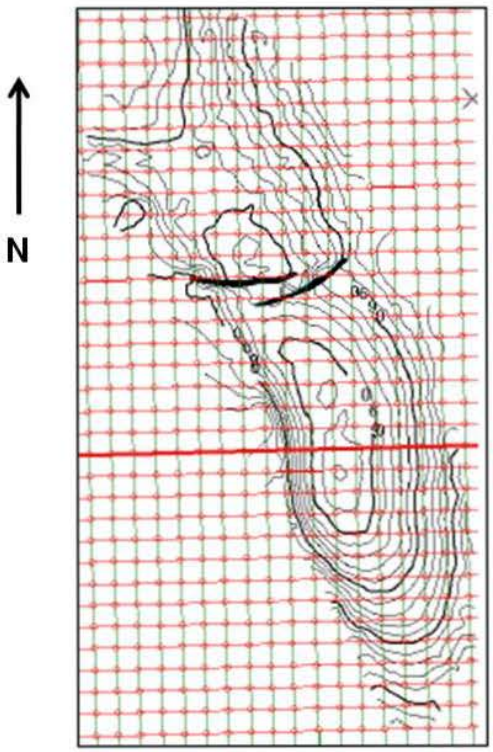
N

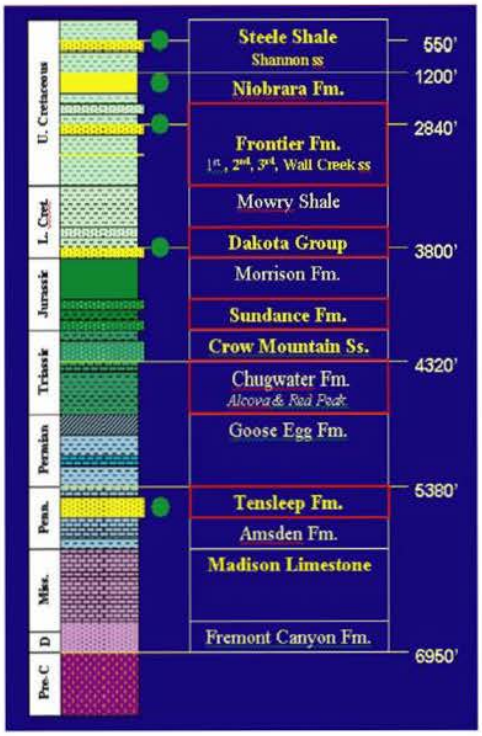
U. Cretaceous
L. Cret.
Jurassic
Triassic
Permian
Penn.
Miss.
D
Pre-C
Steele Shale
Shannon ss
Niobrara Fm.
Frontier Fm.
1st, 2nd, 3rd, Wall Creek ss
Mowry Shale
Dakota Group
Morrison Fm.
Sundance Fm.
Crow Mountain Ss.
Chugwater Fm.
Alcova & Red Peak
Goose Egg Fm.
Tensleep Fm.
Amsden Fm.
Madison Limestone
Fremont Canyon Fm.
550'
1200'
2840'
3800'
4320'
5380'
6950'

3. Project Location

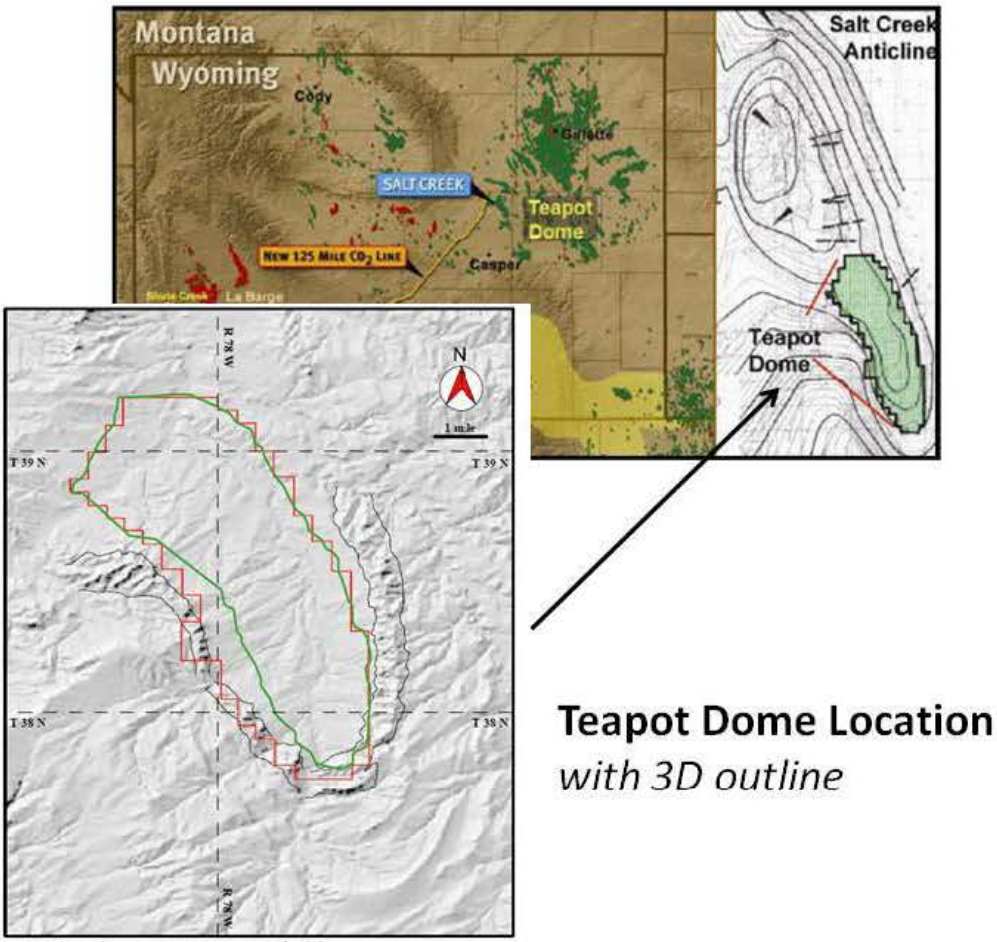

Teapot Dome Location
with 3D outline

Red outlines Teapot Dome field
Green outlines 3D area

4. Acquisition Summary

Area	~ 28 square miles
Contractor	WesternGeco crew 780
Date Shot	January 2001
Design	10 x 120 channel
Instruments	I/O System 2
Number of live groups	1200
Sample Period	2ms
Field Filters	OUT- 0.5 Nyquist
Source	Vibroseis AVH III 392
Source Pattern	4 units inline
Sweep Length	12 seconds, 16 second listen
Sweep Frequency	8-96Hz,
Source Interval	220ft
Source Line Spacing	2200ft
Receiver Interval	220ft
Receiver Line Spacing	880ft
Bin Size	110ft x 110ft
Nominal Fold	~48

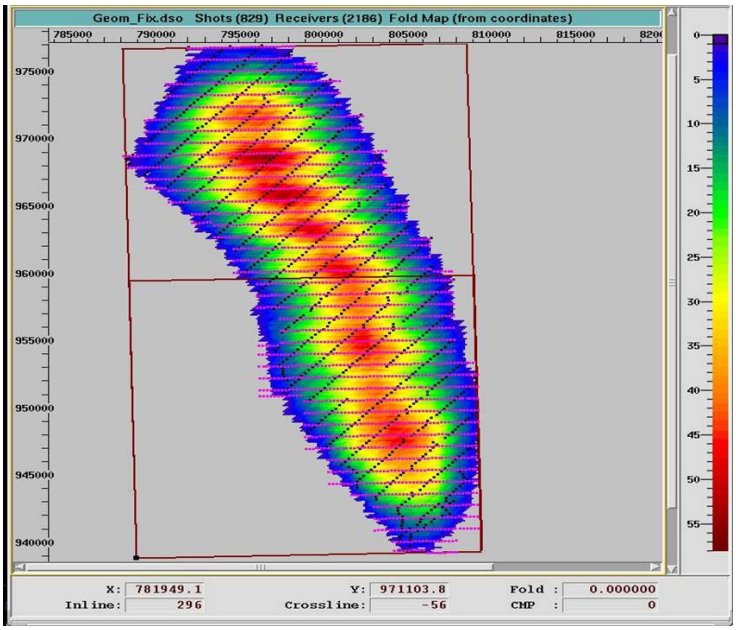

Source/Receiver Layout with Fold Coverage

5. Processing Sequence

TIME PROCESSING

1. **Data Load and conversion to internal format**
2. **Geometry Application and QC**
3. **3D Refraction Statics (Seismic Studio system)**
    a. Tomography solution
    b. Replacement Velocity: 9600ft/sec
    c. Datum: 6700ft
4. **Trace Edit**
5. **True Amplitude Recovery**
    a. Spherical Divergence Corrections, V^2T
6. **Noise Attenuation: Shot Domain (WIND 1)**
7. **Velocity Analysis (0.5 mile grid)**
8. **3D Surface-Consistent Amplitude Correction (Shot, Receiver)**
9. **3D Surface-Consistent Residual Statics (Pass 1)**
10. **Minimum Phase Correction**
11. **Surface-Consistent Deconvolution**
    a. Type: Spike
    b. Operator Length: 240ms
    c. % White Noise: 0.1
12. **Spectral Equalization** (see Discussion section)
13. **Velocity Analysis (0.5 mile Grid)**
14. **3D Surface-Consistent Residual Statics (Pass 2)**
15. **3D Surface-Consistent Amplitude Correction (Shot, Receiver – Pass2)**
16. **Trim Statics**
    a. 3D model trace created, coherency enhanced.
    b. Production Maximum Shift: 12ms
17. **3D Interpolation and Regularization** (see Discussion section)
18. **Noise Attenuation: Common Offset domain (WIND II)**
19. **Pre-Stack Time Migration (PSTM)**
    a. Type: Curved Ray Kirchhoff 3D Pre-Stack Time Migration
    b. Aperture: 15º- 30º @ 10000ft
    c. Offset Bins: 220 – 10780ft (at 440ft increments)
20. **Velocity Analysis and Update using PSTM gathers (0.5 mile grid)**
21. **Residual Normal Moveout**
22. **Final Stack with Mute**
23. **Post-Processing including FXY Deconvolution**
    a. 7pt filter
    b. 60% addback
24. **Spectral Equalization**
25. **Time-Variant Bandpass Filter**

DEPTH PROCESSING

1. **Velocity Model Building**. Using relevant structural information and the available PSTM RMS velocity field, an initial velocity model was generated by converting from PSTM Vrms velocity-Time to Interval Velocity-Depth.
2. **Pre-stack Depth Migration with 3-D tomographic updating.** Kirchhoff 3-D pre-stack depth migration algorithm.
3. **Model Building and Velocity Update.** Common Image Gather-based (CIG) for residual velocity estimation with model updating using 3-D tomography followed by PSDM for updated CIG gathers and evaluation.
4. **Final Pre-stack Depth Migration**. Output depth gathers at 110x110ft spacing, up to 40 offsets, 330ft apart, 10 ft depth step, up to 20000ft aperture with Zmax at 15000ft.
5. **Residual NMO**. Applied to all depth gathers.
6. **Stack** with selected Mute schedule.
7. **Convert from Depth to Time,** using final velocity field (if required)
8. **Post migration processes** (FXY Decon, Spectral Equalization, Bandpass filter)
9. **Output SEG Y** PSDM Gathers and Volume

6. Deliverables

1. Stacks
    1. PSTM, RMO, Stack (non-interpolated gathers)
    2. PSTM, RMO, Stack, Post-Processing (non-interpolated gathers)
    3. PSTM, RMO, Stack (interpolated gathers)
    4. PSTM, RMO, Stack, Post-Processing (interpolated gathers)
    5. PSTM, RMO, Stack (spectral equalization, interpolated gathers)
    6. PSTM, RMO, Stack, Post-Processing (spectral equalization, interpolated gathers)

    7. PSDM, RMO, Stack
    8. PSDM, RMO, Stack, Post-Processing
    9. PSDM, RMO, Stack – converted to Time
    10. PSDM, RMO, Stack, Post-Processing – converted to Time

2. Report
    1. Final Report

3. Gathers
    1. CMP Gathers (non-interpolated)
    2. CMP Gathers (interpolated)
    3. PSTM, RMO, Gathers (interpolated pre-migration)
    4. PSDM ,RMO, Gathers (interpolated pre-migration)
    5. PSDM ,RMO, Gathers (interpolated pre-migration) – converted to Time

4. Velocity
    1. PSTM RMS Velocity Field
    2. PSDM Vint-Z Velocity Field

7. Time Processing

Since the objective of the seismic processing program was to provide a 3D volume that fully reflected the subsurface structural and stratigraphic characteristics of the Teapot Dome field to facilitate the later Tasks in this CO2 MVA program, great care was taken to remove unnecessary distorting effects while preserving valid subsurface information. As the production processing flow evolved, several key factors emerged as critical to success of the project:

- Removal of near-surface travel-time distorting effects.
- Noise Attenuation of the diverse coherent noises encountered on the shot as well as high "random" noise degrading signal-noise ratio.
- Optimizing signal bandwidth
- Accurate definition of the RMS velocity variations across the Teapot Dome field
- 3D Pre-stack Imaging
    - Algorithm selection
    - Aperture design
    - Velocity Modeling
- Post-Stack signal enhancement

These are discussed in the following sections.

A. Survey Grid

For spatial positioning purposes of the 3D survey, the grid was defined as follows.

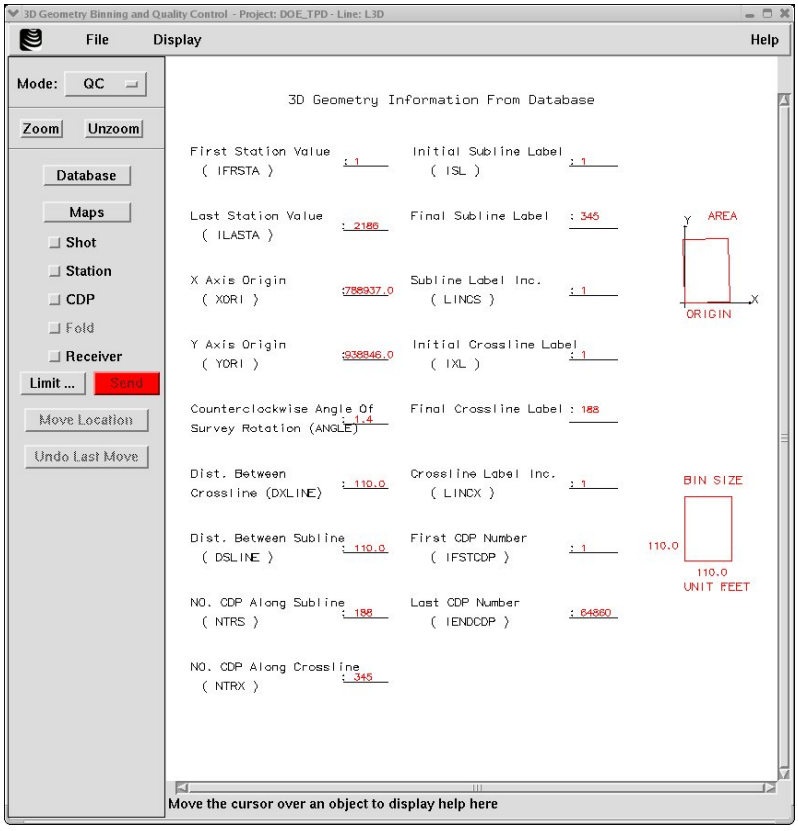

GRID: 110FT X 110FT @ 1.36DEG AZIMUTH

X	Y	ILINE	XLINE	Location
788937.0	938846.0	1	1	SW (origin)
788039.0	976675.0	345	1	NW
808603.0	977164.0	345	188	NE
809501.0	939334.0	1	188	SE

B. 3D Refraction Statics

Fusion invoked a 3D hybrid tomography solution for the 3D near surface model building stage wherein both long wavelength and higher frequency travel-time variations may be computed and removed to allow the structural detail presented in the 3D data volume to fully represent geology undistorted by near-surface variability. The near surface conditions proved to present no significant long wavelength structure-disrupting effects. However, the high frequency variations calculated and applied to the Teapot Dome 3D data did noticeably improve the stack response. The example for XL99 below illustrates the typical improvement.

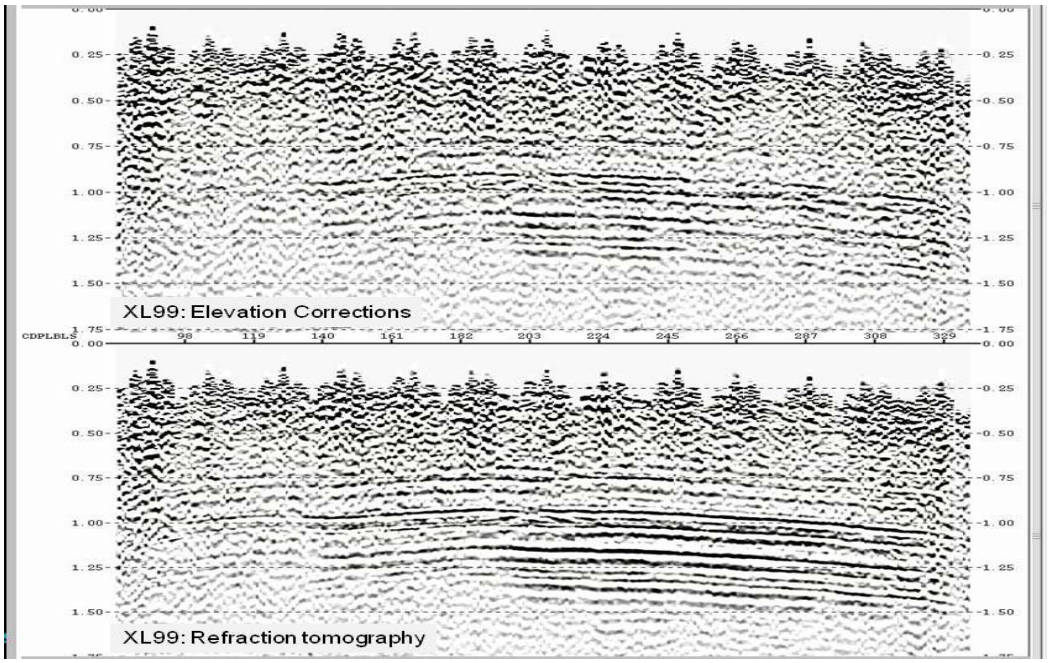

C. Coherent and Random Noise Attenuation

Ground roll of varying degrees was present with its strength and complexity appearing related to surface conditions.
Early testing indicated that a single application of LFAF (Low Frequency Array Forming) was not adequate to fully address noise removal. After a series of tests and analysis a cascaded application of Fusion's WIND workflow-based noise attenuation was adopted. WIND attempts to decompose the data ideally separating signal and noise so that a custom-designed workflow specific to the identified noise conditions can act on the noise and avoid disrupting the previously separated signal energy. Subsequent addition of the attenuated "noise" and "signal" component provides an improved output gather. Decomposition may occur in frequency, F-K or tau-p space as required. The following workflow outlines the concept as applied during the first WIND-based application to the data in the shot domain (WIND2). In this scenario, the data were decomposed into low and high frequency components with separation at 45Hz.

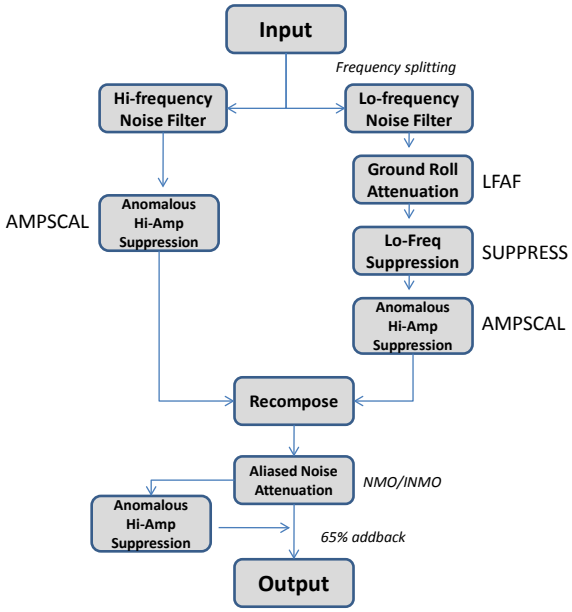

The WIND workflow leveraged several individual processes including low frequency array filtering (LFAF) designed to attenuate ground roll, band limited noise suppression (SUPPRES) separating signal and noise based on their dominant frequency components, and attenuation of anomalously high amplitudes (AMPSCAL). In combination, and custom-designed to the specific characteristics of each noise type, these processes are very effective in eliminating dominant noises and allowing useful signal energy to be maximized for subsurface evaluation.

To fully address the suite of noises identified on these data, two cascaded passes of WIND were implemented as shown in Section 5. The two passes were applied first in the shot domain addressing anomalous noisy trace edit, air blast and ground roll elimination and later in common offset domain to remove residual random noise effects before PSTM.

The effectiveness of the WIND noise attenuation workflow is demonstrated with the examples in the Images Appendix of this report.

D. Preprocessing

The initial parameter testing strategy allowed processing decisions for the following pre-processing steps to be defined:

- Spherical divergence corrections – V^2T
- 3D Surface-consistent Deconvolution - Spiking
- 3D Surface-consistent Amplitude Compensation

Goeometric spreading corrections were applied to the data using an averaged RMS velocity function to correct for the spherical divergence energy decay using a V^2T calculation.

The selected 3D surface consistent deconvolution process using a 240ms spiking operator across a band-limited frequency range provided a broader frequency spectrum (within the limits of the 8-96Hz Vibroseis sweep frequency range). This provided finer temporal resolution for later stratigraphic assessment. The spectral broadening is illustrated below.

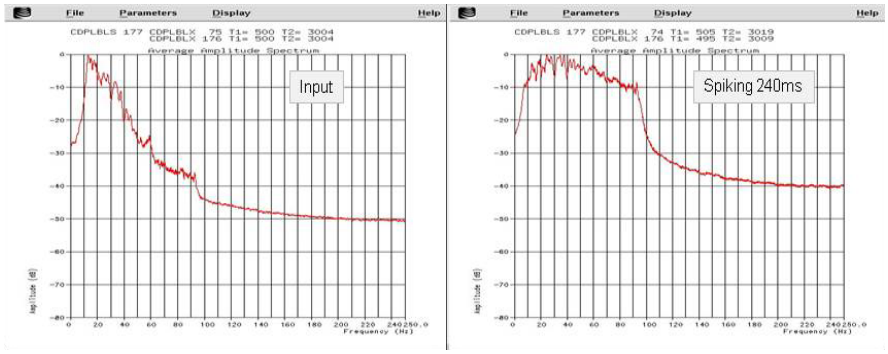

It was observed that further flattening of the spectrum was possible by applying Spectral Equalization (SPEQ) as shown below.

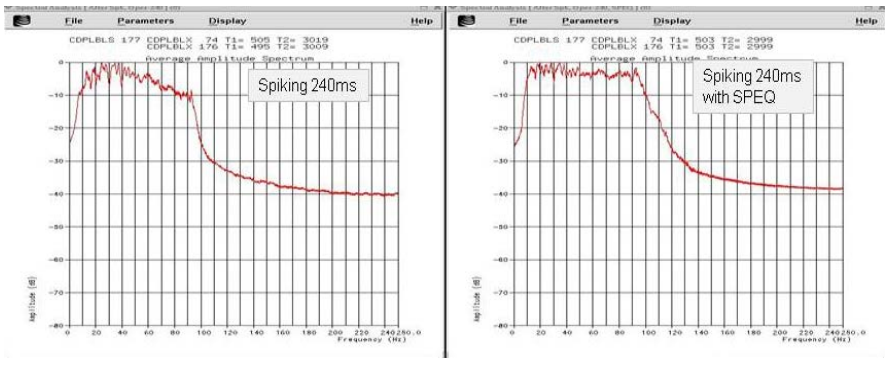

However, since stratigraphic processing using ThinMAN™ followed the PSTM imaging stage, and SPEQ was potentially disruptive to the this broadband spectral inversion process, both a

SPEQ CMP gather volume and a non-SPEQ CMP gather volume were made available as deliverables from this imaging Task stage.

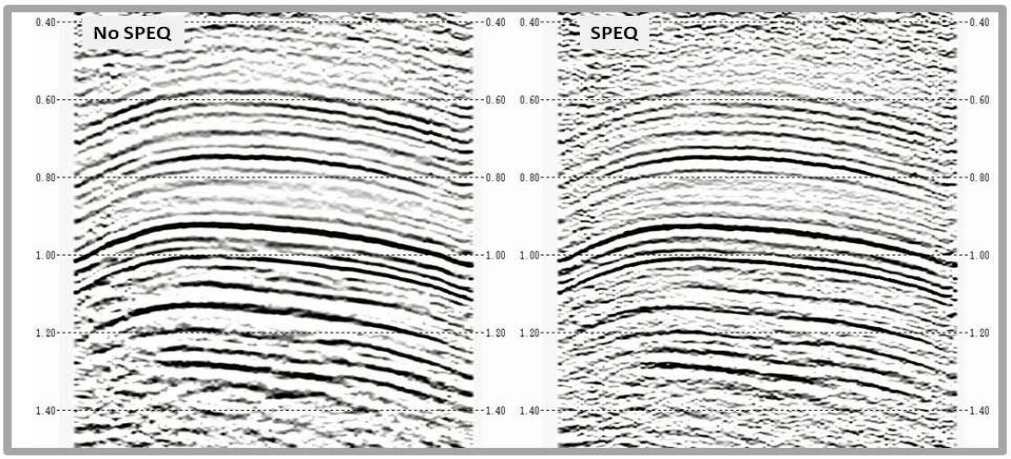

To stabilize amplitude relationships within the data volume and to correct for surface-related coupling effects and/or variations in the strength of the energy source, 3D surface consistent amplitude compensation (SCAC) was applied. This ensured that the amplitude energy level for all sources was at the same level as well as at each receiver location on the surface. This stabilized amplitudes without the need for AGC-type scaling processes that may disrupt internal amplitude relationships associated with subsurface reflectivity variations.

E. Velocity

After initial velocity analyses were generated every 0.5 miles, an initial velocity model provided the basis for a first pass of 3D reflection residual statics. An additional suite of velocity analyses at 0.5 mile after 3D residual reflection statics were estimated and applied to further tune the stacking velocity model. Within the limited areal extent of the survey the velocity field demonstrated good stability and subsequent testing with additional velocity tools indicated a good general fit across the area and a suitable basis for developing an accurate PSTM velocity model. The smoothed stacking velocity model was used to generate a 3D PSTM volume with PSTM gathers generated. Inspection of the 3D SPTM volume and associated gathers, however, indicated that a further RMS velocity estimation stage would provide further improvement especially in the shallower section. After picking a revised RMS velocity field from PSTM velocity analyses, the final curved ray PSTM volume was generated. Residual moveout corrections and CDP-based trim statics removed minor local remnant variations and provided a final PSTM volume with excellent stack response.

F. Regularization and Binning via 3D Interpolation

While CDP fold was relatively stable albeit weighted to the center of the 3D area due to the nature of the acquisition geometry, it was decided to assess the potential of 3D regularization using 3D interpolation methods applied in the common offset domain before migration. The effect was to stabilize trace contribution for PSTM purposes. The results as seen below provided improvement in data stability and improved continuity in the shallow section. As a result, both interpolated and un-interpolated volumes were produced with the interpolated CMP gather volume used for primary 3D pre-stack imaging.

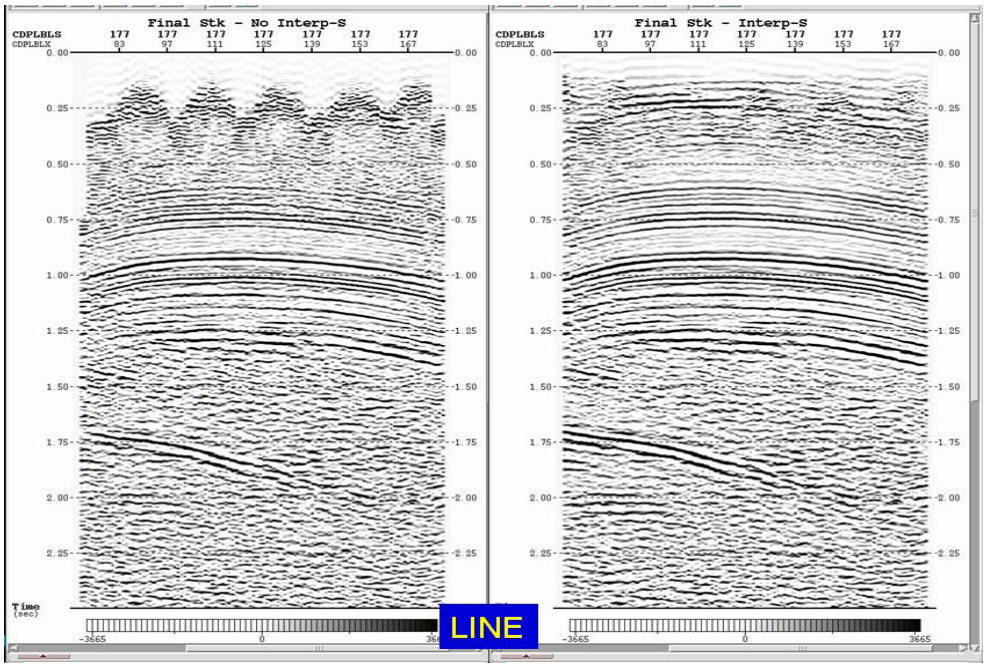

CMP Stack without (left) and with 3D interpolation (right)

G. Pre-Stack Time Migration Parameterization

Following assessment and QC of average input fold (48) and various group offset fold distribution plots, it was decided to utilize 27 output offsets at 440ft intervals centered on 220-11660ft for PSTM purposes.

Initial testing with opening and final angles of 30 and 60 degrees exhibited excessive migration noise in the shallow section. As a result, after follow-up tests, a 15 degree opening angle and 30 degree outside angle was selected with 10000ft aperture radius. This limited migration noise and provided effective 3D image focusing. The final impulse response is shown below.

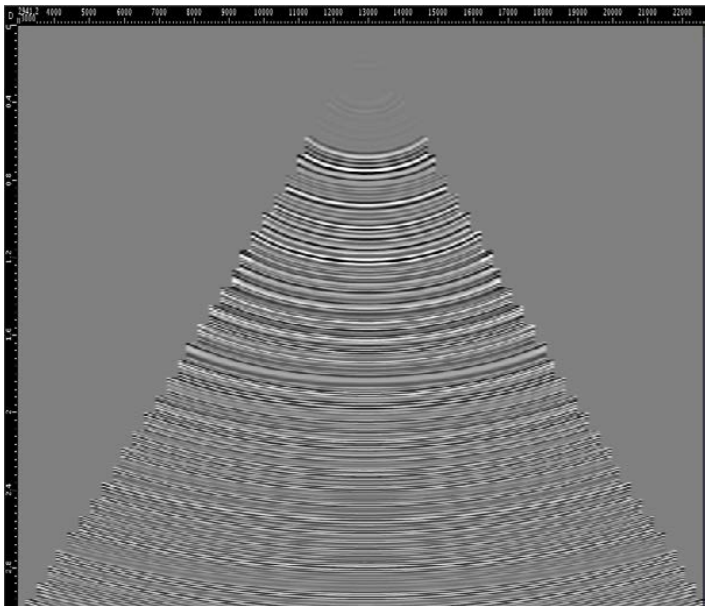

Since the curved ray PSTM velocity model required a smooth interval velocity for ray tracing purposes, the RMS velocity field derived from 3D stacking velocities was smoothed laterally and temporally.

H. Post-PSTM Processing

Residual Normal Moveout (RMO):
Semblance-based residual velocity analyses were generated every output PSTM gather location. Maximum allowable residual velocity was constrained to +/-30% of the starting velocity and spatial smoothing implemented to the output residual velocity field with a 900m radius around each bin. Temporal gate width for smoothing was 100ms. RMO was applied to the PSTM gathers using this smoothed residual velocity field. An output gather data set was generated for archival purposes

Pre-Stack Muting of PSTM Stack Volume
Although a single mute was used, its selection was particularly critical to optimize the shallow section.

Offset	Time
110	0ms
1430	296ms
2090	512ms
6050	768ms
8030	1082ms
10010	1298ms
13310	1614ms

As a result of above testing, pre-stack processing of PSTM gathers was as follows:
Residual normal moveout
Pre-stack Mute

After PSTM gather data were muted and stacked, post-stack processes were as follows:
FX-FY Deconvolution-based WIND workflow
Spectral Equalization
Time-variant Bandpass Filtering

3D FXY Deconvolution
Testing of varying filter lengths (3, 5, and 7) indicated little difference between the varying filter lengths while 50% or greater addback provided a balanced improvement. 7pt filter and 60% addback were selected.

Time-variant Bandpass Filtering

Two-way Time	F0(Hz)	F100	F100	F0
0.0 – 0.3 secs	20	30	70	80
0.35 - Tmax	10	20	70	80

8. Depth Processing

3D Pre-Stack Depth Migration (PSDM) was undertaken to provide a data volume that could most effectively tied to wells for the later reservoir-related stages of the CO2 MVA program. A typical workflow utilizes the following approach

- Velocity Model Building: Vint-Z from PSTM-derived RMS-Time field
- Iterative Pre-stack Depth Migration with 3-D Tomographic Updating.
- Model Building and Velocity Update: at each iteration stage.
- Final Pre-stack Depth Migration
  - 20 degree opening, 50 degree final angle
  - 20000ft aperture
  - 40 output offset bins, 330ft spacing
  - 10ft depth step
- Residual NMO: applied to all depth gathers.
- Gather Mute and Stack
- Convert from Depth to Time, using final velocity field (if required)
- Post migration processes
- Output SEG Y PSDM Gathers and Volume

Graphically, each PSDM iteration may be described as follows to allow the process to converge on an accurate Vin-Z model for the final PSDM migration.

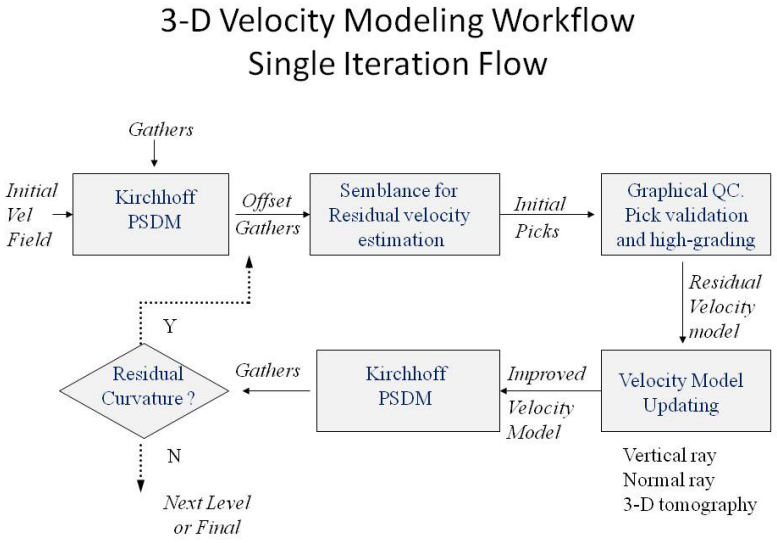

For velocity model updating at each stage, a 3D tomography process is employed that back-projected residual velocity estimates derived from CIG gathers from the previous stage to update the overlying velocity environment. The method is outlined as follows:

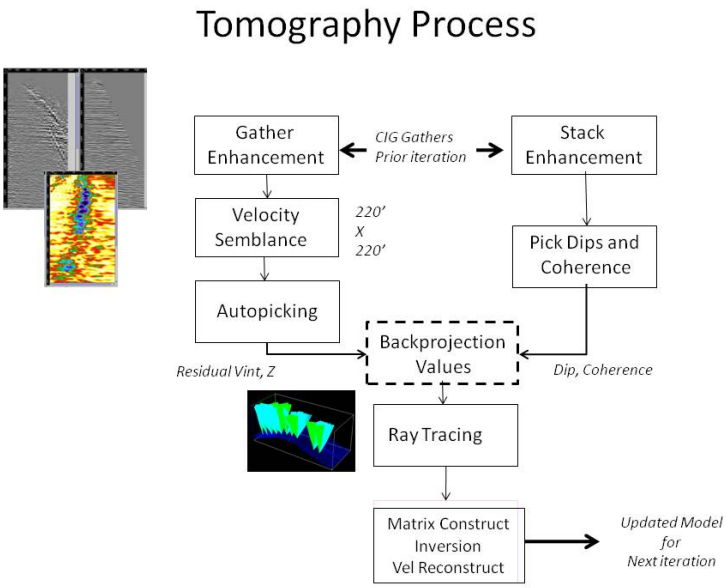

The Teapot Dome iterative process was simplified by the limited areal extent of the data volume and the geologic column extending only to around 7000ft. As a result, a stable velocity regime required minimal updating for the velocity model to converge on a final model. The following two example common image gathers exhibit only minor residual changes to attain the desired gather flatness. Minor depth changes can be observed as the velocity model updated and minor improved focusing of gather reflectors can also be observed.

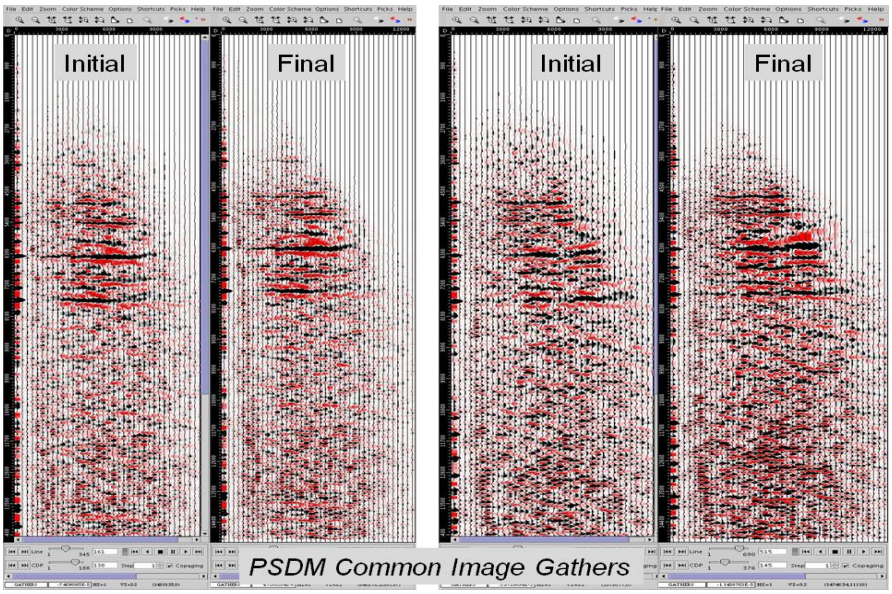

9. Summary and Conclusions

The processing of the Teapot Dome 3D data delivered a high quality pre-stack imaged data base in both two-way-time and depth for the continuing stages of the CO2 MVA project. No major problems were encountered during the project and the primary emphasis was assuring the amplitude integrity and frequency resolution of the data for the subsequent attribute and modeling stages.

3D refraction modeling using Fusion's Seismic Studio™ system provided a three-dimensional near surface model that removed any possible long-wavelength or high frequency near-surface travel time distortions. It noticeably improved stack response of the data versus a basic elevation-based correction. Coherent noise energy was effectively removed using Fusion's WIND noise attenuation workflow allowing later processes such as deconvolution to be more properly designed on valid signal energy without noise contaminating the design. The use of 3D surface-consistent processes provided robust design of deconvolution filters and also allowed amplitude variations associated with differing near-surface conditions, source and or receiver coupling problems etc to be corrected without damaging the integrity of the seismic amplitudes containing valid subsurface stratigraphic and/or fluid content information. Two passes of 3D surface consistent reflection residual statics removed minor high-frequency near surface-related travel-time variations before the detailed 3D velocity estimation stage.

The geologic column of interest only extended to around 7000ft and with offsets extending to greater than 13000ft, RMS velocity estimates could be accurately determined using one-half mile spacing. While velocity variation across the Teapot Dome 3D area proved to be stable, it was noted that an additional one-half mile grid generated after PSTM did improve the stability of the velocity model and, hence, the PSTM result and the final PSTM stack.

Within the limits of the 8-96 Hz Vibroseis sweep frequency range, a broadband spectrum was achieved. Consistent with the expectations of later processes, a volume with and without spectral equalization before stack was produced. Post-processed imaging volumes with spectral equalization applied were generated. Amplitude fidelity was preserved wherever possible and no processes likely to distort the temporal or offset amplitude relationships were applied.

Pre-stack imaging in both time and depth indicated a slowly varying velocity model laterally and consistent with vertical velocity relationships. The 3D area was elongate along the crest of the anticline with the narrower E-W dimension in the dominant dip direction. It was noted, therefore, that, after 3D migration, the anticlinal feature was compressed and, as energy migrated in the generally E-W updip direction, there was loss of useful information at the edges of the survey. The original 3D design with limited E-W aperture limited the useful fully migrated 3D area available for analysis. From observation of the time and depth slices through the final 3D volumes, however, a clearly focused 3D image emerged over the center of the interest area.

10. Fusion Personnel

Houston Processing,

Todd Hibbitts, Senior Processing Geophysicist, Time Processing
Carmen Lupascu, Processing Geophysicist, Time Imaging
Mihai Popovici, Chief Geophysicist, Depth Imaging

Final Report

for
U.S. Department of Energy

INTEGRATED REFLECTION SEISMIC MONITORING AND RESERVOIR MODELING FOR GEOLOGIC CO2 SEQUESTRATION
Phase 1 Task 3.0

Appendix: Images

Images

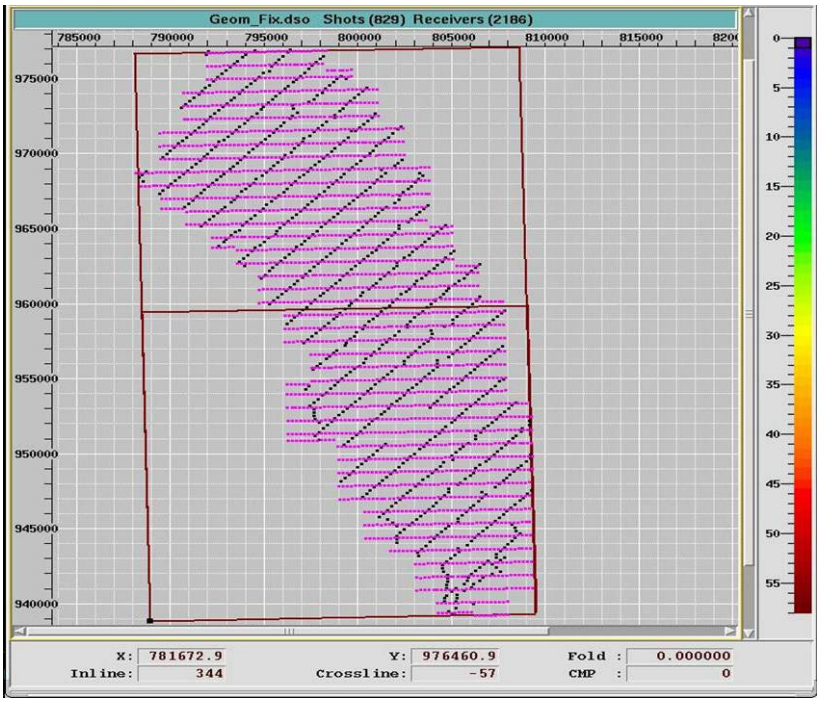

Map: Source-Receiver Locations

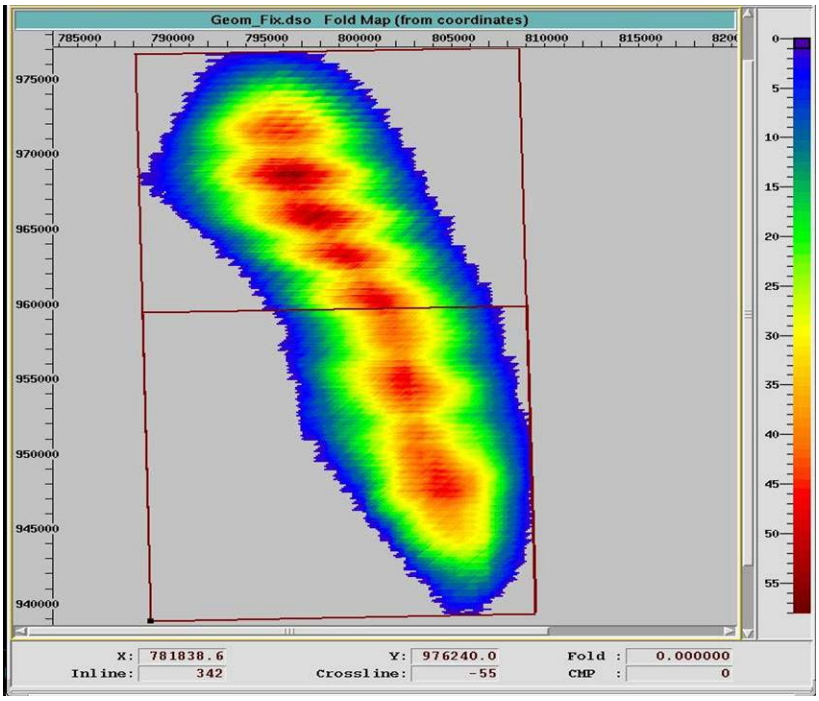

Map: CDP Fold Distribution

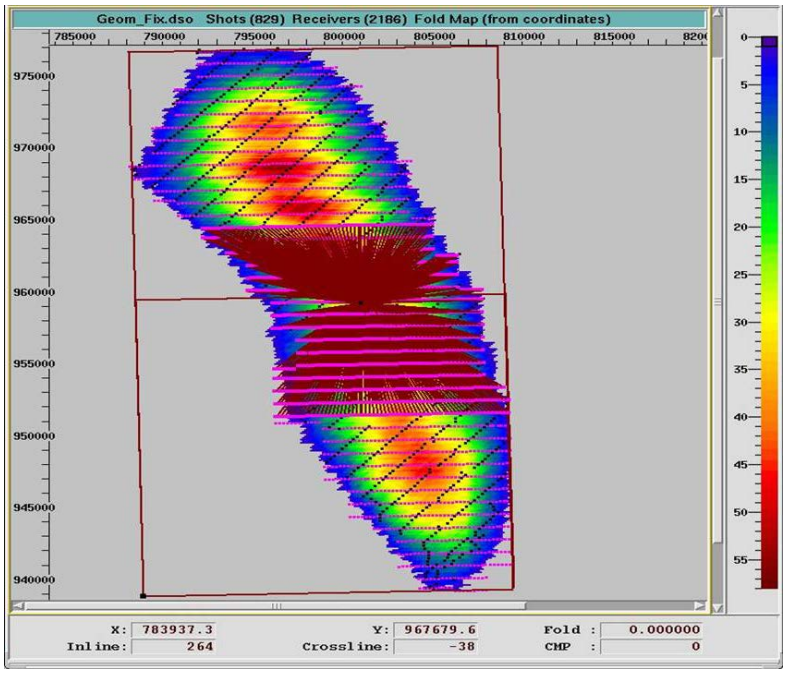

Map: Example Source-Receiver Layout

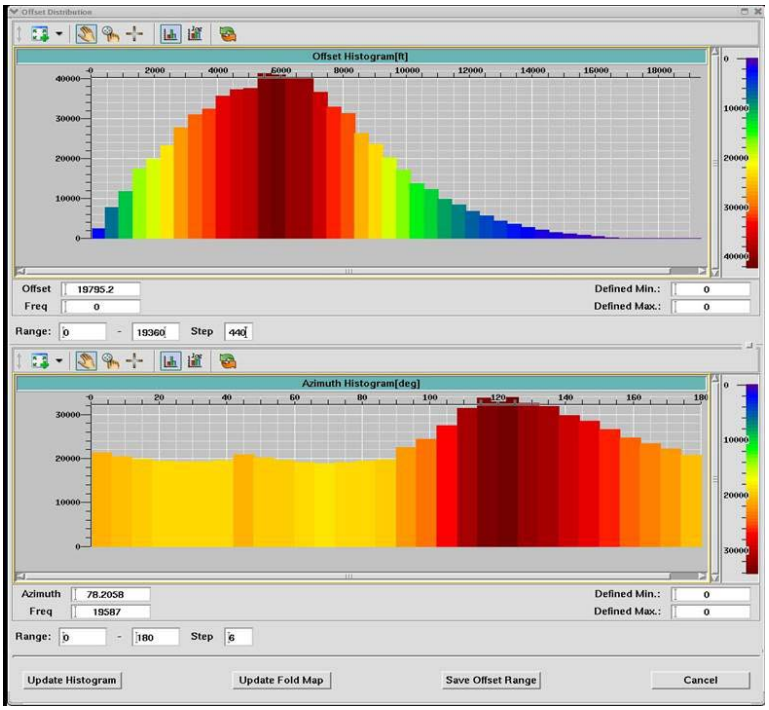

Offset (top) and Azimuth (bottom) Distribution

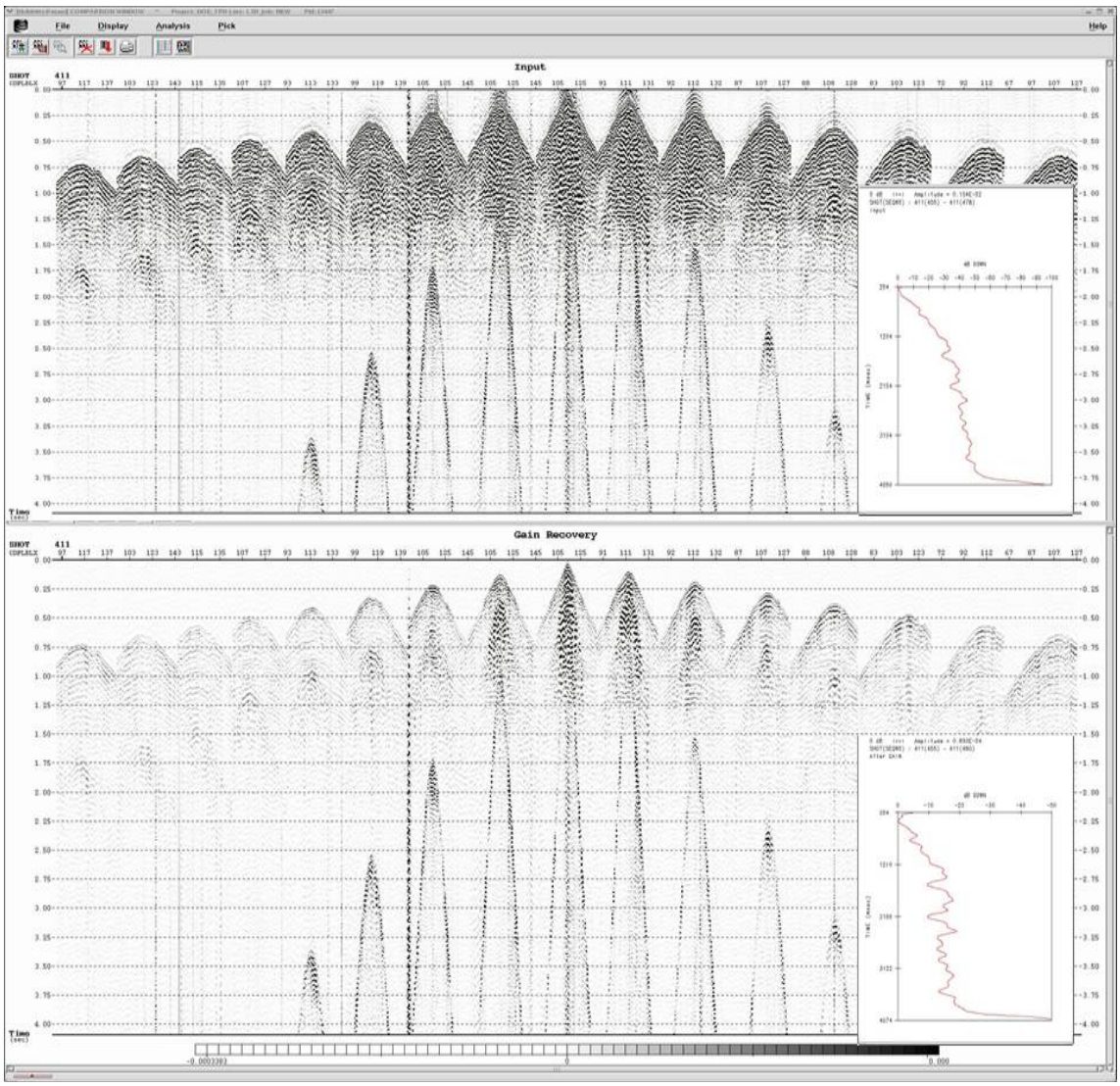

Before and After V^2T Geometric Spreading Corrections

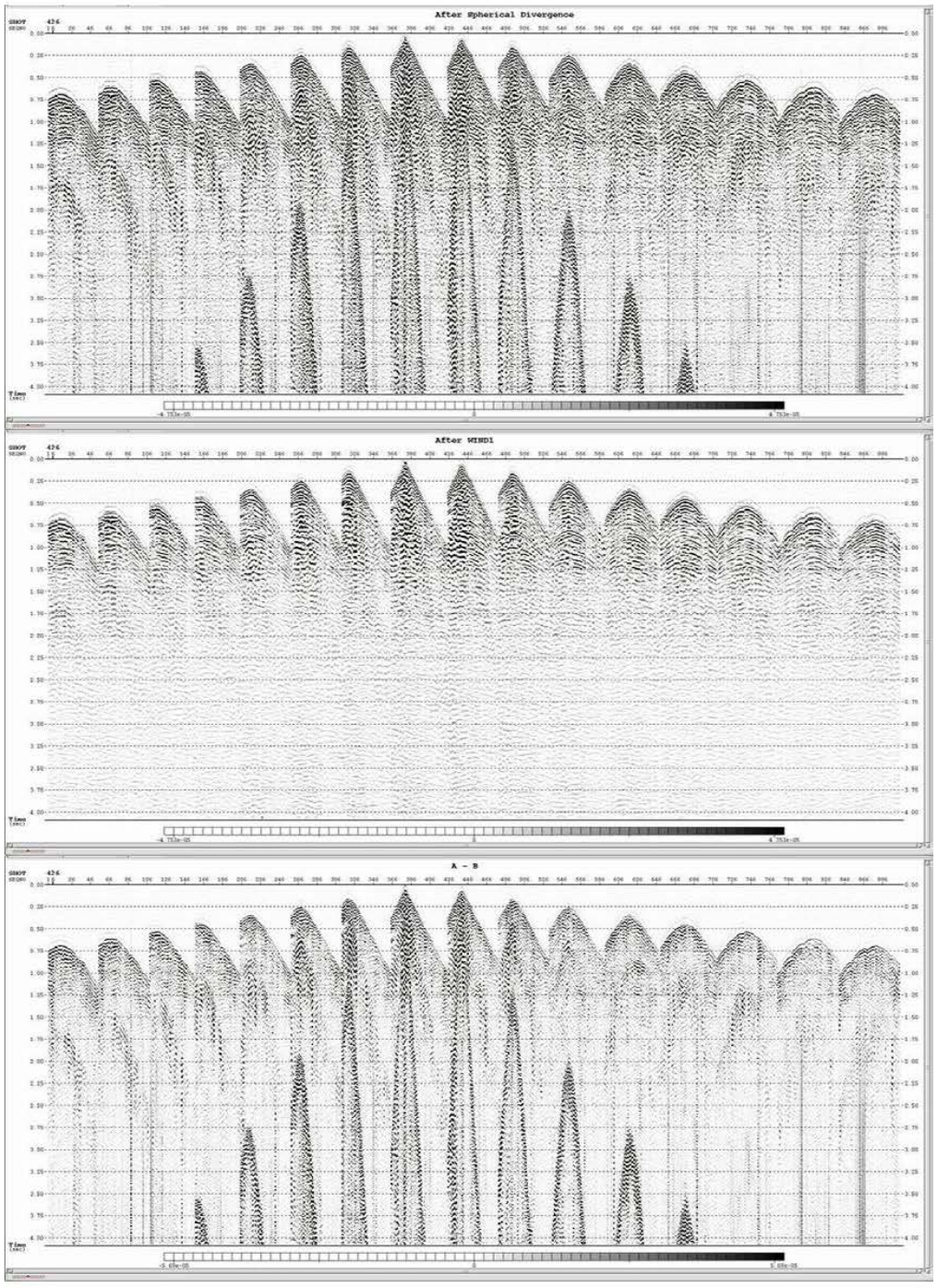

Noise Attenuation (WIND workflow): Before (top), After (middle), Difference (bottom)

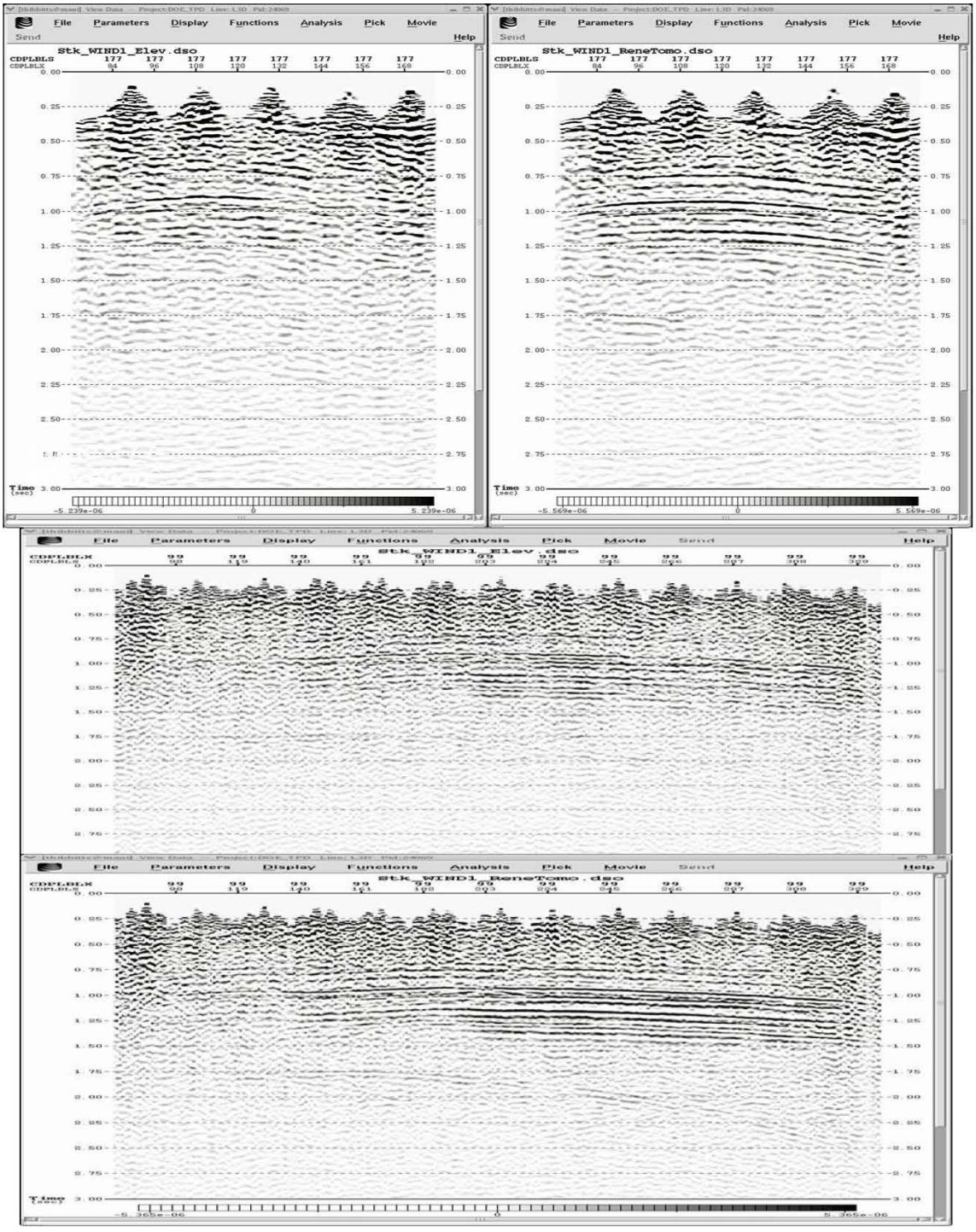

Before and After 3D Refraction Statics solution: Top – Crossline, Bottom - Inline

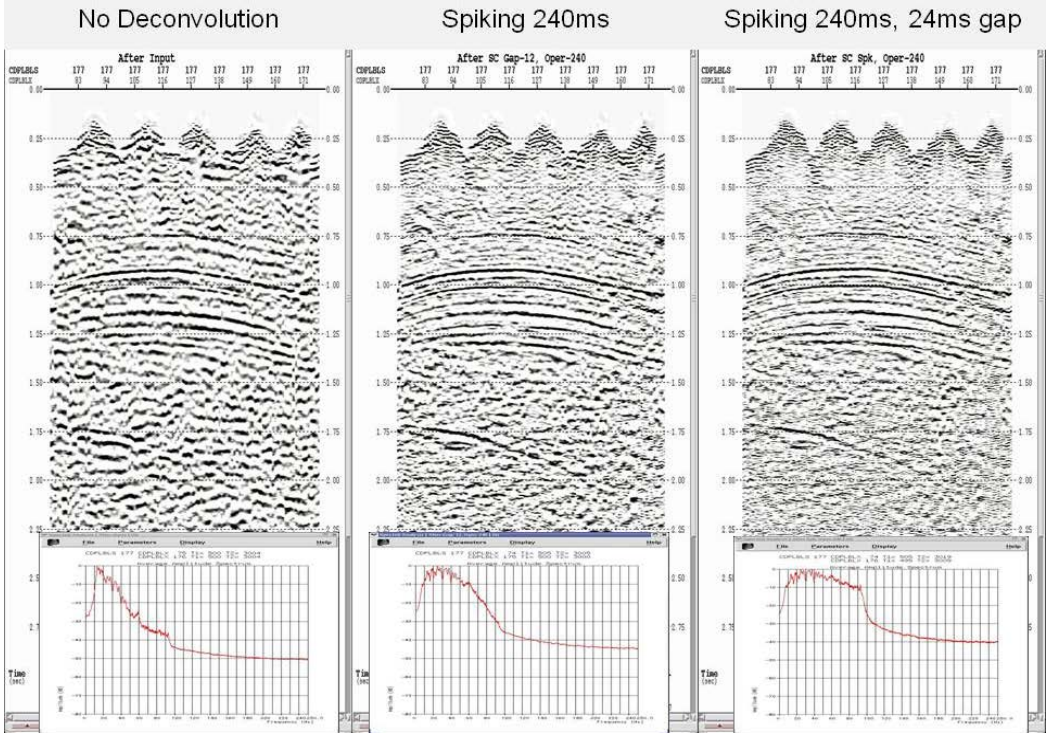

Subset of Deconvolution test applications with Power Spectra (240ms Spiking was selected)

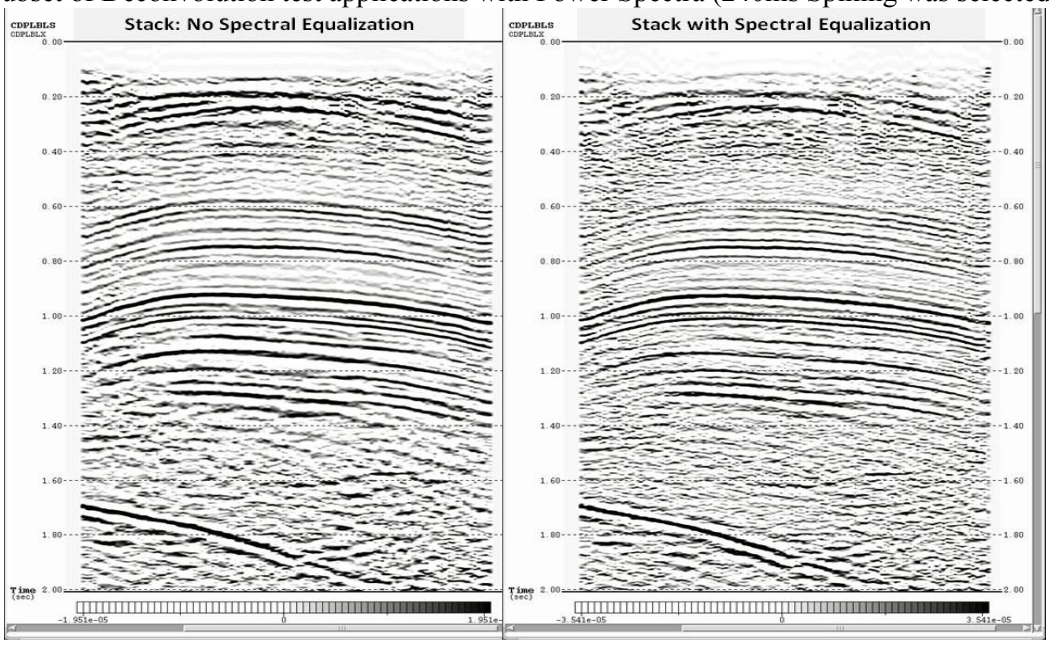

Example Inline without and with Spectral Equalization

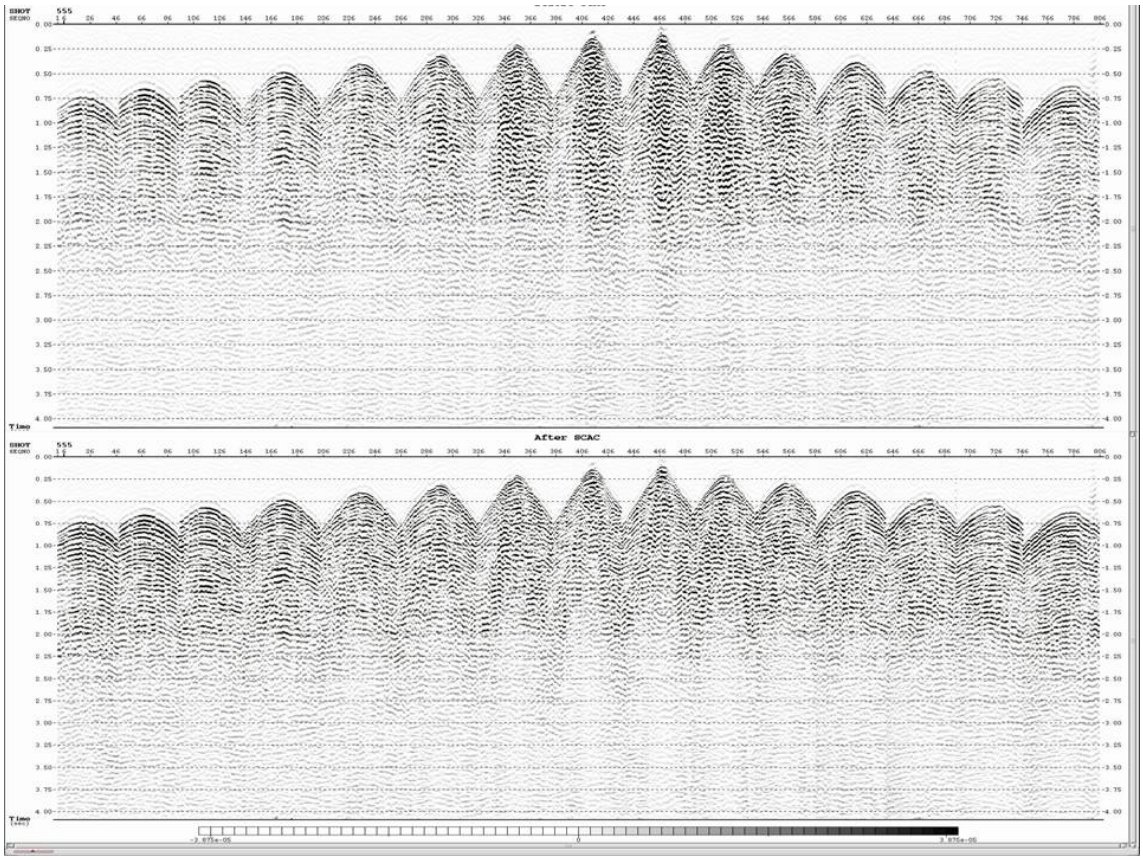

Example Shot: Before and After 3D Surface Consistent Amplitude Compensation

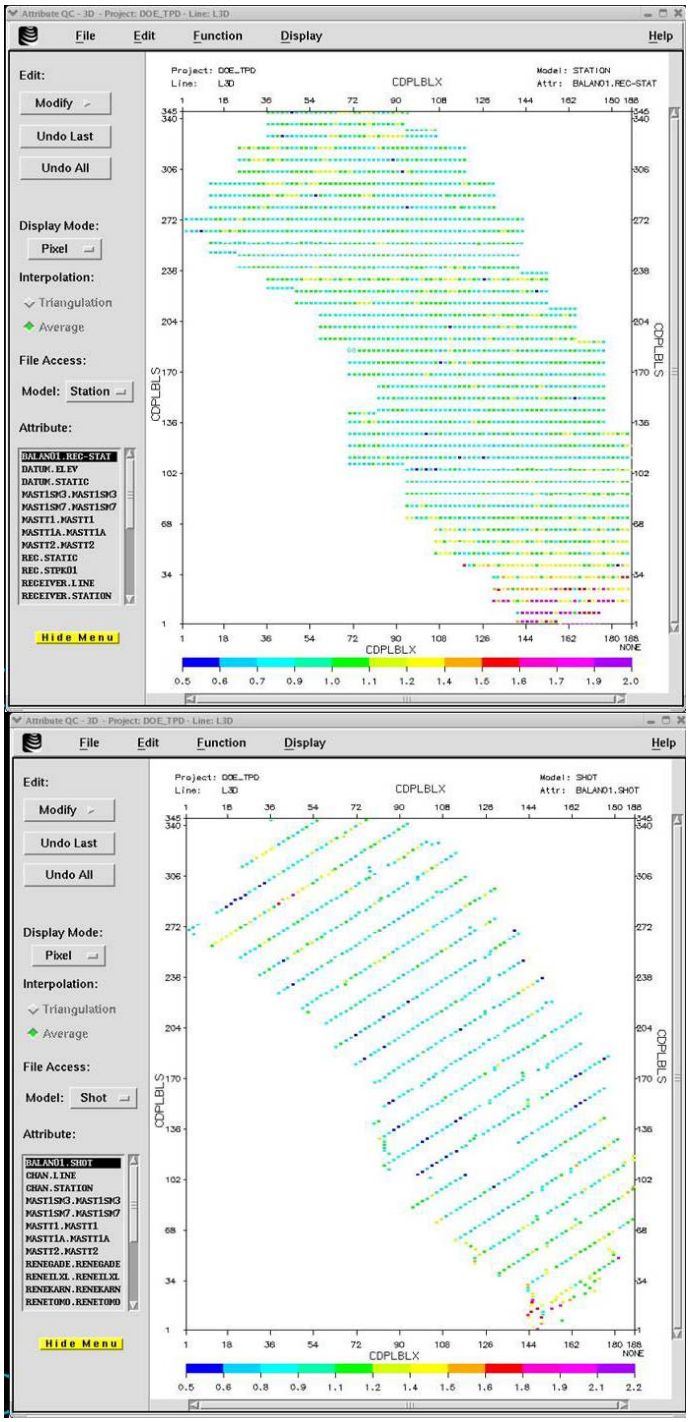

Calculated 3D Surface Consistent Scalars: Receiver (top), Shot (bottom)

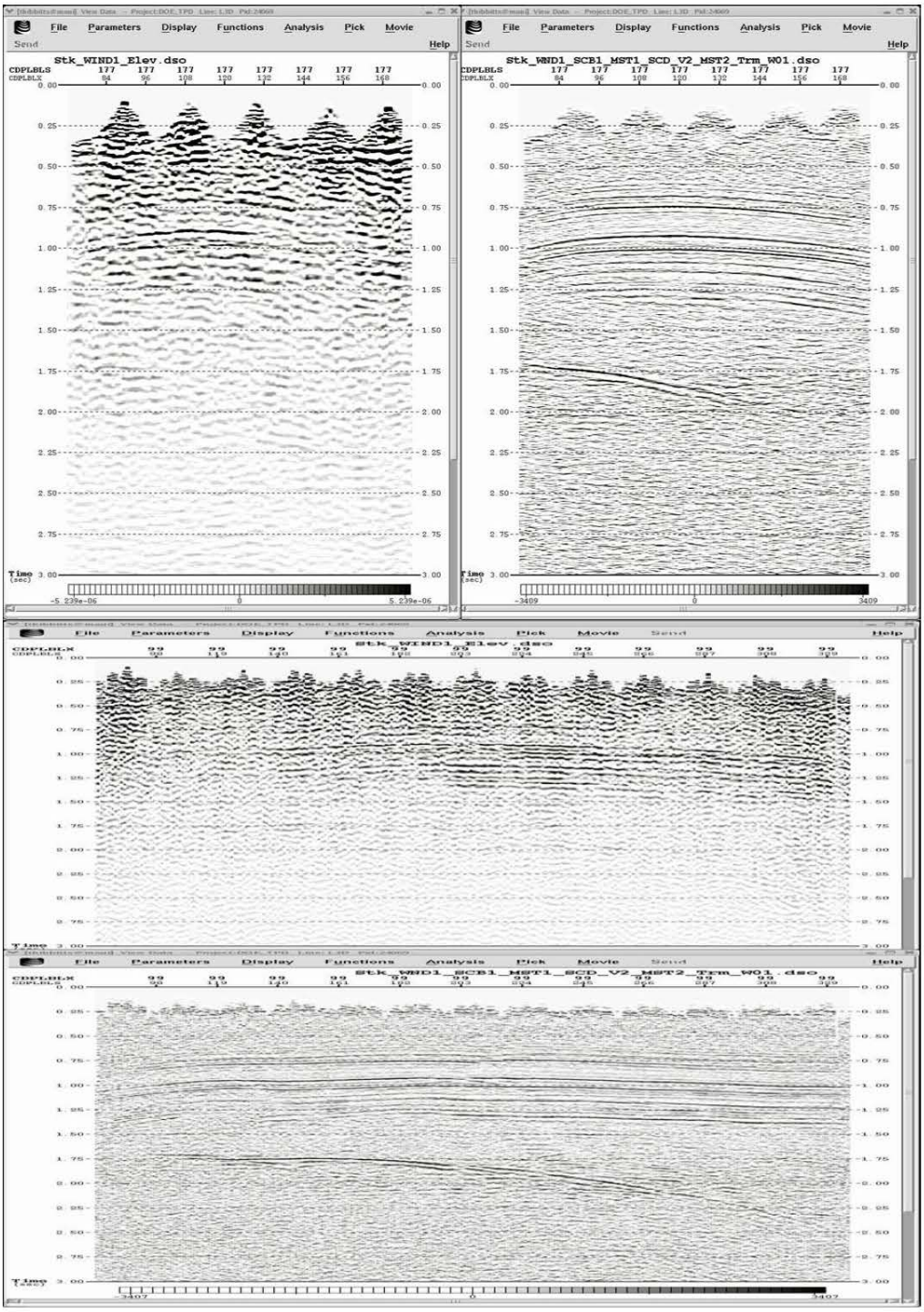

From Initial Stack to Final CDP Stack: Crossline (top), Inline (bottom)

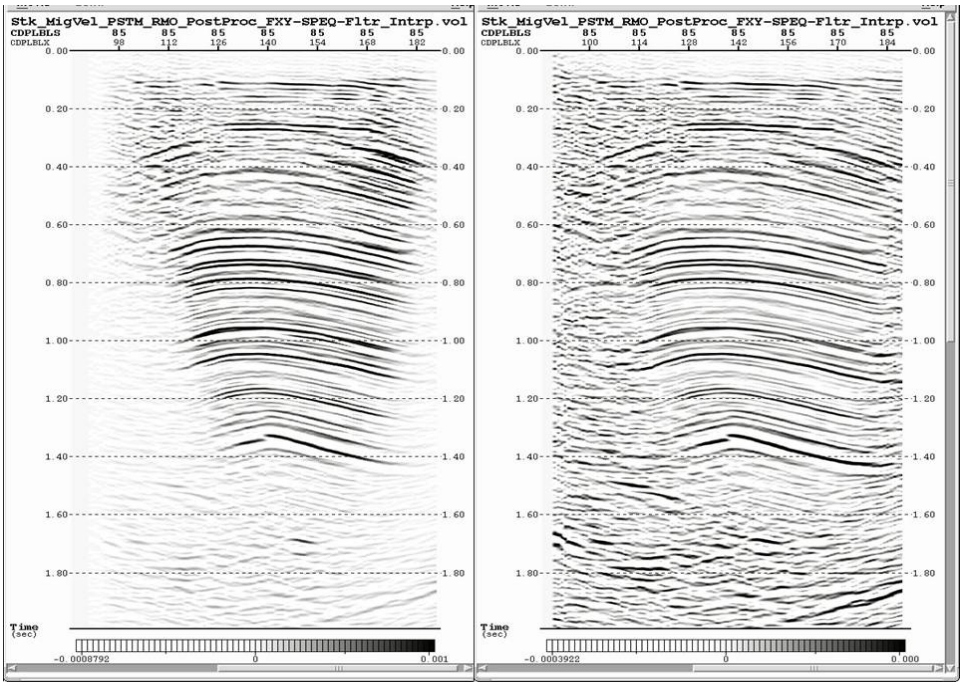

Inline 85: PSTM without and with post-processing

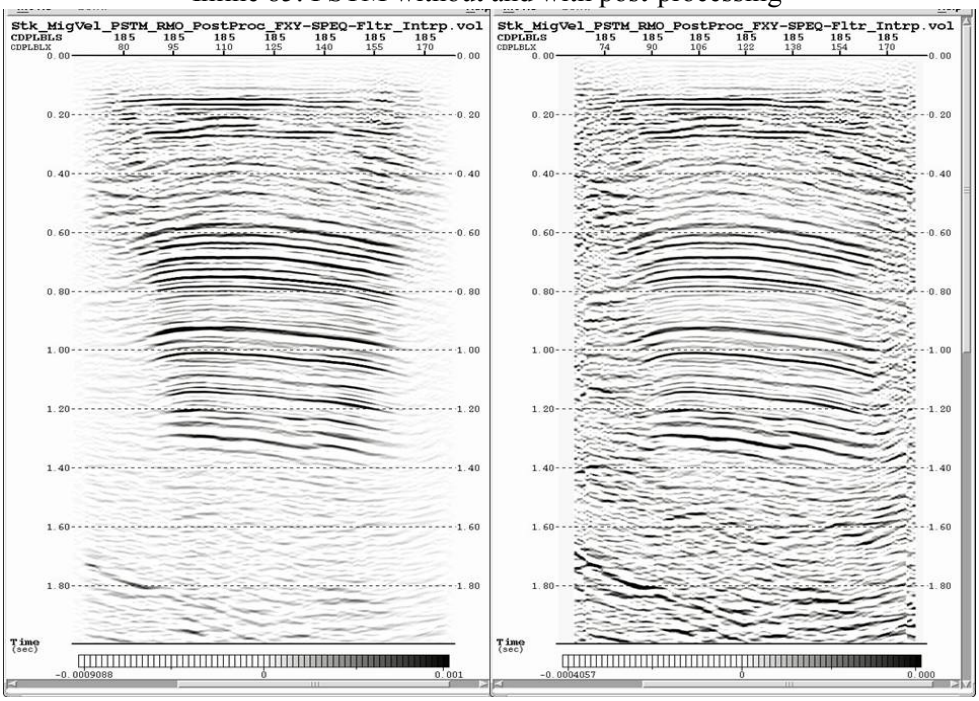

Inline 185: PSTM without and with post-processing

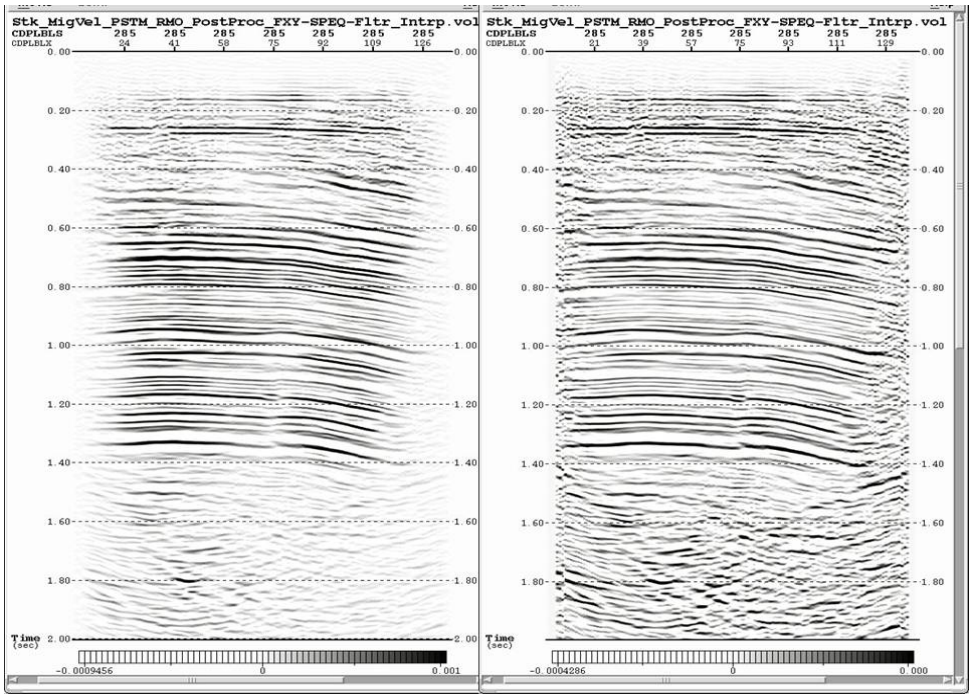

Inline 285: PSTM without and with post-processing

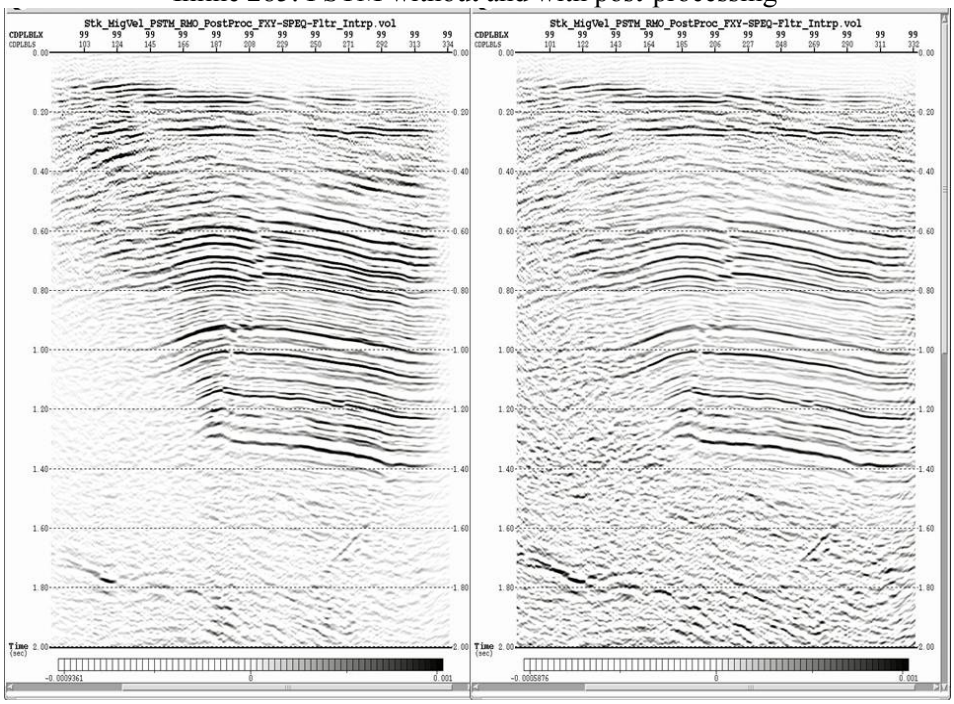

Crossline 99: PSTM without and with post-processing

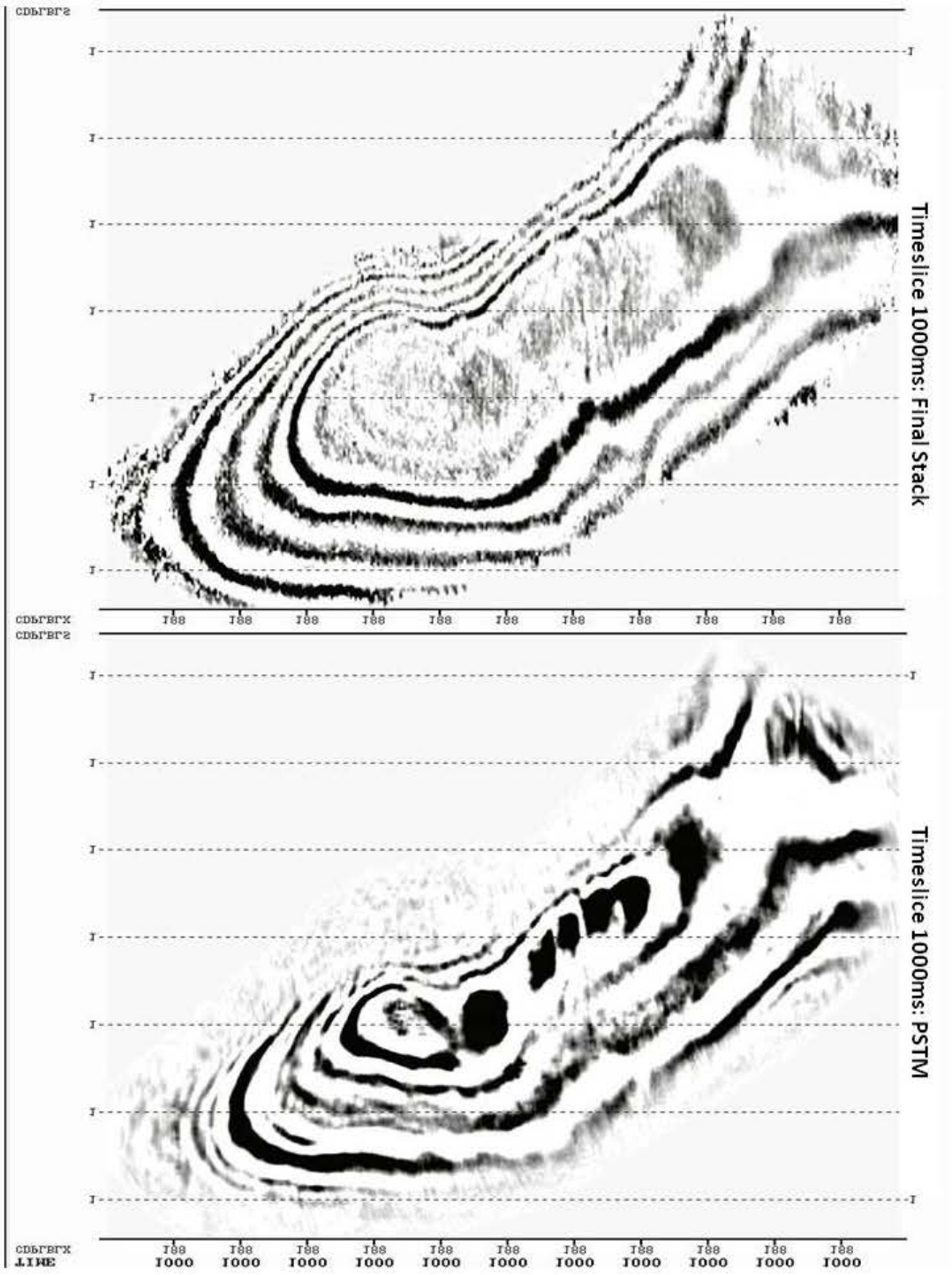

Timeslice 1000ms: Final Stack versus Final PSTM

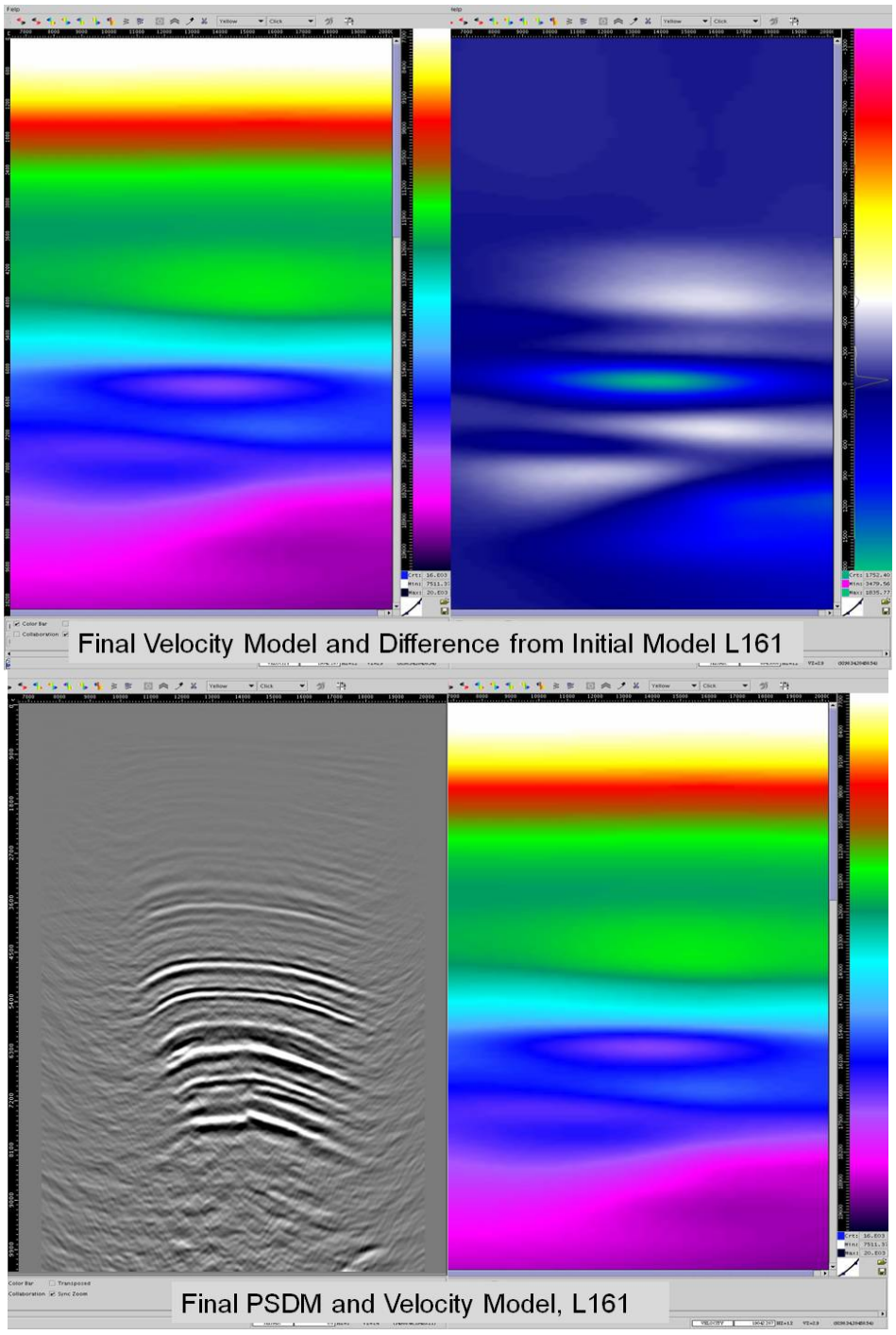

Final PSDM (no post-processing) with Velocity Model: Inline 161

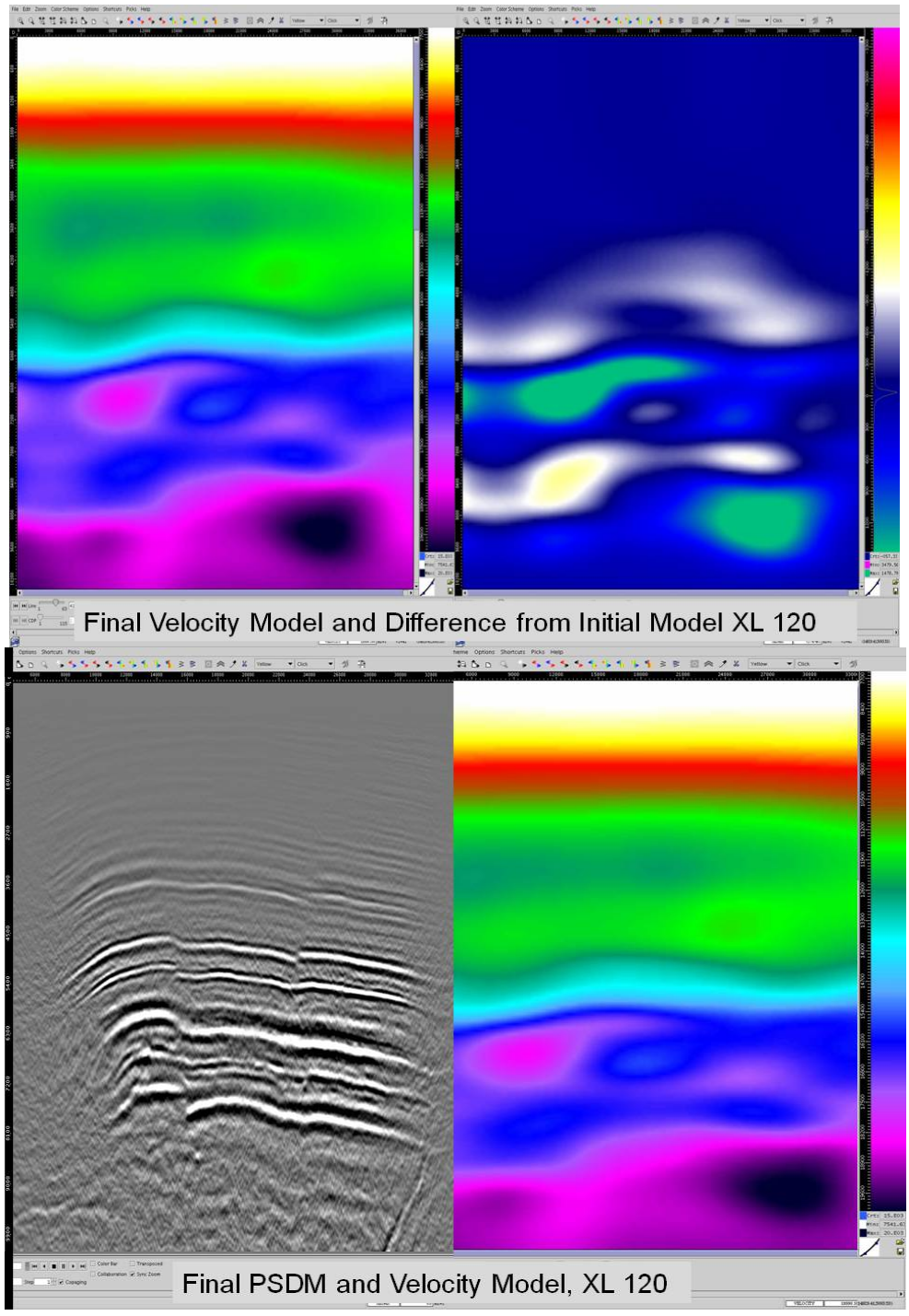

Final PSDM (no post-processing) with Velocity Model: Crossline 120

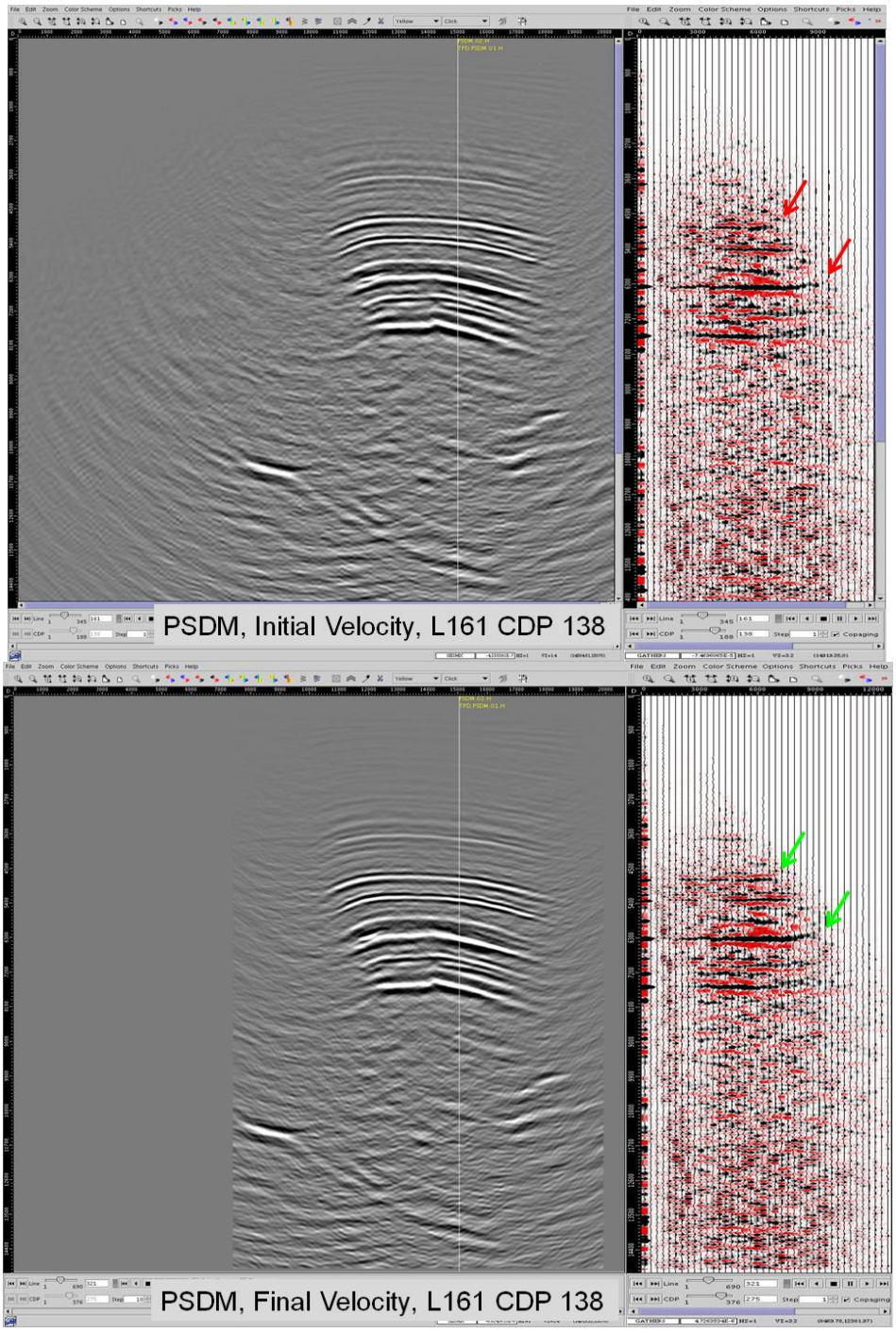

Initial and Final PSDM with Selected Common Image Gather: Inline 161

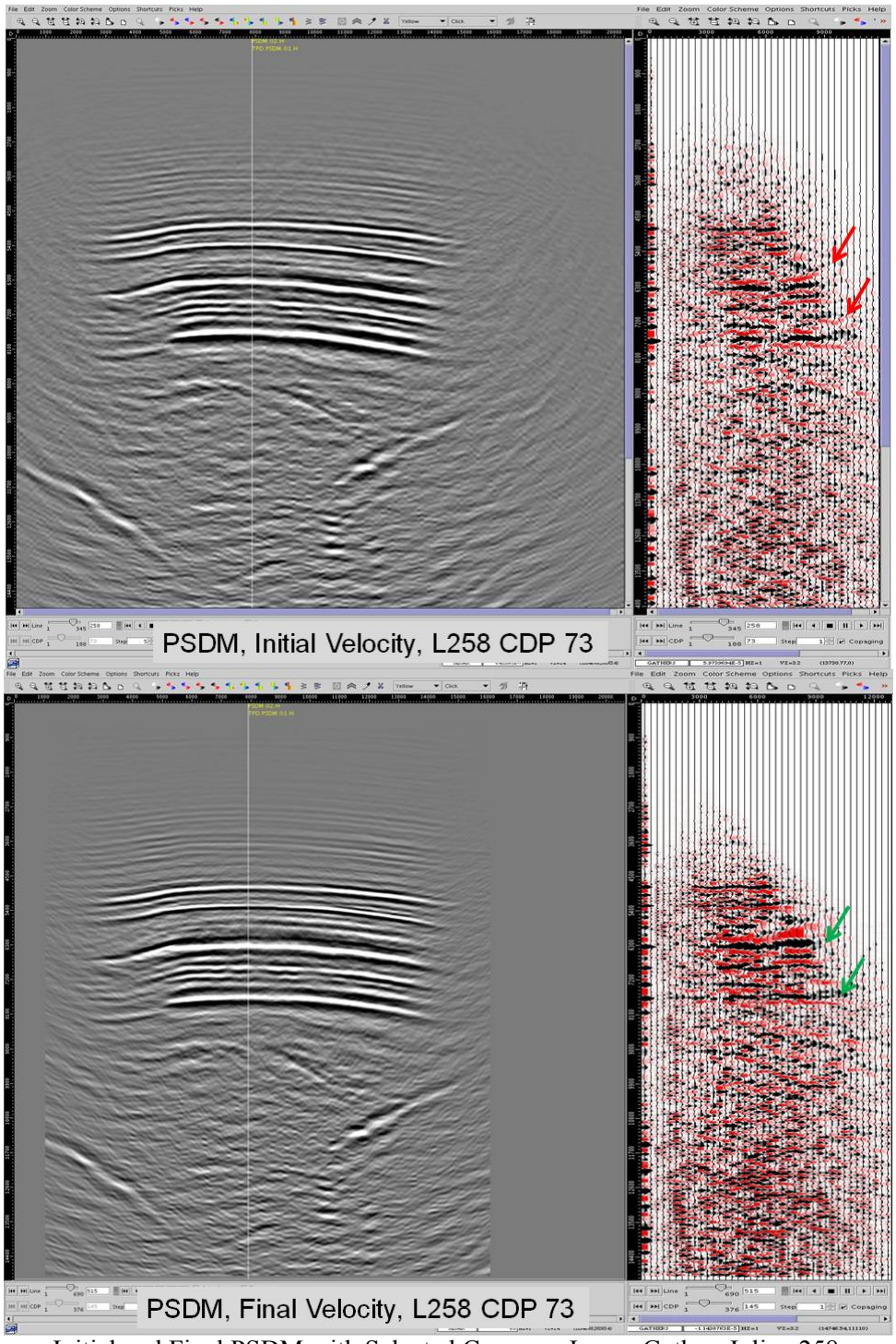

Initial and Final PSDM with Selected Common Image Gather: Inline 258

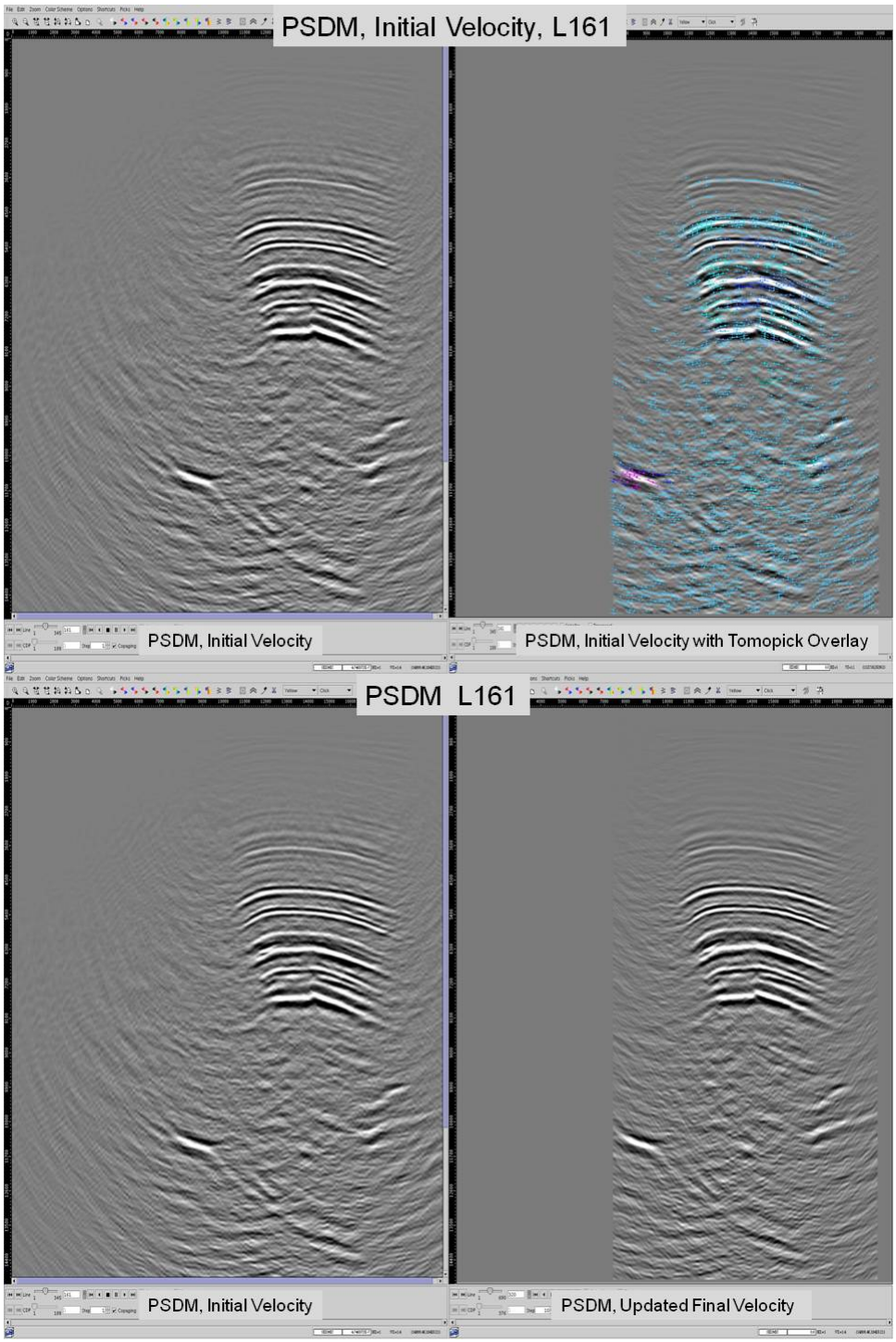

From Initial to Final Velocity showing tomography pick locations for back-projection: Inline 161

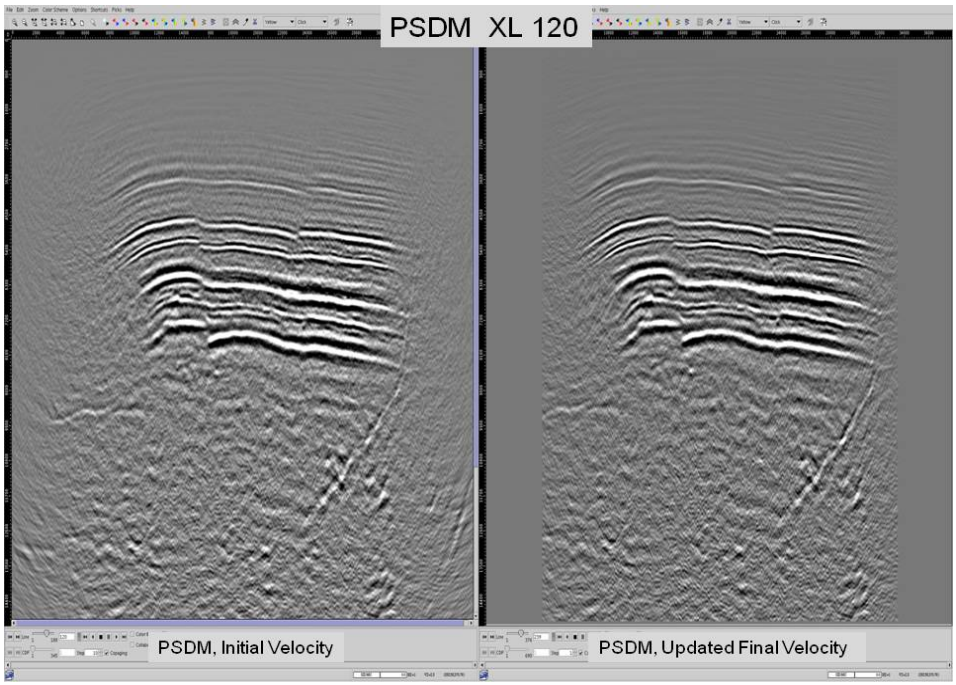

From Initial to Final PSDM: Inline 161 (no post-processing)

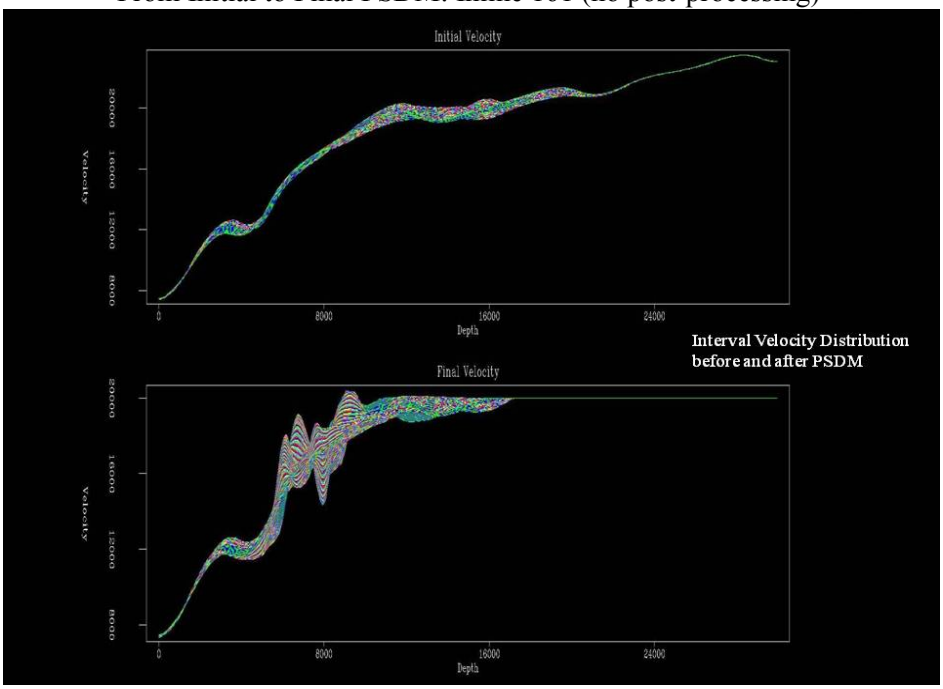

Interval Velocity Distribution before and after PSDM

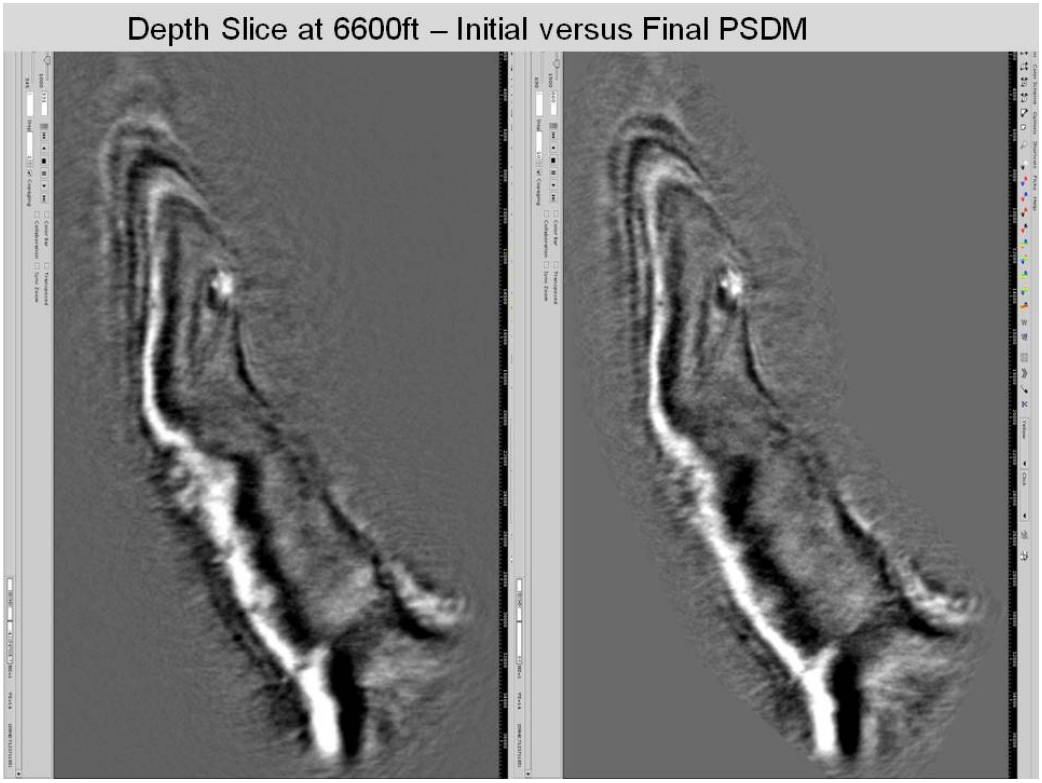

Depthslice @ 6600ft from Initial to Final PSDM (no post-processing)

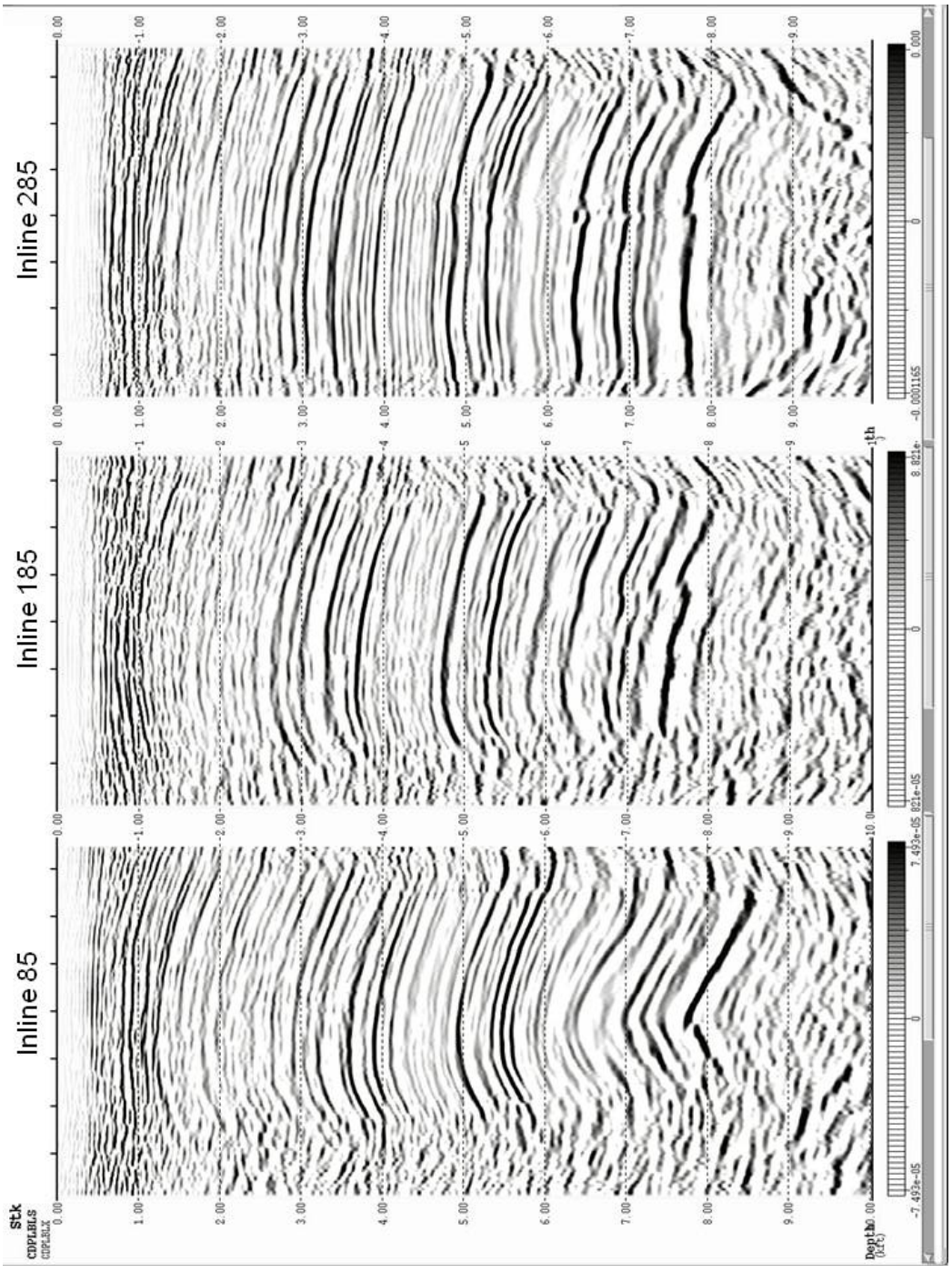

Final PSDM with Post-Processing: Inlines 85, 185, 285

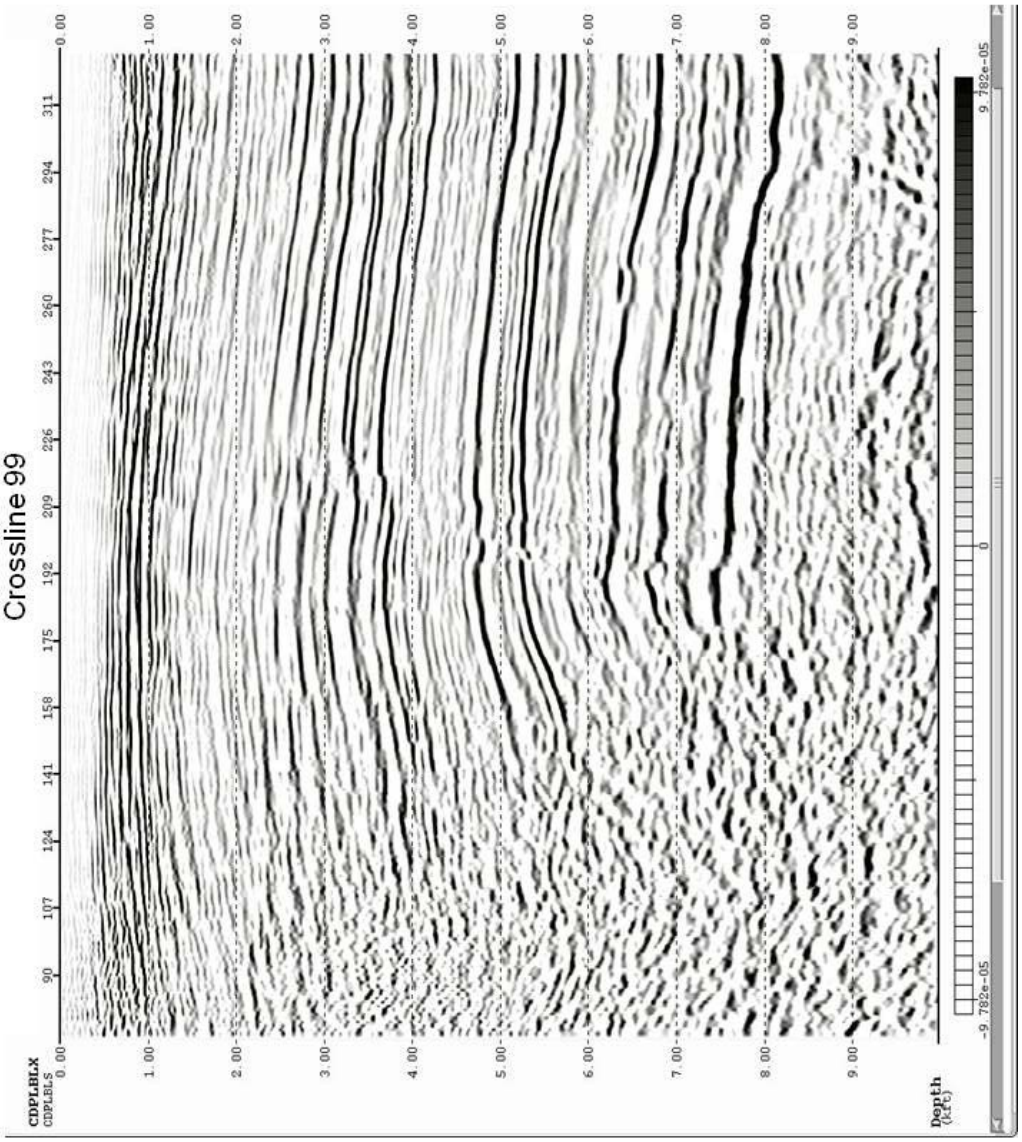

Final PSDM with Post-Processing: Crossline 99

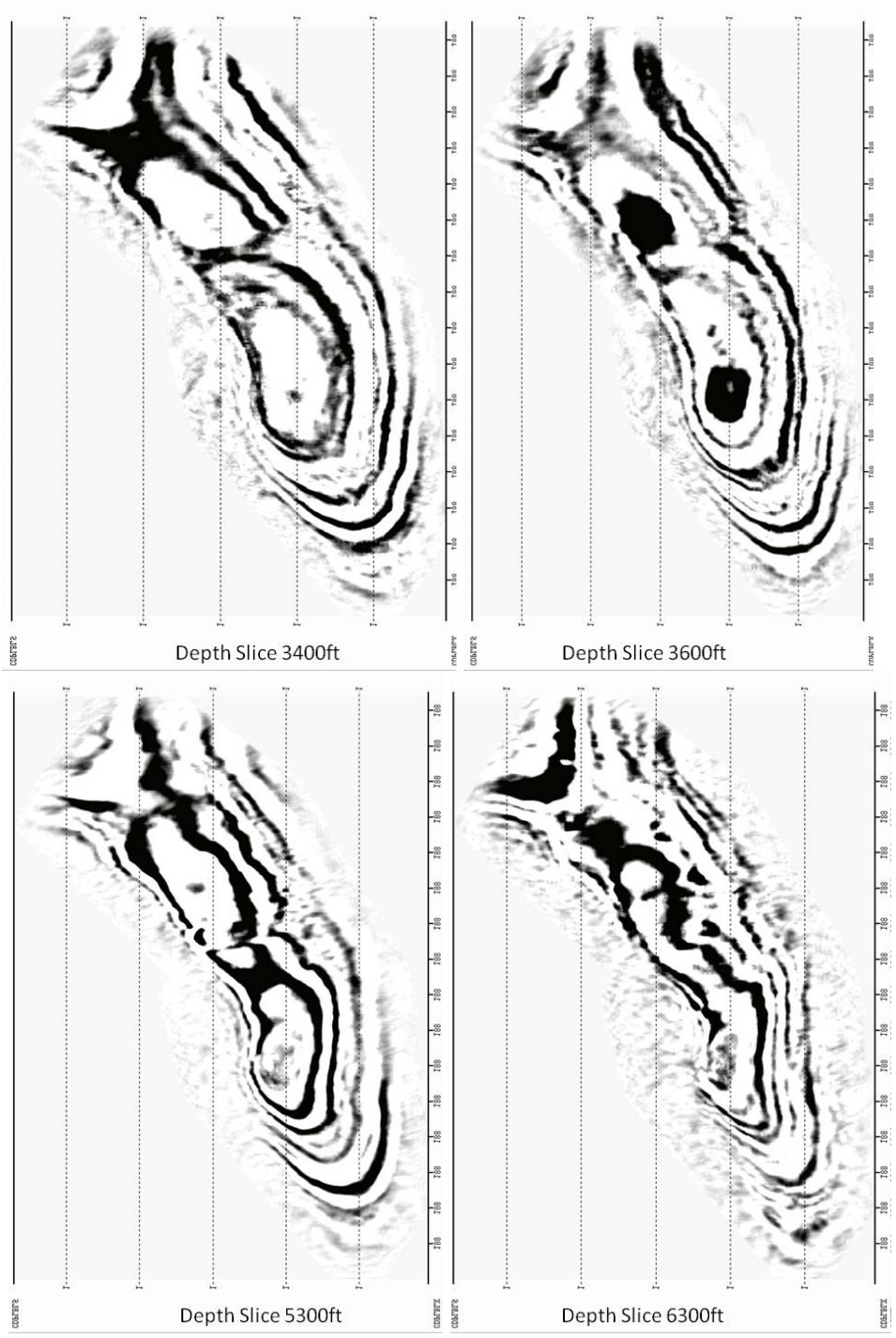

Final PSDM with Post-Processing: Example Depth Slices

Appendix B: Crow Mountain Geopressure Analysis

RMOTC GEOPRESSURE PREDICTION
FINAL REPORT
U.S. DEPARTMENT OF ENERGY

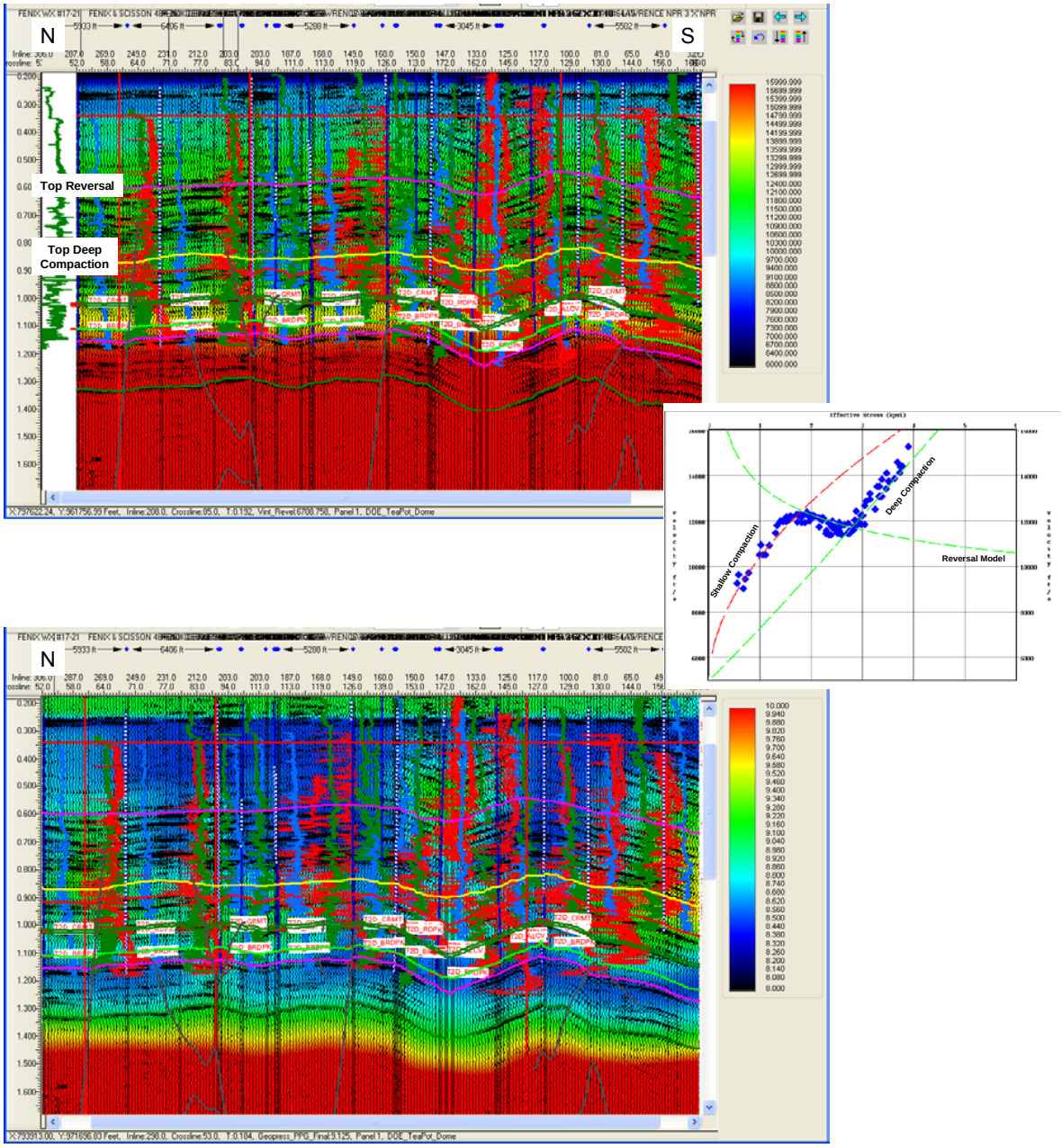

Dr. Alan R. Huffman and Jeff Meyer
Fusion Petroleum Technologies Inc.
8665 New Trails Suite 125
The Woodlands, TX 77381

CONTENTS

Report Date: September 13, 2010

Cover Images: Velocity and pore pressure sections for Arbitrary Line A-A' and the three-layer earth calibration model for the study area.

LIST OF FIGURES IN THIS REPORT

I. EXECUTIVE SUMMARY

As part of the DOE CO2 Sequestration project, Fusion Petroleum Technologies Inc. (FPTI) was requested to perform an integrated geopressure prediction on 28 square miles of 3D seismic in the Teapot Dome Rocky Mountain Oilfield Technology Center (RMOTC) area and perform fracture pressure interpretation based on well control and seismic interval velocities. Well control included 12 wells located within the seismic survey area. These wells contained mud weight data and wireline logs.

The dense velocities were input to REVEL™, a proprietary software developed by FPTI for residual velocity analysis, which refined the velocity field for pressure prediction. The velocity data were used to calibrate for pressure using the control well locations, and then predict pressures in 3D across the prospective area using the GEOPRESS™ tool. Attributes were generated for pore pressure (PP), overburden pressure (OB), fracture pressure (FP), effective stress (ES) in pounds per square inch (PSI) and gradients of these attributes in pounds per gallon (PPG).

II. INTRODUCTION

Pressure Prediction Methodology

Pressure prediction is typically performed using time-migrated gathers along with well logs and borehole geophysical data from local well control. The method requires detailed velocity analysis on properly imaged seismic gathers, some conditioning of the well data, followed by calibration of the seismic with the well data and prediction of fluid pressures on whatever grid was picked on the seismic data. The final velocity picks from the seismic data are calibrated using well control, and a velocity-effective stress transform is determined that honors the well and seismic data at the control wells locations. The overburden for the prediction area is calculated by integrating the density log data to obtain a vertical stress versus depth relationship referenced to the mudline or land surface. This equation usually takes the form of

$$\text{Vertical Stress} = a*Z^b$$

where Z is depth, a is a coefficient and b is an exponent.

For this study, a three-layer earth model was constructed starting with a Bowers-type relationship for velocity-effective stress in the shallow section where mechanical compaction is the dominant pressure mechanism. The Bowers equation is a power law relationship between velocity and effective stress that has been proven to be very effective worldwide for interpreting stress and predicting fluid pressure. The basic equation is of the form

$$V = V_0 + A\sigma^{\mathbf{B}}$$

where V is the velocity, σ is the effective stress, A is a coefficient and B is an exponent. The Bowers relationship was then expanded in the deep section to address unloading effects due to

shale diagenesis, and a deep chemical compaction model was used for the section below the unloaded interval where increasing velocities indicate a thermal-chemical compaction model is the primary mechanism.

The vertical stress and effective stress are then combined to calculate the pore pressure using Terzhagi's basic relationship:

Vertical Stress = Fluid Pressure + Effective Stress.

The last item to be calculated is the fracture pressure and fracture gradient. The fracture pressure is usually determined with offset well calibration using a constant percentage of overburden, or using a Matthews and Kelly approach where the fracture pressure is defined as

$$P_{fr} = P_p + K*(OB-P_p)$$

where P_{fr} is the fracture pressure, K is the stress ratio, P_p is the fluid pressure and OB is the overburden (vertical stress). For this study, a Matthews and Kelly approach was employed.

III. VELOCITY ANALYSIS

The geopressure prediction for the RMOTC project started with data conditioning of the seismic gathers that were generated as part of the pre-stack time migration (PSTM) work performed by Fusion as part of the CO_2 sequestration project. The data used for the geopressure work included the final PSTM seismic gathers, migration velocities used for flattening the gathers and the final stacked data in time domain.

Quality control was performed on the well data, final seismic gathers and velocity data. The 3D survey included a 28 square mile area. Twelve wells were used for calibration of the seismic velocities. The seismic survey area is shown in Figure 3.1.

Following the data conditioning, a dense velocity analysis was performed on the gathers. The final dense velocity data were used as the input to residual velocity analysis. REVEL™ was performed on the seismic volume using a spatial smoothing of 33 x 33 CDP's and a temporal smoothing of 480 milliseconds to stabilize the variations in the velocities without distorting the variations across faults and other primary structures.

An arbitrary line A-A' and three in-lines (IL280, IL200 & IL120, see Figure 3.1) were chosen to demonstrate spatial variations in the velocity field. These velocity sections are shown in Figures 3.2-3.5. The seismic velocities across the area show a mild velocity reversal (magenta horizon) in Figures 3.2-3.5 that again starts to increase in velocity at the top of deep compaction (yellow horizon).

IV- STRESS CALIBRATION

The fluid pressure interpretation was developed by generating vertical stress and seismic velocity/effective stress models from the control wells. Pressure data which consisted of mud weights from the 12 control wells were employed in the calibration procedure. Figure 4.1 shows all of the available drilling mud weight data from the twelve calibration wells as a function of depth that were used in the study. The velocity data from the sonic logs was also compared to the final REVEL velocities, and the trends between the well log and seismic data are consistent, but do show some differences as expected between the different sampling interval and source frequencies of the measurements (Figures 4.2 to 4.11).

Vertical Stress Model:

Well logs available for this study included density logs which were used to fit the density vs. depth relationship (Figure 4.12). The red points in the left hand track indicate the density log data and a representation of formation density extrapolated down to 10,000 feet below ground level elevation. The blue points in the right hand track indicate the calculated vertical stress (overburden) from this density model determined by integrating the density values. The red curve in the right hand panel indicates a mathematical model of the calculated vertical stress that has been calculated with the following power law equation and then high-sided slightly to provide a conservative estimate of the vertical stress:

$$\text{Vertical Stress} = \text{Overburden} = 0.0009823 * d^{\wedge 1.01277}$$

where stress is in kpsi and depth (d) is in feet below surface elevation.

This mathematical model is applied at all locations throughout the velocity survey datumed to surface elevation. In regions where the depth to the top of undercompaction varies spatially, or the extent of undercompaction varies, the use of a single vertical stress function can lead to over/under estimation of the vertical stress. The vertical stress curve defined in Figure 4.12 employs density logs with no indication of substantial density reversal. The vertical stress will be slightly lower if severe density reversals are present within the study area. Alternatively, if higher densities are present in the survey area then the model will underestimate the vertical stress. The overburden model is calibrated slightly to the 'high-side' of the data to ensure that vertical stress is not underestimated.

Fracture Pressure Model

Leak-off test data were not available from the Crow Mountain or near-by formations. The stress ratio/depth trend for the wells is shown in Figure 4.13. Relatively large errors in the stress ratio calibration can result in relatively small errors when calculating fracture pressure. This results because the stress ratio is multiplied with the difference between the fluid pressure and the overburden pressure. That difference can become quite small as depth increases (overpressure) so that the calculated fracture pressure becomes insensitive to small variations in the stress ratio. The stress ratio curve was applied in the prediction process using Mathews and Kelly's equation which is

$$\text{Fracture Pressure} = PP + K*(OB - PP)$$

where K is stress ratio, PP is pore pressure and OB is overburden pressure.

Velocity vs. Effective Stress Model

The calibration of velocity to effective stress starts with an assessment of the sonic log velocities and seismic velocities from REVEL to determine whether the velocities are reasonably consistent. A comparison of the sonic logs for 10 wells (Figures 4.2 to 4.11) with the seismic velocities shows that the calibration wells track reasonably with the seismic velocities.

The next step in the process is to integrate the overburden curve at each calibration well then using the mud weight, RFT and MDT data to calculate effective stress, and then cross-plot the effective stress data versus the seismic velocities in the wells. The typical result of this process is then used to construct a model for the primary compaction, diagenetic unloading and chemical compaction regimes. In this study, the calibration was performed using all 12 calibration wells (Figure 4.14).

A boundary horizon between the normal compaction and the small velocity reversal was mapped on the seismic data. The "top of reversal" surface was integrated with the seismic velocities to predict pressures. Likewise, the boundary horizon between the small velocity reversal and the "top deep compaction" model was also mapped from the seismic data guided by well ties and the onset of increasing velocity. This top of deep compaction was also used in the prediction process.

Fluid Pressure Calibration

The calibration process included a calibration of each well to the final multi-layer earth model (Figures 4.15 to 4.26). The pressure data for each well were displayed against the seismic velocity and resulting pore pressure to assure that the 3D calibration honors all of the well data. The goal of the calibration process is to assure that the sediment velocities will do a reasonably good job of predicting the observed pressure data in each mechanism interval. Figures 4.27 to 4.38 show the composite calibration for all three pressure models; shallow primary compaction, depths between the velocity reversal and the deep compaction surface and finally below the top of deep compaction. The pore pressure gradient curves in the figures 4.27-4.38 that are valid from each of the mapped surfaces, shallow clip surface (red boundary) to the top of reversal surface (magenta boundary) are shown on the right side panel as individual curves. Between the top reversal and the top secondary compaction (blue boundary) surfaces, the red pore pressure curve (right panel) is applicable. Below the second compaction surface, the second green curve for deep compaction is applicable. The composite of these curves represents the actual pore pressure profile at each well location.

Time/Depth Adjustment

The pressure prediction process relies on the quality of the pressure calibration as well as the time-depth conversion calculated from the seismic velocities. Where possible, the seismic velocities should be calibrated with check shot or VSP data to assure that the

time-depth relationship will produce the smallest error possible. In this case, the time-depth relationship from the REVEL velocities was used for the depth conversion.

V. Fluid Pressure Interpretation

Fluid and fracture pressure predictions were performed on a sub-sampled grid of the 3-D velocity volume (Figure 3.1). Time values were converted to depth within GEOPRESS^{TM}, utilizing the seismic interval velocity data. The calibrations defined in section 4 of this report were applied to the data and depth and time values of effective stress, pore pressure, fracture pressure and overburden pressure were generated along with their gradients. The calculations were performed using the application of Bowers compaction from the shallow clip surface (red horizon) to the top reversal surface (magenta horizon). Below the magenta horizon, the Bowers reversal model was applied down to the second compaction surface (blue horizon), followed by a deep Bowers calculation below the blue horizon.

The fluid pressure calculation set a minimum gradient of 8.5 pounds/gallon (hydrostatic). The time-depth relationship at each calculation function allowed generation of time-based calculations of vertical stress, effective stress, fluid and fracture pressure. The output data volume for this project contains time-based data for fluid pressure and its gradient, fracture pressure and its gradient, vertical stress and its gradient and effective stress. For display and interpretation purposes, the same 4 lines from section 3 of this report are used for illustrating the results of both sets of pressure calculations.

The fluid pressure gradient and fracture pressure gradient results along Arbitrary Line A-A' are shown in Figures 5.1 and 5.2. The pore pressure above the "top reversal surface" (magenta) is in a regime of normal compaction. Below the TUL surface, the

regime changes from normal compaction to the inverted Bowers trend. The fluid pressure gradients below the top second compaction surface increase however the pressures remain generally benign throughout. The changes in compaction models reflect changes in the age and stratigraphy of the rocks, and do not reflect a change in the mechanism of pressure generation with depth.

The fracture pressure gradient consistently demonstrates that the predicted fracture gradient gently increase to approximately 20 PPG in the formation above the vicinity of the Crow Mountain formation at approximately 1.0 seconds two way time.

Figures 5.3 and 5.4 show the pore pressure gradient and fracture pressure gradient results for both cases for Inline 280. Figures 5.5 and 5.6 show the same displays for Inline 200. Figures 5.7 and 5.8 show the same displays for Inline 120. The maps for the "top velocity reversal" and "top second compaction" surfaces are also shown in Figures 5.9 and 5.10.

As part of the prediction process, a prediction was extracted from the 3D volume at each calibration well location. These raw predictions are generated within GEOPRESS™ and are used to double-check the results. Figures 5.11 to 5.24 show the results for the 14 available wells in the study area. The Top Reversal and Top Second Compaction surfaces are shown on each prediction panel as magenta and blue lines that cut across the figure. The small changes in pressure can be observed at each boundary.

VI - CONCLUSIONS

Mud weights and pressure data in 12 wells were used to calibrate a three-layer earth model for pressure prediction in the Teapot Dome RMOTC 3D survey that included a three-layer compaction model.

The 3D data was conditioned, followed by dense velocity analysis and residual velocity analysis using REVEL^{TM}. The resulting velocities were used to generate effective stress volume for the 3D survey which was then used with overburden stress to calculate attributes of overburden gradient, fluid and fracture pressure and their gradients.

The pressure regime in the RMOTC area is basically normally pressured at all levels penetrated by wells in the study area. The low pore pressures and much higher fracture pressures in the RMOTC area will allow substantial amounts of CO_2 to be sequestered at this site without significant risk of seal failure.

VII - LIST OF DATA INCLUDED WITH THIS REPORT

The final deliverables for this project included the following items:

- Final conditioned gathers
- Final velocity results from REVEL for the study area
- Calibration data for the pressure prediction
- Digital data for final GEOPRESS^{TM} outputs for pore pressure and pore pressure gradient, fracture pressure and fracture pressure gradient, overburden pressure and overburden pressure gradient, and effective stress for the study area. The data are output in SEG-Y format in time and in depth.
- Final edited well logs for each well in LAS format

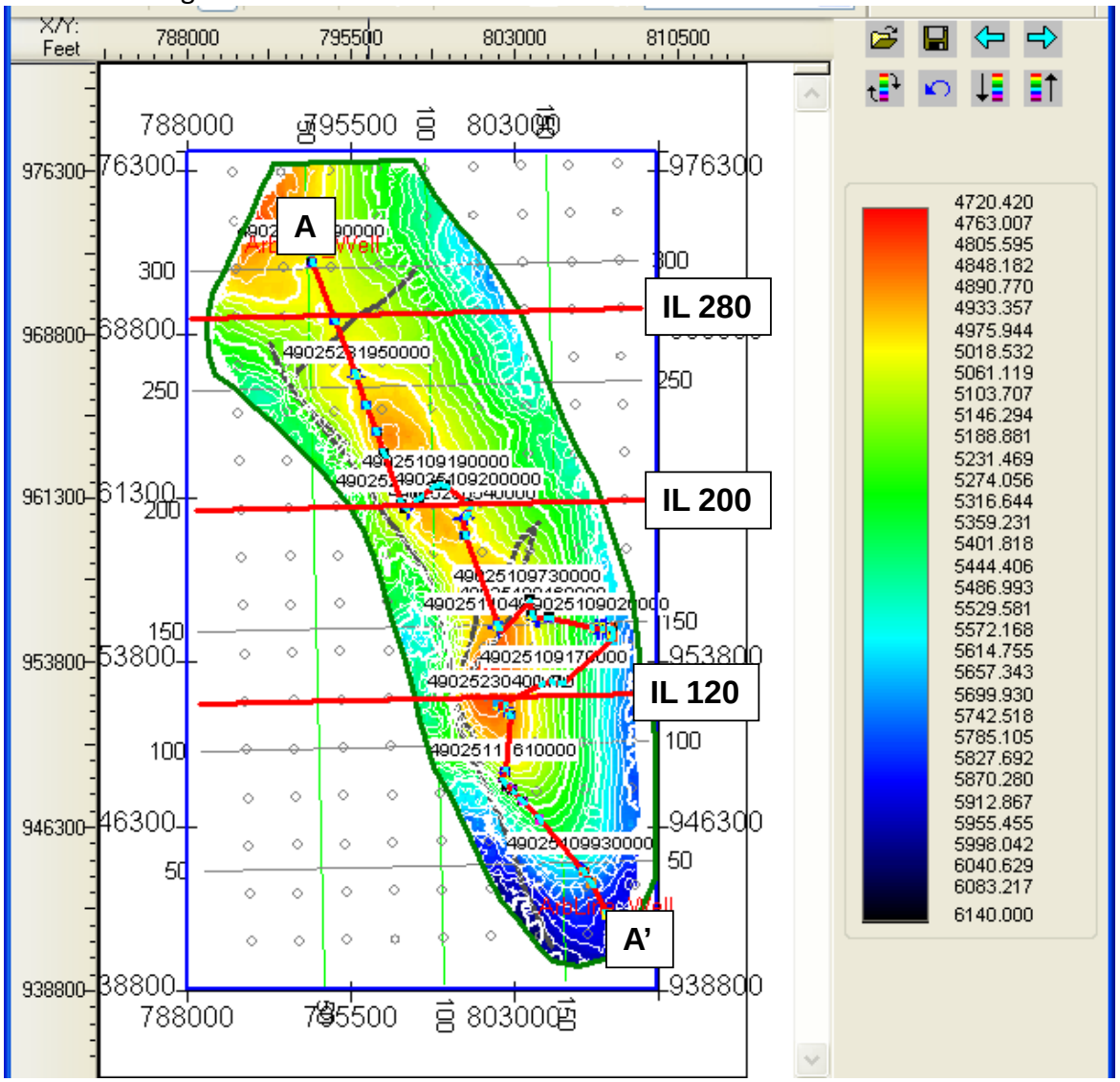

Figure 3.1: Base map for study area showing the 4 display lines used in this report (arbitrary line A-A', IL 120, IL 200 and IL 280).

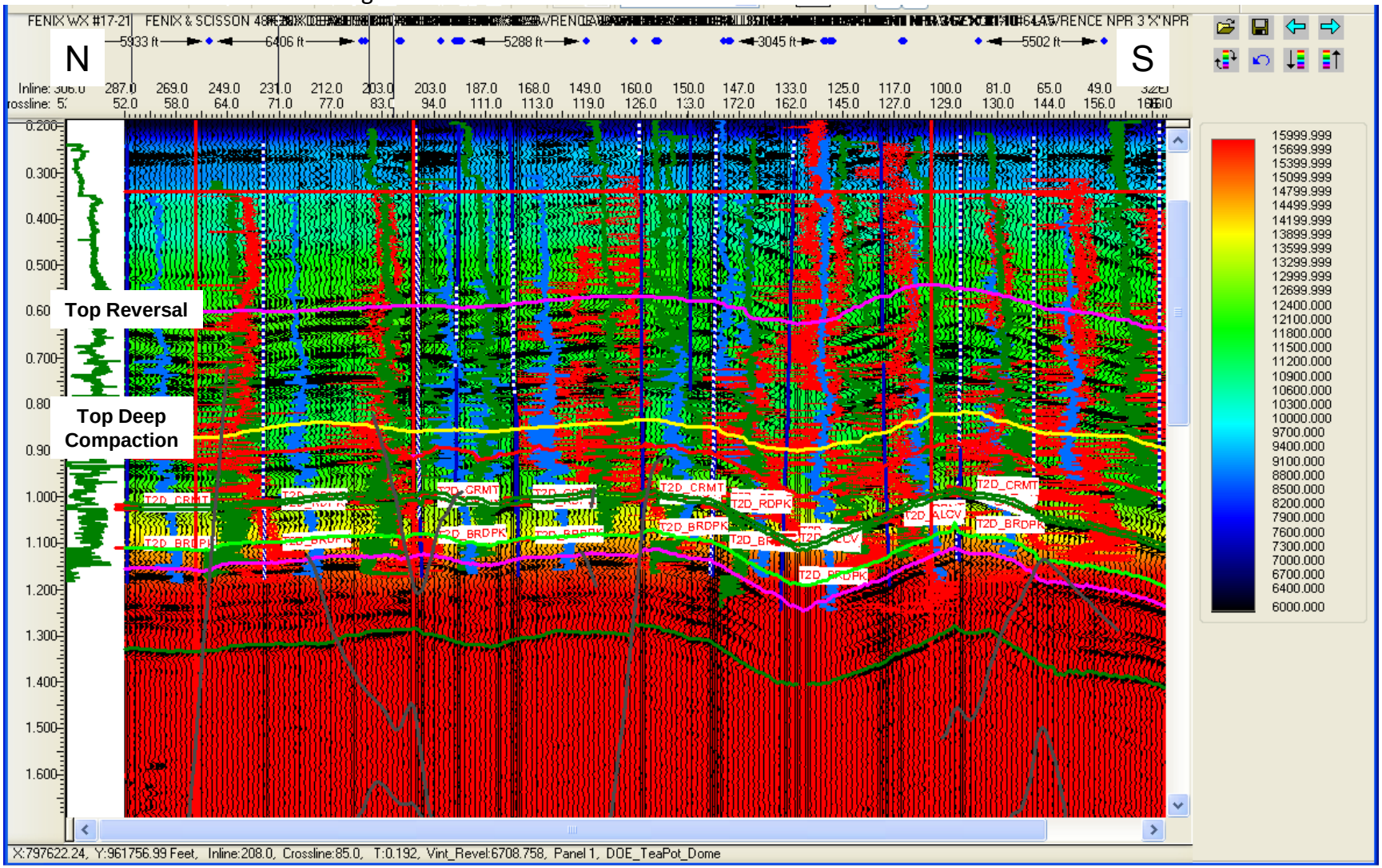

Figure 3.2: REVEL interval velocity section for <u>Arbitrary Line A-A</u>' showing the top of the velocity reversal (magenta) and top of the deep compaction (yellow) horizons. Velocity units are in ft/sec.

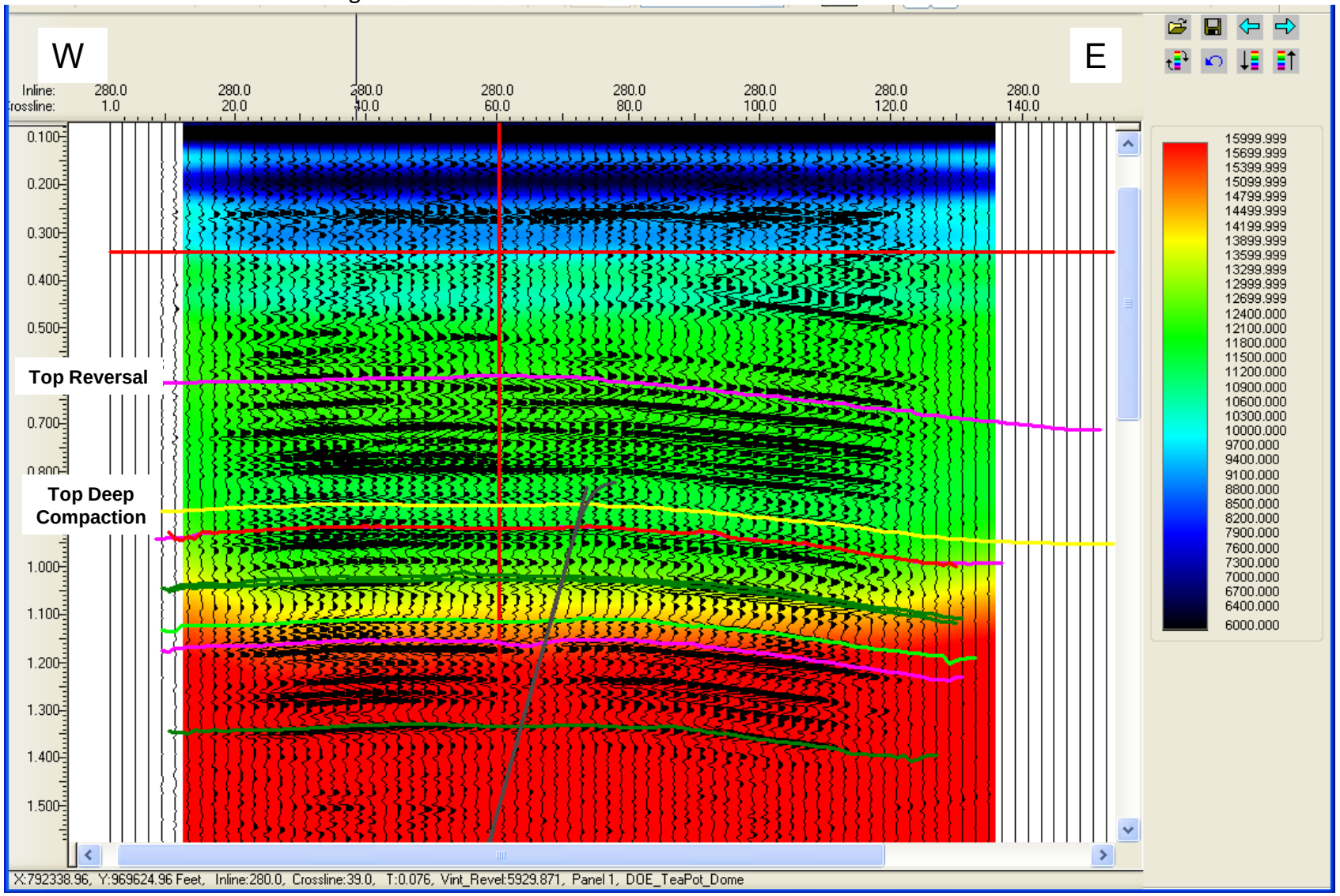

Figure 3.3: REVEL interval velocity section for Inline 280 showing the top of the velocity reversal (magenta) and top of the deep compaction (yellow) horizons. Velocity units are in ft/sec.

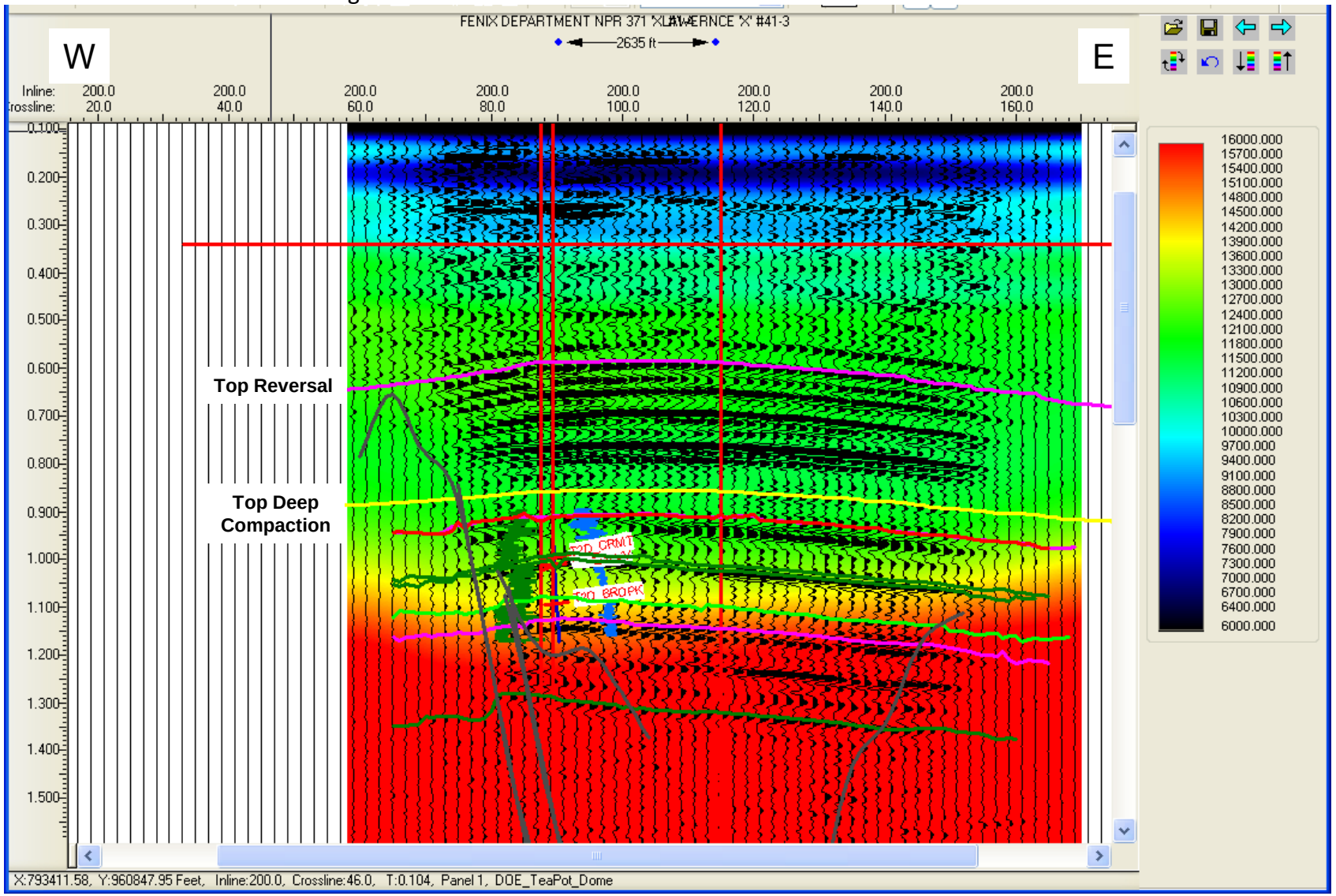

Figure 3.4: REVEL interval velocity section for <u>Inline 200</u> showing the top of the velocity reversal (magenta) and top of the deep compaction (yellow) horizons. Velocity units are in ft/sec.

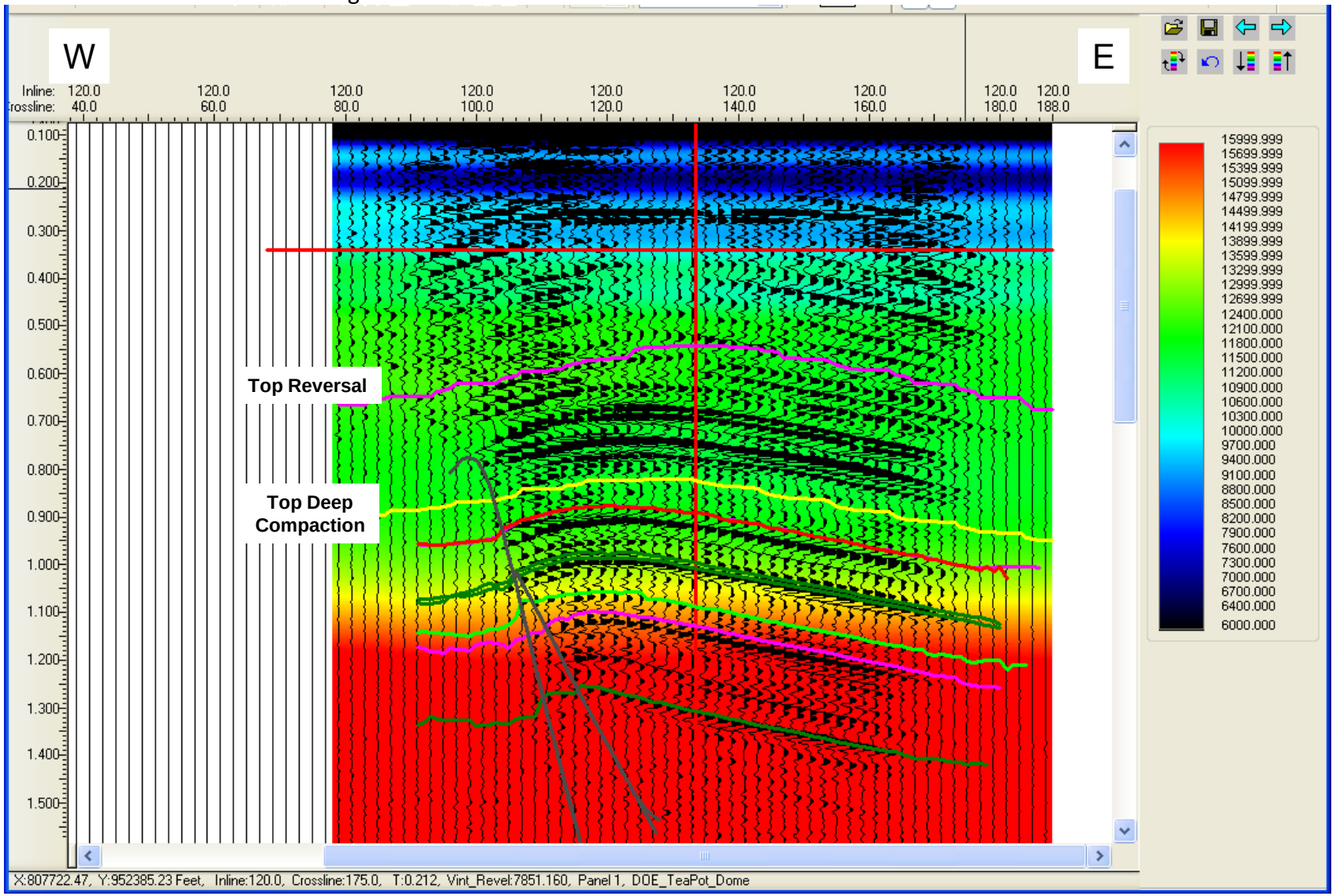

Figure 3.5: REVEL interval velocity section for <u>Inline 120</u> showing the top of the velocity reversal (magenta) and top of the deep compaction (yellow) horizons. Velocity units are in ft/sec.

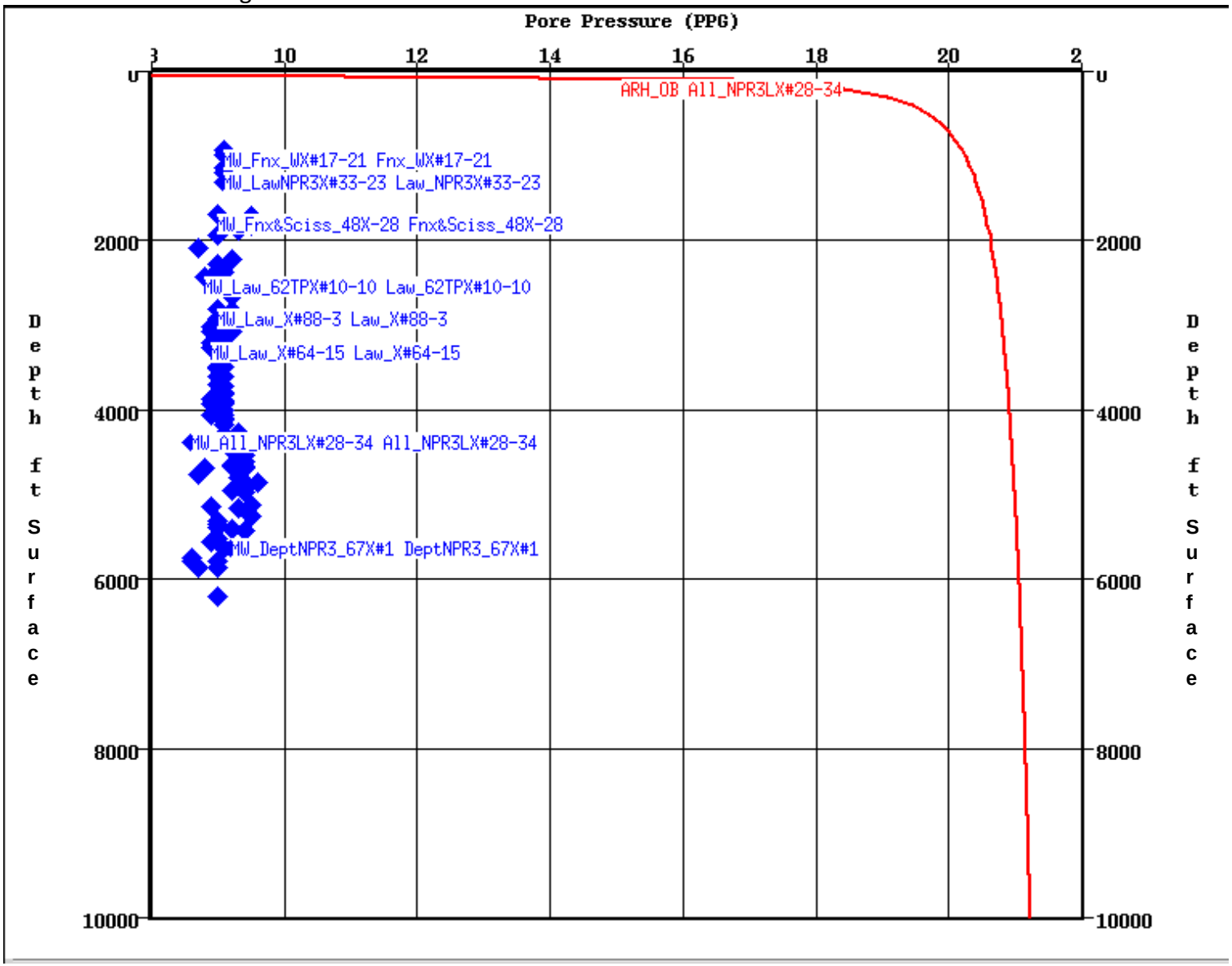

Figure 4.1: Pressure vs. depth plot for all mud weight data from the calibration wells used in the study.

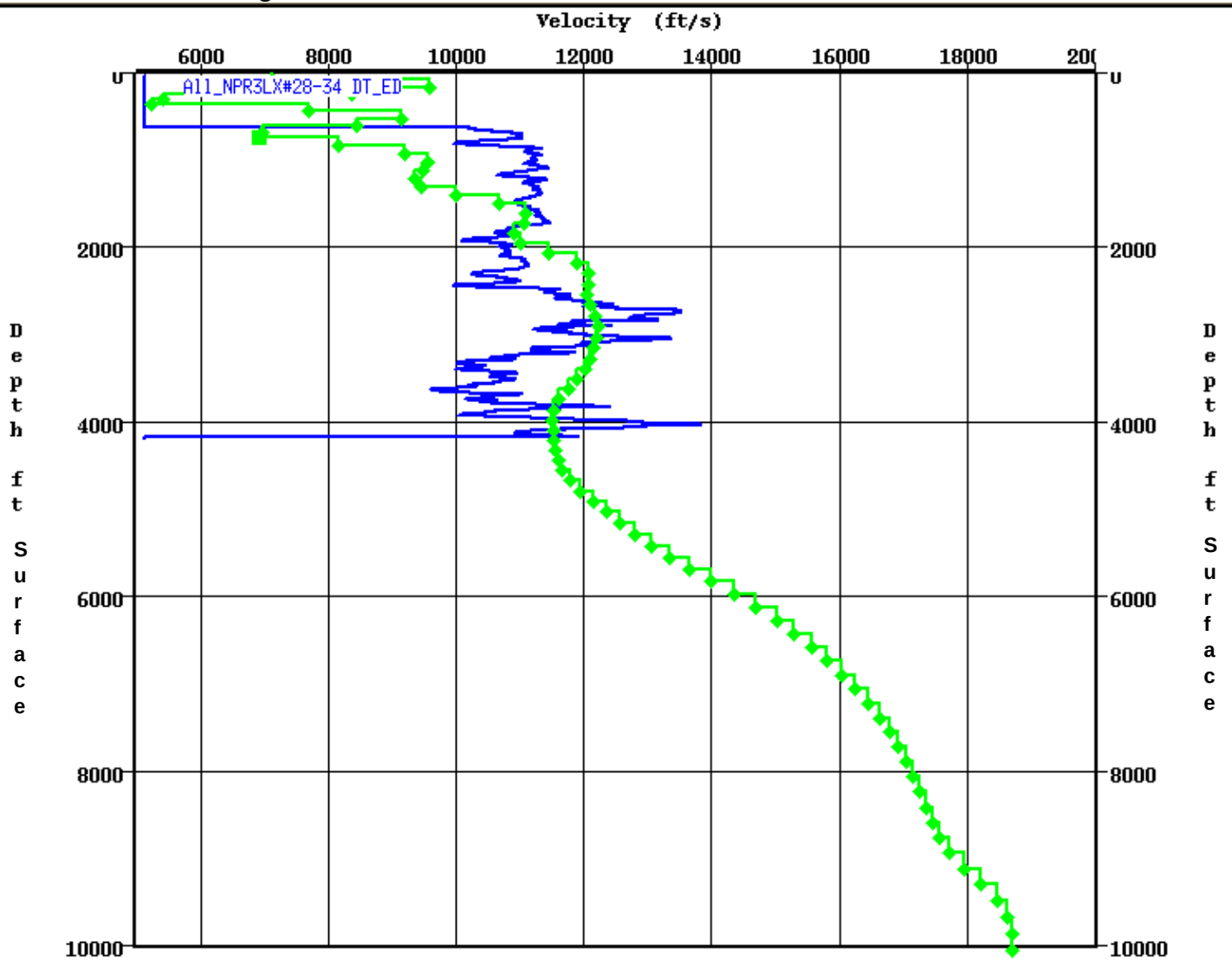

Figure 4.2: Sonic velocity (blue) and check shot velocity (purple) vs. REVEL seismic interval velocity (green) for the NPR 3LX #28-34 well.

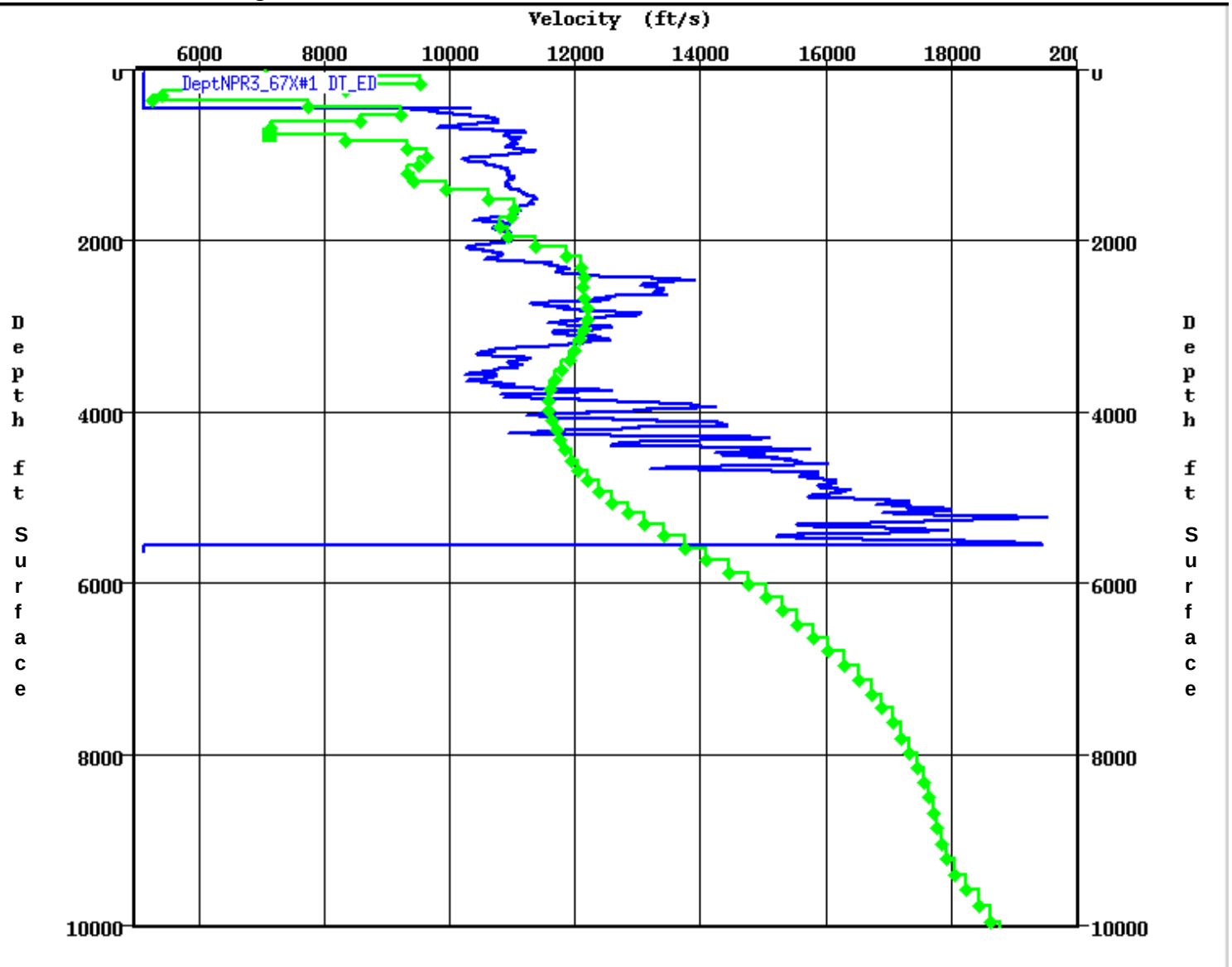

Figure 4.3: Sonic velocity (blue) vs. REVEL seismic interval velocity (green) for the NPR3 #67X-1 well.

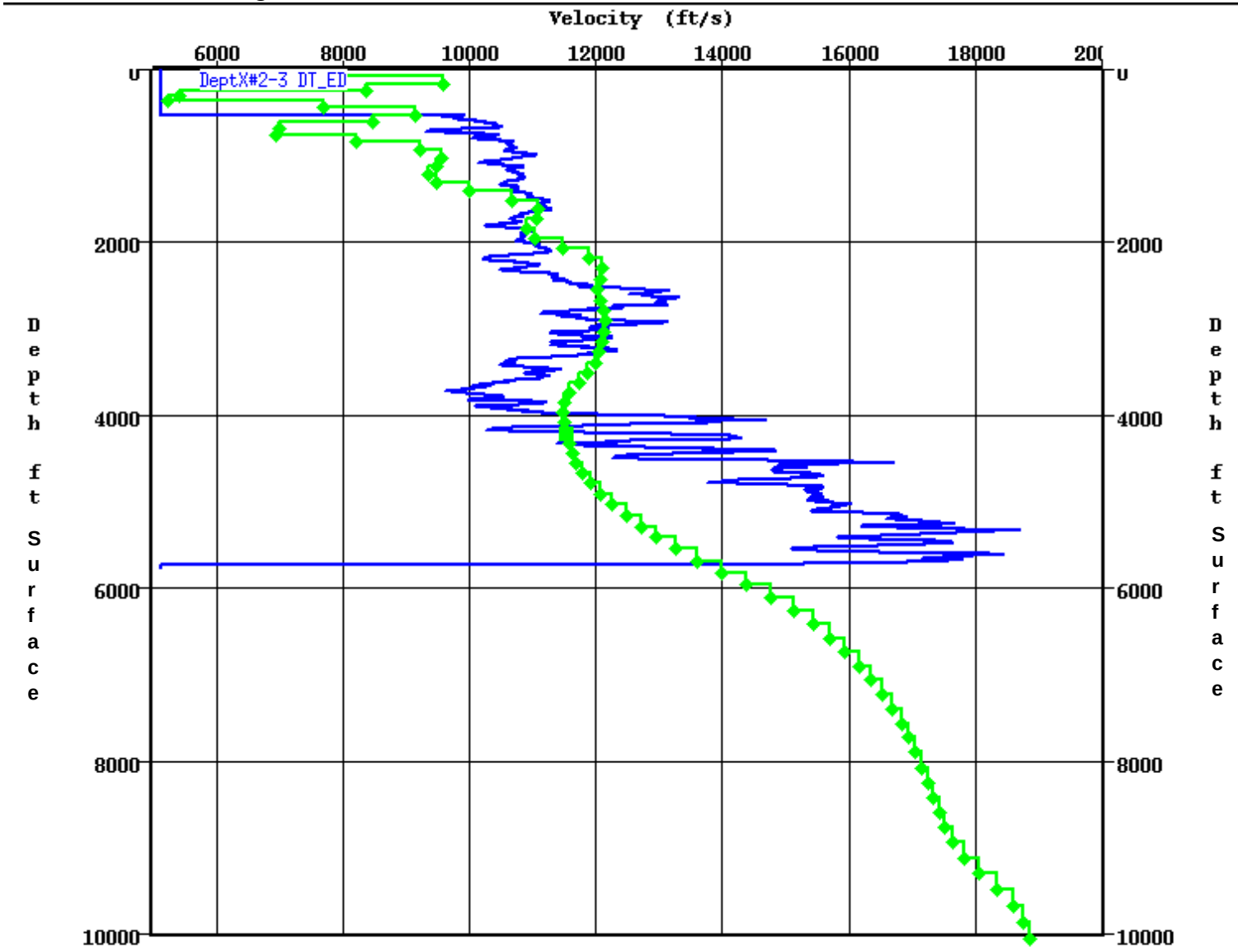

Figure 4.4: Sonic velocity (blue) vs. REVEL seismic interval velocity (green) for the Dept X #2-3 well.

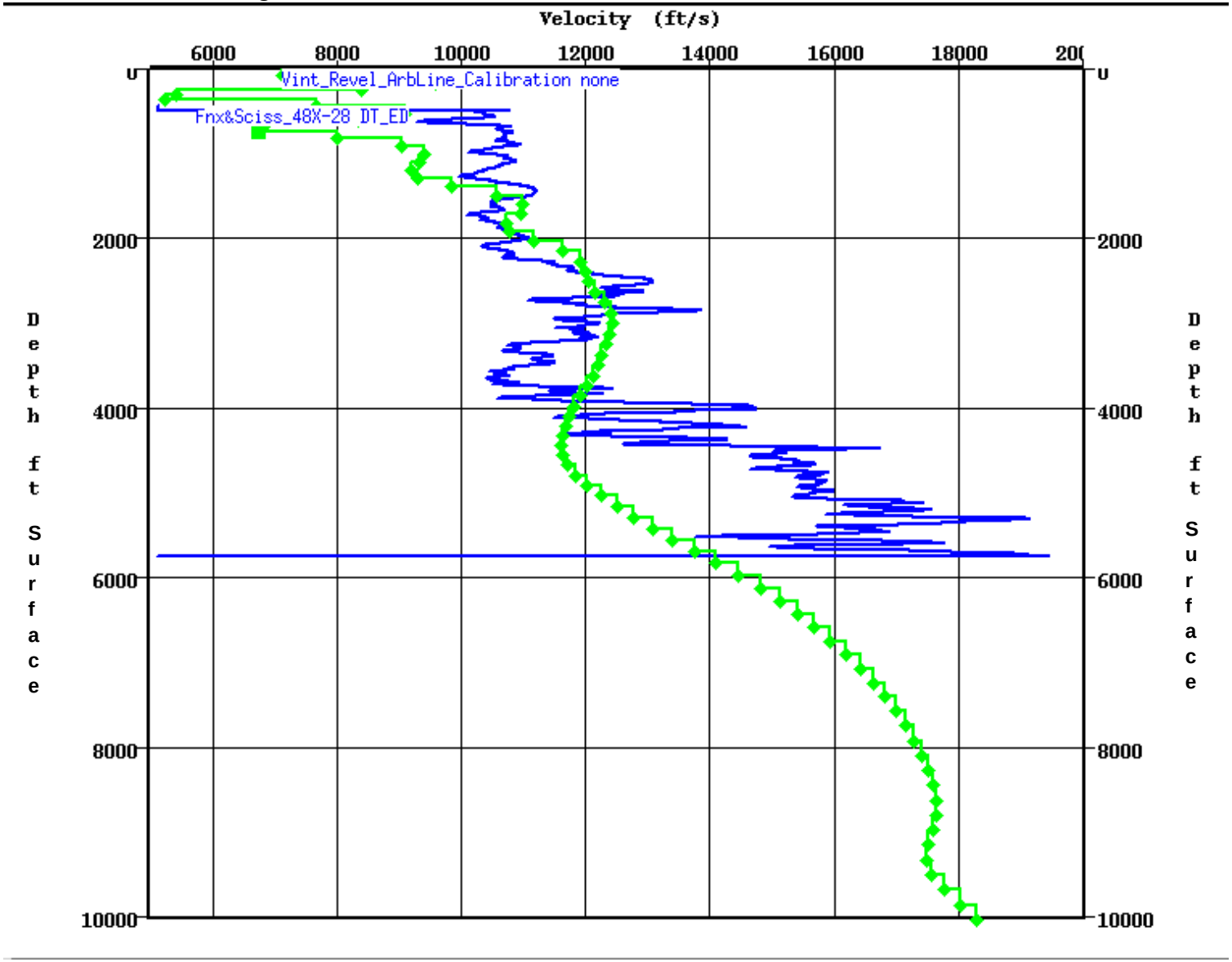

Figure 4.5: Sonic velocity (blue) vs. REVEL seismic interval velocity (green) for the FNX X #48-28 well.

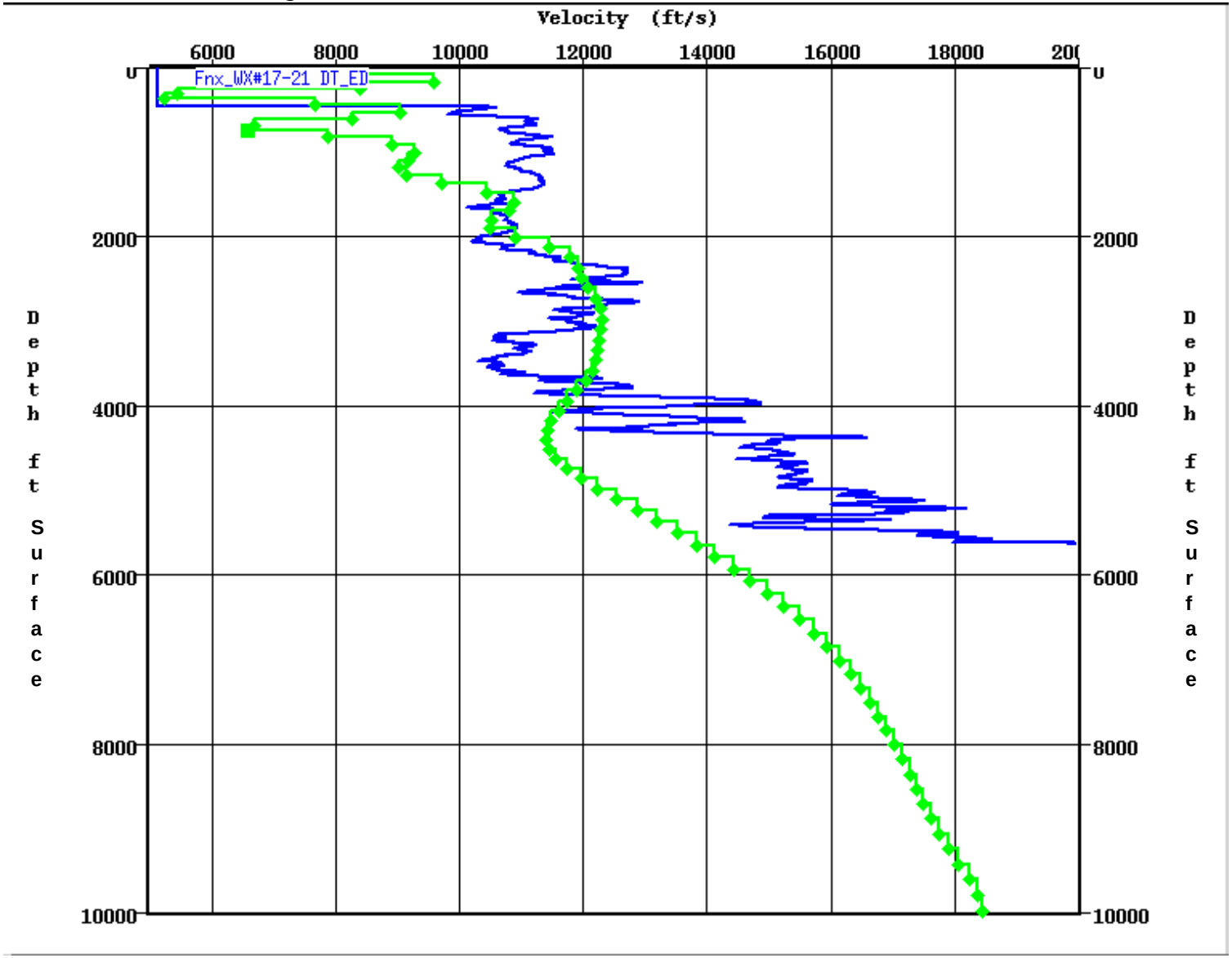

Figure 4.6: Sonic velocity (blue) vs. REVEL seismic interval velocity (green) for the FNX WX #17-21 well.

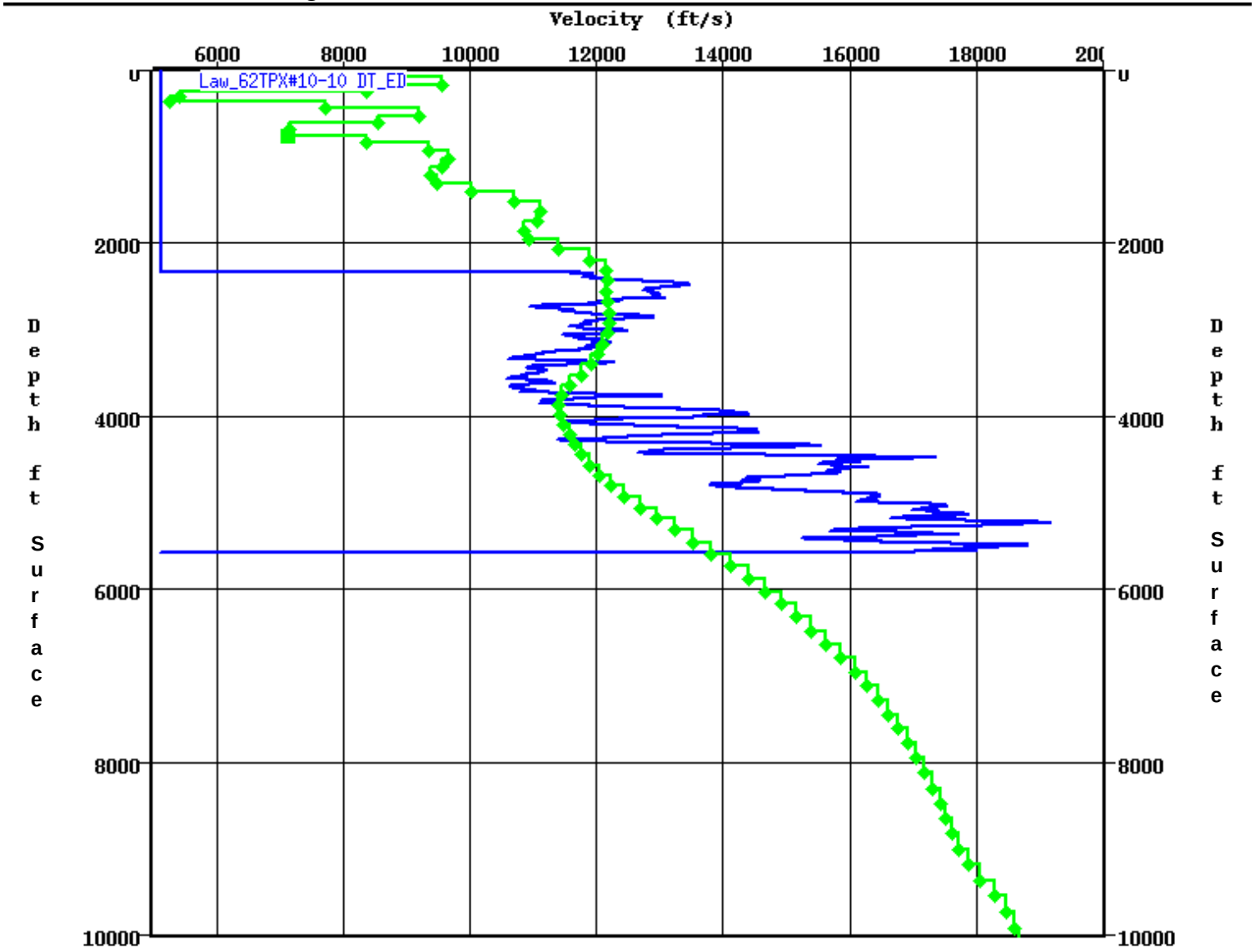

Figure 4.7: Sonic velocity (blue) vs. REVEL seismic interval velocity (green) for the Law 62TPX #10-10 well.

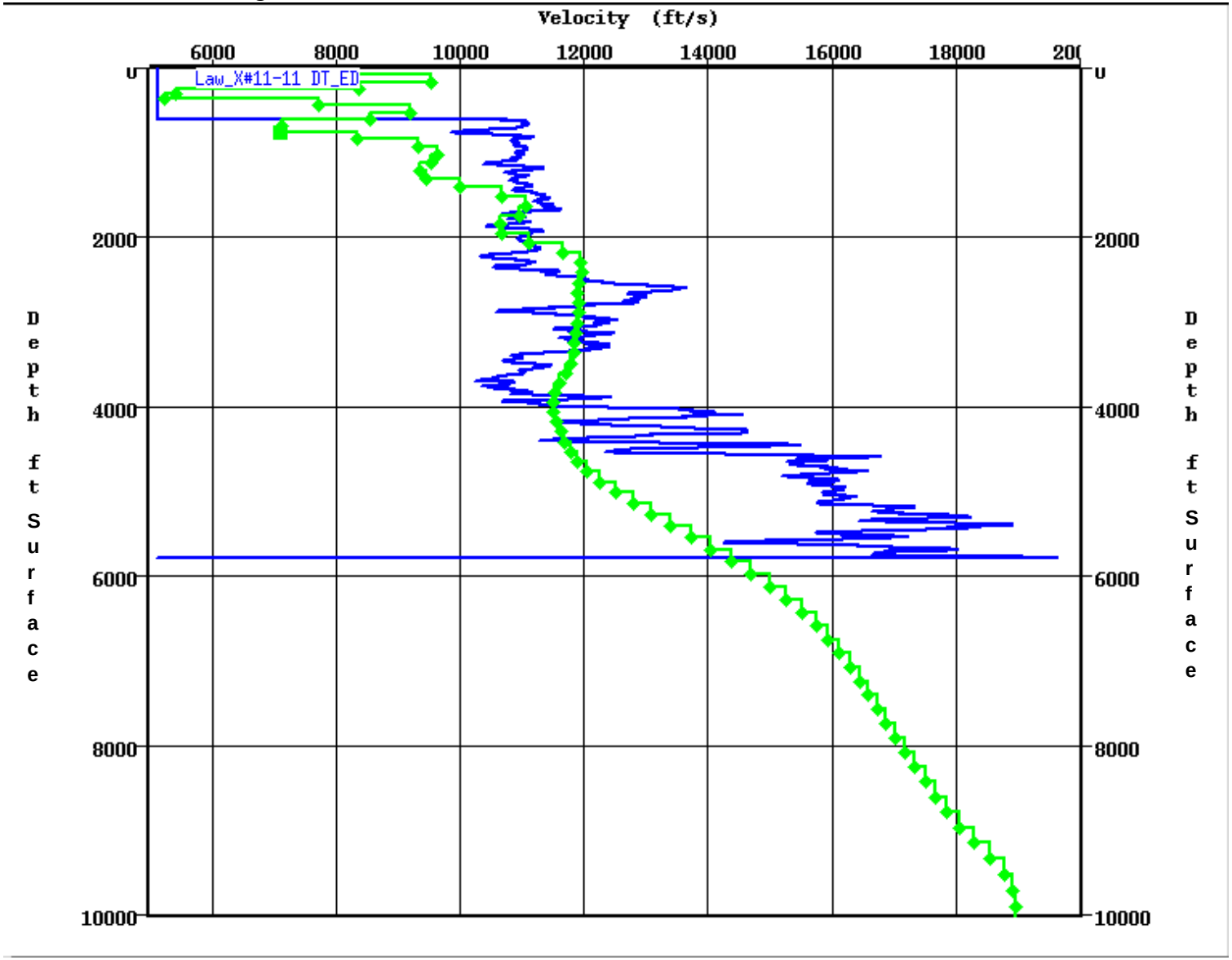

Figure 4.8: Sonic velocity (blue) vs. REVEL seismic interval velocity (green) for the Law X #11-11 well.

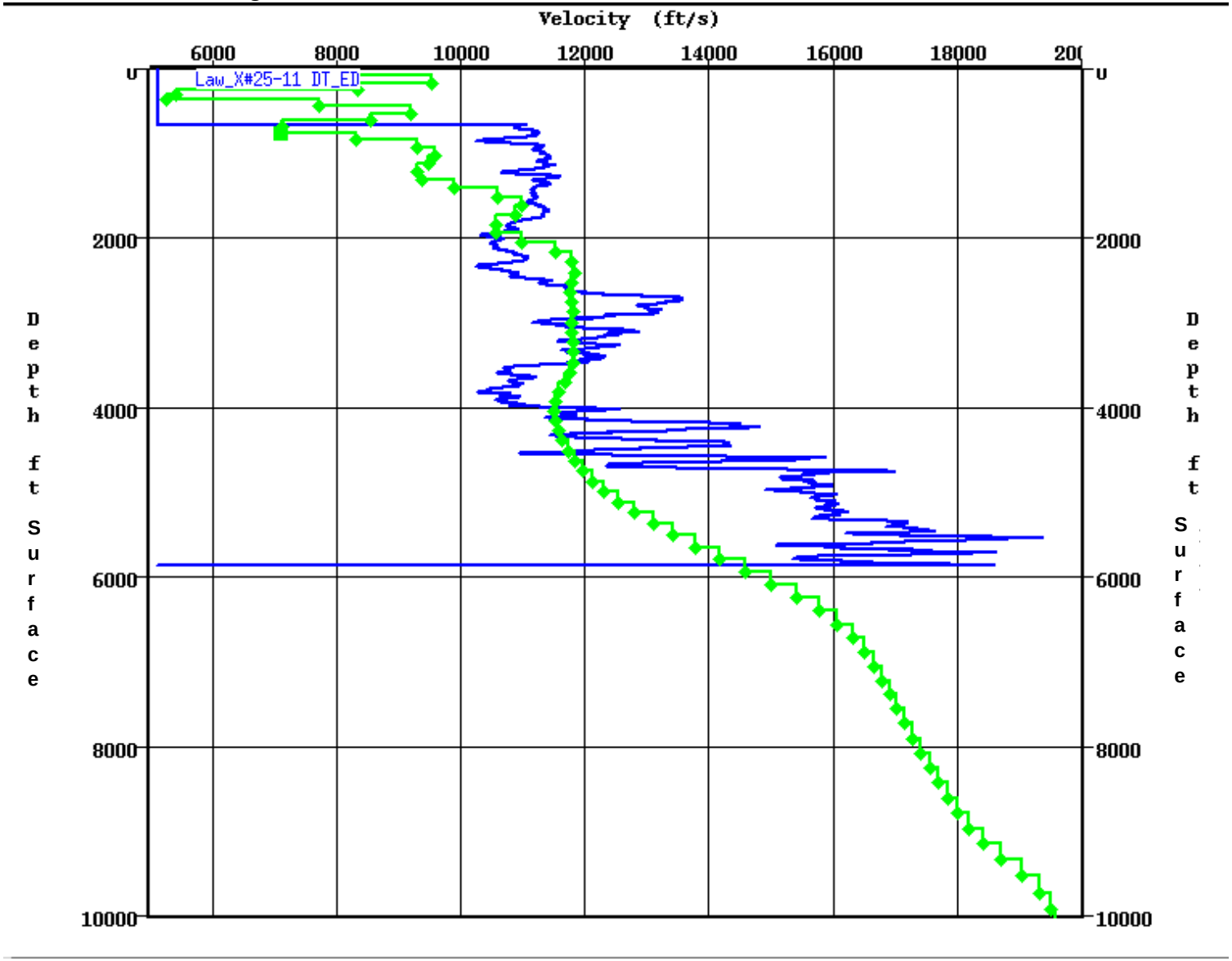

Figure 4.9: Sonic velocity (blue) vs. REVEL seismic interval velocity (green) for the Law X #25-11 well.

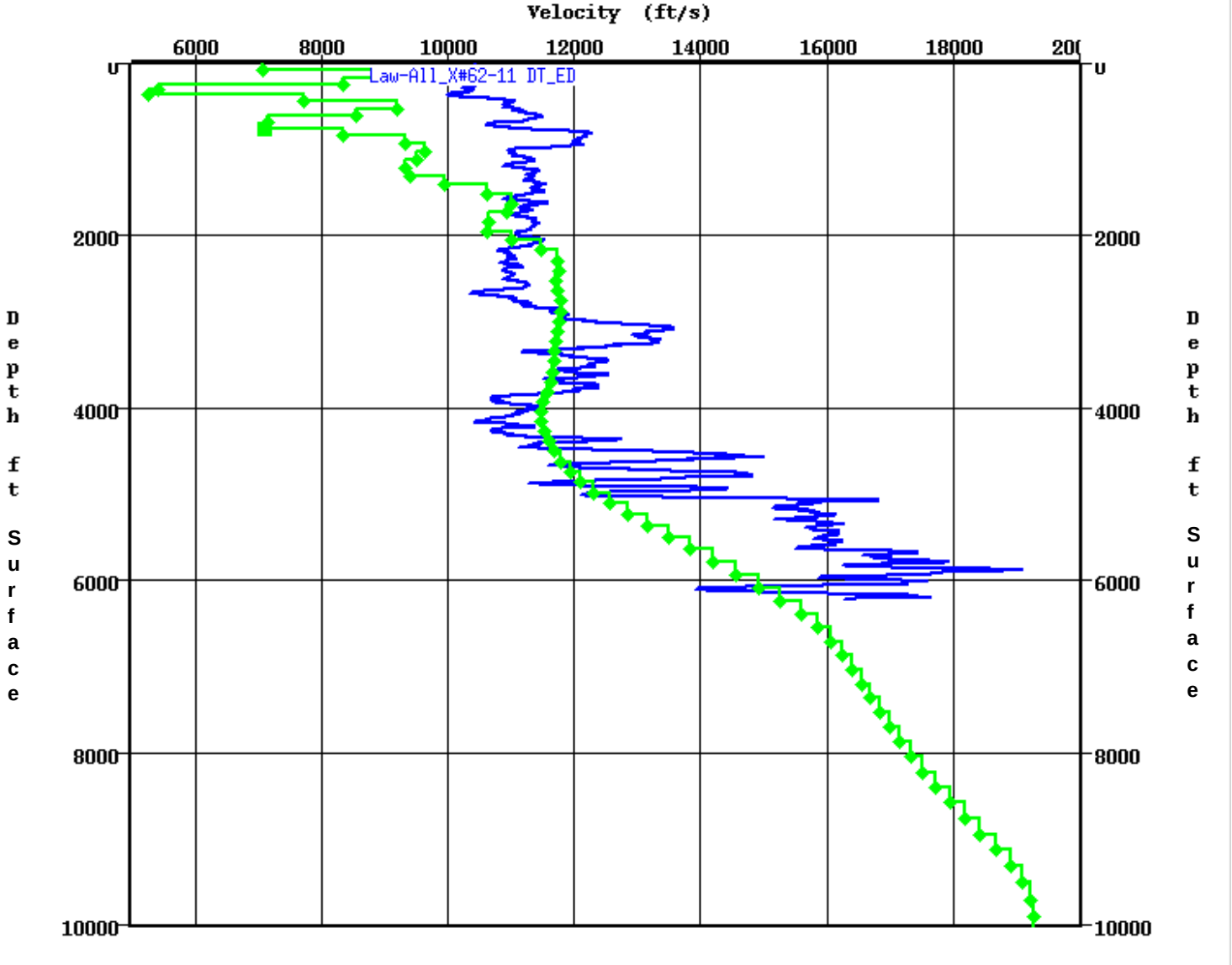

Figure 4.10: Sonic velocity (blue) vs. REVEL seismic interval velocity (green) for the Law X #62-11 well.

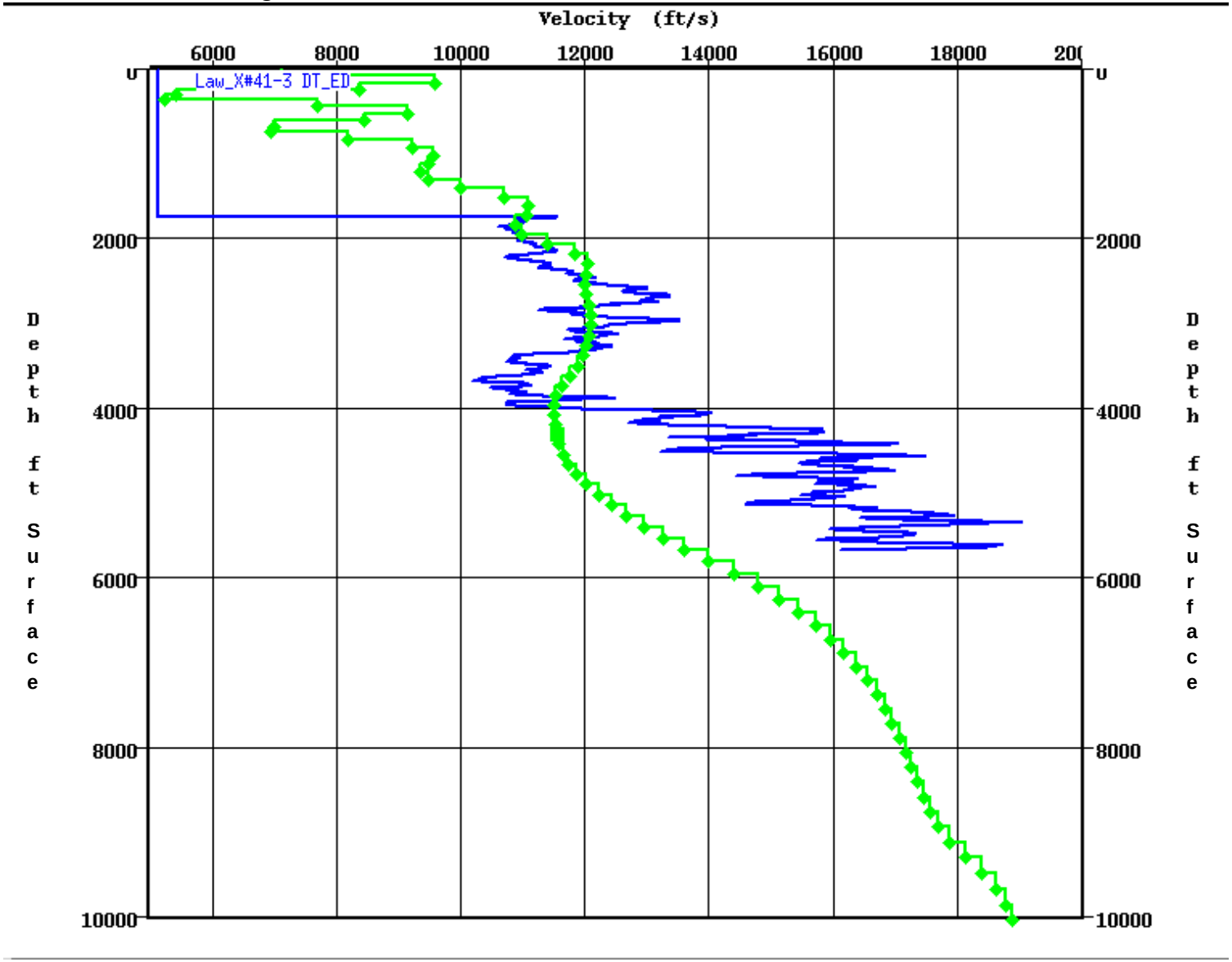

Figure 4.11: Sonic velocity (blue) vs. REVEL seismic interval velocity (green) for the Law X #41-3 well.

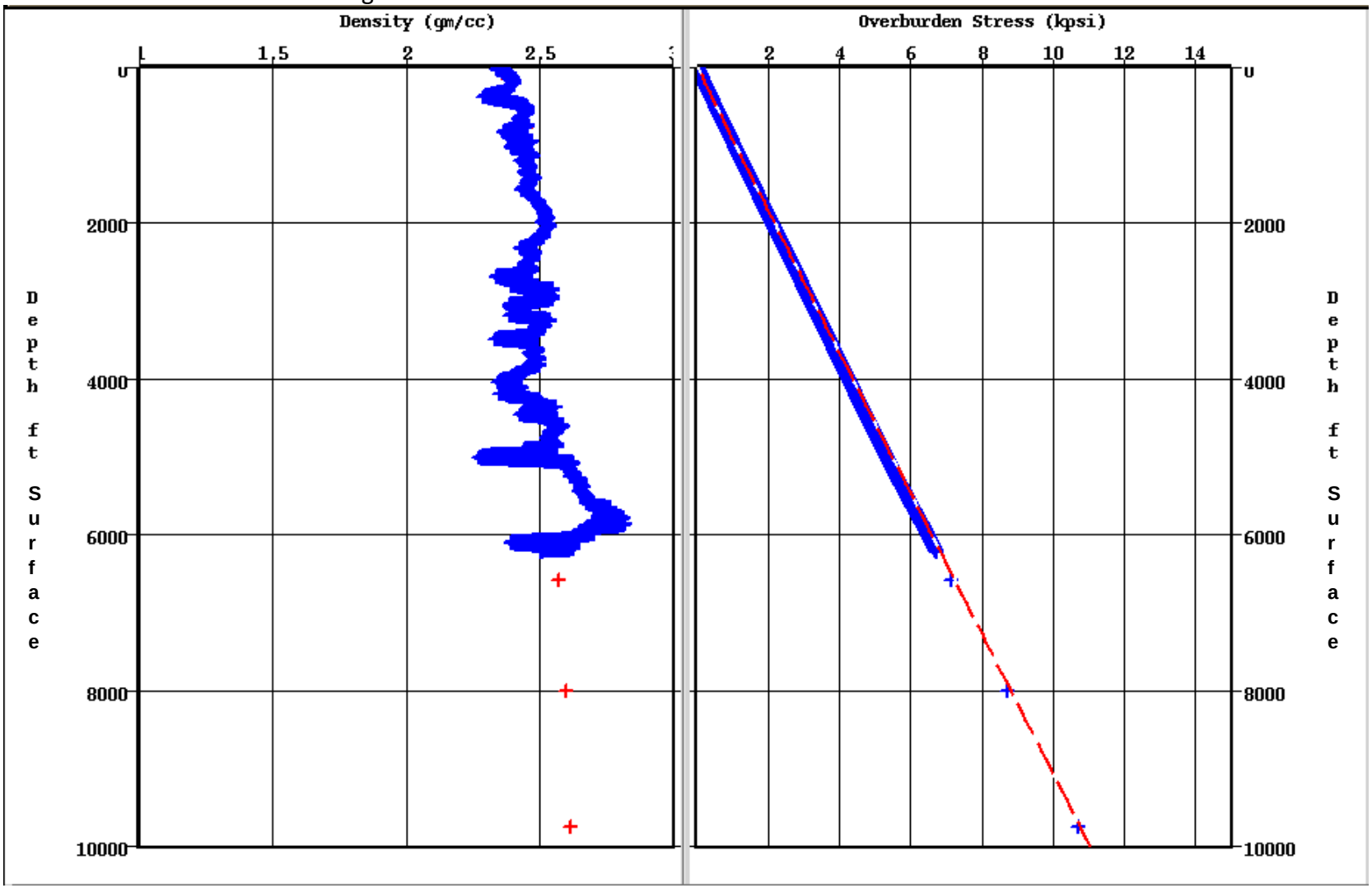

Figure 4.12: Density vs. depth plot (left panel) showing the density trend from the Law X #62-11 well, and overburden stress plot (right panel) showing the integration of the density data and curve fit to overburden stress in Kpsi.

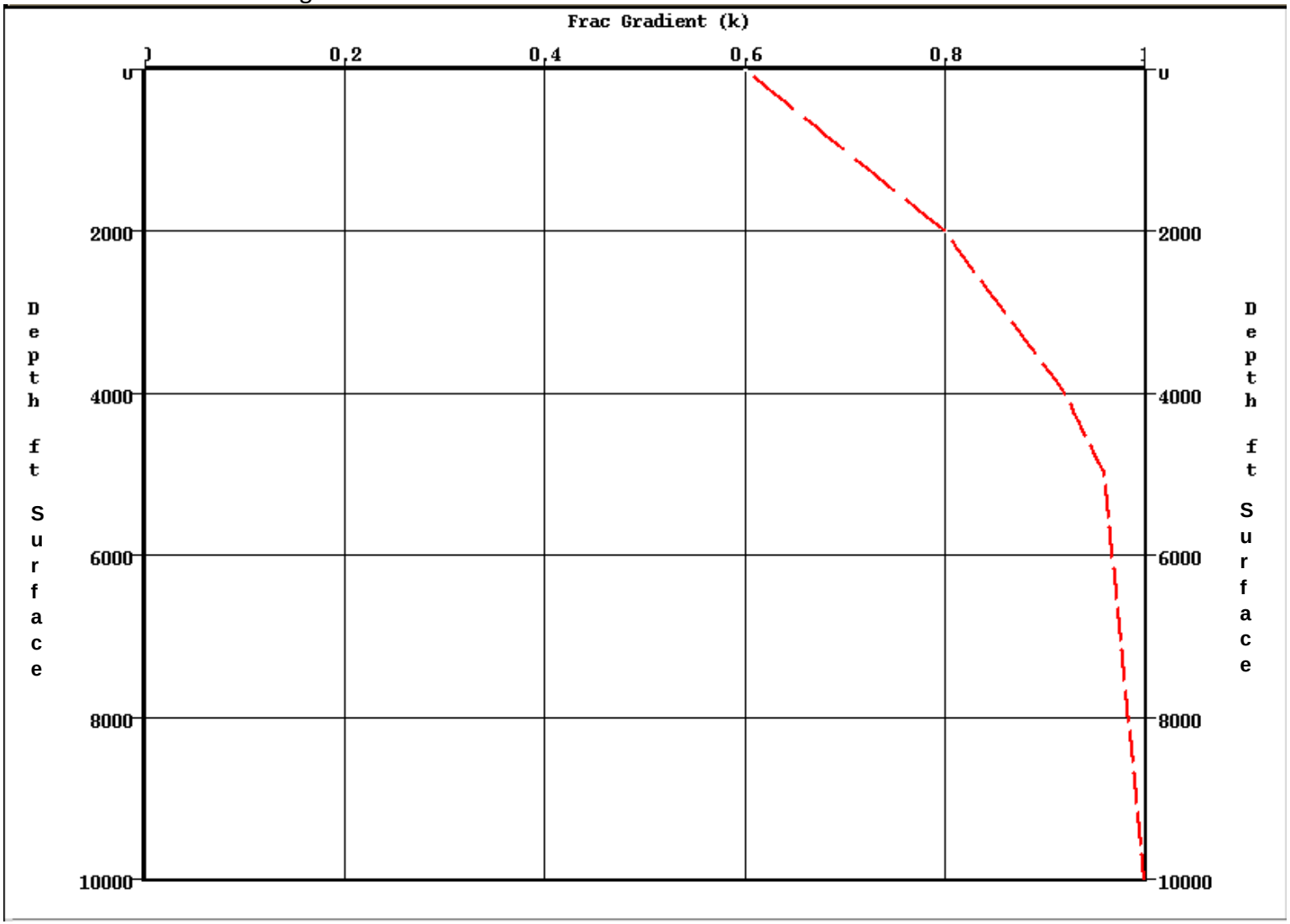

Figure 4.13: Stress ratio cross-plot (red curve) showing the curve used to generate the fracture gradients for the study. No Leak Off Test (LOT) data were available for the wells in the seismic survey. Stress ratio cross-plot (red curve) showing the curve used to generate the fracture gradients for the study.

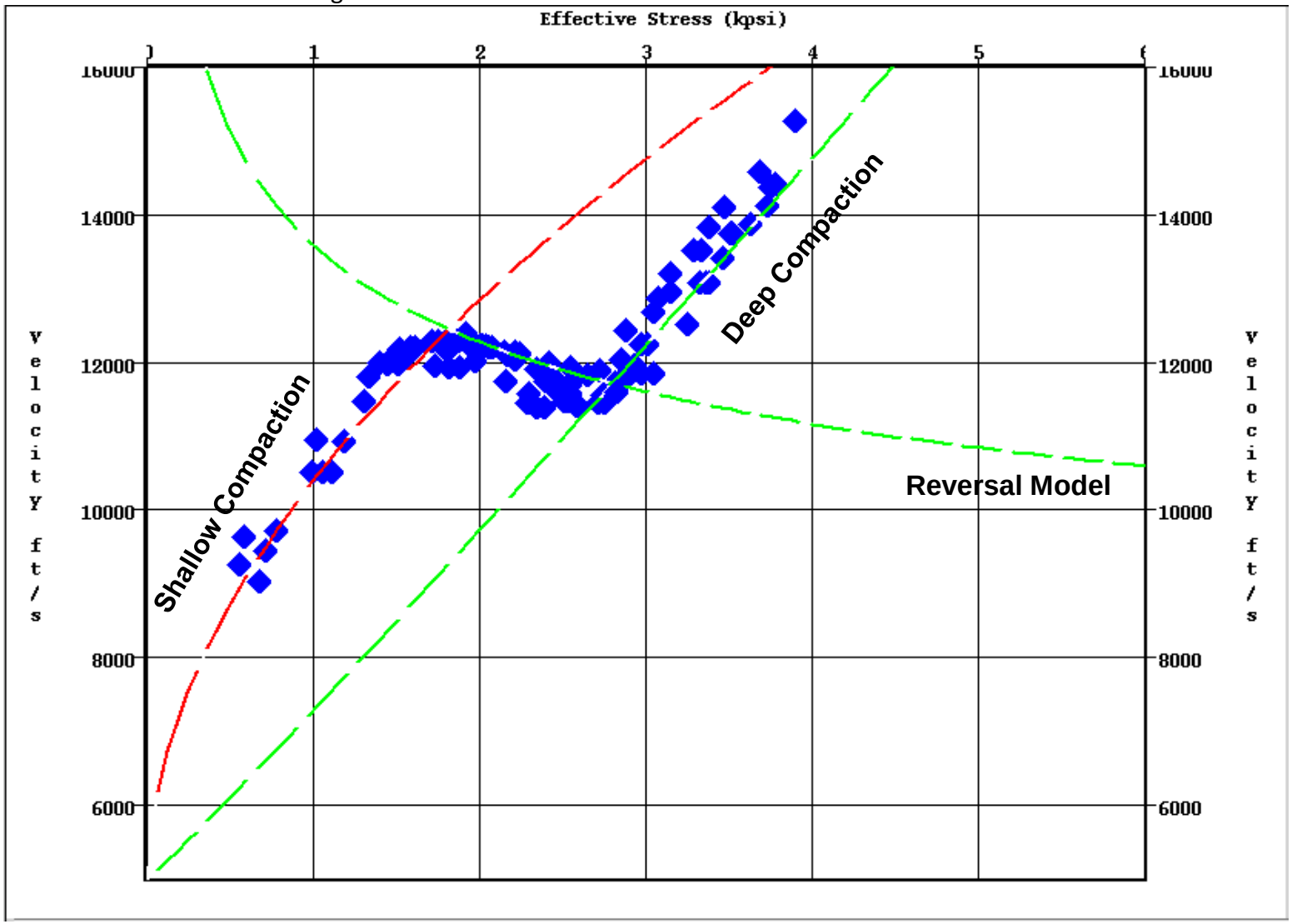

Figure 4.14: Effective stress cross-plot showing the mud weight data for all calibration wells plotted against the REVEL interval velocity. The curves for shallow compaction, reversal interval and deep compaction are also shown.

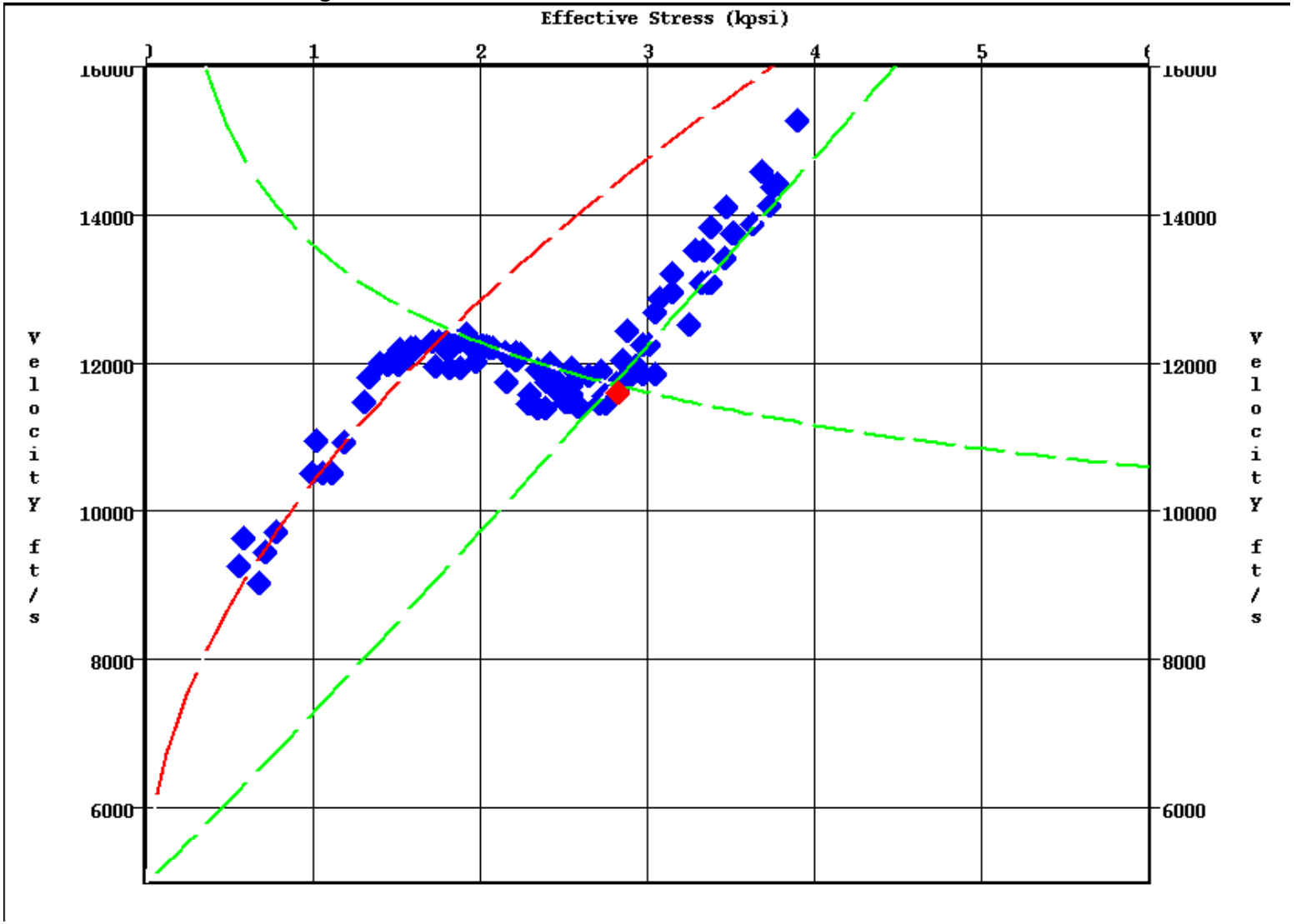

Figure 4.15: Effective stress cross-plot showing the mud weight data for all calibration wells plotted against the REVEL interval velocity. The curves for shallow compaction, reversal interval and deep compaction are also shown. The red data points are from the NPR3 LX #28-34 well.

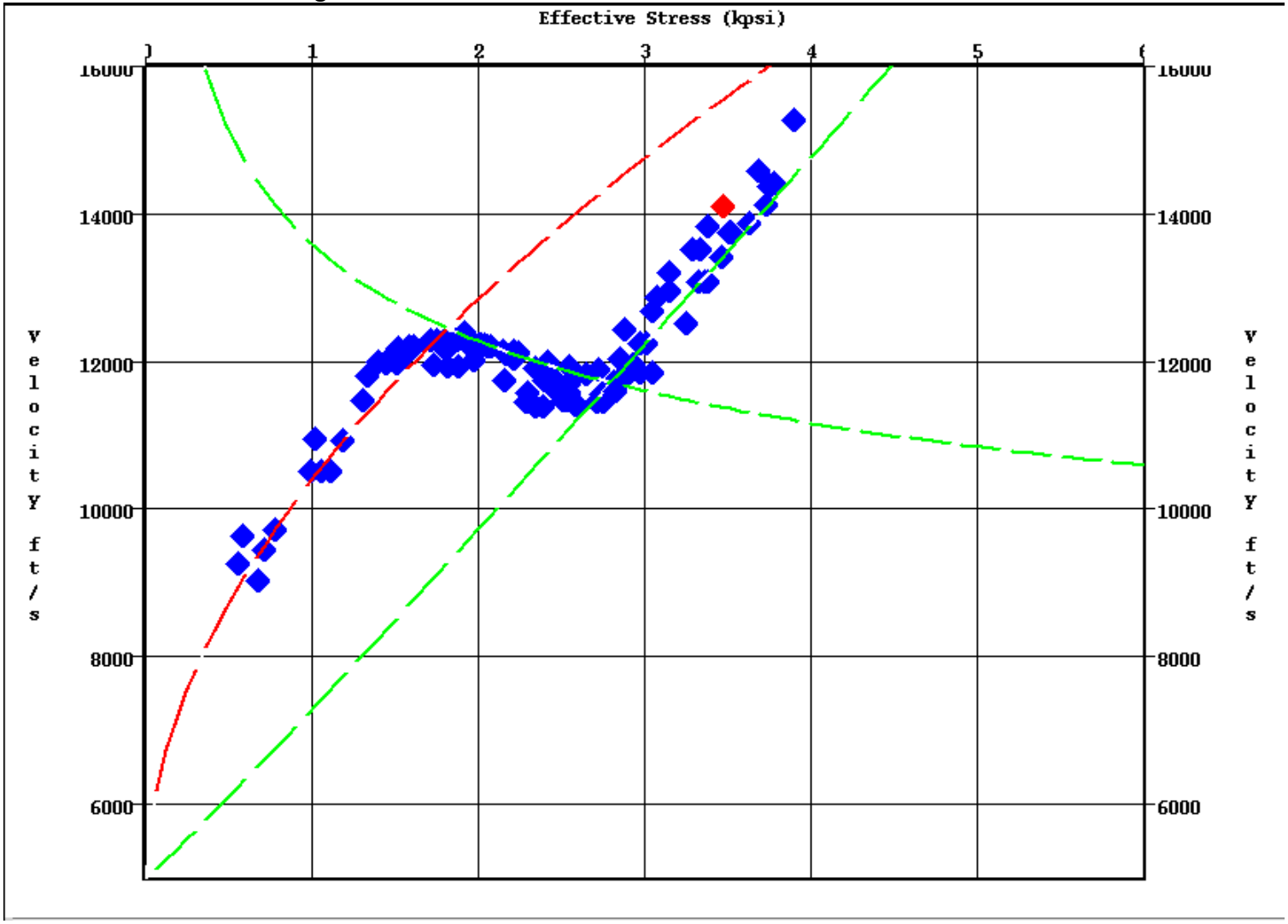

Figure 4.16: Effective stress cross-plot showing the mud weight data for all calibration wells plotted against the REVEL interval velocity. The curves for shallow compaction, reversal interval and deep compaction are also shown. The red data points are from the NPR3 #67X-1 well.

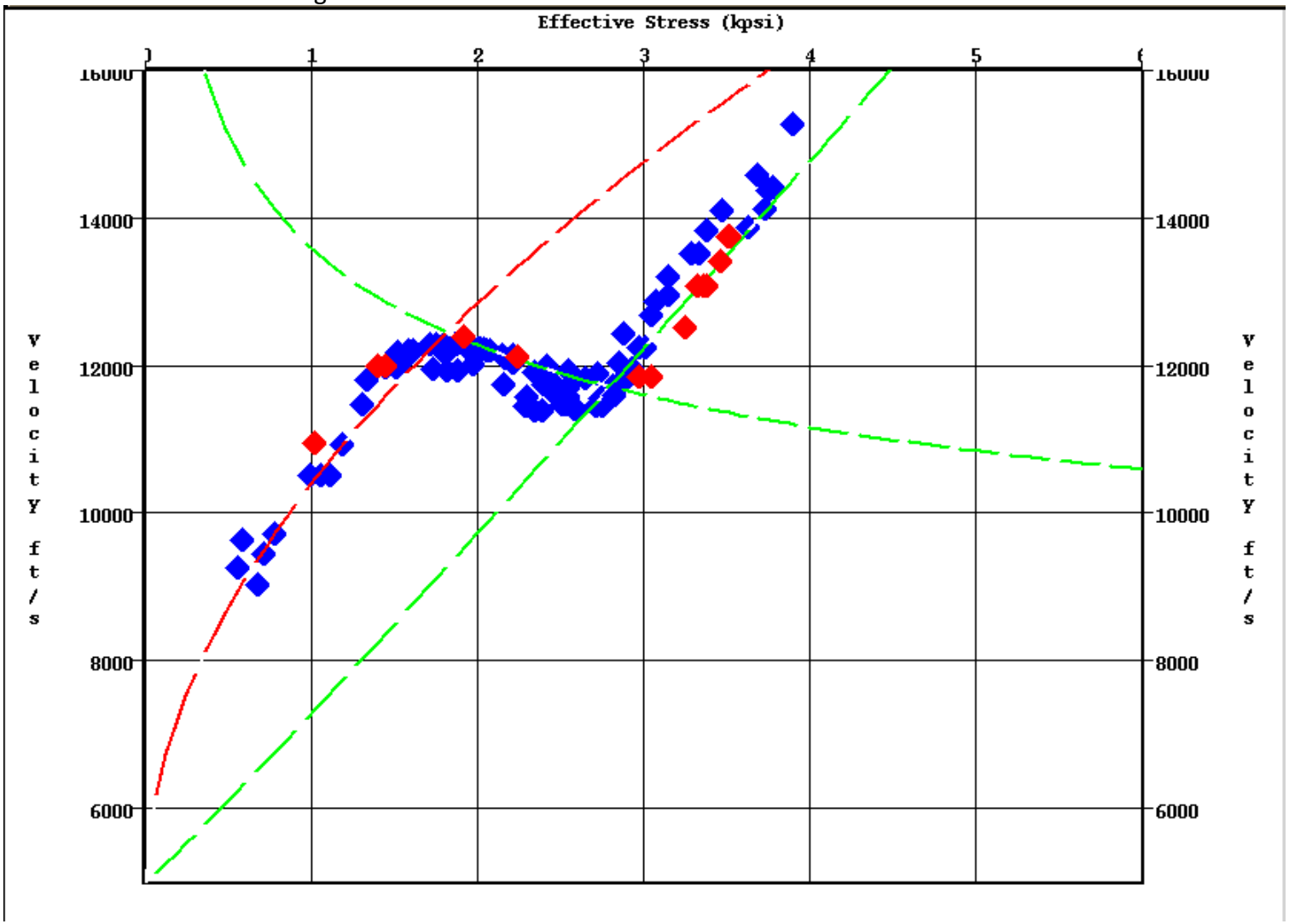

Figure 4.17: Effective stress cross-plot showing the mud weight data for all calibration wells plotted against the REVEL interval velocity. The curves for shallow compaction, reversal interval and deep compaction are also shown. The red data points are from the Dept X #2-3 well.

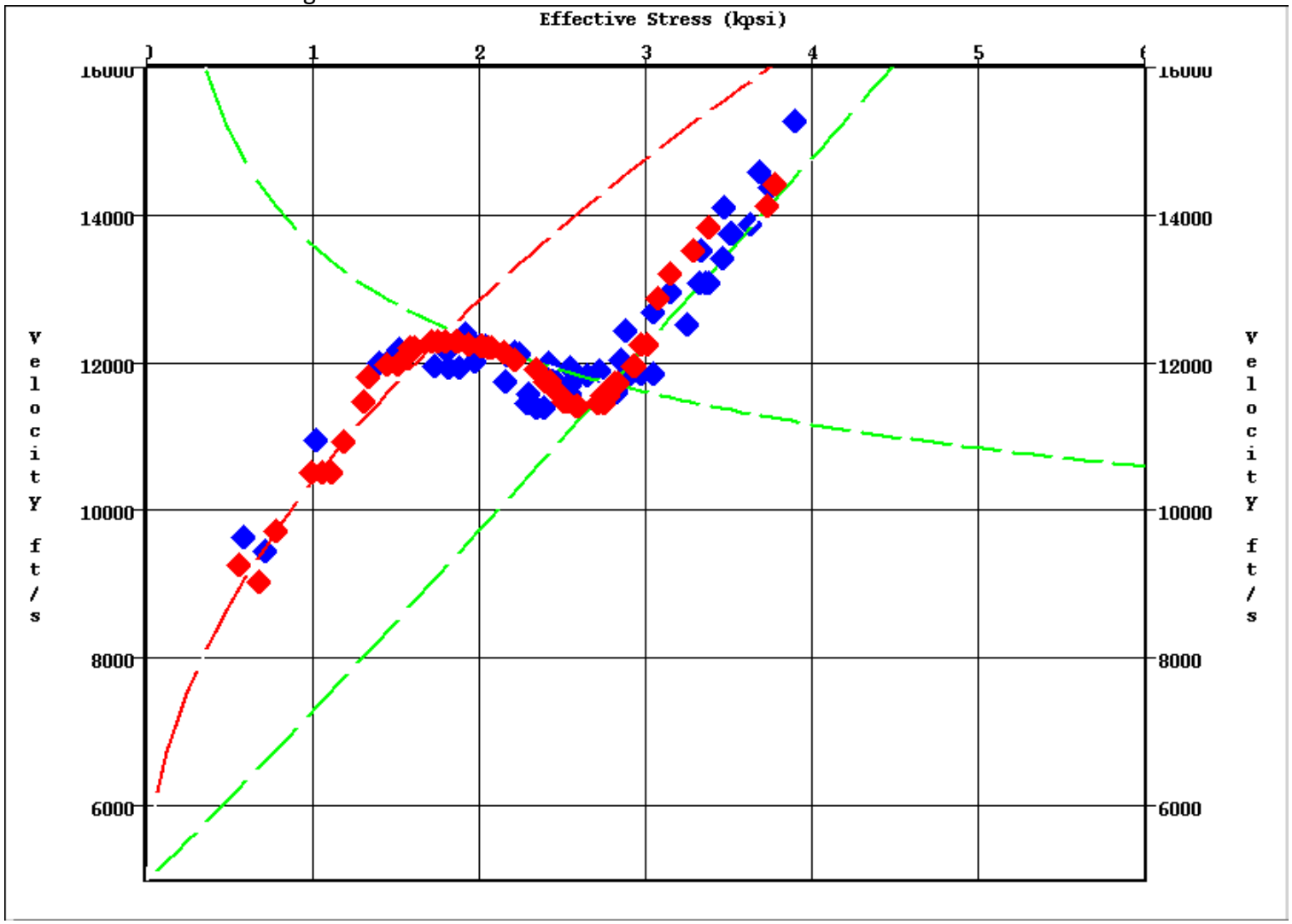

Figure 4.18: Effective stress cross-plot showing the mud weight data for all calibration wells plotted against the REVEL interval velocity. The curves for shallow compaction, reversal interval and deep compaction are also shown. The red data points are from the FNX WX #17-21 well.

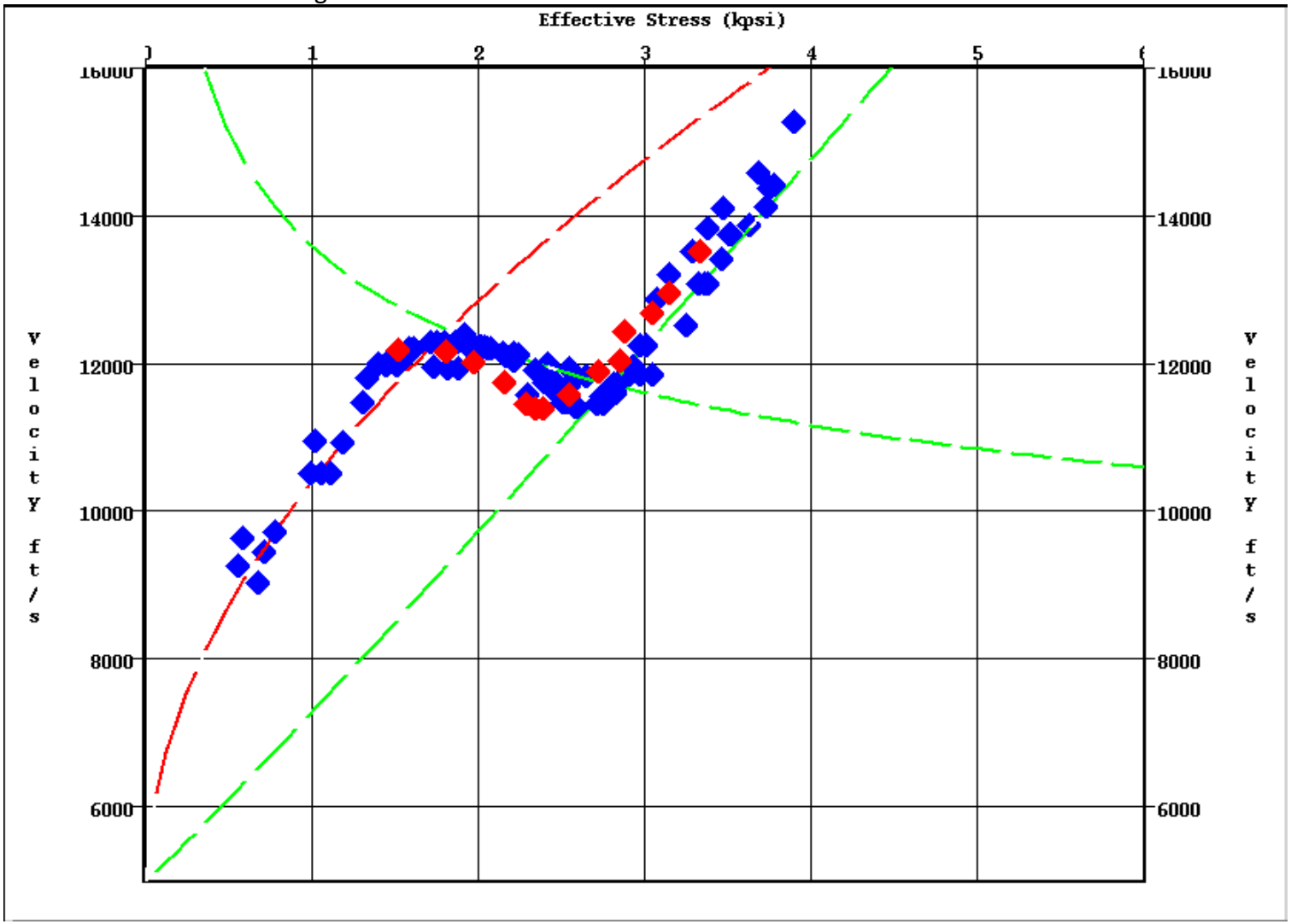

Figure 4.19: Effective stress cross-plot showing the mud weight data for all calibration wells plotted against the REVEL interval velocity. The curves for shallow compaction, reversal interval and deep compaction are also shown. The red data points are from the Law 62 TPX #10-10 well.

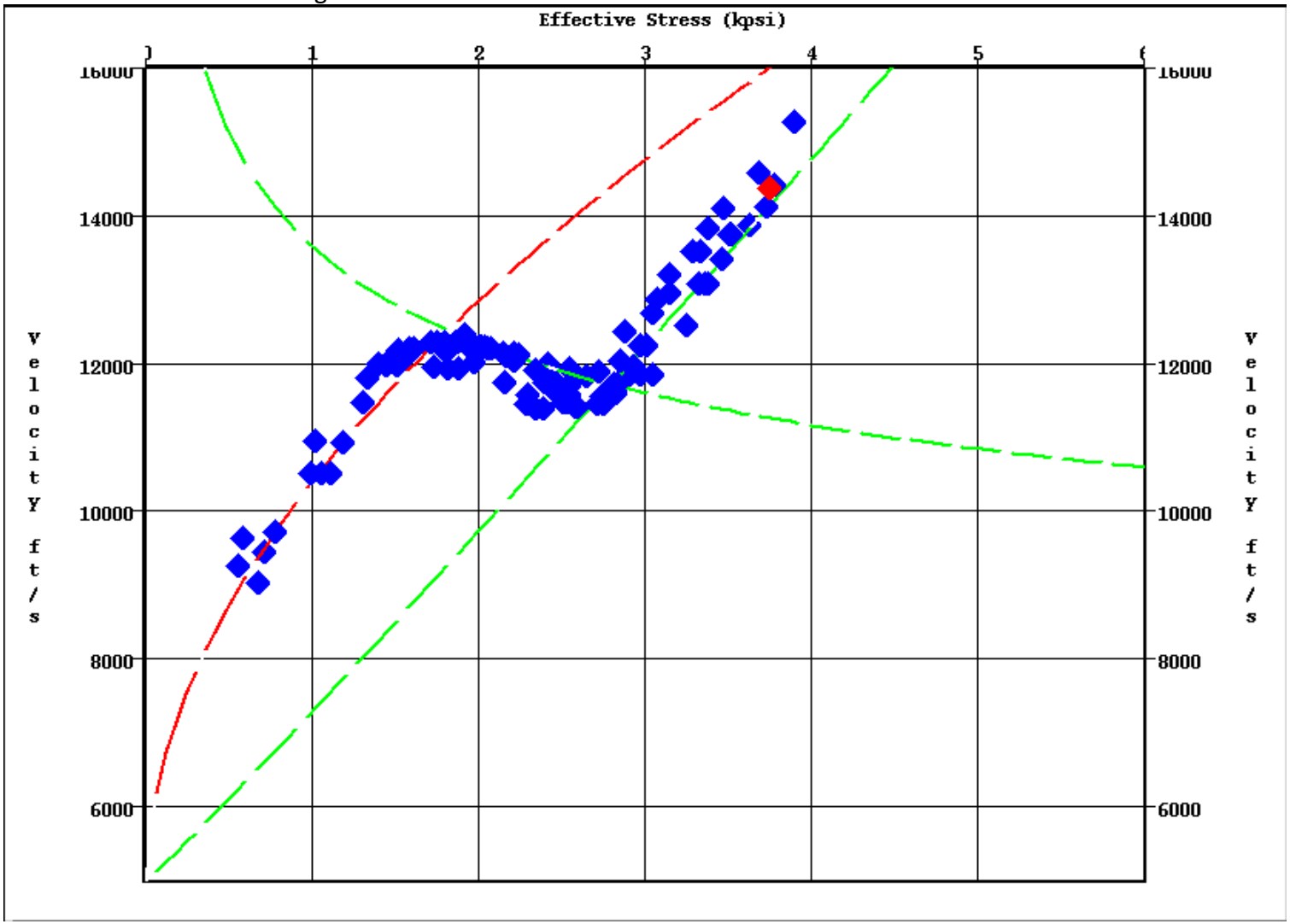

Figure 4.20: Effective stress cross-plot showing the mud weight data for all calibration wells plotted against the REVEL interval velocity. The curves for shallow compaction, reversal interval and deep compaction are also shown. The red data points are from the Law X #11-11 well.

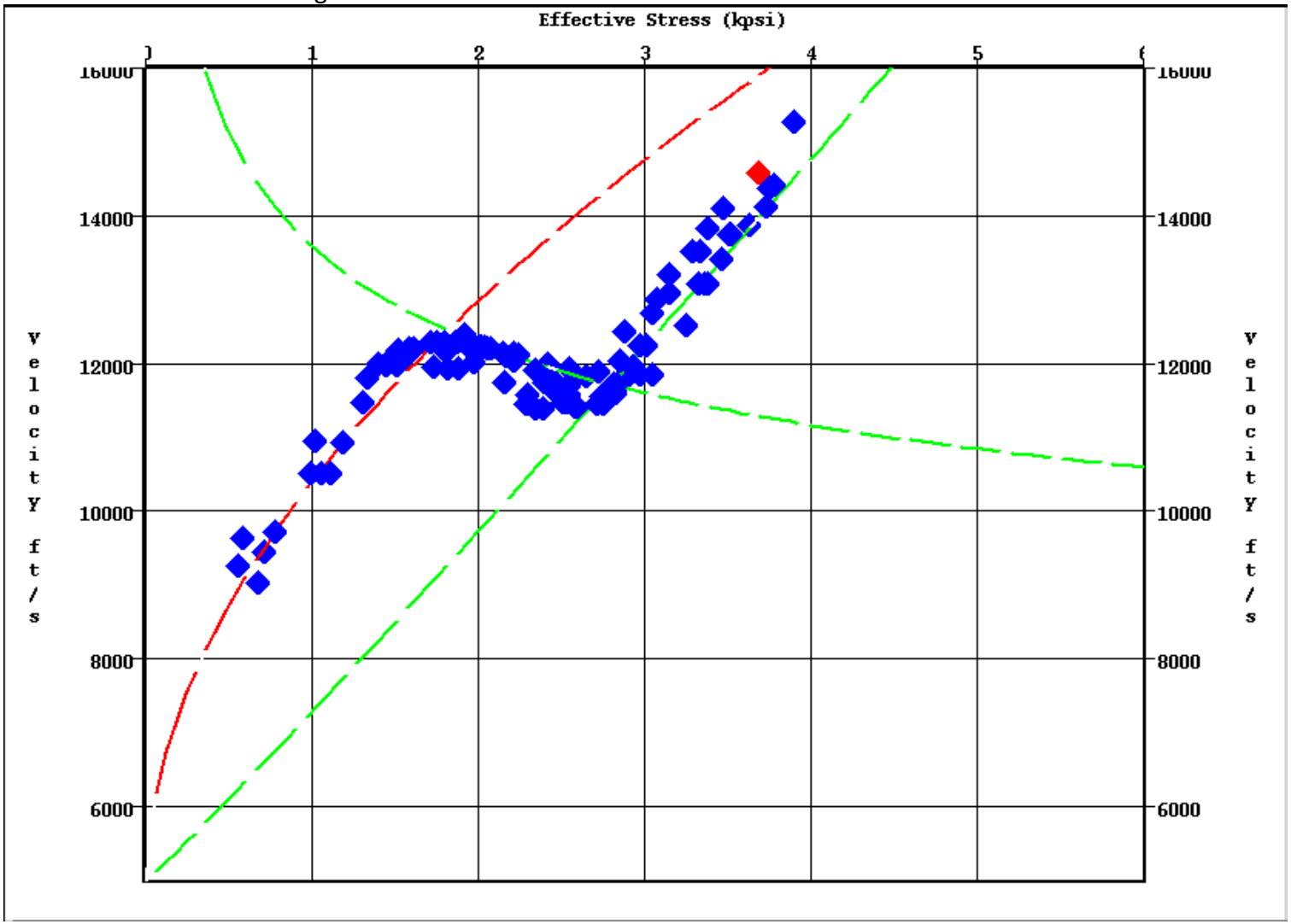

Figure 4.21: Effective stress cross-plot showing the mud weight data for all calibration wells plotted against the REVEL interval velocity. The curves for shallow compaction, reversal interval and deep compaction are also shown. The red data points are from the Law X #25-11 well.

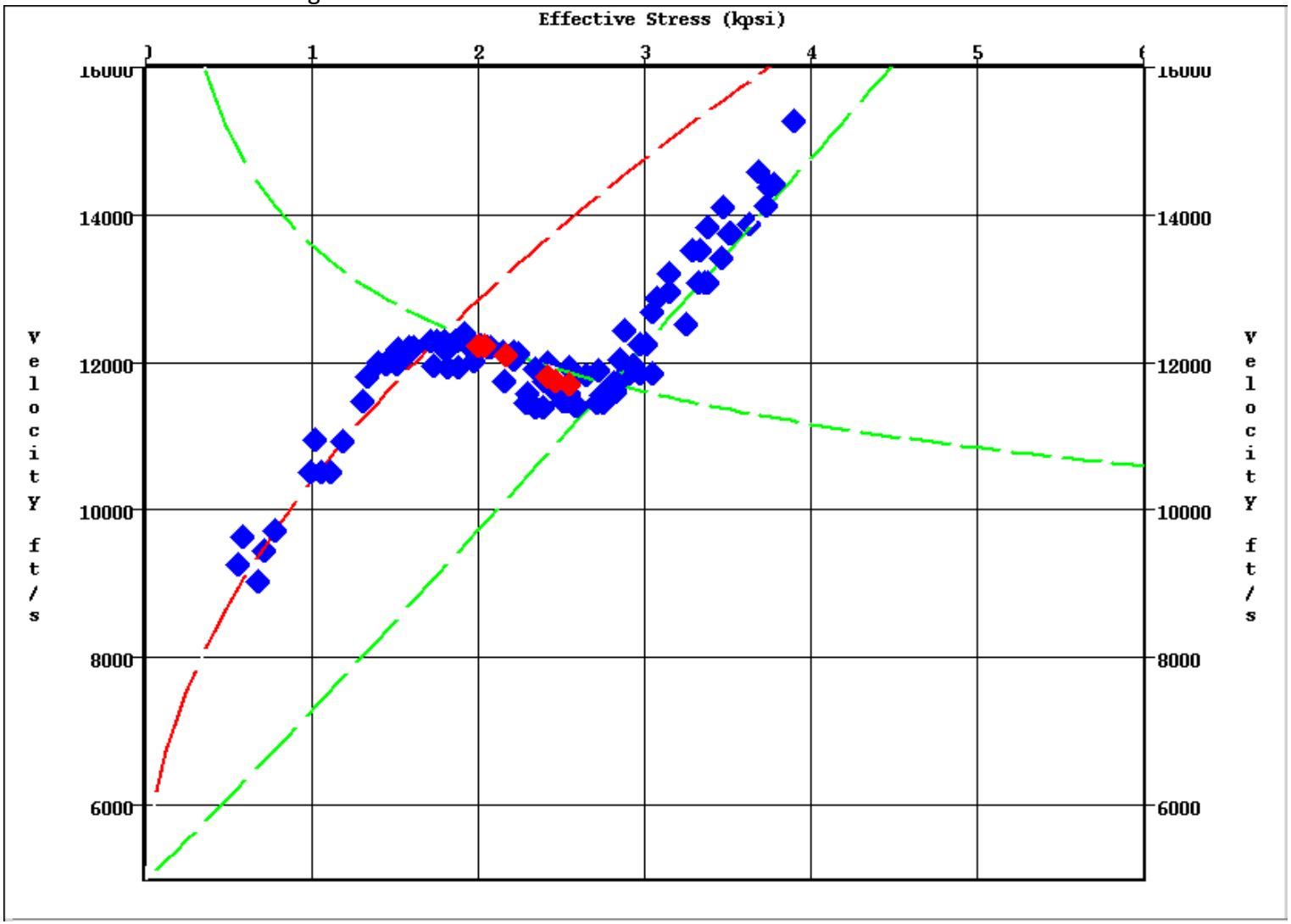

Figure 4.22: Effective stress cross-plot showing the mud weight data for all calibration wells plotted against the REVEL interval velocity. The curves for shallow compaction, reversal interval and deep compaction are also shown. The red data points are from the Law X #64-15 well.

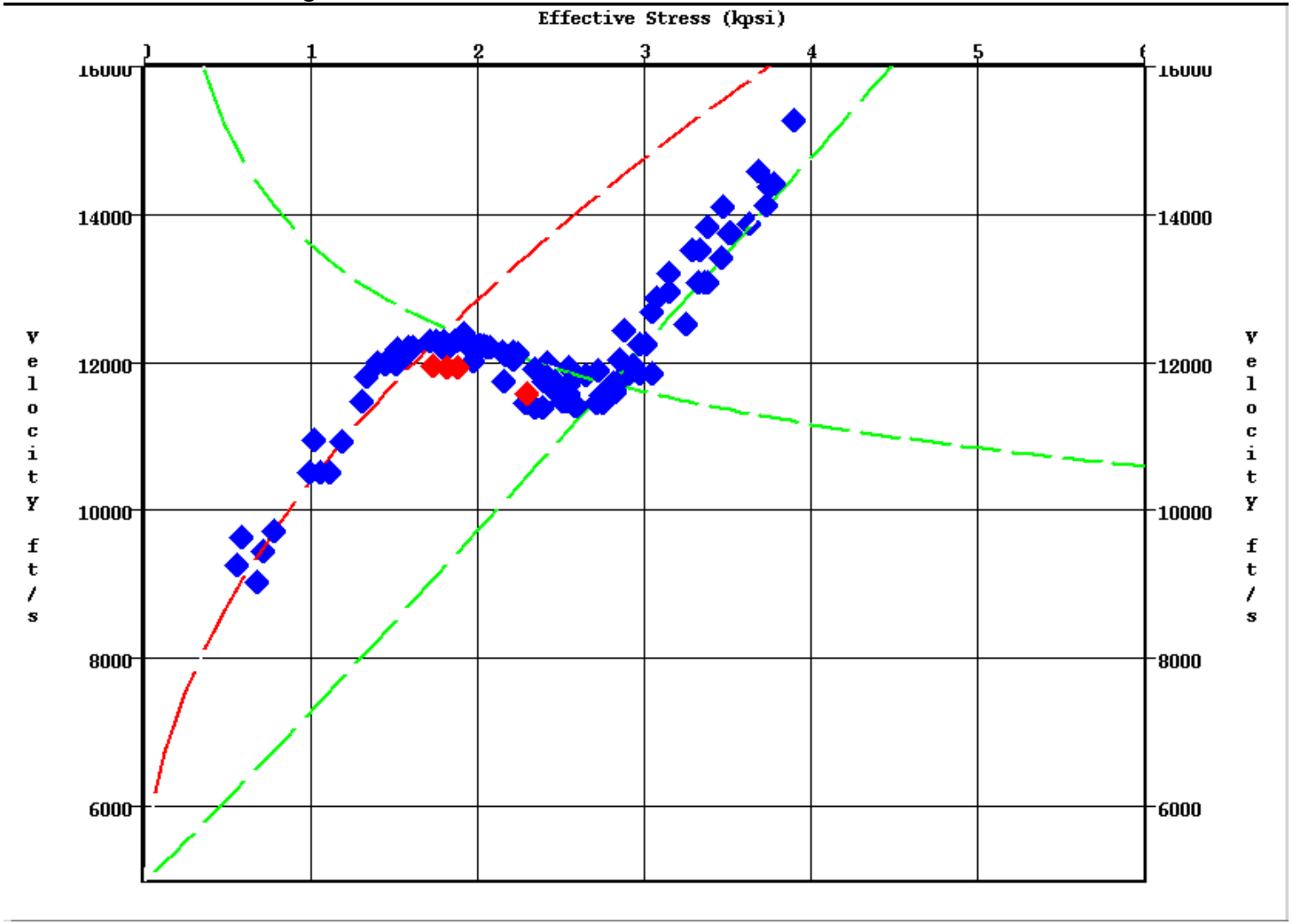

Figure 4.23: Effective stress cross-plot showing the mud weight data for all calibration wells plotted against the REVEL interval velocity. The curves for shallow compaction, reversal interval and deep compaction are also shown. The red data points are from the Law X #88-3 well.

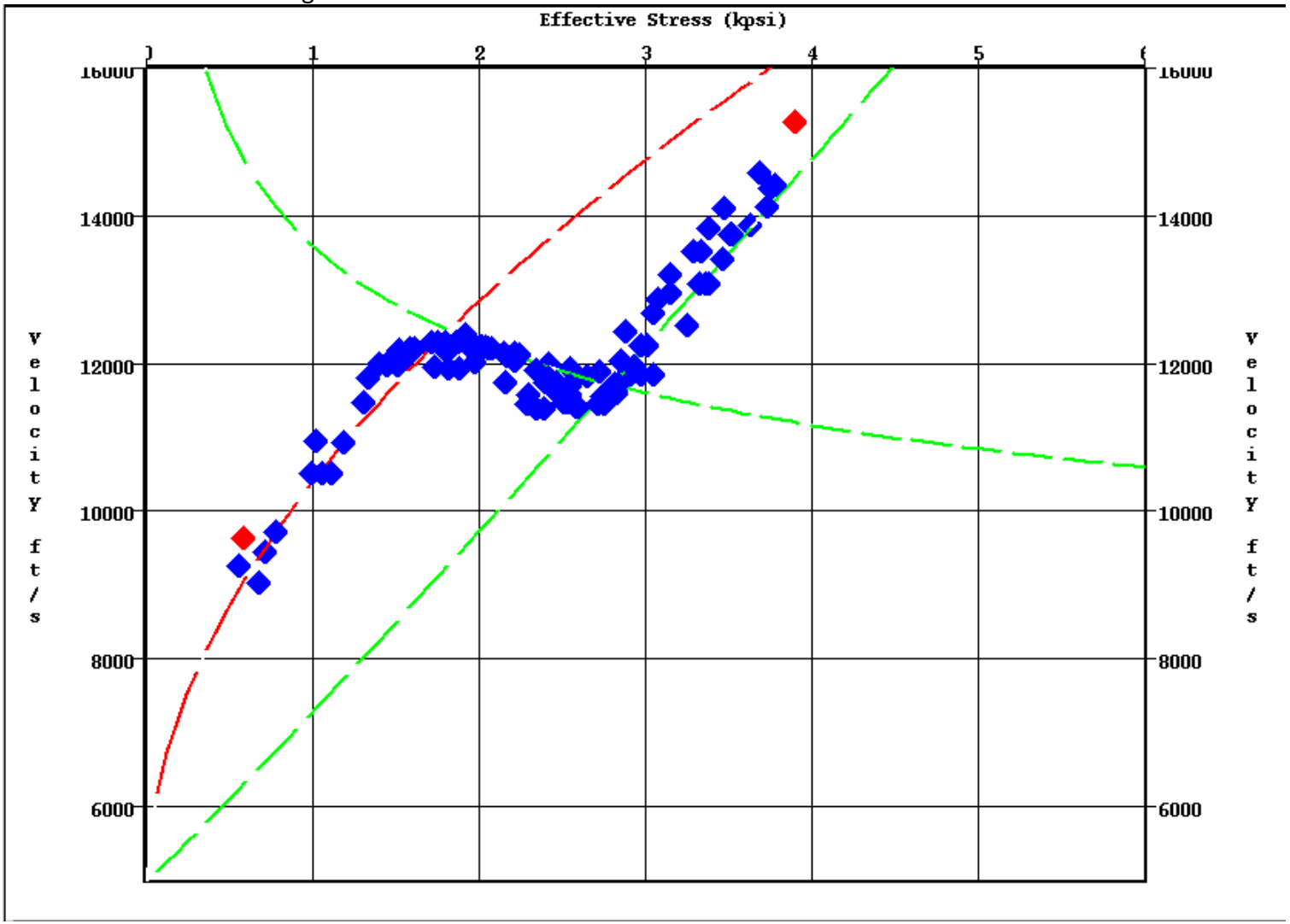

Figure 4.24: Effective stress cross-plot showing the mud weight data for all calibration wells plotted against the REVEL interval velocity. The curves for shallow compaction, reversal interval and deep compaction are also shown. The red data points are from the Law X #62-11 well.

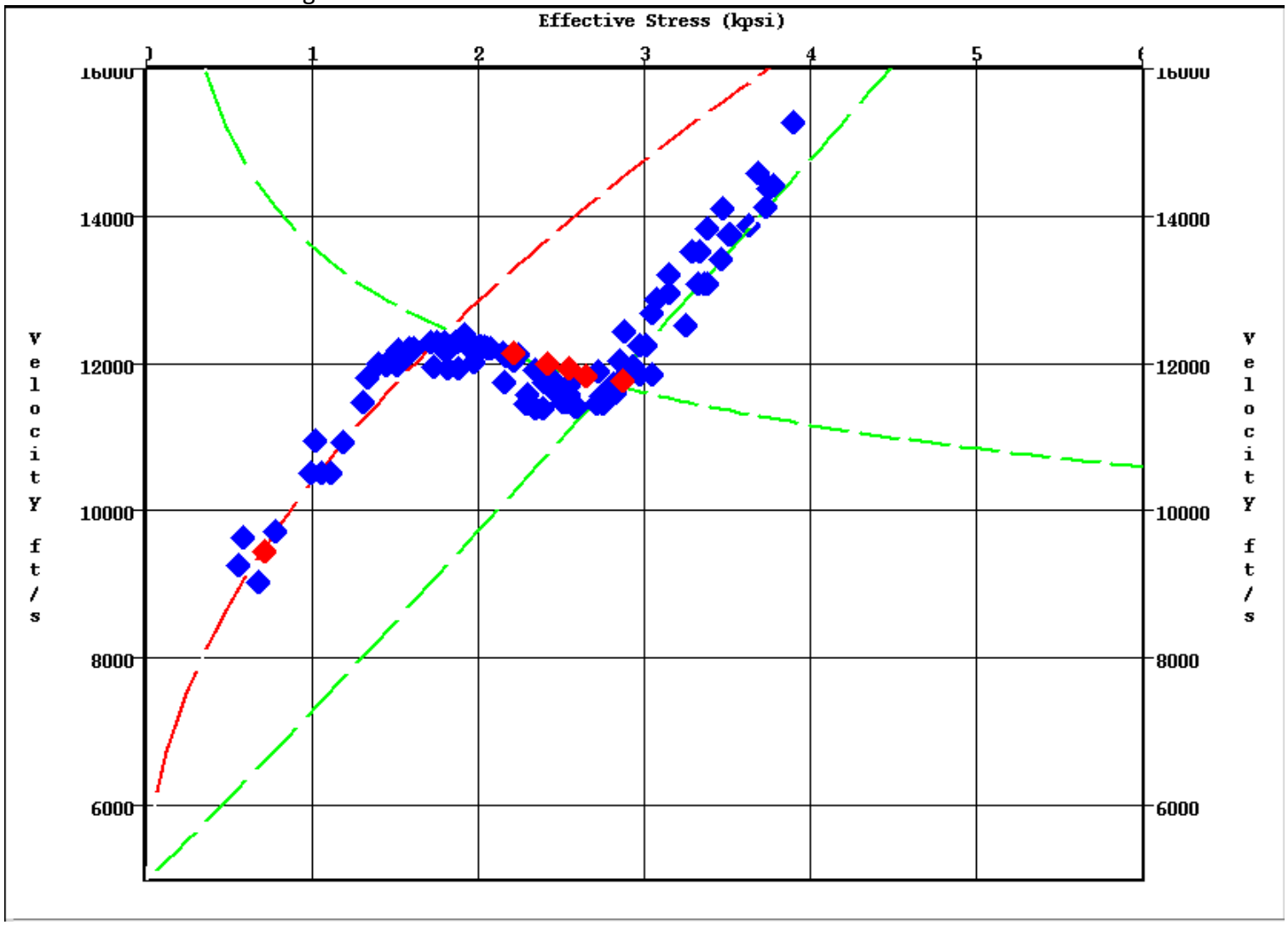

Figure 4.25: Effective stress cross-plot showing the mud weight data for all calibration wells plotted against the REVEL interval velocity. The curves for shallow compaction, reversal interval and deep compaction are also shown. The red data points are from the NPR3 X #33-23 well.

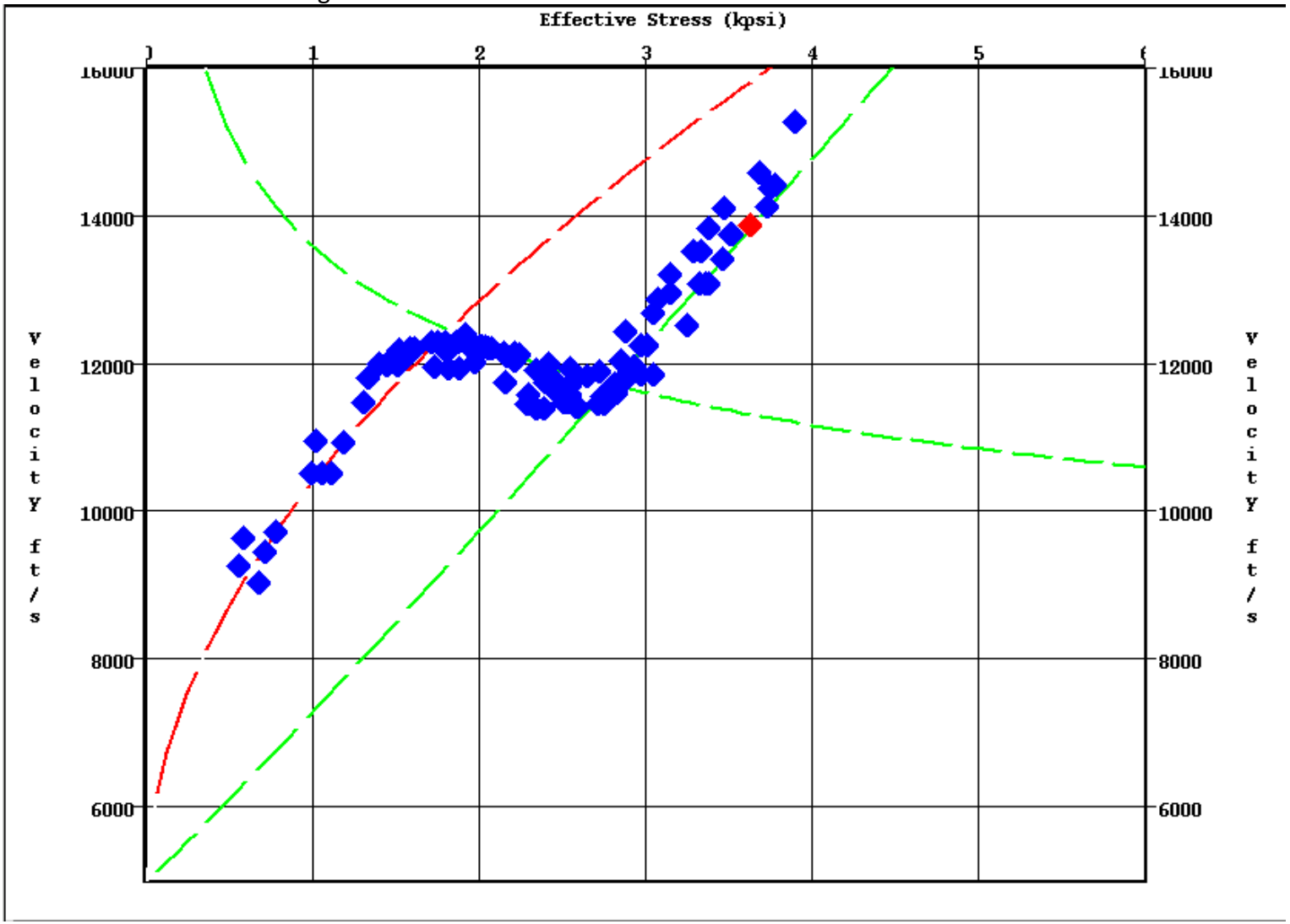

Figure 4.26: Effective stress cross-plot showing the mud weight data for all calibration wells plotted against the REVEL interval velocity. The curves for shallow compaction, reversal interval and deep compaction are also shown. The red data points are from the FNX NPR #371X well.

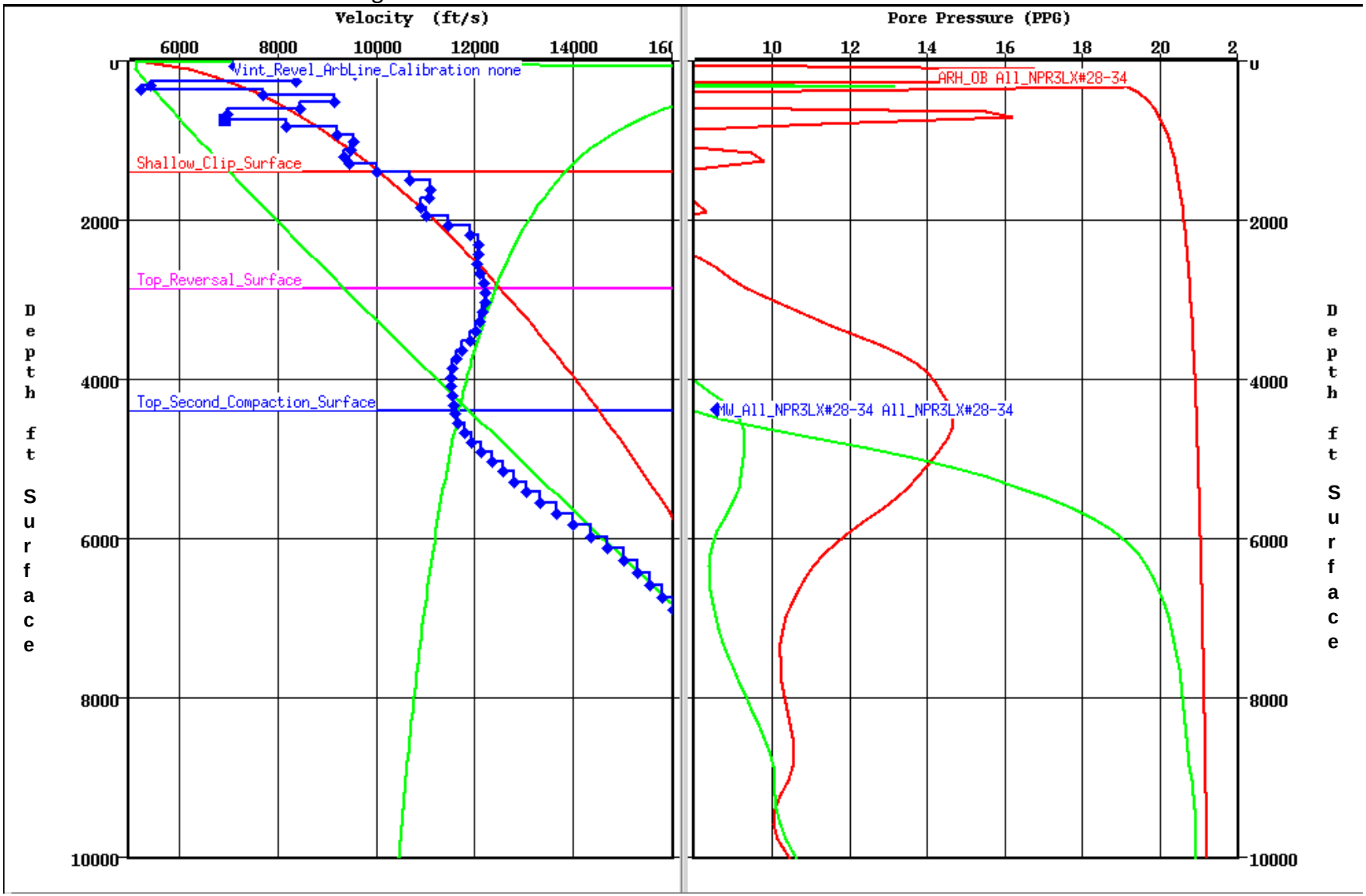

Figure 4.27: Calibration display for the NPR 3LX #28-34 well showing the REVEL interval velocity (left panel) and the resulting pressure predictions for the three layer earth model. Mud weights are shown as blue diamonds.

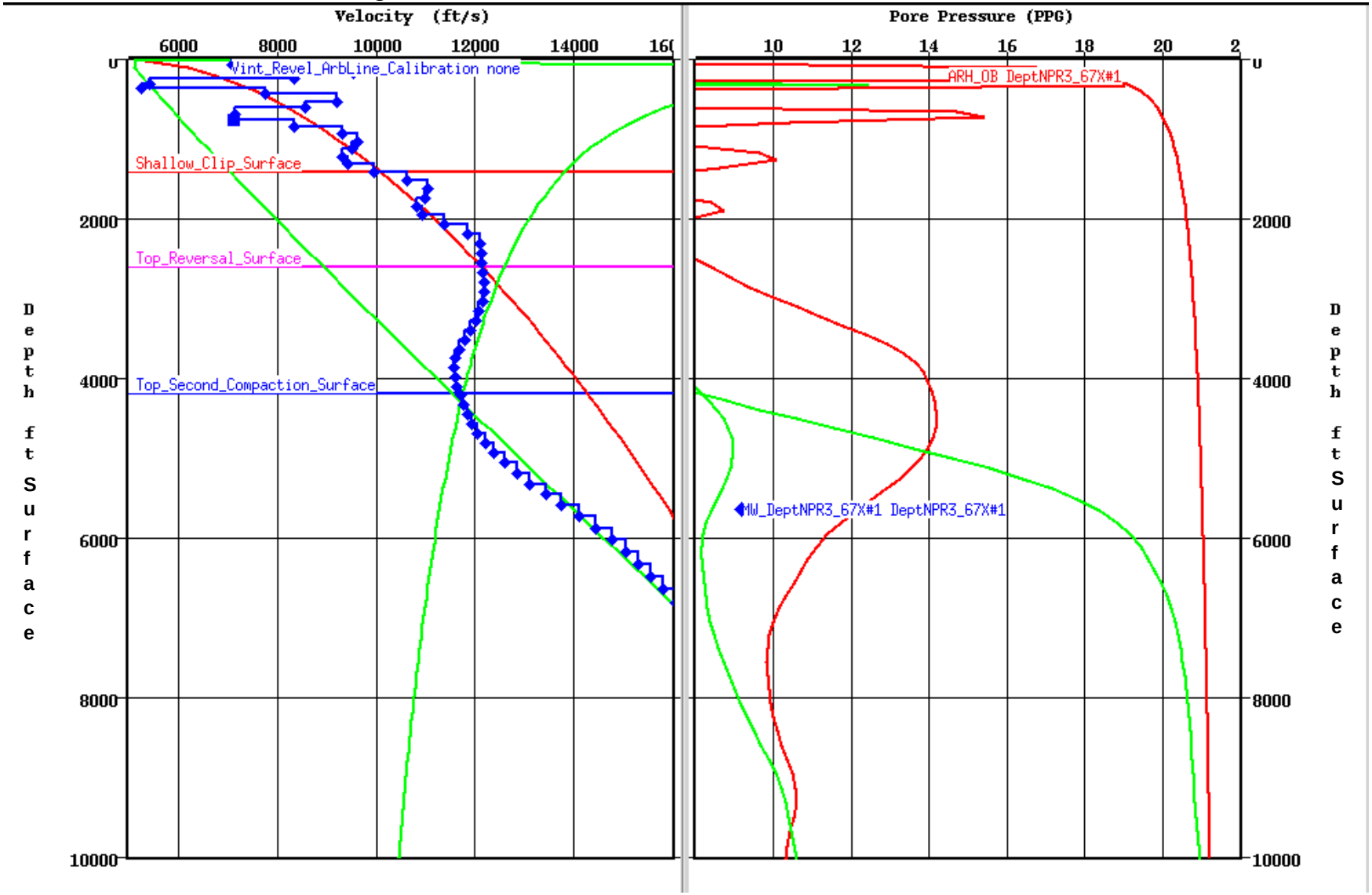

Figure 4.28: Calibration display for the NPR3 67X #1 well showing the REVEL interval velocity (left panel) and the resulting pressure predictions for the three layer earth model. Mud weights are shown as blue diamonds.

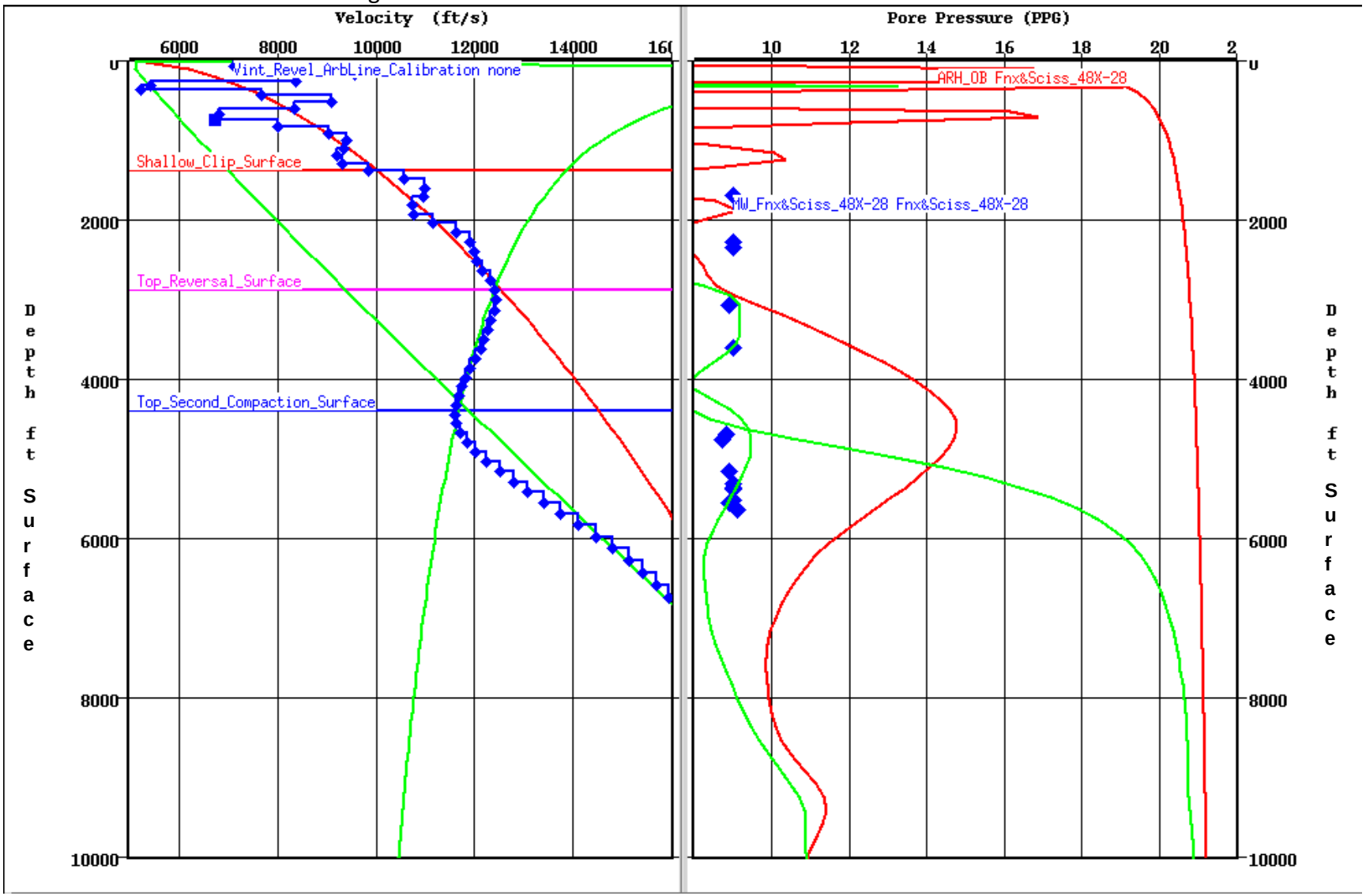

Figure 4.29: Calibration display for the FNX X #48-28 well showing the REVEL interval velocity (left panel) and the resulting pressure predictions for the three layer earth model. Mud weights are shown as blue diamonds.

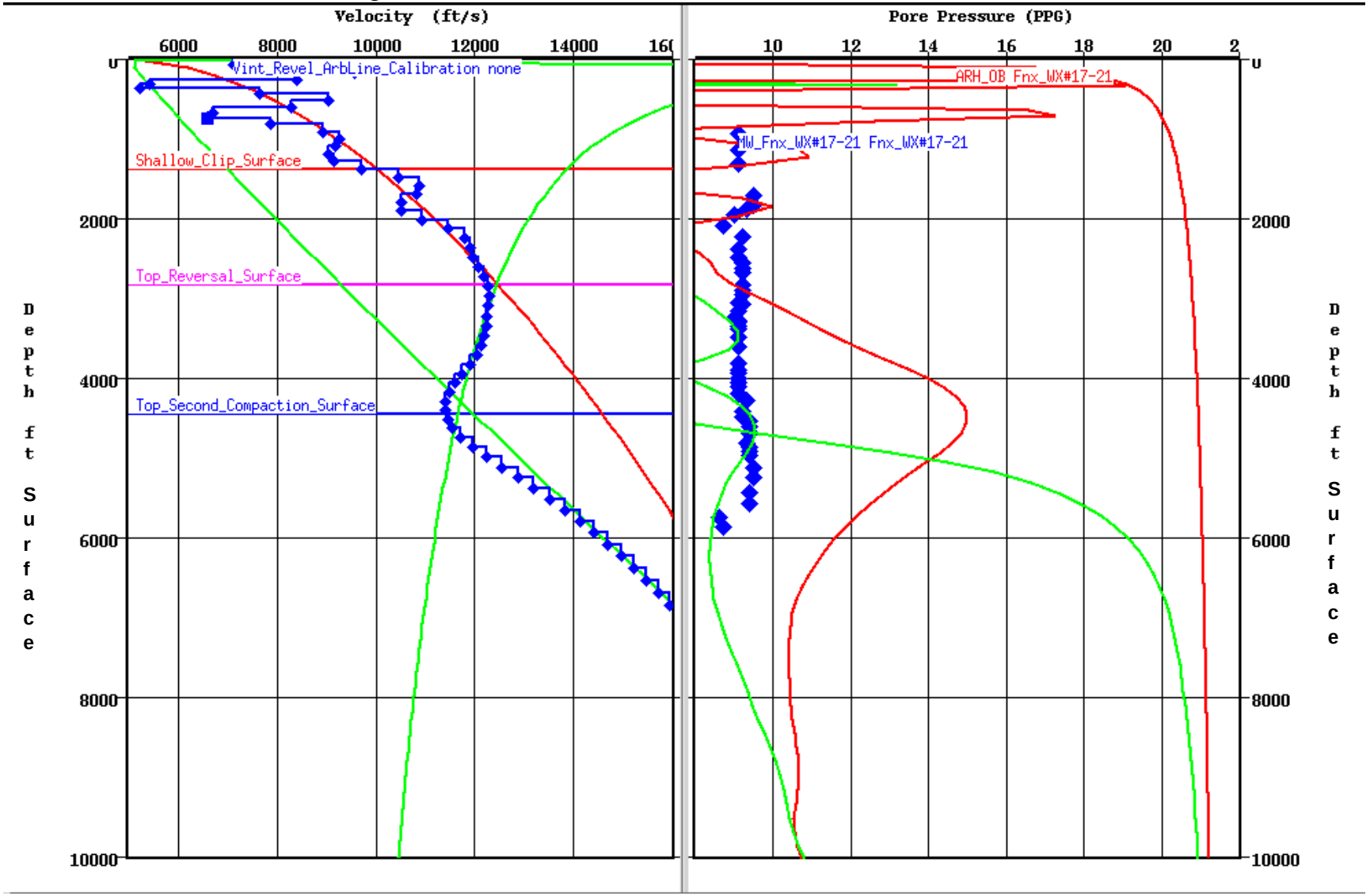

Figure 4.30: Calibration display for the FNX WX #17-21 well showing the REVEL interval velocity (left panel) and the resulting pressure predictions for the three layer earth model. Mud weights are shown as blue diamonds.

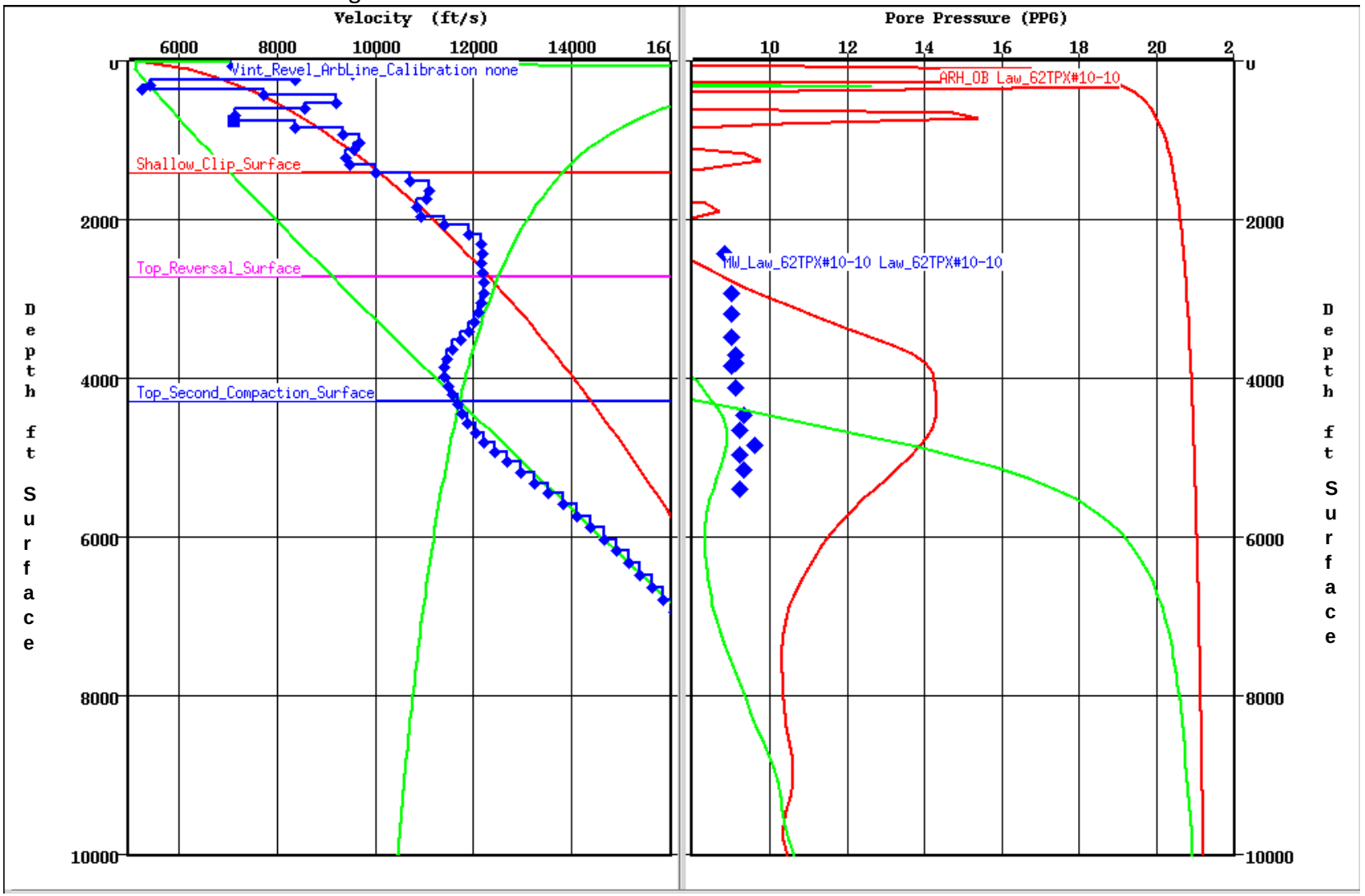

Figure 4.31: Calibration display for the Law 62 TPX #10-10 well showing the REVEL interval velocity (left panel) and the resulting pressure predictions for the three layer earth model. Mud weights are shown as blue diamonds.

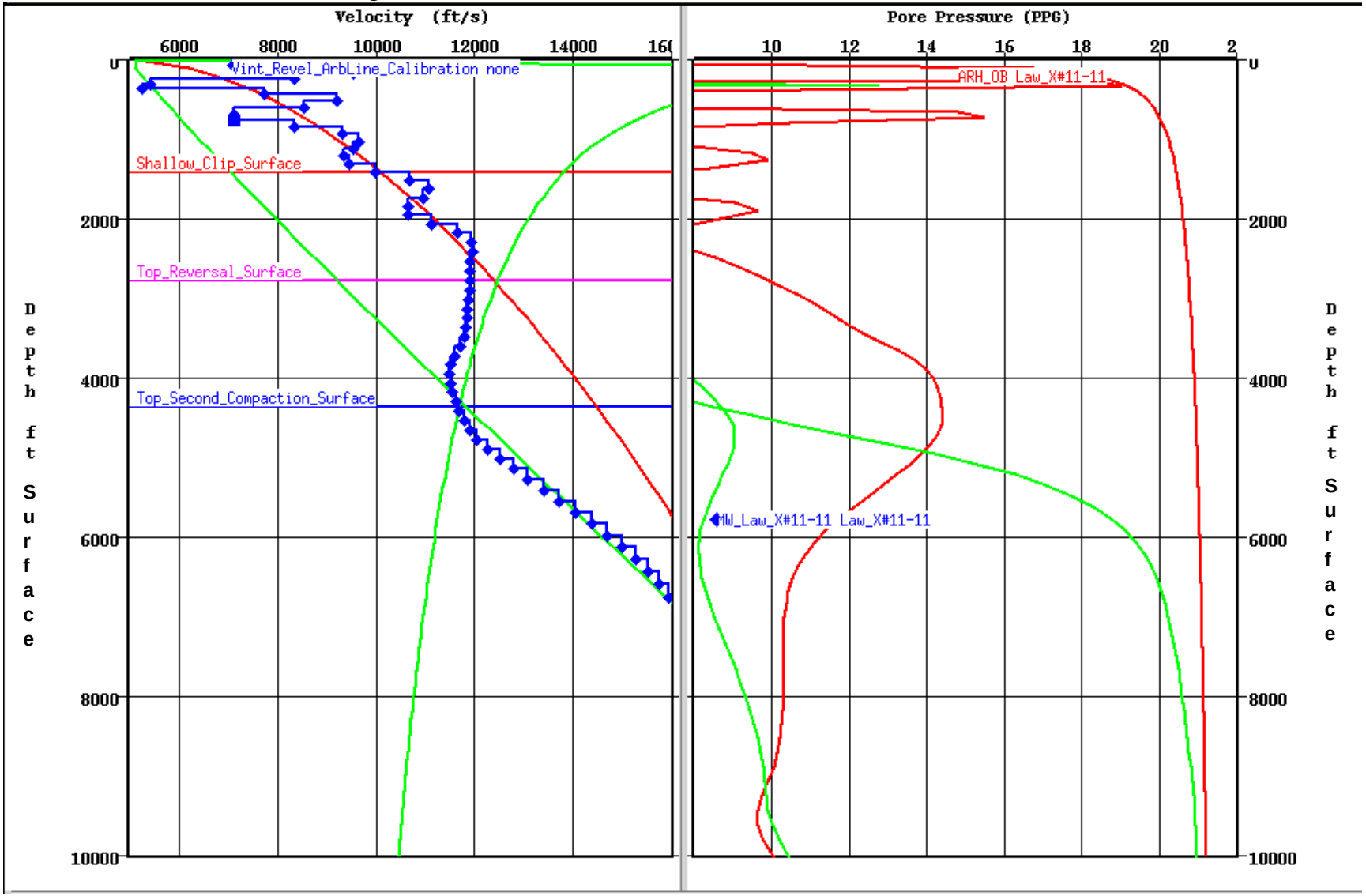

Figure 4.32: Calibration display for the Law X #11-11 well showing the REVEL interval velocity (left panel) and the resulting pressure predictions for the three layer earth model. Mud weights are shown as blue diamonds.

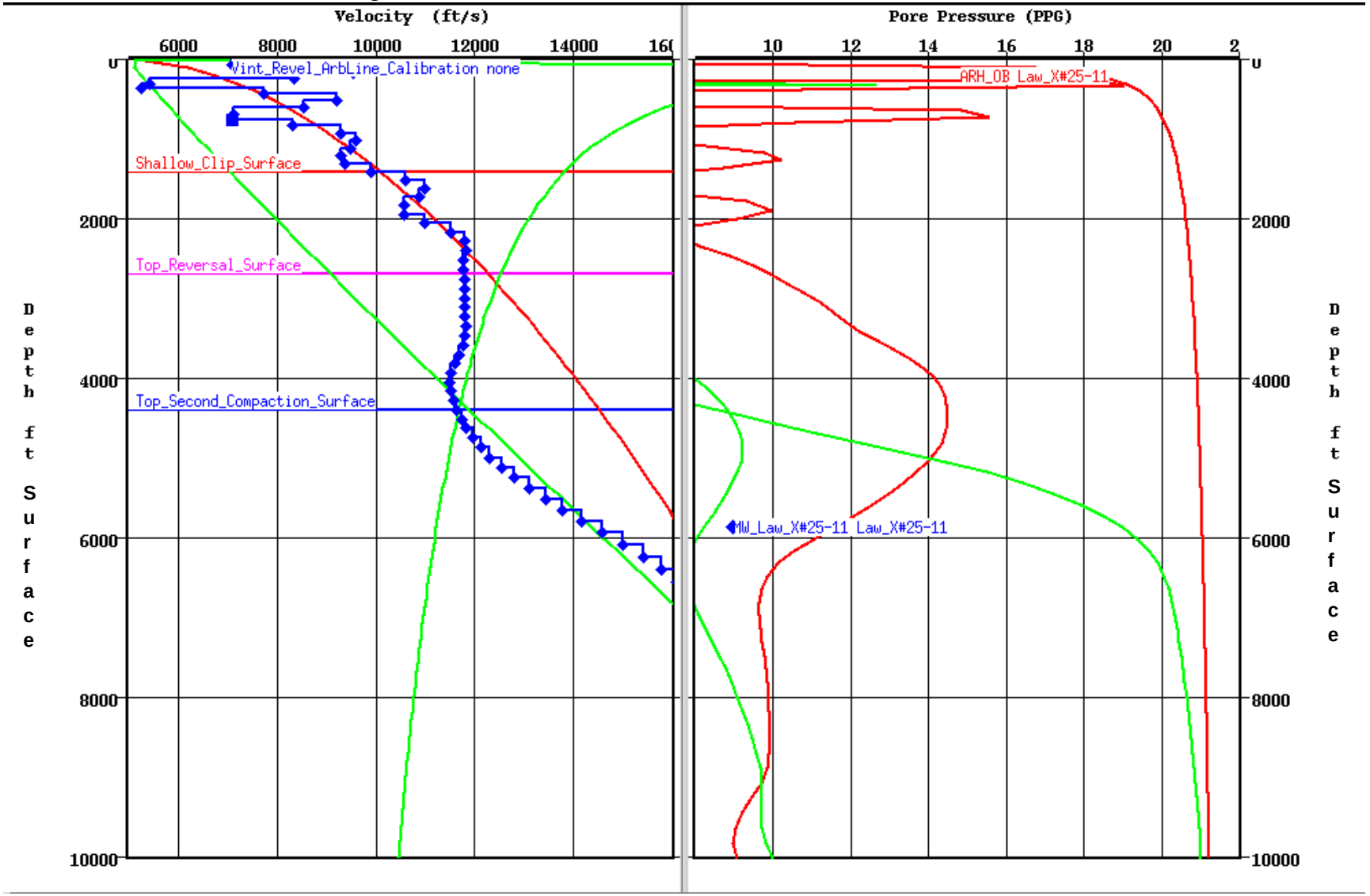

Figure 4.33: Calibration display for the Law X #25-11 well showing the REVEL interval velocity (left panel) and the resulting pressure predictions for the three layer earth model. Mud weights are shown as blue diamonds.

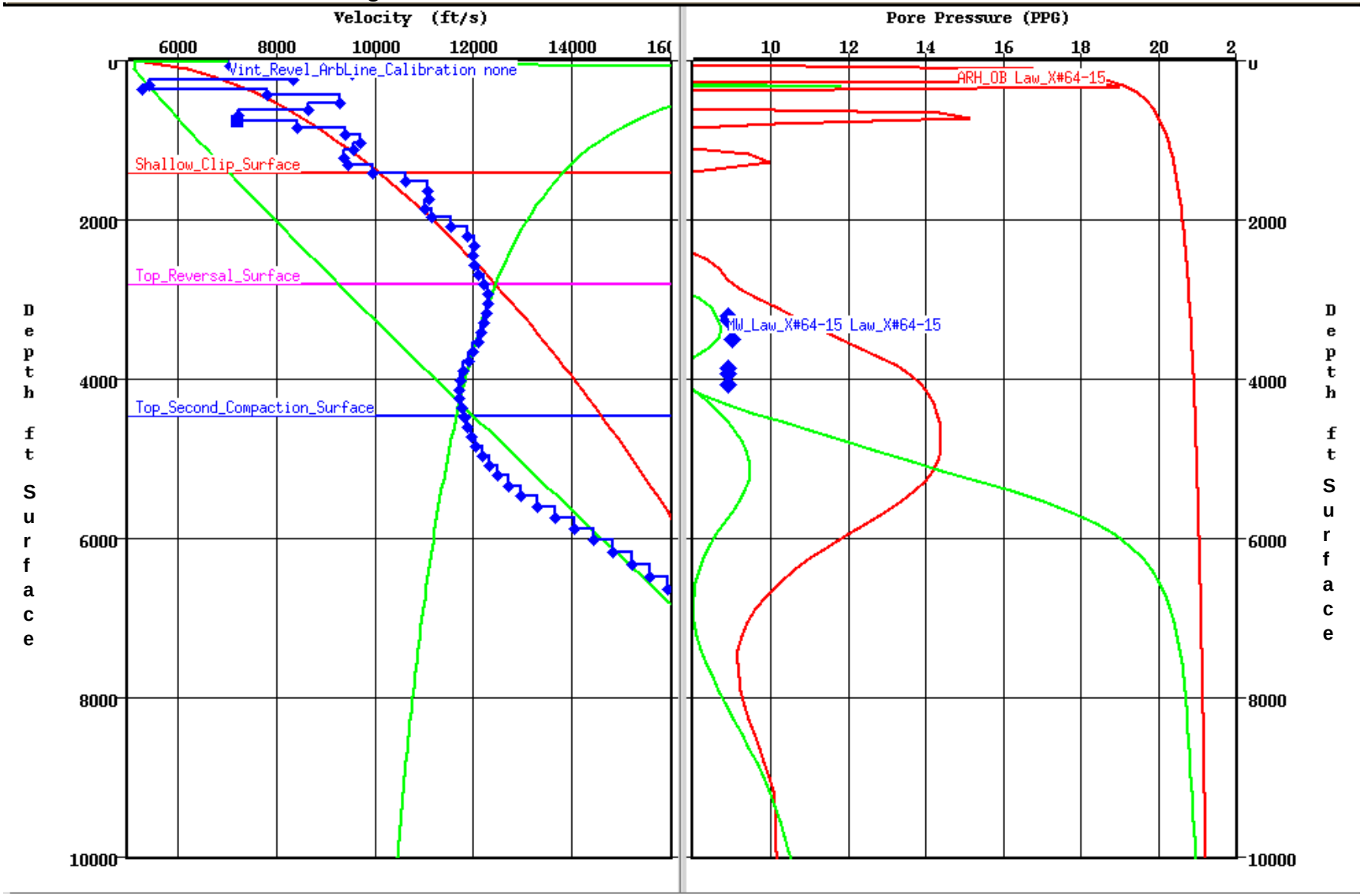

Figure 4.34: Calibration display for the Law X #64-15 well showing the REVEL interval velocity (left panel) and the resulting pressure predictions for the three layer earth model. Mud weights are shown as blue diamonds.

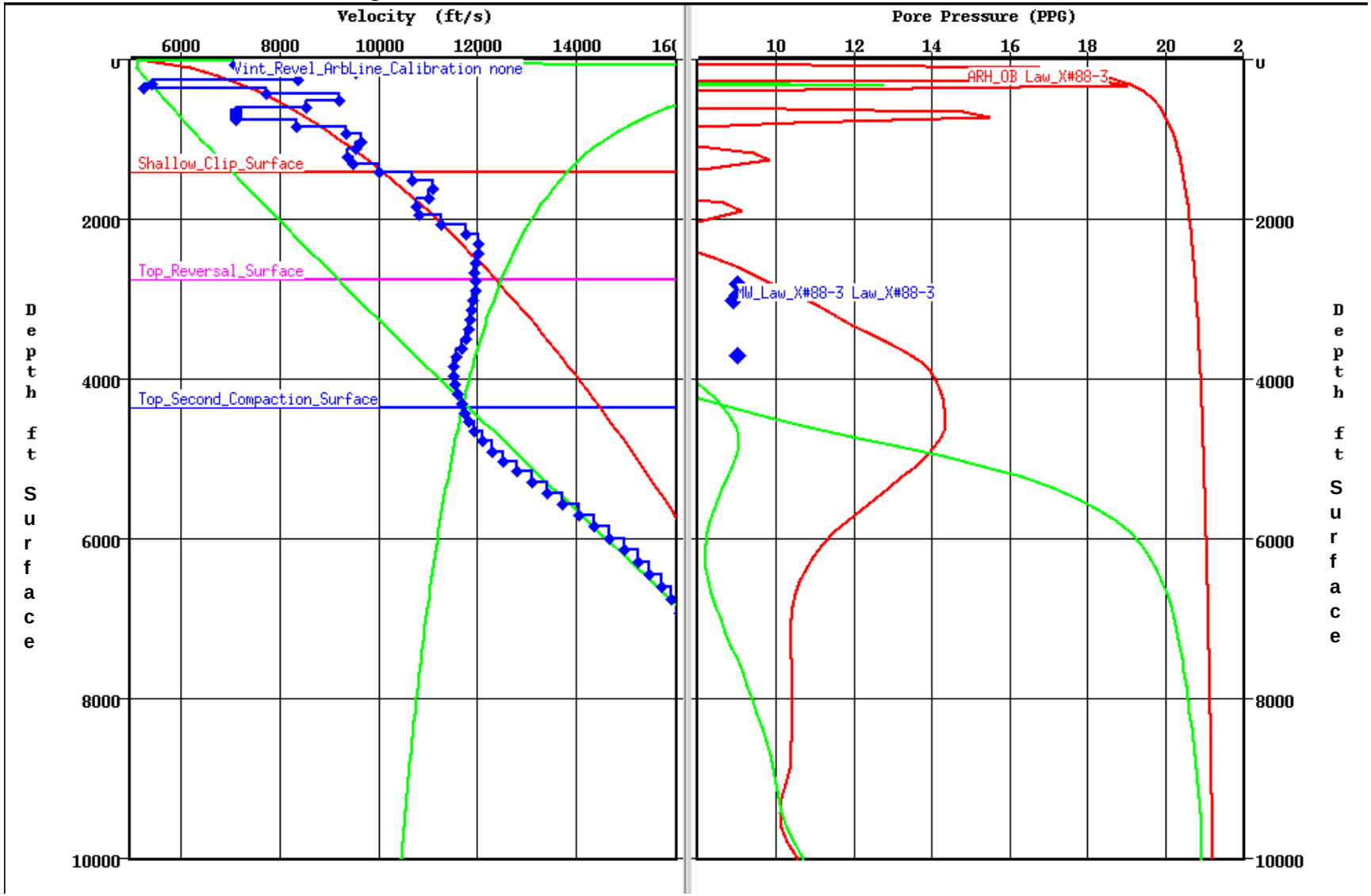

Figure 4.35: Calibration display for the Law X #88-3 well showing the REVEL interval velocity (left panel) and the resulting pressure predictions for the three layer earth model. Mud weights are shown as blue diamonds.

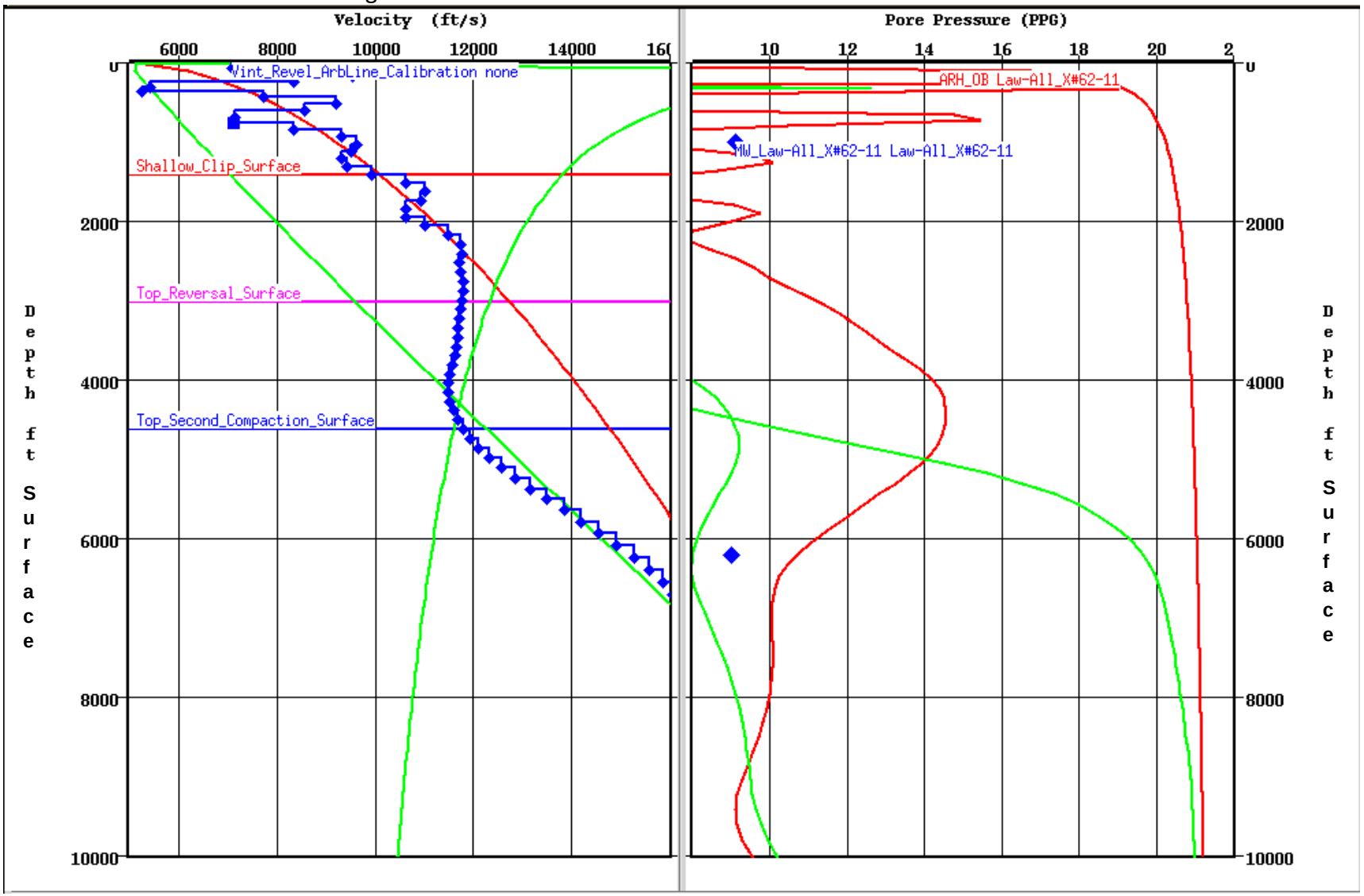

Figure 4.36: Calibration display for the Law X #62-11 well showing the REVEL interval velocity (left panel) and the resulting pressure predictions for the three layer earth model. Mud weights are shown as blue diamonds.

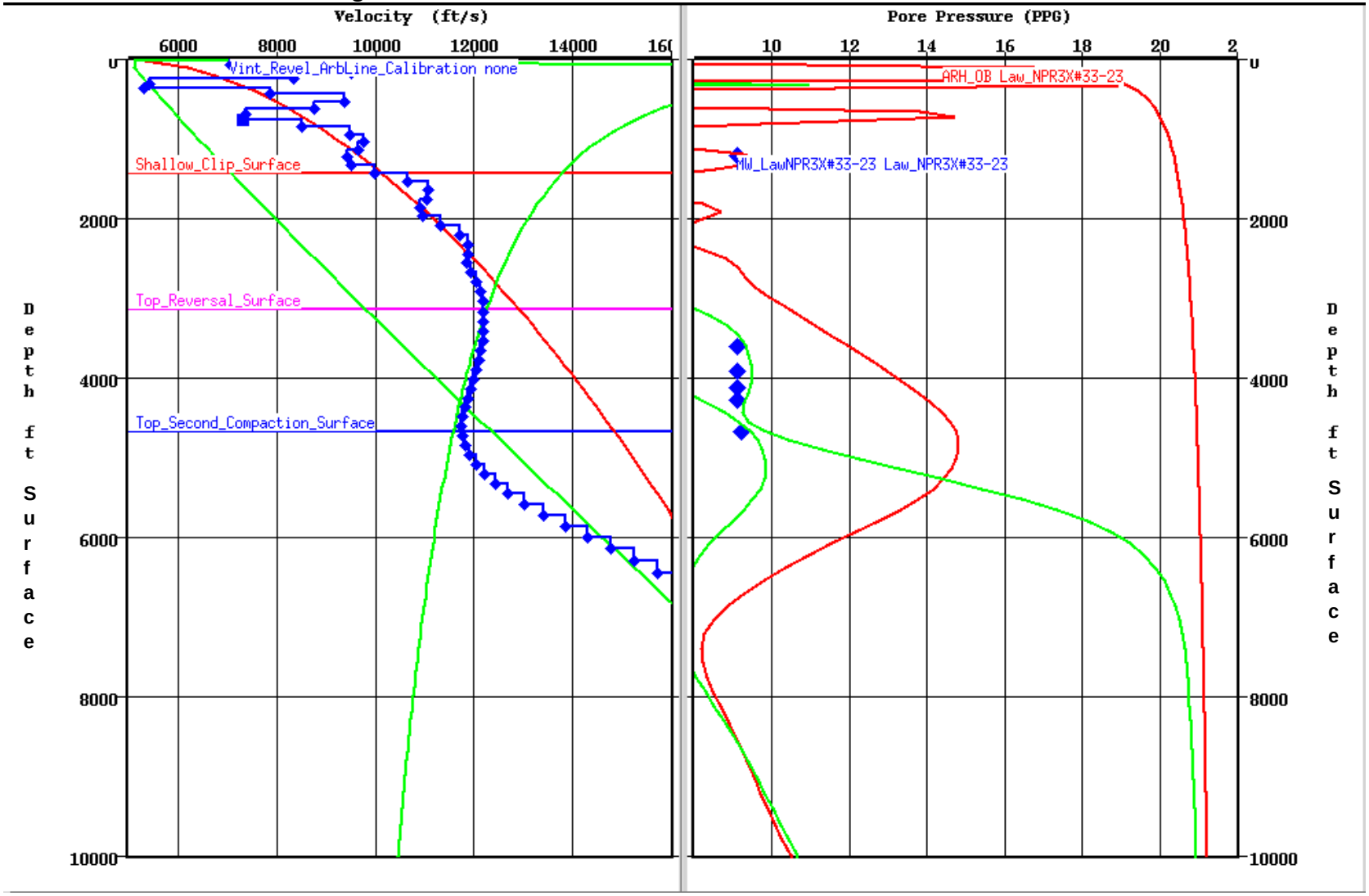

Figure 4.37: Calibration display for the Law NPR3X #33-23 well showing the REVEL interval velocity (left panel) and the resulting pressure predictions for the three layer earth model. Mud weights are shown as blue diamonds.

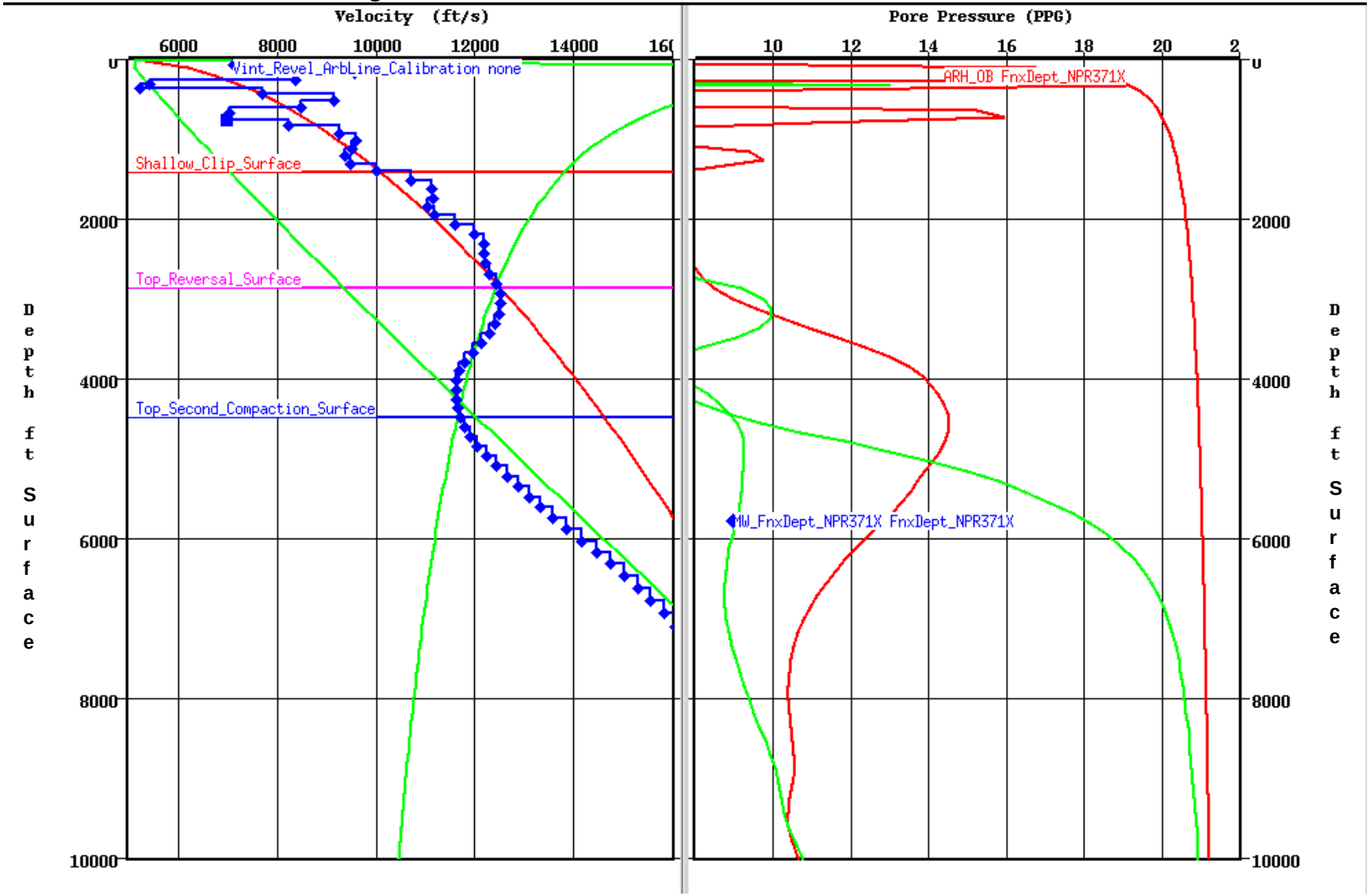

Figure 4.38: Calibration display for the FNX NPR #371X well showing the REVEL interval velocity (left panel) and the resulting pressure predictions for the three layer earth model. Mud weights are shown as blue diamonds.

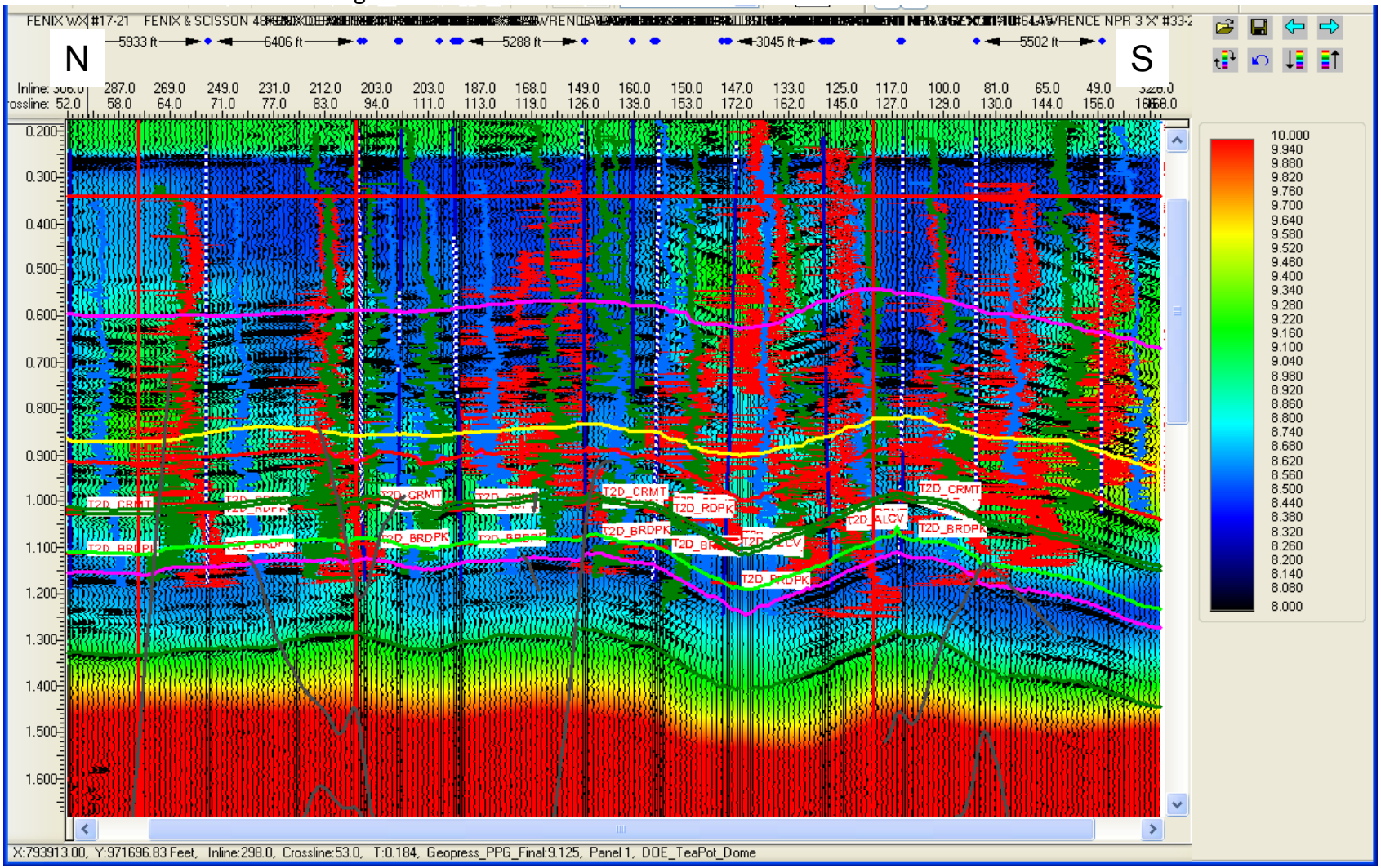

Figure 5.1: Pore pressure gradient section for Arbitrary Line A-A' showing the top of velocity reversal (magenta) and top of the deep compaction (yellow) horizons. Color-bar units are PPG.

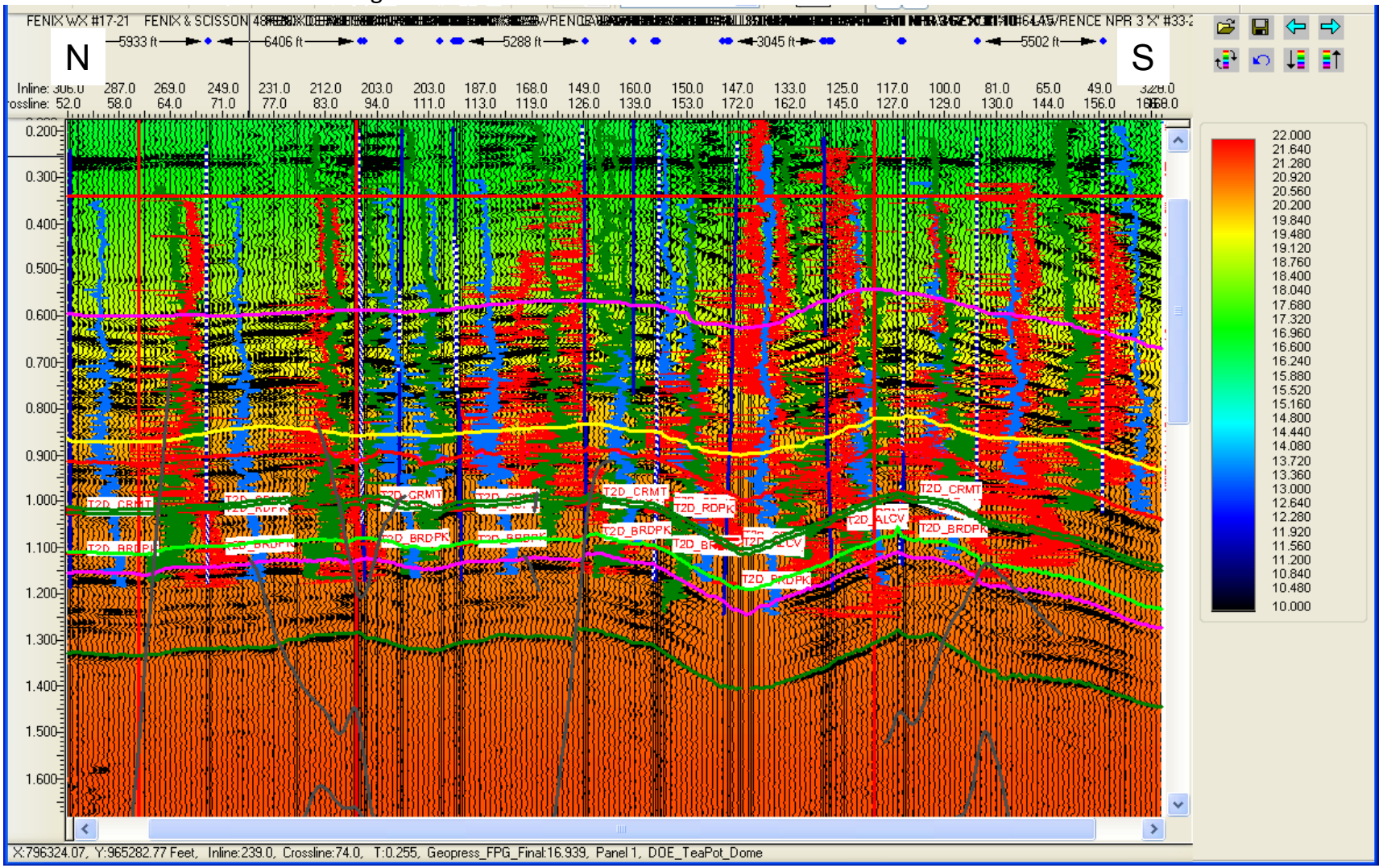

Figure 5.2: Fracture pressure gradient section for Arbitrary Line A-A' showing the top unloading (magenta) and top chemical compaction (yellow) horizons. Color-bar units are PPG.

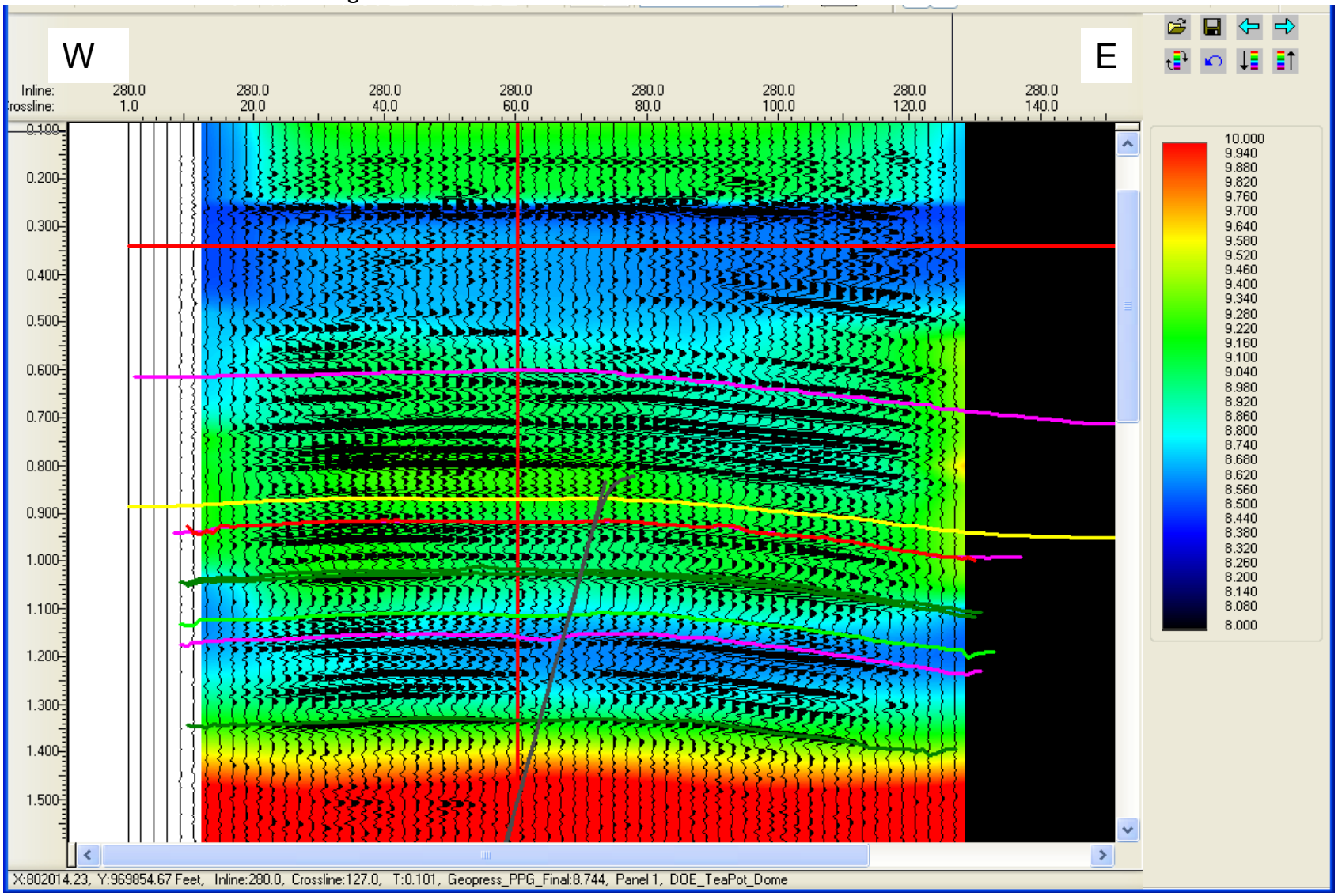

Figure 5.3: Pore pressure gradient section for <u>Inline 280</u> showing the top of velocity reveral (magenta) and top of the deep compaction (yellow) horizons. Color-bar units are PPG.

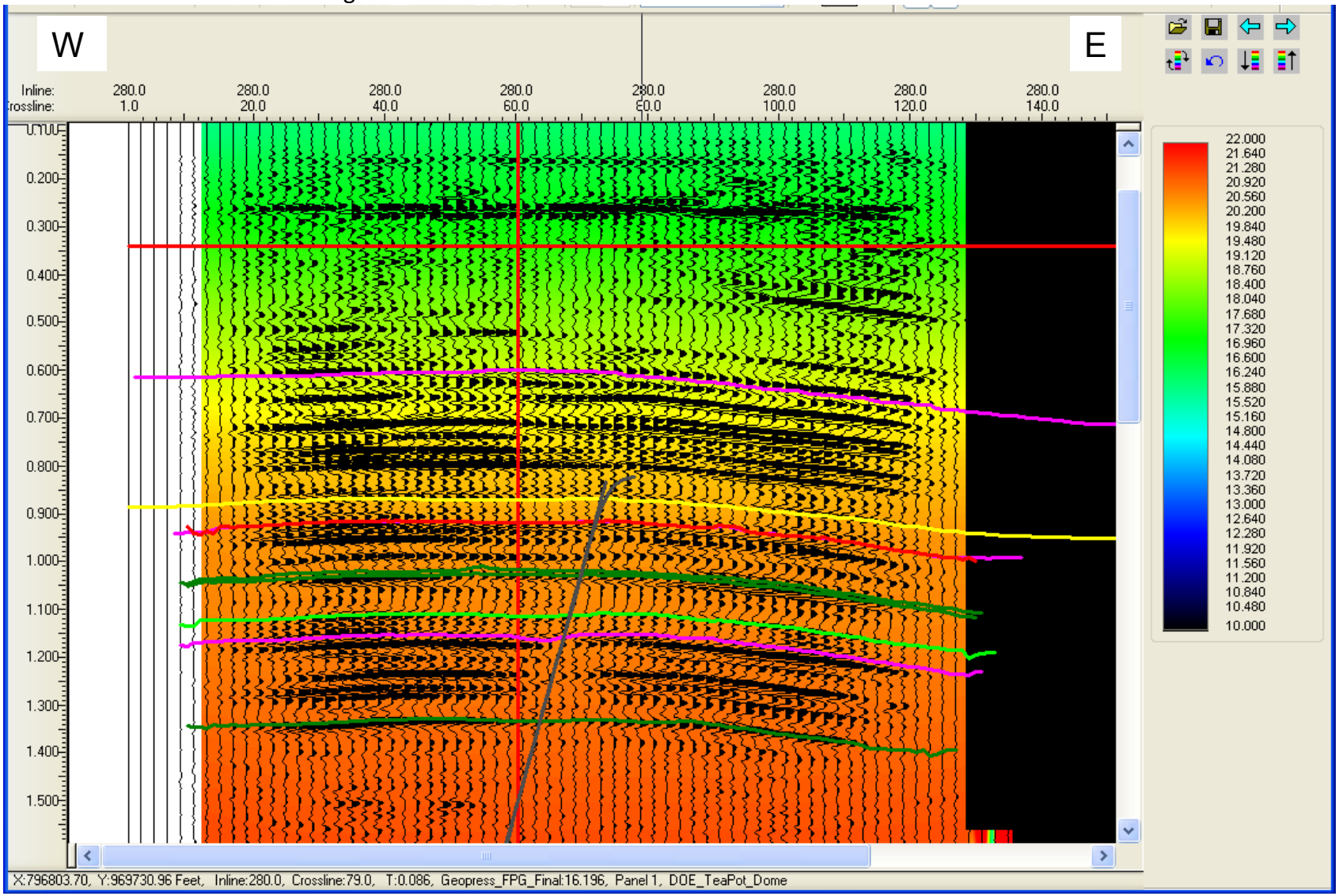

Figure 5.4: Fracture pressure gradient section for <u>Inline 280</u> showing the top of velocity reversal (magenta) and top of the deep compaction (yellow) horizons. Color-bar units are PPG.

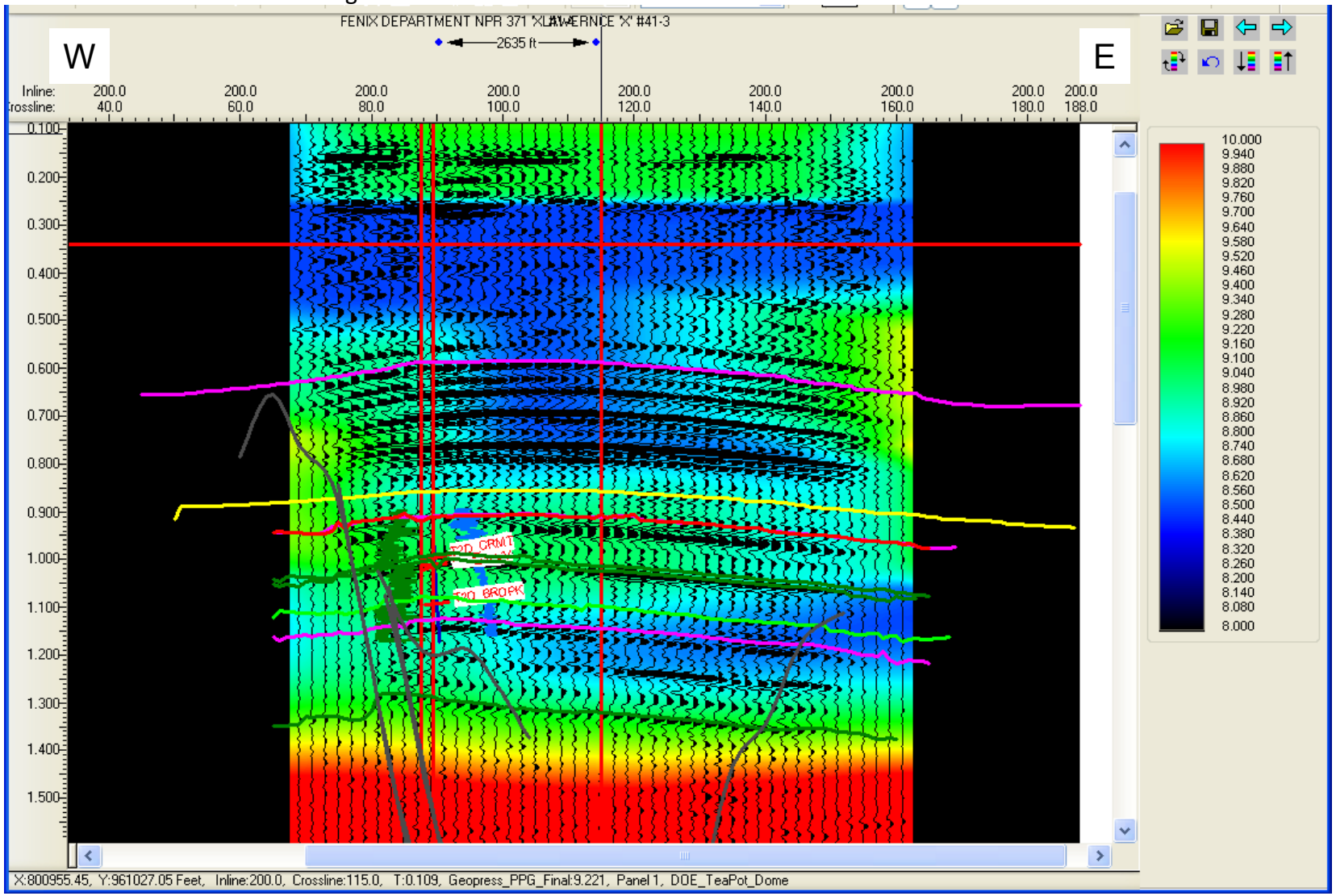

Figure 5.5: Pore pressure gradient section for <u>Inline 200</u> showing the top of velocity reversal (magenta) and top of the deep compaction (yellow) horizons. Color-bar units are PPG.

.

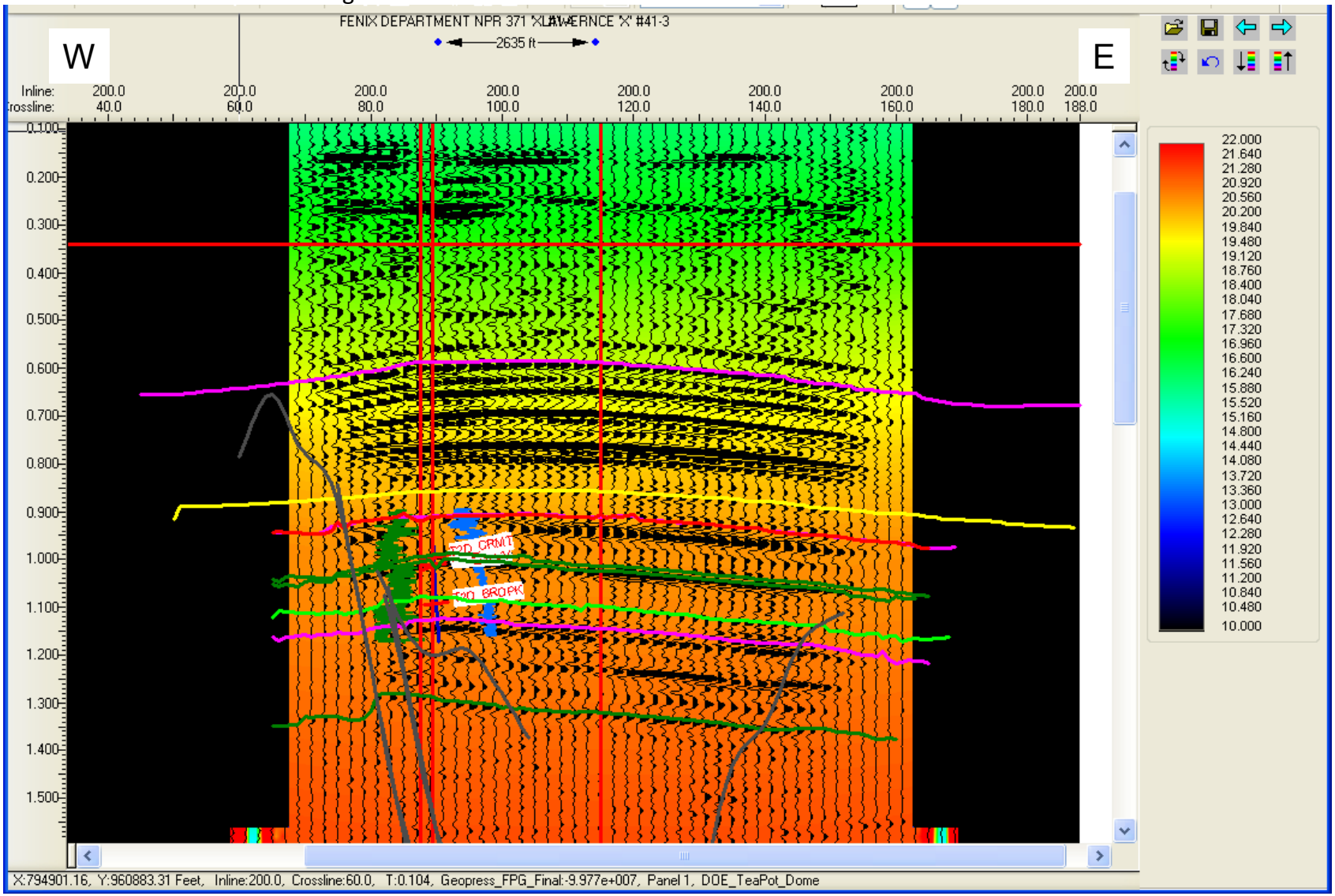

Figure 5.6: Fracture pressure gradient section for <u>Inline 200</u> showing the top of velocity reversal (magenta) and top of the deep compaction (yellow) horizons. Color-bar units are PPG.

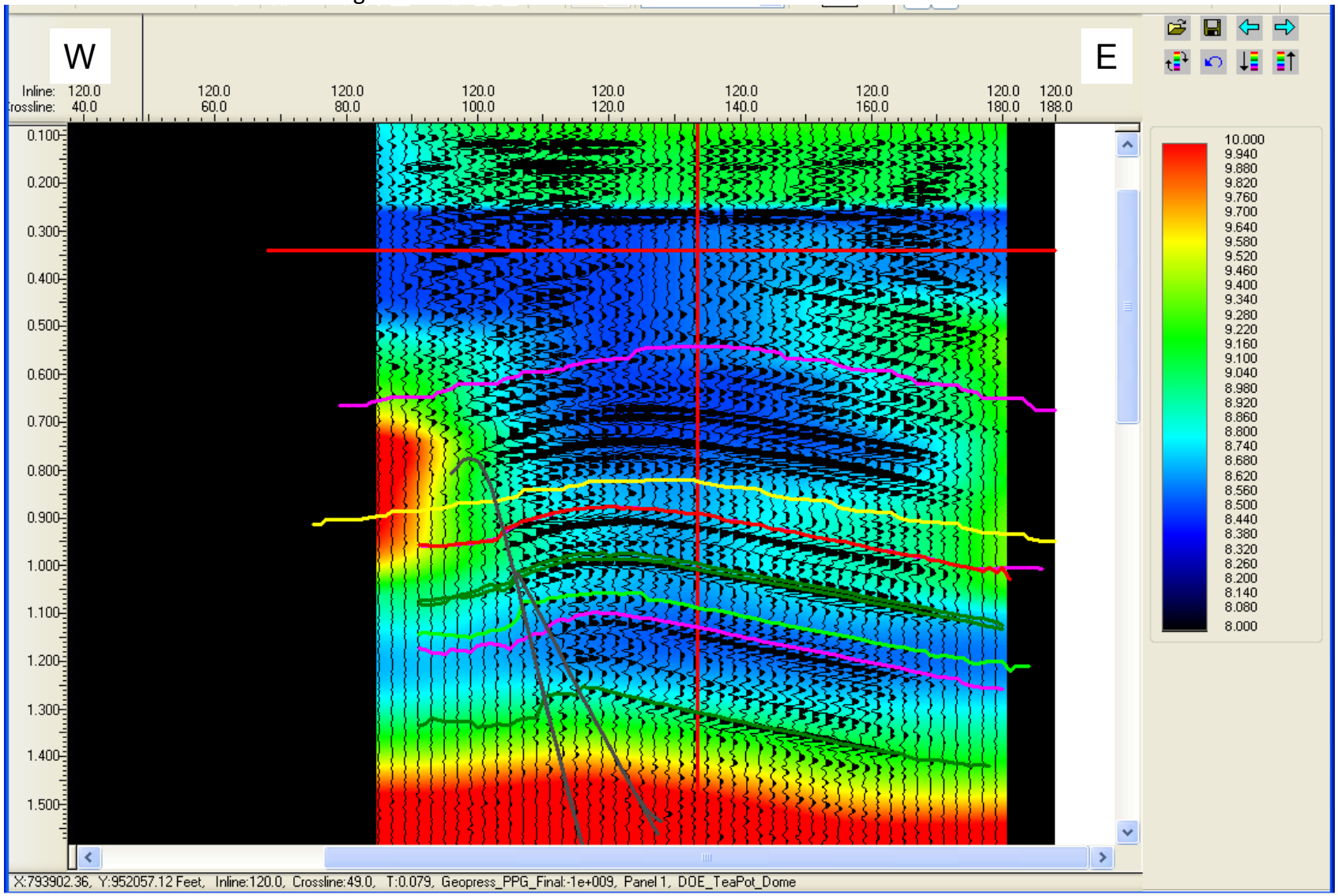

Figure 5.7: Pore pressure gradient section for <u>Inline 120</u> showing the top of velocity reversal (magenta) and top of the deep compaction (yellow) horizons. Color-bar units are PPG.

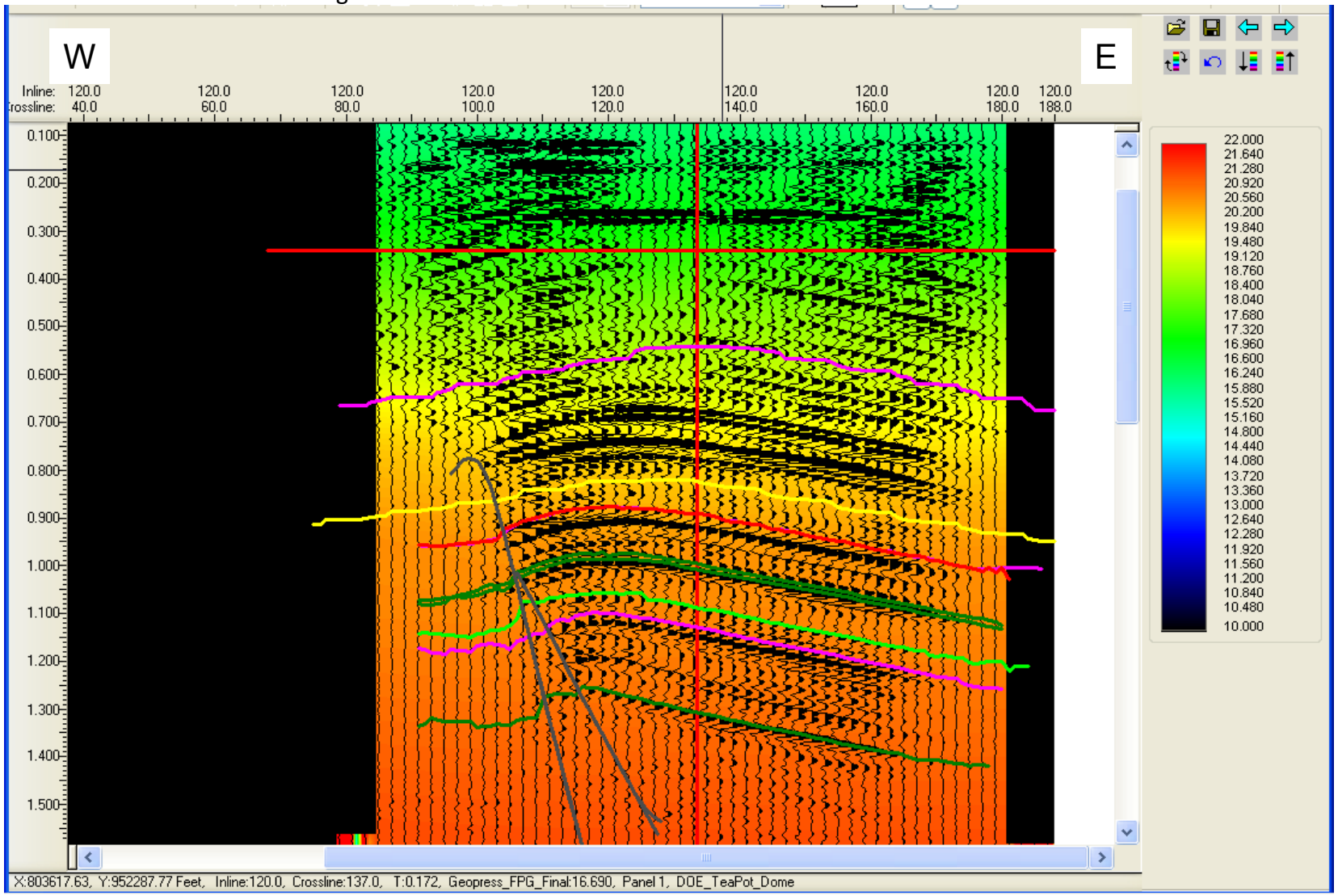

Figure 5.8: Fracture pressure gradient section for <u>Inline 120</u> showing the top of velocity reversal (magenta) and top of the deep compaction (yellow) horizons. Color-bar units are PPG.

.

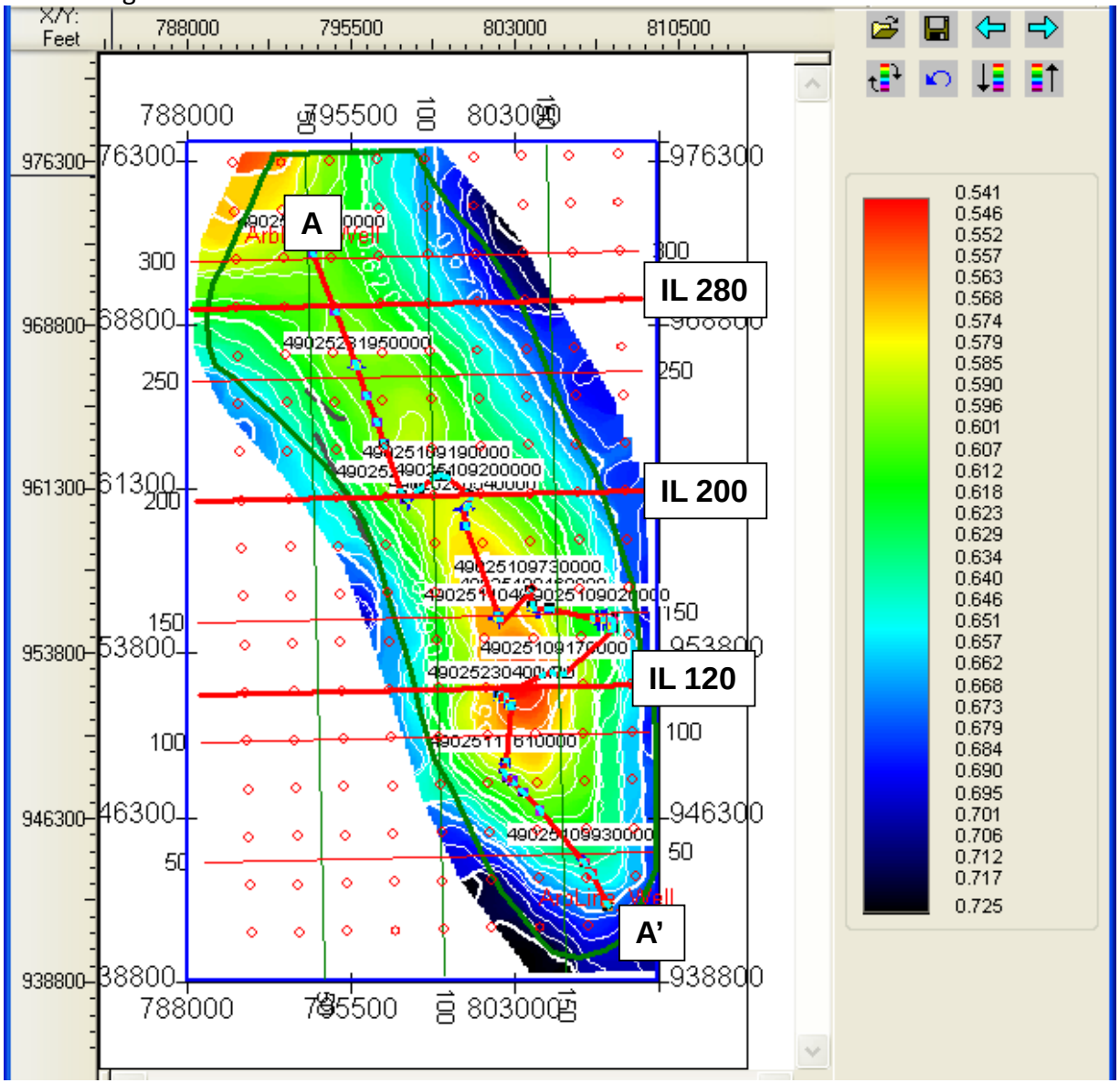

Figure 5.9: Map showing the top of the velocity reversal surface with 10 msec time contours.

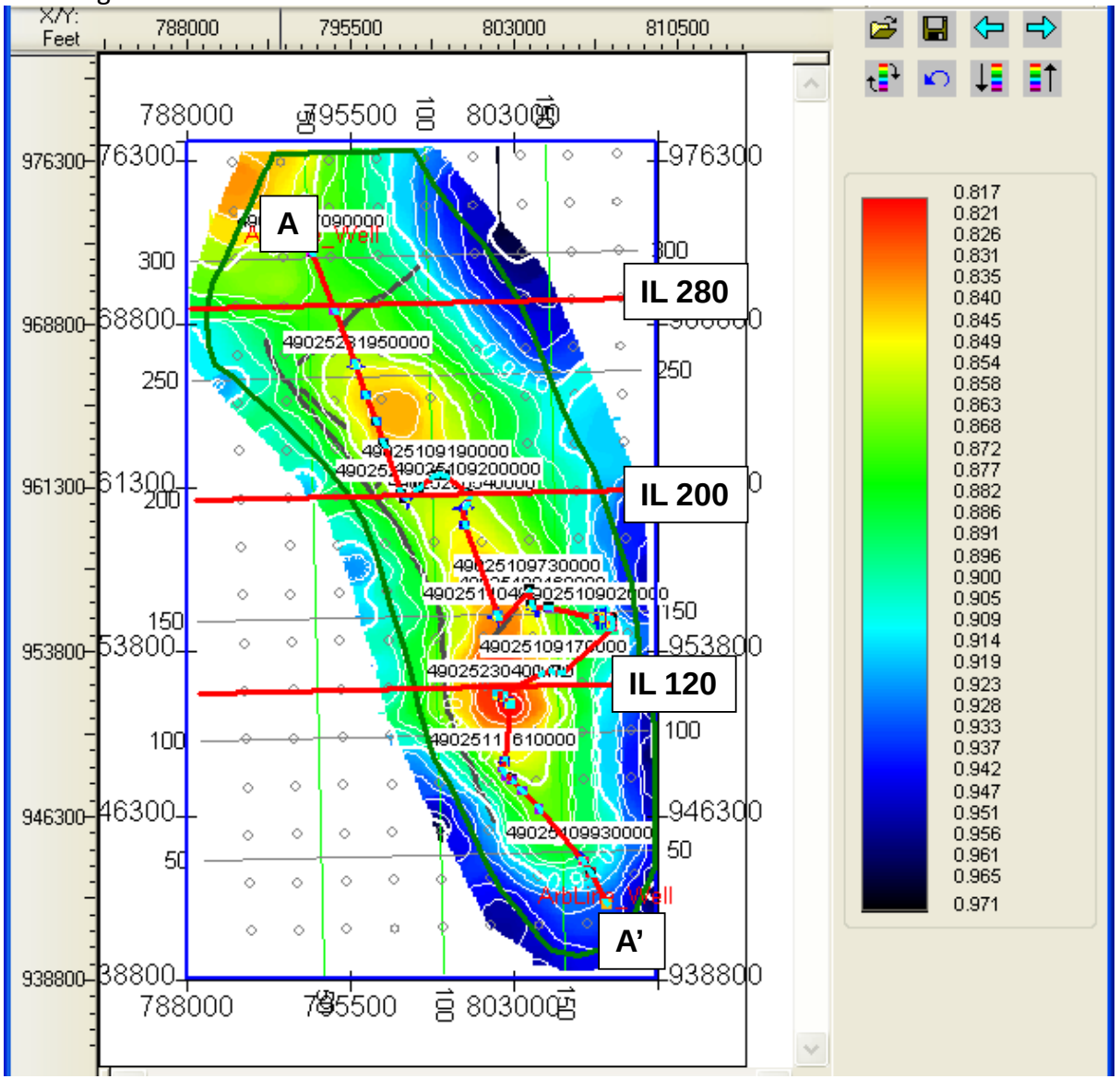

Figure 5.10: Map showing the top of the deep compaction surface with 10 msec time contours.

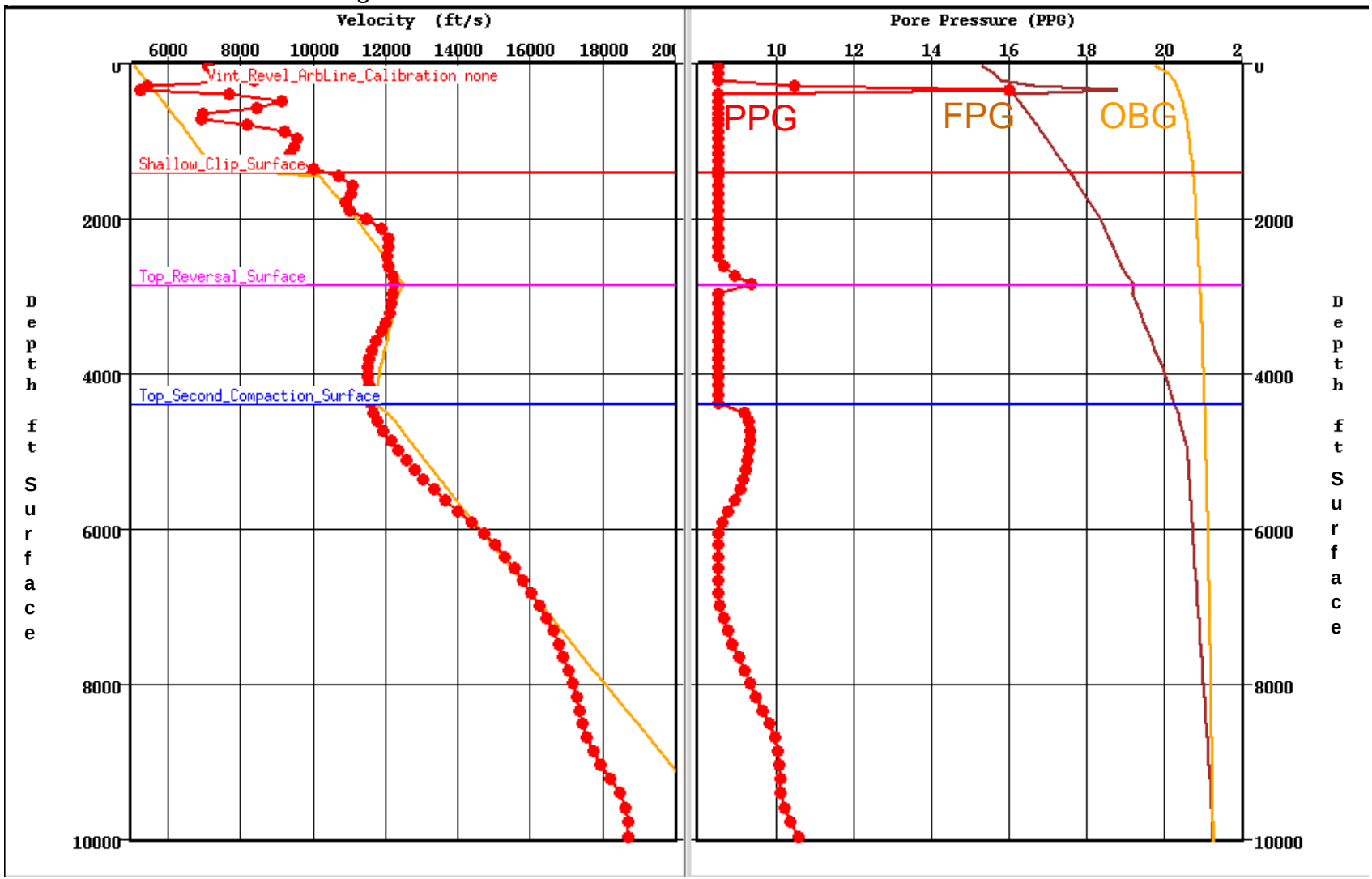

Figure 5.11: Prediction panel for the NPR 3LX #28-34 well. Pore pressure gradient (red), fracture pressure gradient (brown) and overburden gradient (orange) are labeled in the right panel.

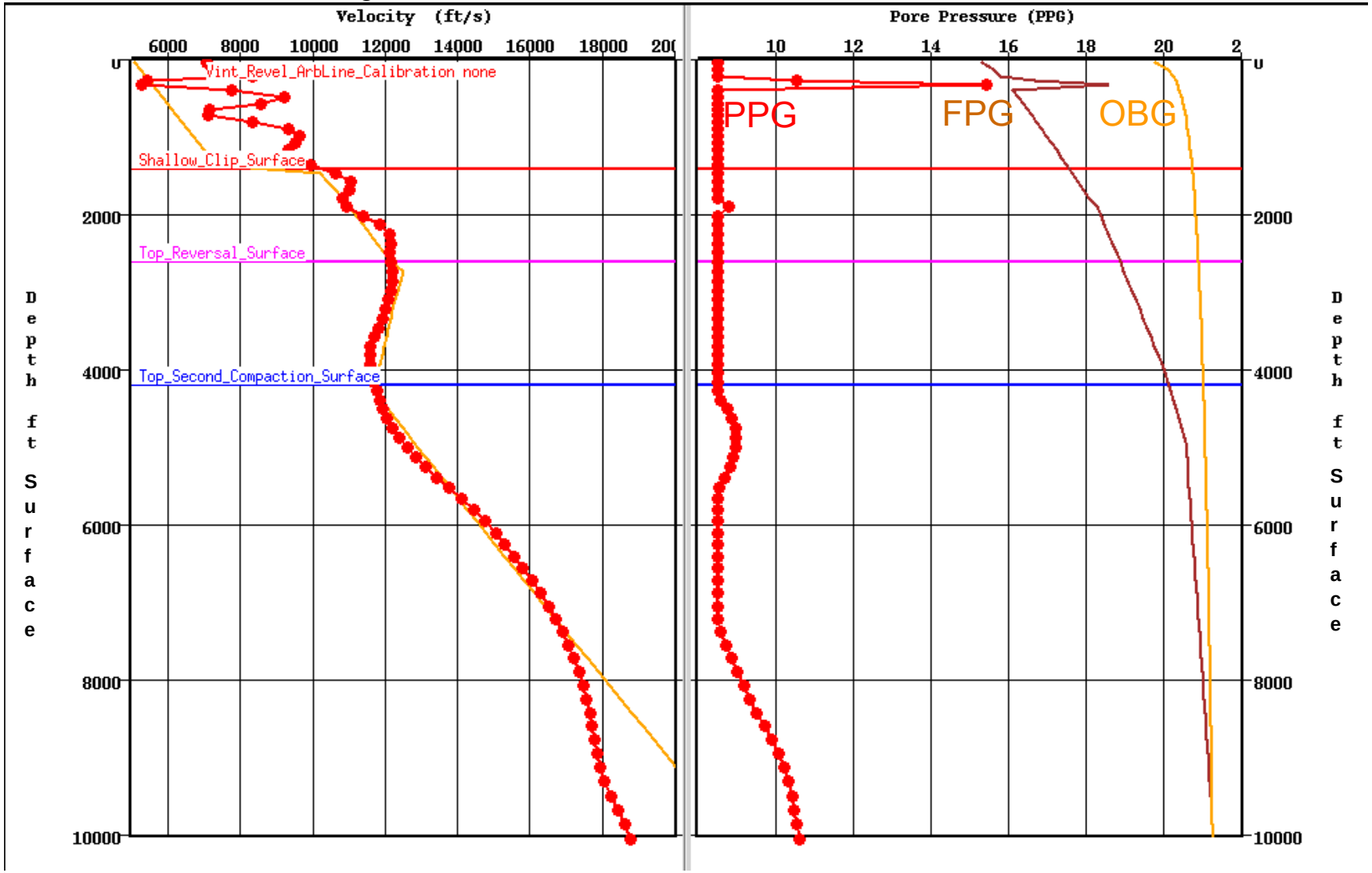

Figure 5.12: Prediction panel for the NPR3 X #67-1 well.

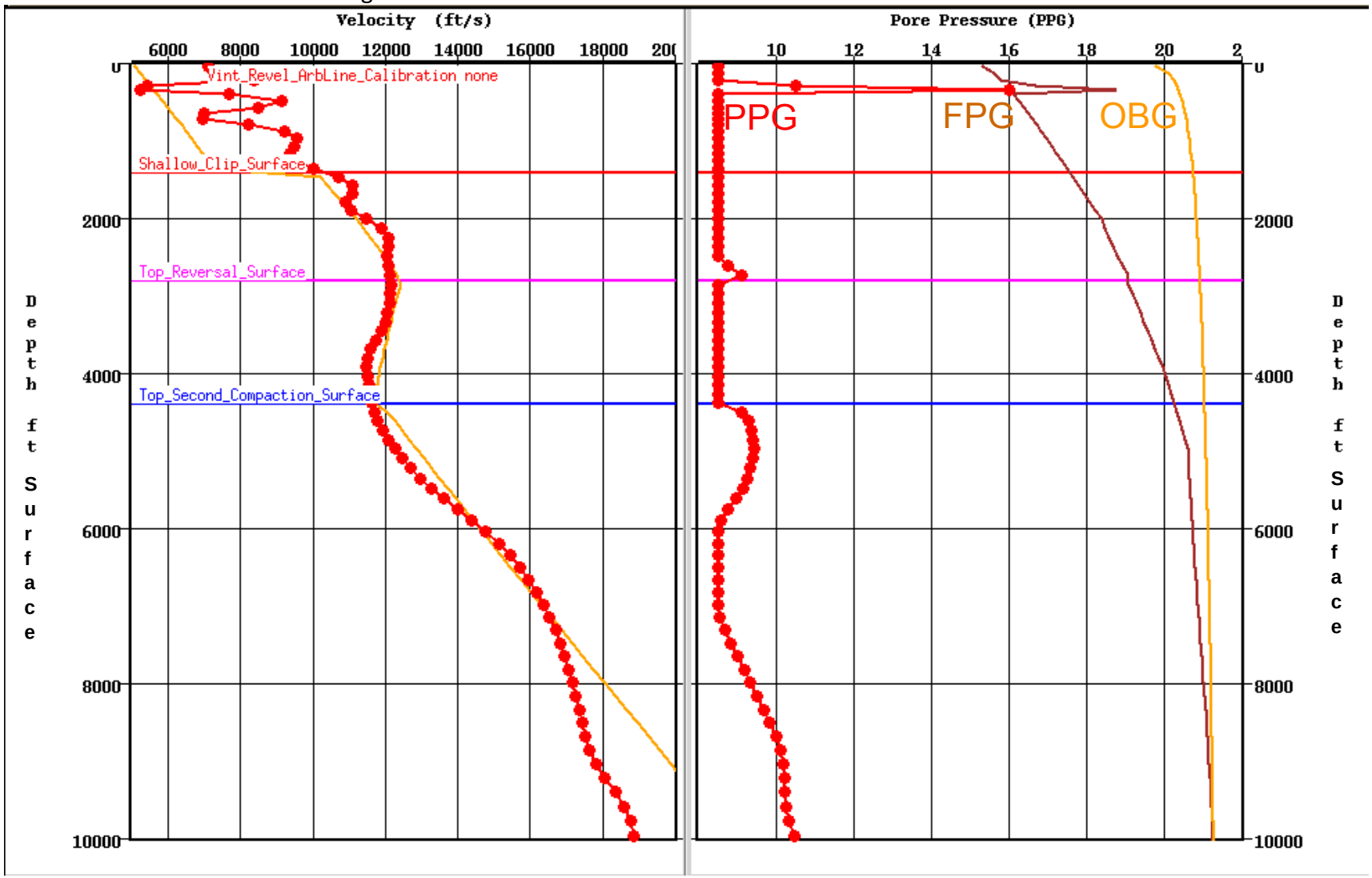

Figure 5.13: Prediction panel for the Dept #2-3 well.

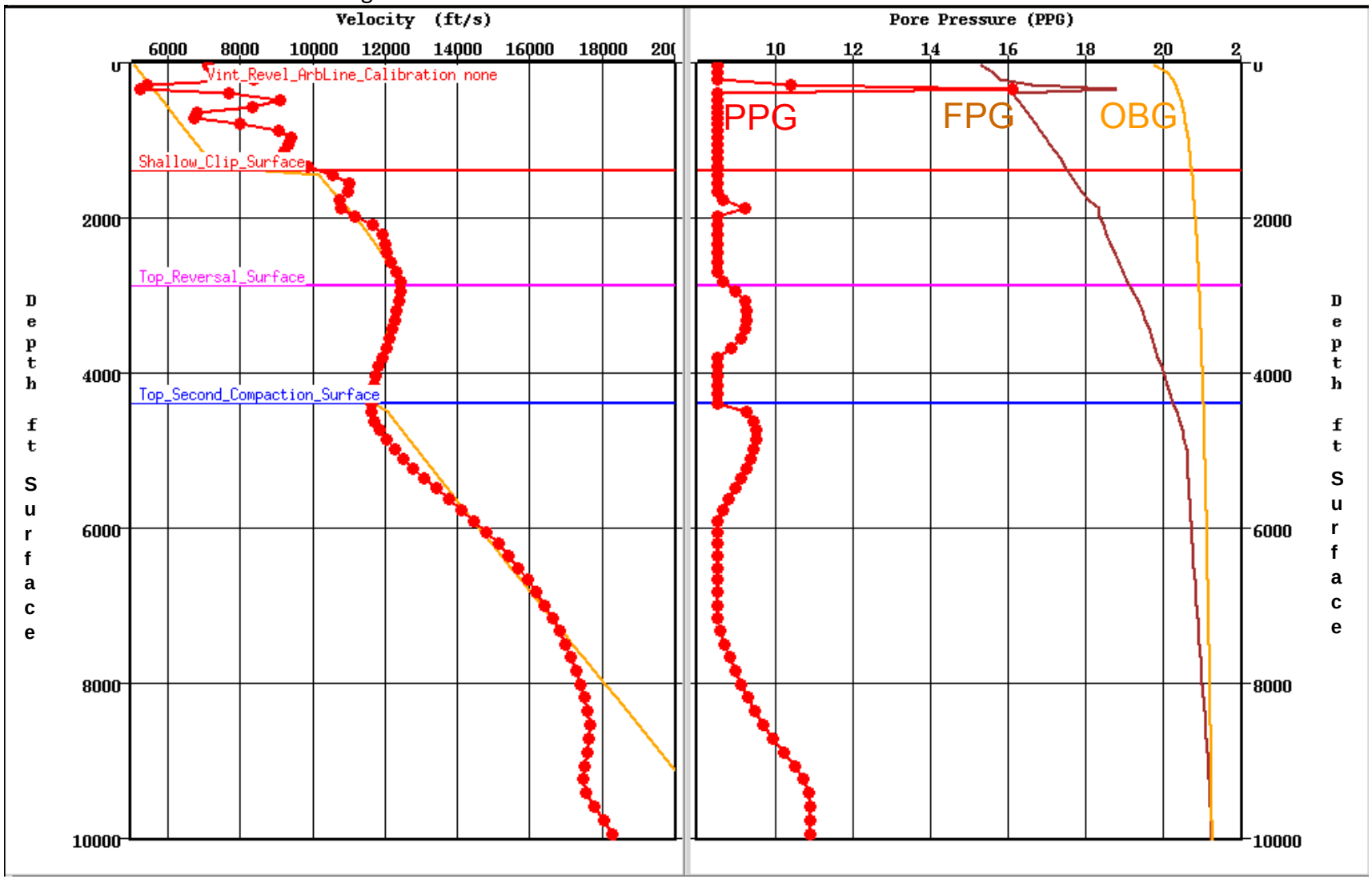

Figure 5.14: Prediction panel for the FNX X #48-28 well.

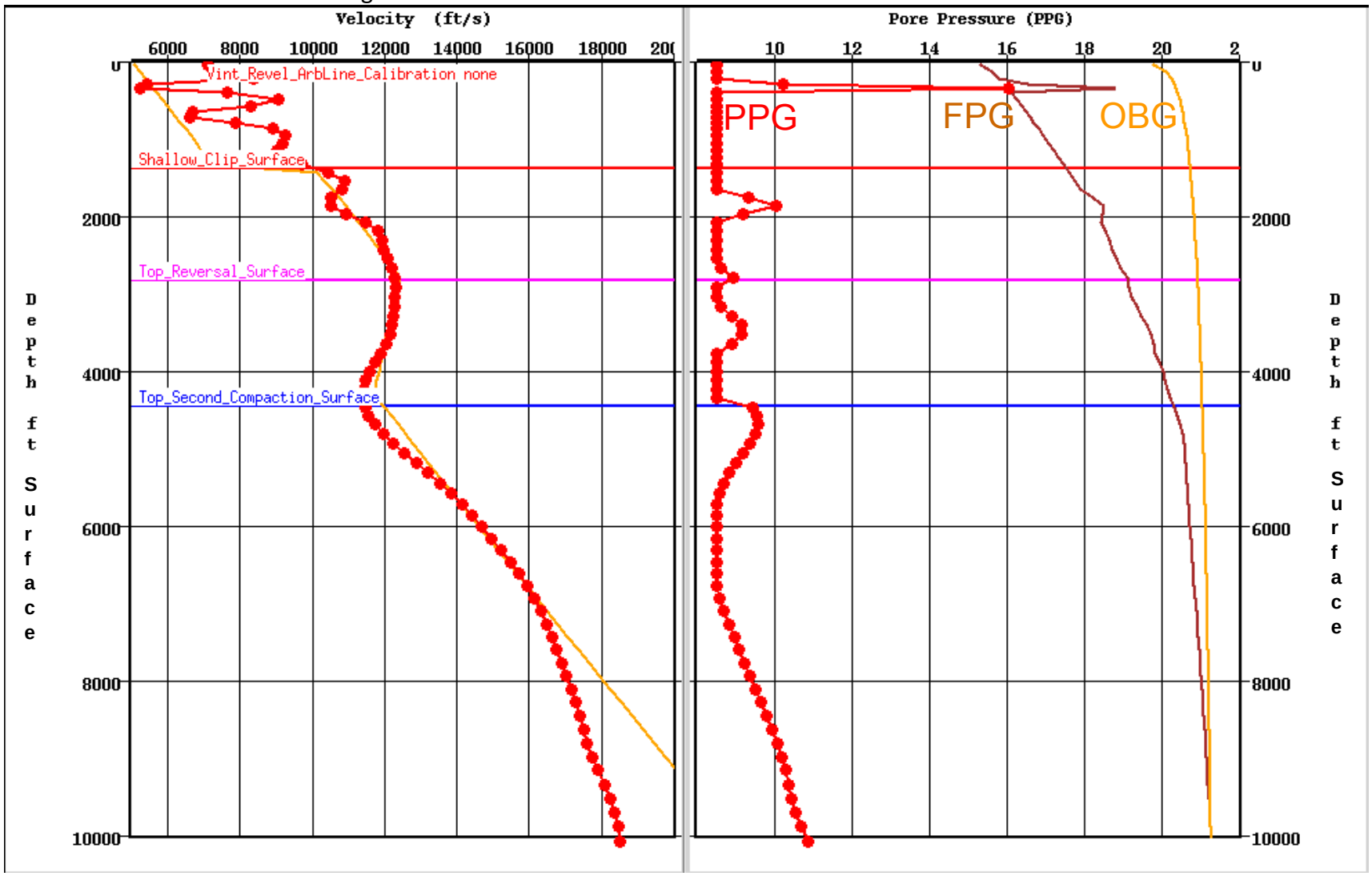

Figure 5.15: Prediction panel for the FNX WX #17-21 well.

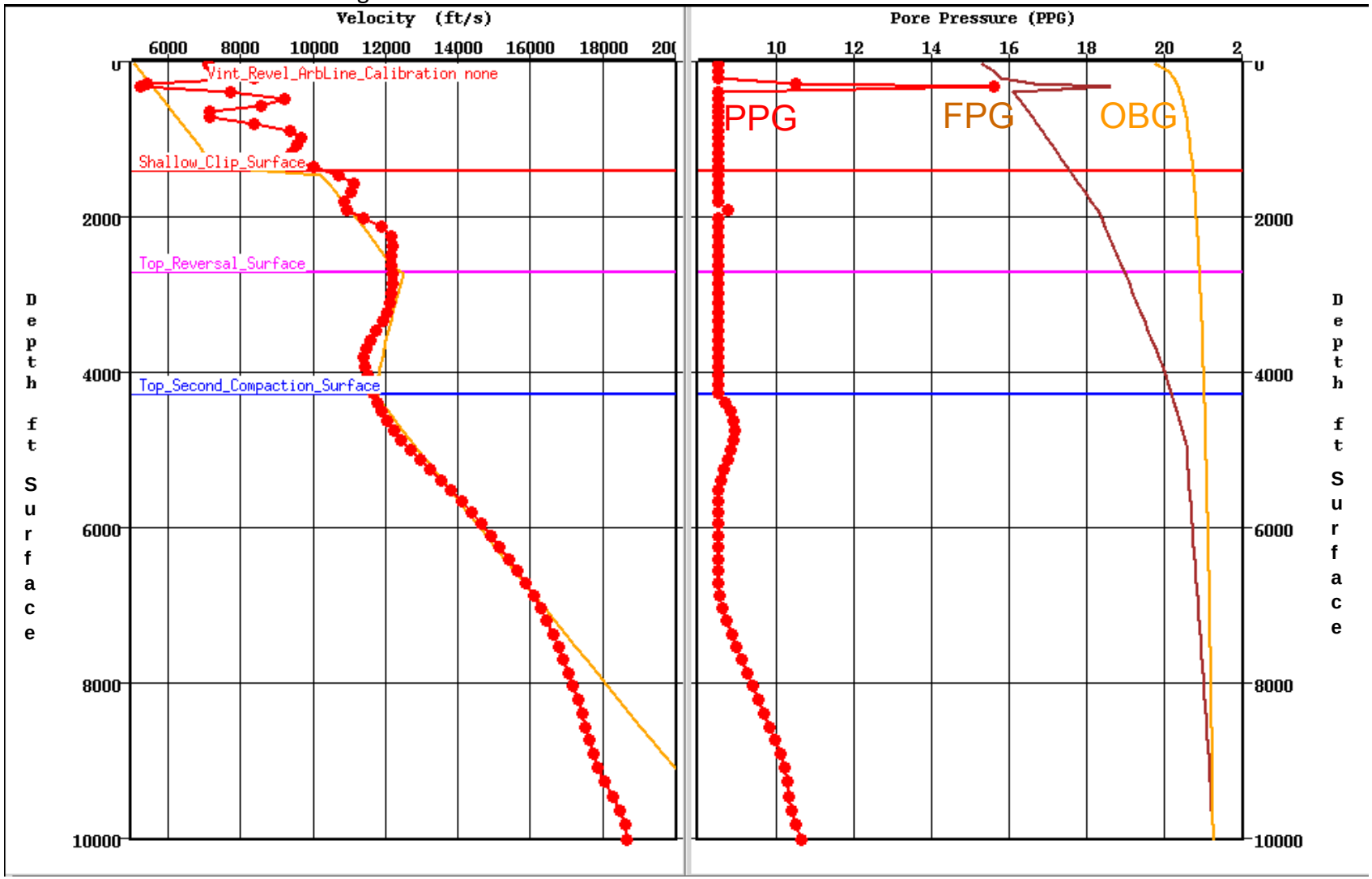

Figure 5.16: Prediction panel for the Law 62TPX #10-10 well.

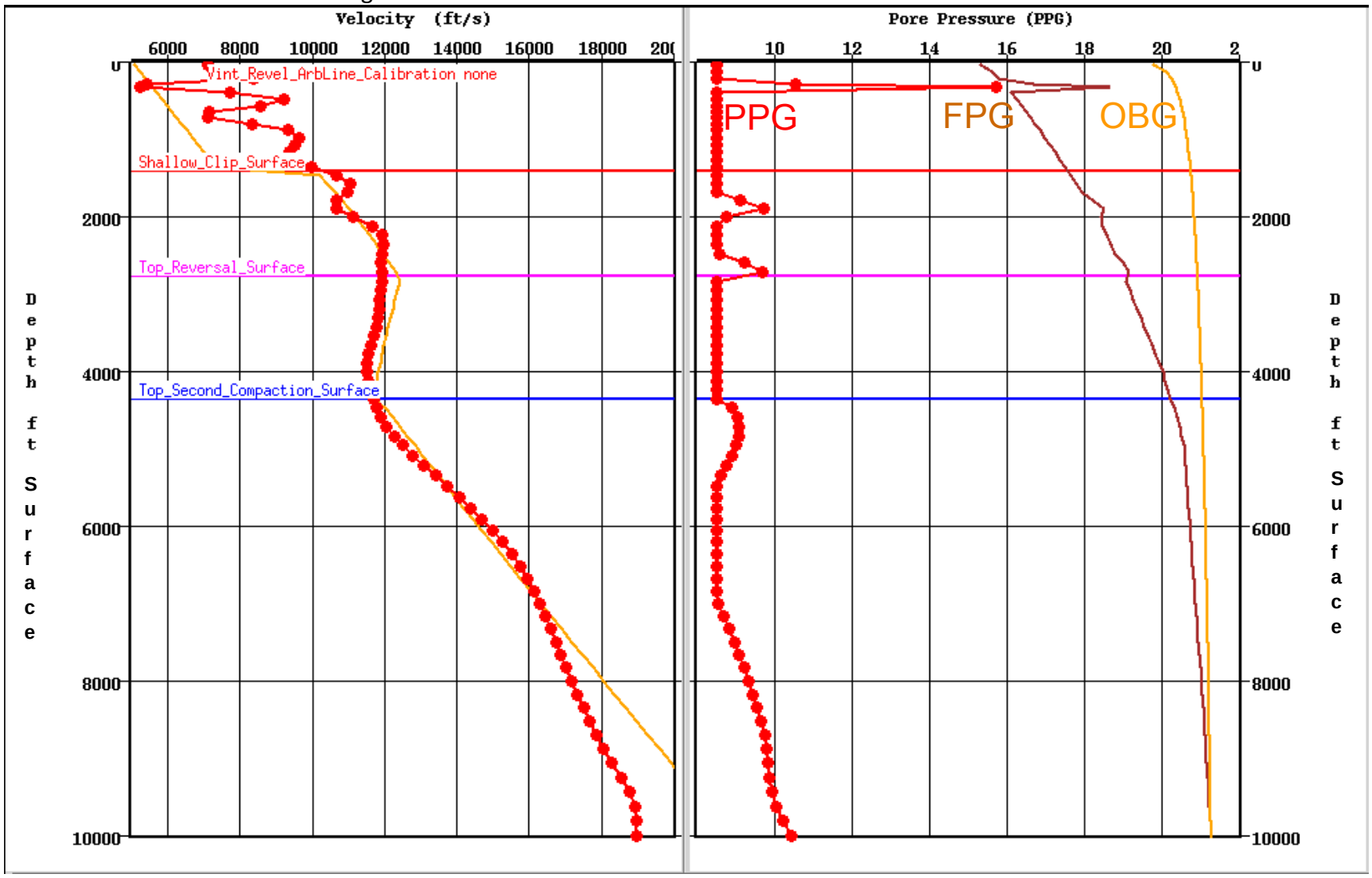

Figure 5.17: Prediction panel for the Law X #11-11 well.

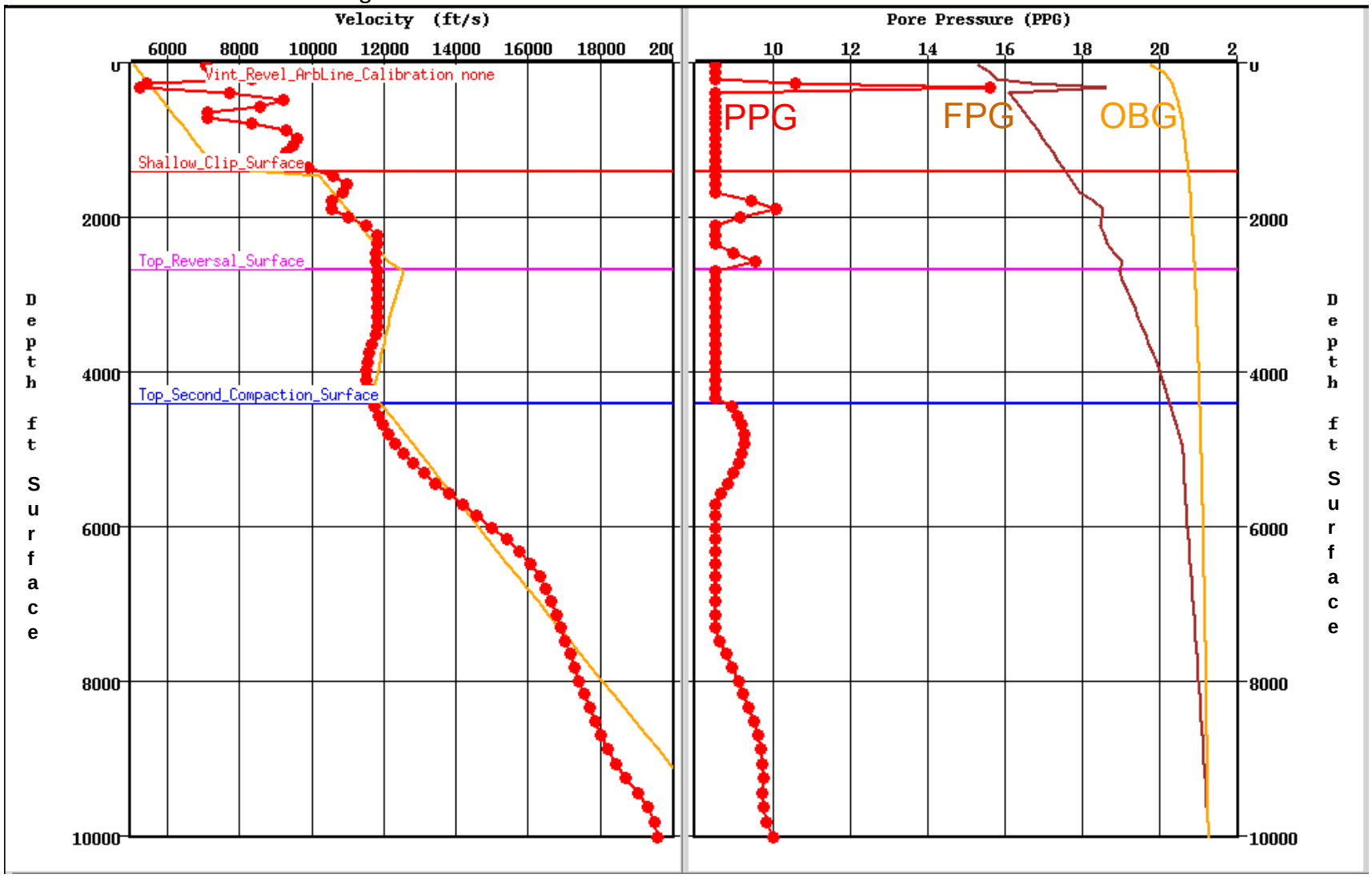

Figure 5.18: Prediction panel for the Law X #25-11 well.

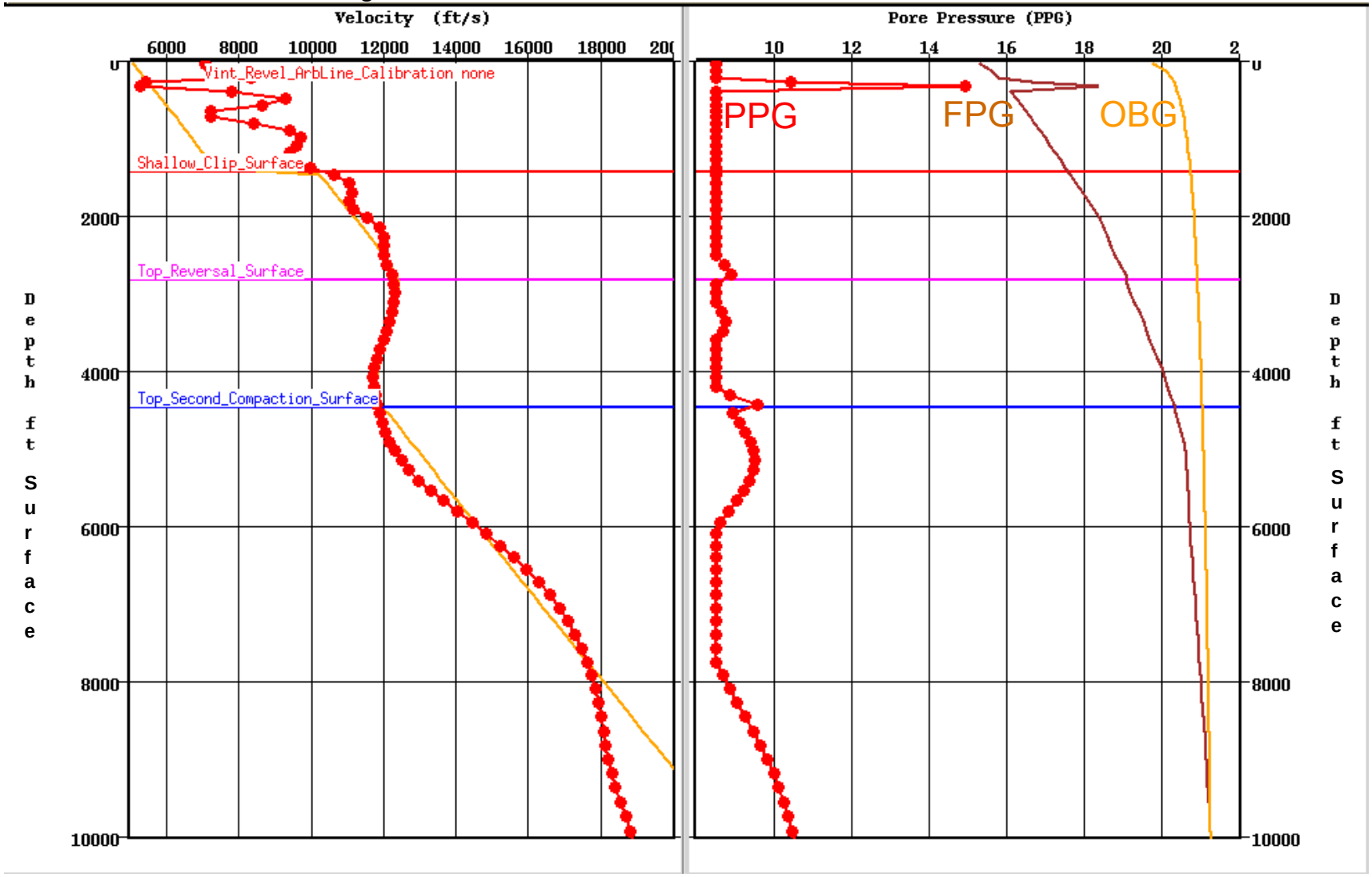

Figure 5.19: Prediction panel for the Law X #64-15 well.

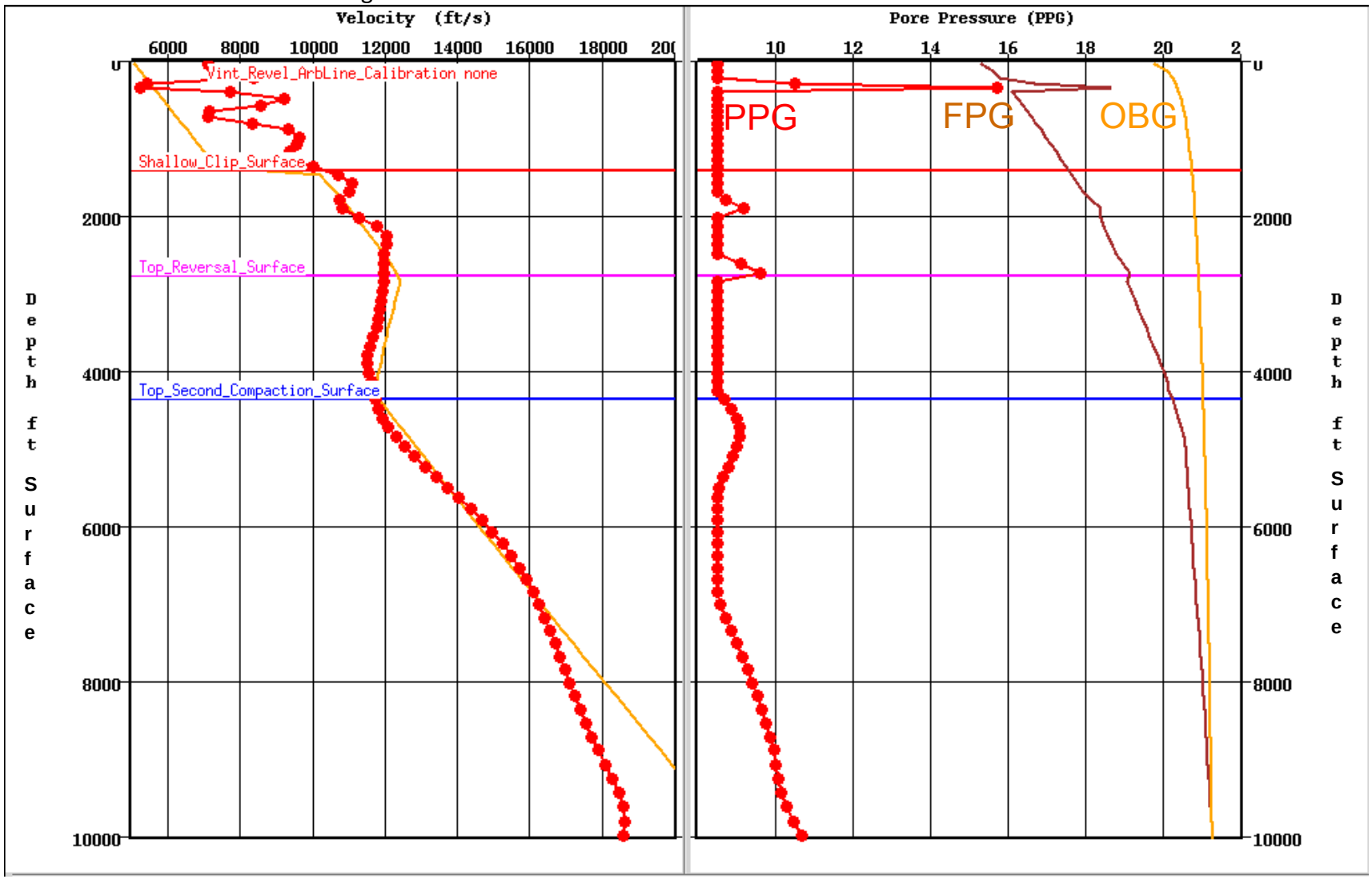

Figure 5.20: Prediction panel for the Law X #88-3 well.

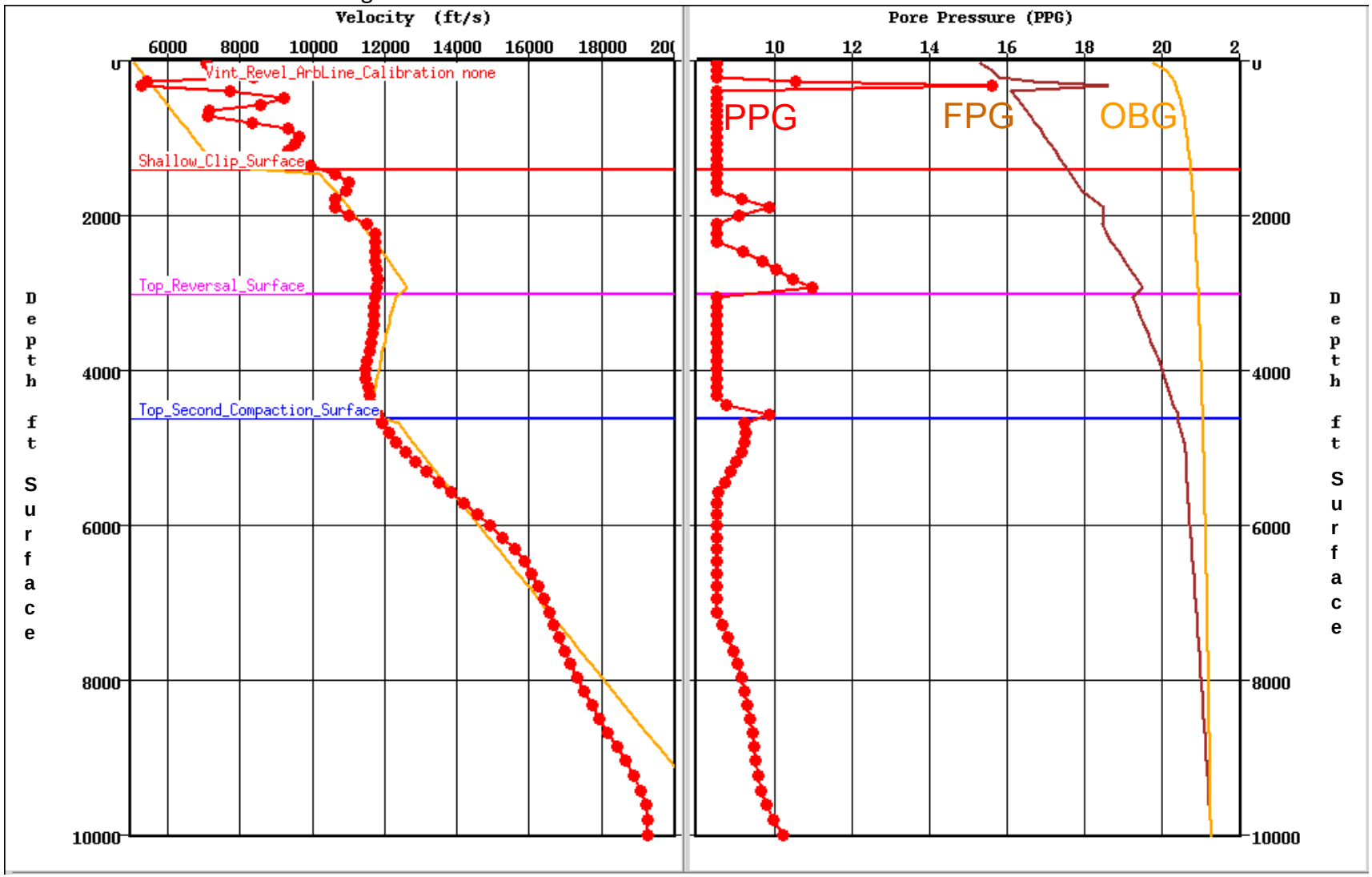

Figure 5.21: Prediction panel for the Law X #62-11 well.

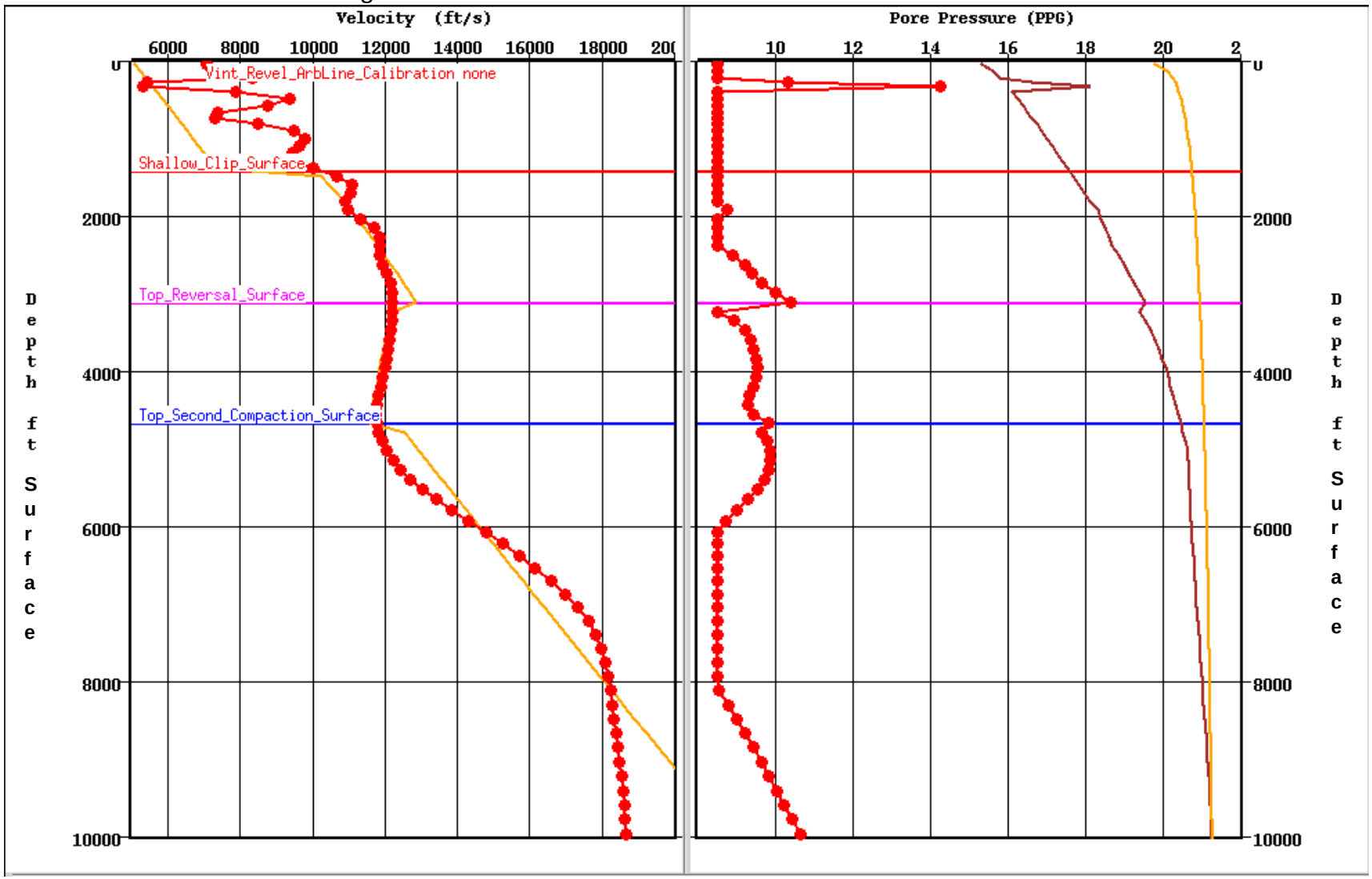

Figure 5.22: Prediction panel for the NPR3X #33-23 well.

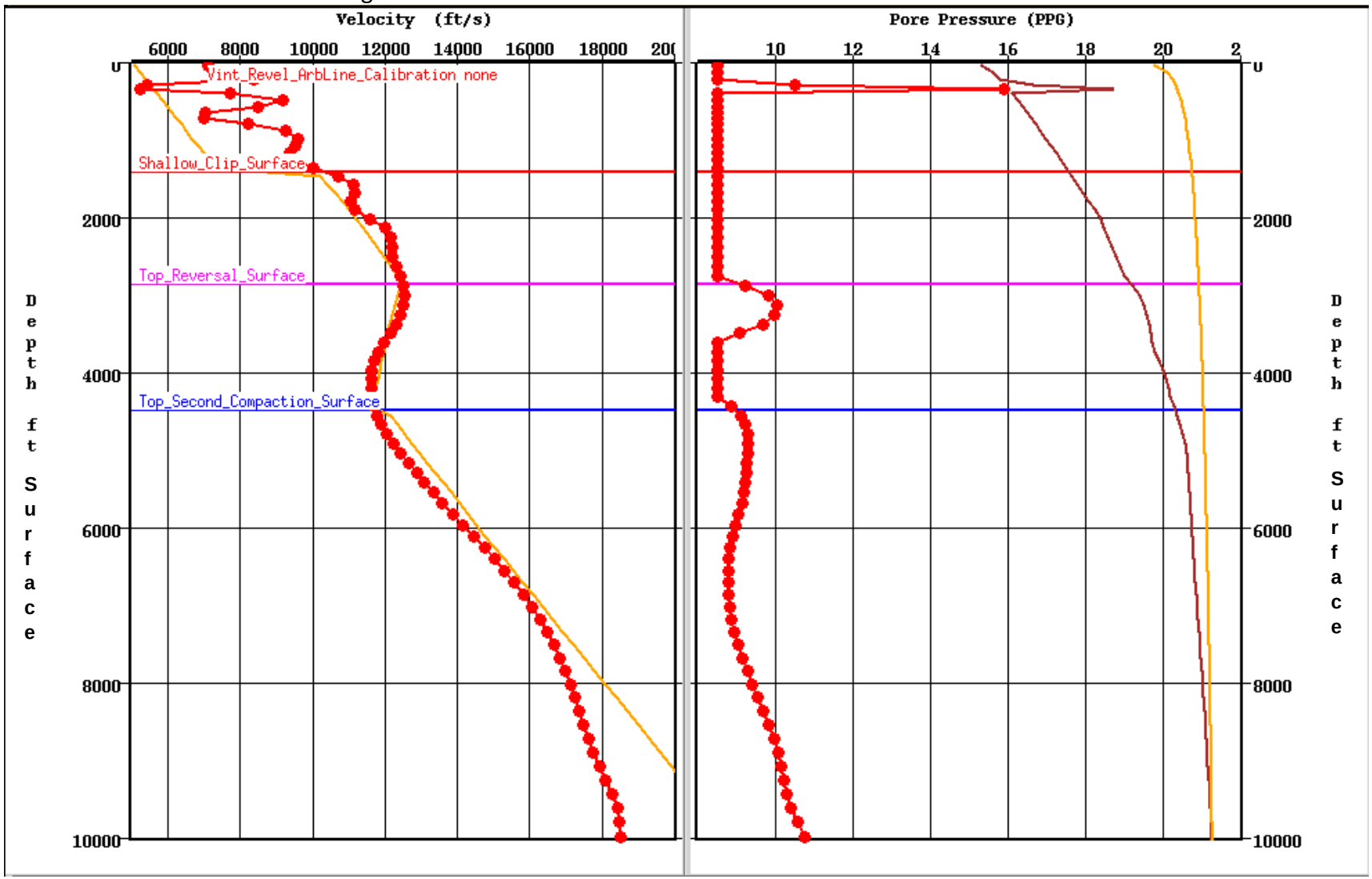

Figure 5.23: Prediction panel for the NPR #371X well.

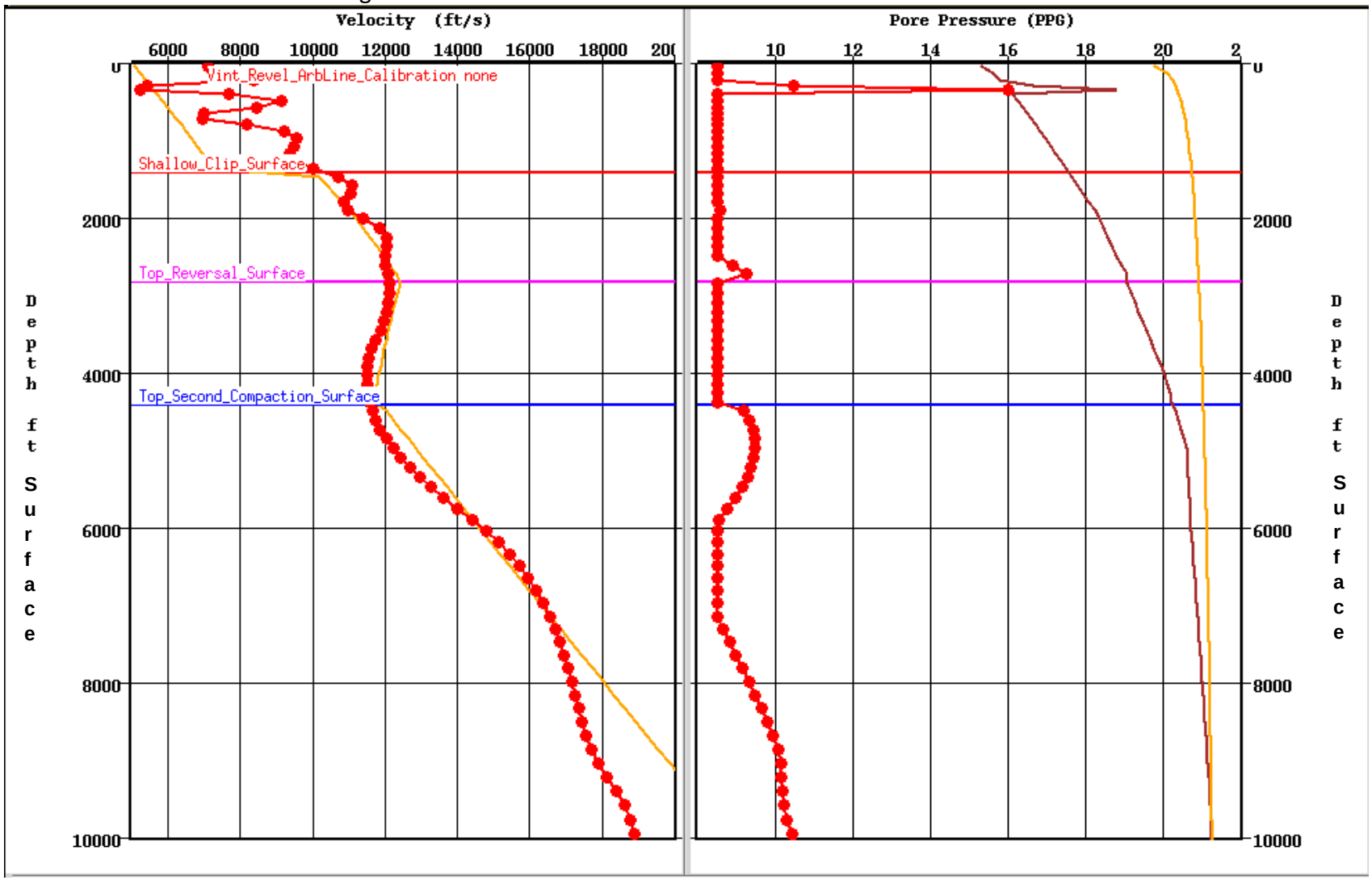

Figure 5.24: Prediction panel for the Law X #41-3 well.

Appendix C: Gantt Chart

ID	Task Name	Start	Finish	Duration	% Complete
1	**CO2 MVA project DEFE0001111**	**Thu 10/1/09**	**Tue 1/31/12**	**610 days**	**99%**
2	**Task 1: Project Management and PlanningPlan**	**Thu 10/1/09**	**Tue 1/31/12**	**610 days**	**100%**
3	Task 1.1: Detailed Project Management Report	Thu 10/1/09	Thu 12/31/09	66 days	100%
4	**Task 1.2: Project administration**	**Fri 10/2/09**	**Fri 12/30/11**	**586 days**	**100%**
240	**Task 1.3 quarterly report**	**Fri 12/4/09**	**Tue 1/31/12**	**564 days**	**100%**
250	**Phase I: Baseline Reservoir Analysis**	**Thu 10/1/09**	**Wed 4/28/10**	**150 days**	**100%**
251	**Task 2: Finalize Area**	**Thu 10/1/09**	**Wed 10/14/09**	**10 days**	**100%**
252	Task 2.1:Teapot RMOTC/Hoskins Mound	Thu 10/1/09	Wed 10/14/09	10 days	100%
253	**Task 3: Seismic Processing**	**Thu 10/15/09**	**Tue 2/2/10**	**79 days**	**100%**
254	Task 3.1: Load & QC	Thu 10/15/09	Wed 10/28/09	10 days	100%
255	Task 3.2: Preprocess	Thu 10/29/09	Mon 11/30/09	23 days	100%
256	Task 3.3: Time imaging	Tue 12/1/09	Thu 12/31/09	23 days	100%
257	Task 3.4: Depth imaging	Fri 1/1/10	Tue 2/2/10	23 days	100%
258	Milestone 1: Kickoff Meeting	Fri 1/1/10	Fri 1/1/10	0 days	100%
259	**Task 4: Reservoir Geophysics**	**Fri 1/1/10**	**Wed 4/28/10**	**84 days**	**100%**
260	Task 4.1: ExSpect	Fri 1/1/10	Thu 2/11/10	30 days	100%
261	Task 4.2: ThinMAN	Mon 2/15/10	Fri 3/12/10	20 days	100%
262	Task 4.3: Geopressure	Mon 3/29/10	Wed 4/28/10	23 days	100%
263	Milestone 2: Site with 3D Seismic Identified & Acquired	Tue 3/30/10	Tue 3/30/10	0 days	100%
264	**Phase II: Proof of Concept**	**Mon 1/25/10**	**Fri 12/30/11**	**504 days**	**99%**
265	**Task 5: Reservoir Model**	**Mon 1/25/10**	**Wed 7/21/10**	**128 days**	**100%**
266	Task 5.1: Load seismic and QC well data	Mon 1/25/10	Fri 2/26/10	25 days	100%
267	Task 5.2: Define Reservoir structure in SMT	Mon 3/1/10	Fri 4/9/10	30 days	100%
268	**Task 5.3: Geocellular grid**	**Mon 4/12/10**	**Thu 6/24/10**	**54 days**	**100%**
269	**Geo-structure**	**Mon 4/12/10**	**Thu 6/24/10**	**54 days**	**100%**
270	Import Reservoir Structure into JS	Mon 4/12/10	Fri 4/16/10	5 days	100%
271	Model definiton and well correlation	Tue 5/4/10	Mon 5/10/10	5 days	100%
272	Structural Framework Modeling	Mon 5/17/10	Thu 6/24/10	29 days	100%
273	Reservoir Definition	Tue 6/8/10	Mon 6/14/10	5 days	100%
274	Build 3D grid	Fri 6/18/10	Thu 6/24/10	5 days	100%
275	**Task 5.4: Populate grid**	**Wed 6/9/10**	**Wed 6/23/10**	**11 days**	**100%**
276	import analyzed logs mineralogy poro/perm	Wed 6/9/10	Thu 6/10/10	2 days	100%
277	upscale logs to grid dimensions	Thu 6/10/10	Mon 6/14/10	3 days	100%
278	property modeling	Thu 6/17/10	Wed 6/23/10	5 days	100%
279	Task 5.5: Upscale	Wed 6/23/10	Wed 6/30/10	6 days	100%
280	Task 5.6: Evaluate and Redo static model	Thu 7/1/10	Wed 7/7/10	5 days	100%
281	Task 5.7: Simulation Prparation	Thu 7/8/10	Wed 7/21/10	10 days	100%
282	**Task 6: Flow & Seismic Simulation**	**Tue 8/3/10**	**Fri 7/15/11**	**249 days**	**100%**
283	Task 6.1: Simulate CO2 injection	Tue 8/3/10	Fri 4/29/11	89.8 days	100%
284	Task 6.2: Rock Physics	Fri 4/29/11	Thu 6/30/11	44.5 days	100%
285	Task 6.3: Seismic modeling	Wed 6/1/11	Fri 7/15/11	33 days	100%
286	Milestone 3: Reservoir Model	Mon 8/30/10	Mon 8/30/10	0 days	100%
287	**Task 7: Analyze Simulation**	**Wed 8/17/11**	**Tue 11/8/11**	**59.9 days**	**99%**
288	Task 7.1: Image synthetics	Wed 8/17/11	Mon 10/31/11	53.9 days	100%
289	Task 7.2: Synthetic and Field seismic Calibration	Mon 10/31/11	Mon 11/7/11	5 days	100%
290	Task 7.3: Analyze images	Mon 10/31/11	Tue 11/8/11	6 days	100%
291	Task 7.4: Reservoir geophysics	Fri 11/4/11	Fri 11/4/11	0 days	0%
292	**Task 8: Sparcity Analysis**	**Tue 11/8/11**	**Tue 12/6/11**	**20 days**	**100%**
293	Task 8.1: Sparcity analysis	Tue 11/8/11	Tue 12/6/11	20 days	100%
294	**Task 9: Establish Methodology**	**Tue 12/6/11**	**Fri 12/30/11**	**17.1 days**	**100%**
295	Task 9.1: Establish CO2 MVA workflow	Tue 12/6/11	Tue 12/20/11	10 days	100%
296	Milestone 4: Sparcity Analysis	Fri 12/30/11	Fri 12/30/11	0 days	100%
297	**Phase III: SeisPRO CO2 MVA system**	**Thu 10/1/09**	**Fri 9/30/11**	**522 days**	**100%**
298	Task 10: Enhanced GeoPRO	Thu 10/1/09	Mon 11/30/09	43 days	100%
299	Task 11: Database	Tue 12/1/09	Fri 9/30/11	479 days	100%
300	Task 12: Infrastructure	Sun 11/15/09	Fri 9/30/11	490 days	100%
301	Task 13: Grid/parallel enhancement	Fri 10/1/10	Fri 9/30/11	261 days	100%
302	Task 14: Unified data format	Thu 2/4/10	Fri 9/30/11	432 days	100%
303	Task 15: Visualization	Sun 11/15/09	Fri 9/30/11	490 days	100%
304	Task 16: Instalation and testing	Mon 8/22/11	Fri 9/30/11	30 days	100%
305	Milestone 5: Debriefing	Wed 1/18/12	Wed 1/18/12	0 days	100%
306	Final report	Mon 11/14/11	Fri 3/30/12	101 days	95%

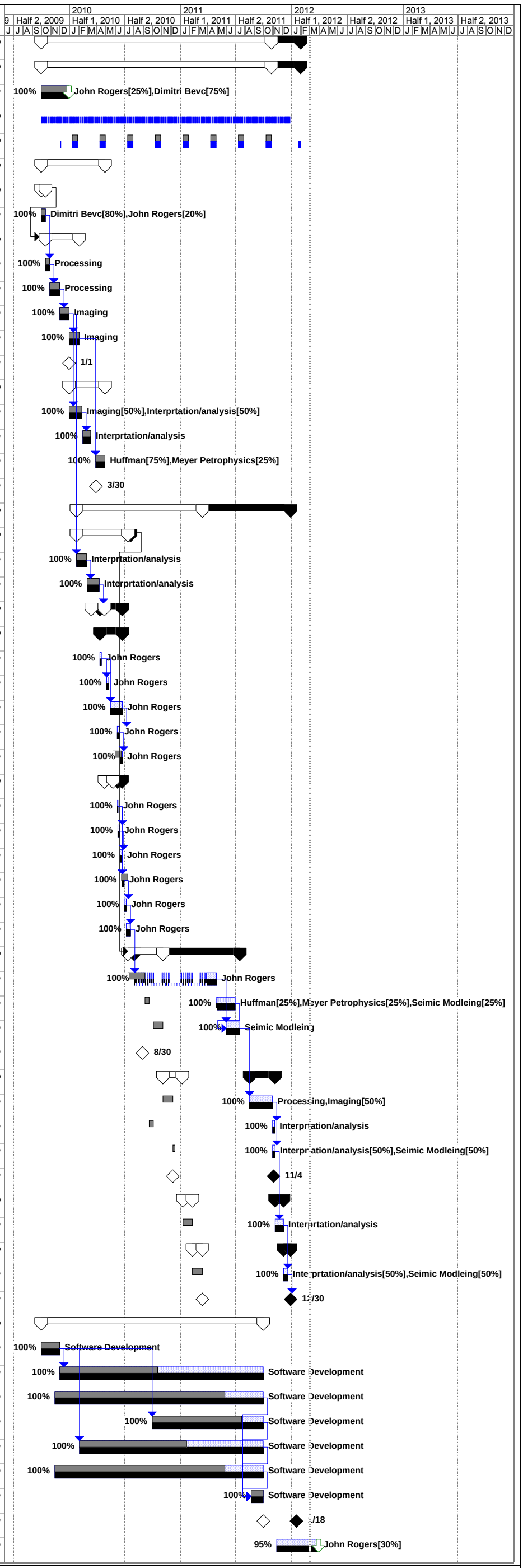

Project: MSProj11
Date: Tue 2/28/12

Task		Summary		Rolled Up Baseline Milestone		Project Summary	
Progress		Rolled Up Task		Rolled Up Progress		Group By Summary	
Baseline		Rolled Up Milestone		Split		Deadline	
Milestone		Baseline Summary		Baseline Split			
Baseline Milestone		Rolled Up Baseline		External Tasks			